CREEP OF HI-NICALON S FIBER TOWS

AT ELEVATED TEMPERATURE IN AIR AND IN STEAM

THESIS

Theodore R. Shillig, Captain, USAF

AFIT-ENY-13-M-31

DEPARTMENT OF THE AIR FORCE
AIR UNIVERSITY

AIR FORCE INSTITUTE OF TECHNOLOGY

Wright-Patterson Air Force Base, Ohio

AFIT-ENY-13-M-31

CREEP OF HI-NICALON S FIBER TOWS AT ELEVATED TEMPERATURE IN AIR AND IN STEAM

THESIS

Presented to the Faculty

Department of Aerospace and Astronautical Engineering

Graduate School of Engineering and Management

Air Force Institute of Technology

Air University

Air Education and Training Command

in Partial Fulfillment of the Requirements for the

Degree of Master of Science in Materials Science

Theodore R. Shillig, B.S.

Captain, USAF

March 2013

AFIT-ENY-13-M-31

CREEP OF HI-NICALON S FIBER TOWS AT ELEVATED TEMPERATURE IN AIR AND IN STEAM

Theodore R. Shillig, B.S.
Captain, USAF

Approved:

Marina B. Ruggles-Wrenn, PhD (Chairman)	Date
Geoff E. Fair, PhD (Member)	Date
Thomas G. Eason, PhD (Member)	Date

AFIT-ENY-13-M-31

Abstract

Structural aerospace components require materials that have superior long-term mechanical properties and can withstand severe environmental conditions, such as high temperatures, high pressures and moisture. Ceramic-matrix composites (CMCs) are capable of maintaining excellent strength and creep resistance at high temperatures, which makes them attractive candidate materials for aerospace applications, particularly in propulsion components. Silicon Carbide (SiC) ceramic fibers have been used as constituent materials in CMCs, although oxidation of the SiC to SiO_2 has been a known fiber degradation mechanism. Recently developed near stoichiometric Hi-Nicalon S fibers have shown significant improvements in thermo-chemical stability. Creep of the Hi-Nicalon S fibers at elevated temperature in air and in inert gas environments has been examined. However performance of these new fibers at elevated temperatures in steam environments has not been studied thoroughly. The objective of this thesis is to investigate creep of near stoichiometric Hi-Nicalon S SiC fiber tows at elevated temperatures in air and in steam.

The creep response of Hi-Nicalon S SiC fiber tows was investigated at 800°C, 900°C, 1000°C and 1100°C in laboratory air and in steam. The creep stresses ranged from 154 MPa to 1250 MPa. Creep run-out was defined as 100 h at creep stress. The presence of steam degraded the creep performance of the fiber tows at all temperatures. However, the negative effects of steam became less pronounced as the temperature increased. Less degradation due to steam at higher temperature is attributed to the transition from passive oxidation at 800°C-1000°C to active oxidation at 1100°C of the Hi-Nicalon S SiC fibers.

Table of Contents

Page

List of Figures

List of Tables

CREEP OF HI-NICALON S FIBER TOWS

AT ELEVATED TEMPERATURE IN AIR AND IN STEAM

I. Introduction

"It is a truism that technological development depends on advances in the field of materials. One does not have to be an expert to realize that a most advanced turbine or aircraft design is of no use if adequate materials to bear the service loads and conditions are not available. Whatever the field may be, the final limitation on advancement depends on materials"[28].

Materials have always been a limiting factor in the advancements of technology. The ever increasing demand for aerospace vehicles that are more fuel-efficient and can fly faster, longer and higher drives the development of lighter, stronger, and more durable materials. Today, composites are some of the most important materials developed for use in aerospace applications.

Although composites are among the most advanced structural materials, their origin can be traced back to ancient Egypt where straw was used as reinforcement in clay bricks. Composite materials have been used in various ways throughout the ages. However, research and development of composite materials for use in engineering applications has grown dramatically since the 1920's. In the 1930's and 1940's, honeycomb structures, powder metallurgy, and glass reinforced plastic were the advanced structural materials. Continuous glass fibers were first produced commercially in 1939 [53]. Advanced fibers such as boron and carbon were developed in the 1950's and 1960's [26]. The United States Air Force began researching the use of composites in the 1960's, investigating the possibility of using boron or graphite fibers in an epoxy resin for aircraft control surfaces. Since then the US Air Force has led the research and development effort to bring high performance fiber composites to engineering applications [12].

Composite materials were first introduced in commercial aircraft in the 1950's when fiberglass made up some two percent of the structure of the early Boeing 707s. Composites make up 9% of the aircraft structural weight in the Boeing 777. Fighter aircraft developed in the late 1970s such as the F-15 and F-16 incorporated about 1-2% (by weight) composites into the airframe. The use of composites increased greatly in the next generation of fighter aircraft. The F/A-18E/F and F-22A aircraft are approximately 25% composites by weight [17]. Today, composites make up a large percentage of aircraft components, for example the fuselage and wings of the Boeing 787 Dreamliner consist mostly of composites which make up 50% of the aircraft by weight [1].

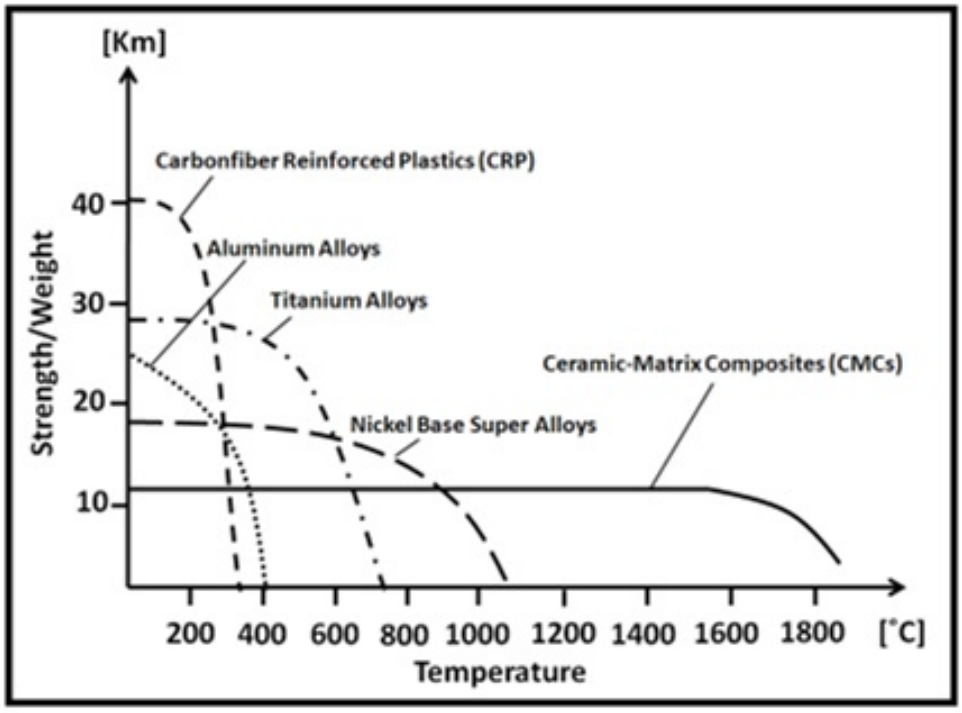

Figure 1.1: Strength to weight ratio as a function of temperature for select aerospace materials [19]

Advances in aerospace propulsion technologies have raised the demand for structural materials that have superior long-term mechanical properties and retain properties under high temperature, high pressure and various environmental conditions such as moisture. Ceramic-matrix composites (CMCs), capable of maintaining excellent strength and fracture toughness at high temperatures, are prime candidate materials for such aerospace applications. Additionally, the lower densities of CMCs and their higher use temperatures allow for improved high-temperature performance when compared to conventional nickel-based superalloys [55]. Replacing traditional metal alloys in the aircraft propulsion

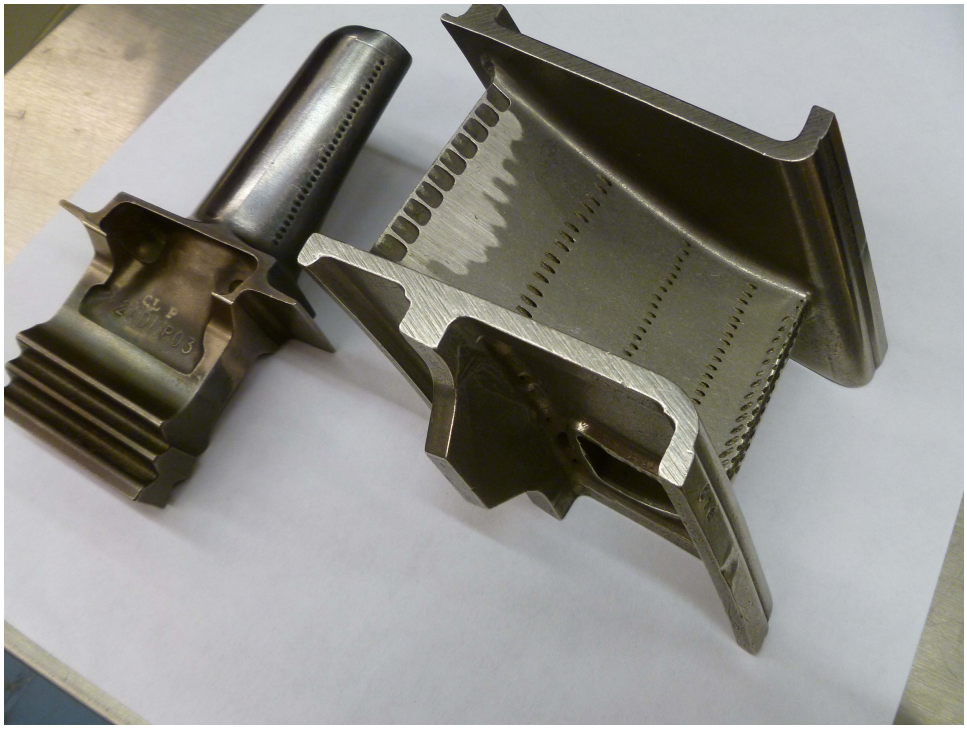

Figure 1.2: Turbine engine blades showing active cooling ports

systems with CMCs can raise the limitations on the operating temperatures that the propulsion systems can attain. In turbine engines, higher operating temperatures allows for increased power, reduced fuel consumption, and a reduction in emissions [18]. Figure

1.1 shows the comparative advantage of the CMCs over other materials commonly used in aerospace applications [51].

Fig.1.2 shows two turbine engine components that due to material property limitations require active cooling ports to prevent failure. With materials that have superior long-term mechanical properties at higher temperatures these turbine components could be operated at higher temperatures, increasing the performance threshold.

II. Background

2.1 Ceramic Matrix Composites

In the recent decades numerous material science and engineering research efforts have focused on the development of CMCs. Ceramic matrix composites are designed to have load-carrying capacity at high temperatures in extreme environments. Ceramic matrix composites are prime candidate materials for structural components in hypersonic vehicles, rocket engines, jet engines, and space vehicles [45]. CMCs are currently being evaluated for use in aerospace turbine engines and are likely to be incorporated in combustion chambers and nozzle extensions of advanced rocket propulsion systems. Some additional examples of military and commercial applications of CMCs are shown in Table 2.1.

Table 2.1: CMC Applications [1]

Applications / Sectors	Continuous Fiber CMCs		
MILITARY	• F414 and F110 Nozzle Flaps and Seals • F117 Aft Deck Heat Shields • Engine Vanes • Flame Holders	• Orbital Transfer Engine Thrusters • Low Cost Large Rocket Thruster (Million Pound) Heavy Lift Launch • Tactical Missile Combustors, Rotors • Divert and Attitude Control Thrusters	• Turboramjet Variable Area Nozzles • Surveillance OTV Thrusters • Hypersonic Leading Edges, Inlet Cowlings and Nozzles • Linear Aerospike Engine, Thrust Cells and Ramp
Commercial/Dual Use	• Heat Exchangers • Radiant Burner Tubes • Land-Based Gas Turbines • Candle Filters	• MDH Air Preheater Tubes • Immersion Heaters • Seal-less Magnetic Pumps • Motorcycle Brakes	• Diesel Components • Valve Guides • Pistons • Turbocharger Rotors

While monolithic ceramics exhibit excellent high-temperature properties, they also exhibit some undesirable properties. One of the inherent limitations of ceramic materials

is their tendency to be brittle. Monolithic ceramics generally have low toughness, low ductility and exhibit catastrophic failure. CMCs were developed specifically to enable the increased use of ceramics in structural applications. The CMC are designed to have the favorable mechanical, thermal, and environmental properties of monolithic ceramics while also exhibiting graceful failure. Hence, the main advantages of CMCs over monolithic ceramics are their superior toughness, tolerance to the presence of defects, and non-catastrophic mode of failure. Typical tensile stress-strain curves for a monolithic ceramic material and for a CMC are shown in Fig. 2.1.

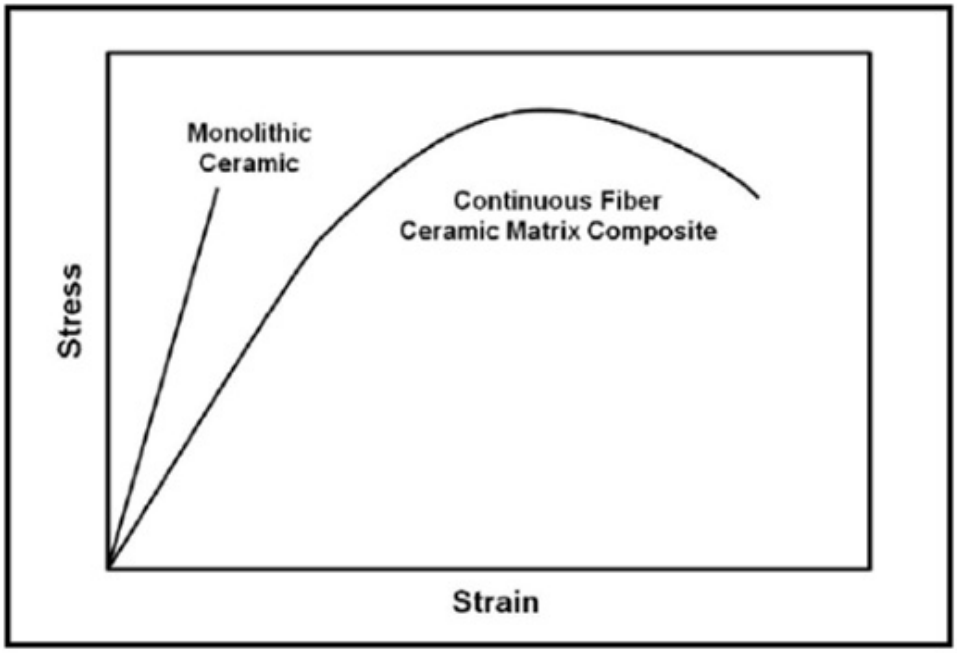

Figure 2.1: Stress-Strain Curves, Monolithic ceramic vs CMC [2]

It is widely accepted that in order to avoid brittle fracture behavior in CMCs and improve the damage tolerance, a weak fiber/matrix interface is needed, which serves to deflect matrix cracks and to allow subsequent fiber pull-out [20, 32–34]. In the presence of a weak fiber/matrix interface, matrix cracks are allowed to propagate within the material

and around the fibers without causing catastrophic failure. As matrix cracks are deflected around the fibers, fiber-bridged cracks form and the loads are gradually transferred to fibers, finally causing uncorrelated fiber fracture followed by fiber pullout [20, 32]. Thus the fibers continue carrying the load as the matrix cracks propagate leading to graceful failure of the composite material system as shown in Fig. 2.2. Example of fiber pullout is shown in Fig.2.3 .

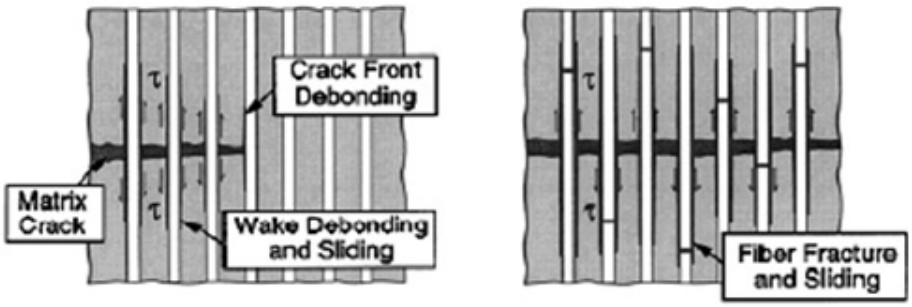

Figure 2.2: Fiber/matrix interface [56]

CMCs offer superior long-term mechanical properties and retained properties under high temperature. SiC fiber-reinforced SiC matrix composites are currently being evaluated for aircraft engine hot-section components [6, 7, 14, 44]. In these applications the composites will be subjected to mechanical loadings at elevated temperatures in oxidizing environments. Therefore the thermodynamic stability and oxidation resistance of the CMCs are vital issues. The most significant problem hindering SiC-fiber-containing CMCs is oxidation embrittlement [39]. Typically the embrittlement occurs once oxygen enters through the matrix cracks and reacts with the fibers and the fiber coatings [27, 37, 49]. The degradation of fibers and fiber coatings is generally accelerated by the presence of moisture [21, 41, 42]. An example of such degradation of fibers and fiber coatings is shown in Fig. 2.4.

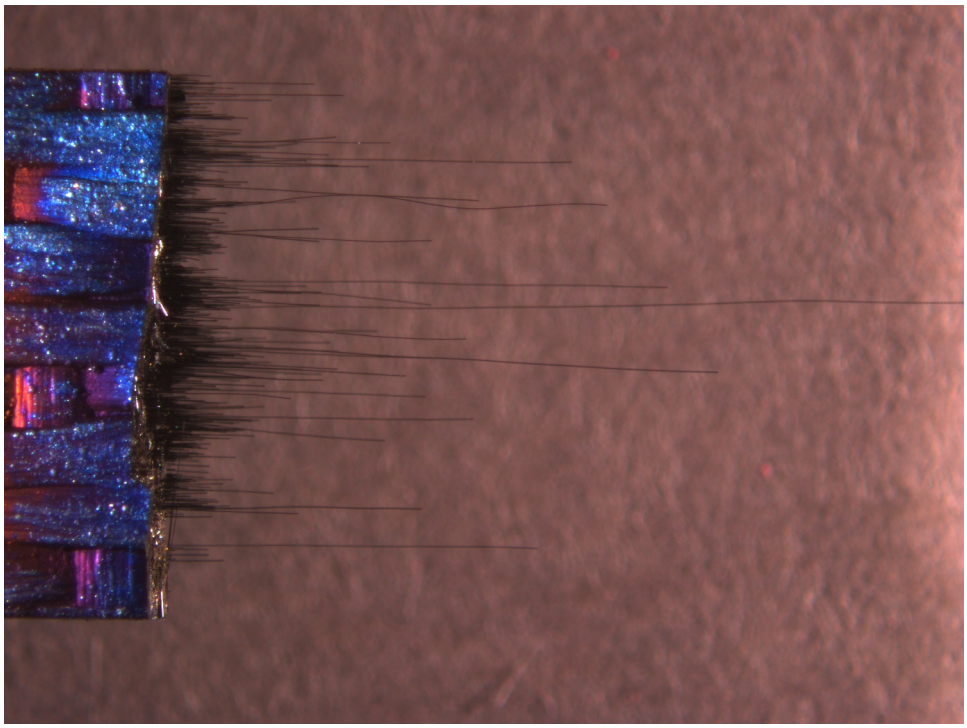

Figure 2.3: Hi-Nicalon/BN/SiC specimen subjected to tension-tension fatigue (1.0 Hz, max stress = 120 MPa) at 1200°C in air. The fracture surfaces show a substantial amount of fiber pullout. [2]

The mechanical properties and performance of the composite with 0°/90° fiber orientation are dominated by the fibers, so fiber degradation is a likely source of composite degradation. Acceptance of the SiC-SiC CMCs for high-temperature structural applications requires a thorough understanding of their mechanical behavior. In order to use SiC-SiC CMCs in combustion environments, like jet engines, their environmental resistance and mechanical performance in such environment must be assured.

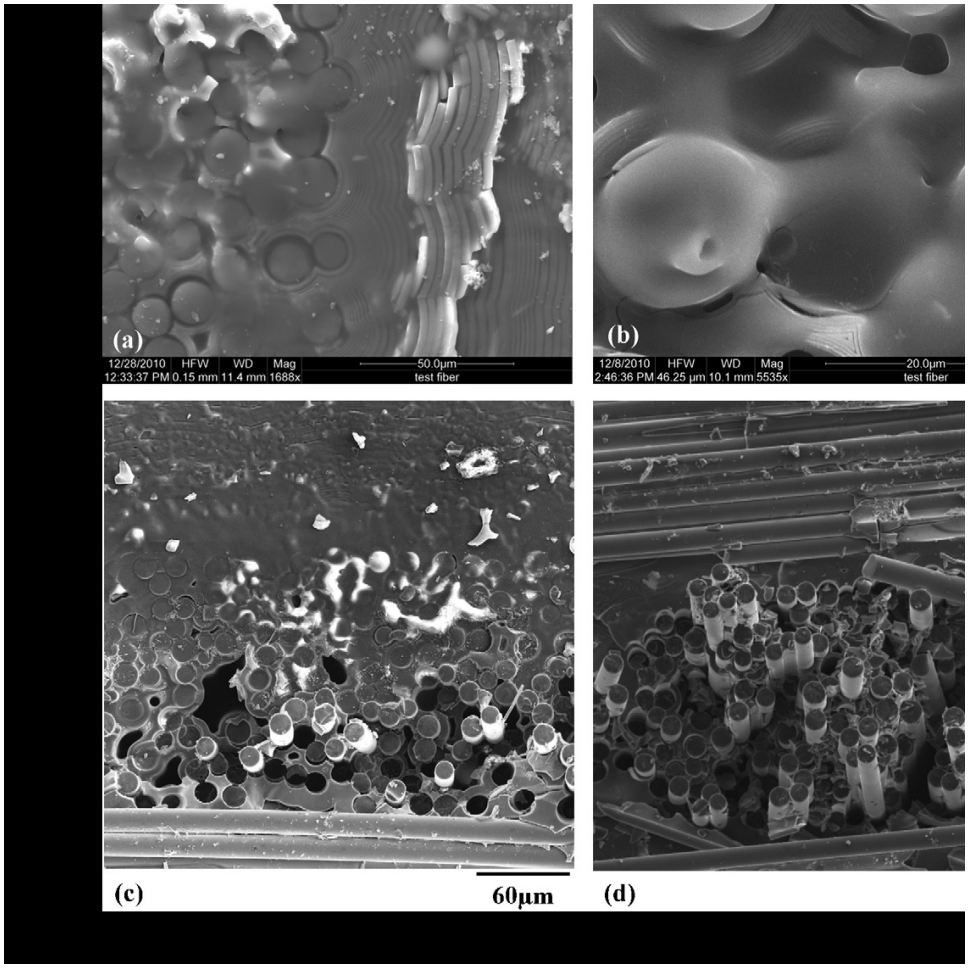

Figure 2.4: Fracture surface of Hi-Nicalon^{TM}. Higher magnification images showing: (a) oxidation of fibers and matrix, (b) glassy phase in the oxidized region, (c) oxidized region in the top half of the image transitioning to the non-oxidized region in the bottom half of the image, and (d) fiber pull-out typical in the non oxidized region. [11]

2.2 Silicon Carbide Based Fibers

SiC-based fibers have been produced since the mid-1960s by chemical vapor deposition (CVD) onto a tungsten or carbon filament core. The resulting fibers had large diameter (100-140μm) and little flexibility, which limited their use. These fibers were mainly utilized as reinforcement for metals such as aluminum, titanium, and intermetallics.

Fine SiC-based fibers with diameters of 10-15μm were first produced in the early 1980s by Nippon Carbon. This development of small-diameter SiC-based fibers opened the possibility of reinforcing ceramic materials with ceramic fibers in order to produce high-temperature structural composites. The schematic in Figure 2.5 shows the process of producing fine silicon carbide fibers by the melt spinning, crosslinking, and pyrolysis of an organosilicon polymer.

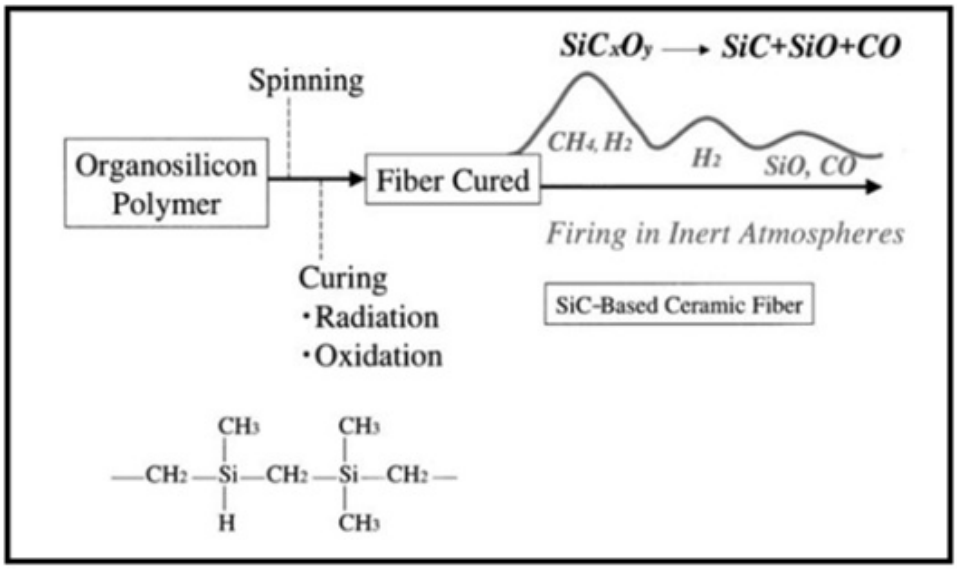

Figure 2.5: Fundamental production process of SiC-based fibers using PCS precursor [30]

It is recognized that all SiC-based fibers are not pure SiC. The Si-based fibers of first generation such as Nicalon fiber (manufactured by Nippon Carbon, Japan), consist of SiC-nanocrystals (1-2nm in size) and free carbon embedded in an amorphous SiC_xO_y matrix. Approximate chemical composition of the Nicalon fibers is: 65% SiC, 23% SiO2 and 12% C. Stiffness of the Nicalon fibers (220 GPa) fell significantly short of that of pure SiC (400 GPa), yet their strain at failure was high (1.4%). This deviation was attributed to the large amount of excess carbon and oxygen contained in the fiber. Additionally, these fibers suffer severe strength degradation at temperatures above 1200°C. Hence, SiC/SiC

composites reinforced with these fibers must be processed at lower temperatures (i. e. using CVI or PIP techniques). Furthermore, the use of these composites would be limited in temperature.

Numerous studies were performed on the first generation SiC-based fibers. It was concluded that the non-stoichiometric composition of the fibers was limiting their performance and physical characteristics. It was found that the oxygen which remained in the fibers after pyrolysis formed an amorphous intergranular Si-O-C phase [8], which was responsible for the loss of fiber strength and creep at temperatures around 1000-1100°C. Note that at 1000-1100°C, bulk SiC exhibits excellent strength and creep resistance. The low Young's modulus of the fibers (only about half of the modulus of bulk SiC) was attributed to a low fraction of a granular SiC phase in the fibers. Results of these studies revealed that in order to improve fibers, it was necessary to achieve a more stoichiometric composition and to considerably reduce the oxygen content in the fiber.

SiC-based fibers of the second generation were developed in an effort to produce fibers with reduced oxygen content. SiC-based fibers of the second generation, such as Hi-Nicalon, are near oxygen-free. They consist of SiC-nanocrystals (average size 5 nm) and free carbon [C/Si (at) ratio=1.39]. Because these fibers contain only negligible amounts of SiC_xO_y phase they do not suffer decomposition at high temperature. The SiC-based fibers of second generation creep at 1200°C. However, subjecting them to heat treatment at 1400-1600°C stabilizes the microstructure and improves their creep resistance. Notably, the Hi-Nicalon fiber did not creep at temperatures below 1000°C. In fact, Hi-Nicalon fiber was shown to possess the highest creep threshold and to produce the lowest creep rate among the first and second generation SiC-based fibers. Still, at 1400°C all first and second generation SiC fibers produced very similar creep rates ($\approx 5\times10^{-7}s^{-1}$ under a stress of 0.3 GPa) [8]. The activation energy for the creep of Hi-Nicalon fibers was determined to be 360 kJ/mol and the predominant creep mechanism was identified as grain boundary sliding accommodated

by interface-controlled diffusion. It was recognized that the carbon layers located between the grains could facilitate the grain boundary sliding. The ultimate failure of the fibers in creep was not due to a lack of accommodation, as is the case for bulk ceramics. Rather the ultimate failure in creep was caused by surface defects, such as cavities or porous zones growing from local chemical heterogeneities [8].

Further improvements in SiC-based fibers were achieved by Nippon Carbon researchers, who recognized that to produce a near stoichiometric fiber they had to reduce the excess carbon in the Hi-Nicalon fiber. The radiation cured precursor route utilized to produce the Hi-Nicalon fiber became an intermediate step in producing a near stoichiometric SiC fiber without the use of sintering aids. Then the Hi-Nicalon fiber was heated to 1500°C in a hydrogen-rich atmosphere in order to reduce the excess carbon. As a result, C/Si ratio in the fiber was reduced from 1.39 to 1.05 and a near stoichiometric fiber called Hi-Nicalon-S was produced [29].

Microstructures of Nicalon, Hi-Nicalon, and Hi-Nicalon-S fibers are schematically depicted in Fig. 2.6.

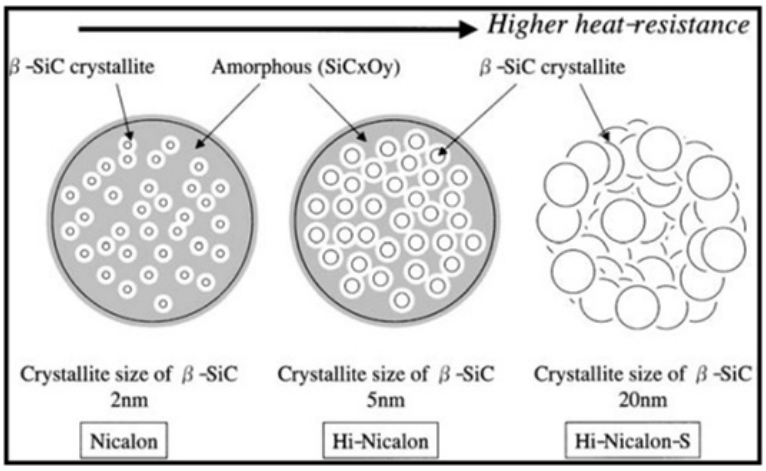

Figure 2.6: Schematic showing microstructures of Nicalon, Hi-Nicalon, and Hi-Nicalon S Fibers [30]

Hi-Nicalon-S fibers, processed in inert atmospheres and crosslinked by radiation have very low oxygen content and nearly stoichiometric chemical composition. Hi-Nicalon S fiber is fabricated from a polycarbosilane (PCS) precursor via the basic process shown in Figure 2.5. The filaments are cured by electron irradiation and pyrolyzed by a modified Hi-Nicalon process in a closely controlled atmosphere at 1600 - 2000°C [46]. Hi-Nicalon-S fibers primarily consist of relatively large (20 - 200nm) SiC grains and several phases, which considerably influence the thermal stability of the fibers. The excess carbon from processing is reduced and a nearly 1 to 1 C/S ratio is achieved, which makes the fiber more chemically stable and therefore more oxidation resistant and more thermally resistant [46]. A summary of the material properties of various SiC fiber tows can be seen in Table 2.2

Table 2.2: Specification and Material Properties of various SiC Fiber Tows [30]

: Nearly stoichiometric SiC fiber

	SiC Fibers							
	Nicalon			Tyranno				Sylramic
	NL-200	Hi-Nicalon	Hi-Nicalon-s	Lox M	ZMI	ZE	SA*	
Atomic Composition	$SiC_{1.34}O_{0.36}$	$SiC_{1.39}O_{0.01}$	$SiC_{1.05}$	$SiTi_{0.02}C_{1.37}O_{0.32}$	$SiZr_{<0.01}C_{1.44}O_{0.24}$	$SiZr_{<0.01}C_{1.52}O_{0.05}$	SiC $O,Al_{<0.008}$	$SiCTi_{0.02}B_{0.09}O_{0.02}$
Tensile Strength (GPa)	3.0	2.8	2.6	3.3	3.4	3.5	2.8	3.0
Tensile Modulu (GPa)	220	270	410	187	200	233	410	420
Elongation (%)	1.4	1.0	0.6	1.8	1.7	1.5	0.7	0.7
Density ($g \cdot cm^{-3}$)	2.55	2.74	3.10	2.48	2.48	2.55	3.02	>3.1
Diameter (μm)	14	14	12	8 & 11	8 & 11	11	8 & 10	10
Specific Resistivity ($\Omega \cdot cm$)	10^3-10^4	1.4	0.1	30	2.0	0.3	—	—
Thermal Expansion coeff. (10^{-6}/K)	3.2 (25-500℃)	3.5 (25-500℃)	—	3.1	4.0	—	4.5 (20-1320℃)	—
Thermal Conductivity (W/mK)	2.97(25℃) 2.20(500℃)	7.77(25℃) 10.1(500℃)	18.4 (25℃) 16.3 (500℃)	—	2.52	—	64.6	40-45

SiC fiber-reinforced SiC matrix composites are currently being evaluated for use in various applications, including aircraft jet engines, gas turbines for electrical power/steam cogeneration, as well as nuclear power plant components. It is recognized that the structural performance of the CMCs is controlled by the strength of the fibers. Therefore, fiber

performance at elevated temperature in service environments is a critical factor in the development of CMCs. Multifilament tows, consisting of several hundreds of filaments, represent a fundamental unit in textile composites. As the matrix becomes increasingly more damaged, fiber tows carry more and more load and control the ultimate failure of the composite. Dassios et al [15] demonstrated that testing of fiber tows rather than testing of single filaments permitted a more accurate measurement of the fiber strength. Multifilament tows are more damage tolerant than single fibers. The ultimate failure of the fiber tows is preceded by breaks of individual fibers. When an intact single fiber is extracted from a fiber tow for testing, it is reasonable to conclude that this fiber is likely to be stronger than those that broke during extraction. Hence testing of a single filament will not yield an average value of strength, but rather will produce a higher than average strength value. Conversely, testing of a fiber tow will yield average values of fiber properties.

High-temperature properties and mechanical performance of SiC-based fibers have been examined by various researchers. Lamon and co-workers studied the delayed failure of SiC fiber tows at 600°C-800°C in air [22–24]. Forio et al [22] investigated static fatigue of Nicalon fiber tows at 600°C-700°C. The delayed failure of the fiber tows was attributed to slow crack growth activated by oxidation. Gauthier and Lamon [23] examined static fatigue of Hi-Nicalon and Hi-Nicalon S multifilament tows and static fatigue of single filaments at 500°C-800°C in air. A model based on slow crack growth in single filaments was shown to successfully predict delayed failure of fiber tows. Gauthier et al [24] investigated oxidation of Nicalon, Hi-Nicalon, and Hi-Nicalon fibers subjected to static fatigue at 500°C-800°C. It was found that the delayed failure of the fiber tows was due to subcritical crack growth of the surface defects by oxidation of the grain boundaries (free carbon) and of the SiC nanograins or silicon oxicarbide at the crack tip.

Subcritical crack growth has been widely studied and was shown to depend on temperature. Ladeveze et al. examined the framework for modeling subcritical crack

growth [36]. It is known that there are two different stages of crack propagation. During the first stage, damage occurs directly at the crack tip. During the second stage, oxygen and water must diffuse through an oxide layer formed on the surface of the fiber prior to further damage occurring. This is aptly called the diffusion-controlled stage. Ladevezes and co-workers developed additional predictive models capable of accounting for oxidation effects at both low and high temperatures [36].

2.3 Research Objectives

The main objective of this research is to investigate mechanical performance of SiC-based fibers at elevated temperature in air and steam. In order for SiC/SiC CMCs to be safely used in advanced aerospace applications such as jet engines, their environmental durability at elevated temperatures in operating environments must be assured. Therefore, a thorough understanding and analysis of the performance of SiC-based fibers at elevated temperature in oxidizing environment is required. This research aims to evaluate the effects of steam on creep performance of Hi-Nicalon S fiber tows at temperatures in the 800-1100°C range.

An experimental facility had been designed and a test method had been developed previously by Major Clint Armani for the testing of oxide fibers in air and steam [2]. In the course of the present effort the experimental facility was used for testing of higher strength SiC fiber tows. A new design of the steam delivery system was developed and implemented in order to achieve a more consistent near 100% steam environment around the test specimens. The test method employed in the present effort permitted accurate load control and, most importantly, accurate strain measurement. Creep strains were measured and creep rates were determined.

III. Material and Test Specimen

3.1 Material

The material to be studied is Hi-Nicalon-S fiber tows with PVA sizing manufactured by Nippon Carbon Co. The fiber tow consists of approximately 500 filaments with a monofilament diameter of 13μm. Material properties for this spool of Hi-Nicalon-S fiber are listed below in Table 3.1. Based on this data, a cross sectional area of 6.6366e^{-8} m^2 was used for all engineering stress calculations.

Table 3.1: Hi-Nicalon-S fiber properties.

Property	Results	Units
Density	3.01	g/cc
Tensile Strength	3.13	GPa
Tensile Modulus	366	GPa
Sizing Amount	.8	wt.%
Oxygen Content	.82	wt.%

3.2 Test Specimen

The test specimens were prepared using primary, secondary and tertiary tabs according to the method developed by Steffens [52]. A model of the three-tab design is depicted in Fig. 3.1. The centerline hole was punched in the fiberglass tabs to permit hanging the fiber tow specimen on the hook fixtures. In preparing the fiber tows test specimens, excess lengths of tow were taken from the manufacturer's spool. Portions of the tow that contained obvious damage, such as broken filaments and bent fibers were discarded. Fiberglass tabs were positioned seven inches apart on the grid of a cutting board. Each tow section was aligned over the tabs, utilizing the gird lines, and taped onto the cutting board. The fiber tow must bisect the centerline holes in each tab to ensure that only axial loading was present during testing. A two part epoxy (Hardman Double Bubble Epoxy, 04001) was applied to

the tow section on top of the primary tab then the secondary fiberglass tab was applied so that the tow and the epoxy were sandwiched between the tabs. Once the adhesive had thickened (after about 5 minutes), the excess tow protruding beyond the tabs was folded toward the test section. The two part epoxy was then applied to the folded tow section on top of the secondary tab. Finally a tertiary fiberglass tab was applied in order to sandwich the folded portion of the tow between the secondary and tertiary fiberglass tabs. After the adhesive has fully cured, the excess tow protruding beyond the tertiary tab was cut with a razor blade. The final length of the fiber tow specimen measured between tabs was seven inches for all experiments. The primary tab was 1.75 in. x 1.0 in., the secondary tab was 1.00 in. x 1.00 in. and the tertiary tab was 0.75 in. x 0.75 in. Steps of the specimen preparation process can be seen in Fig. 3.2

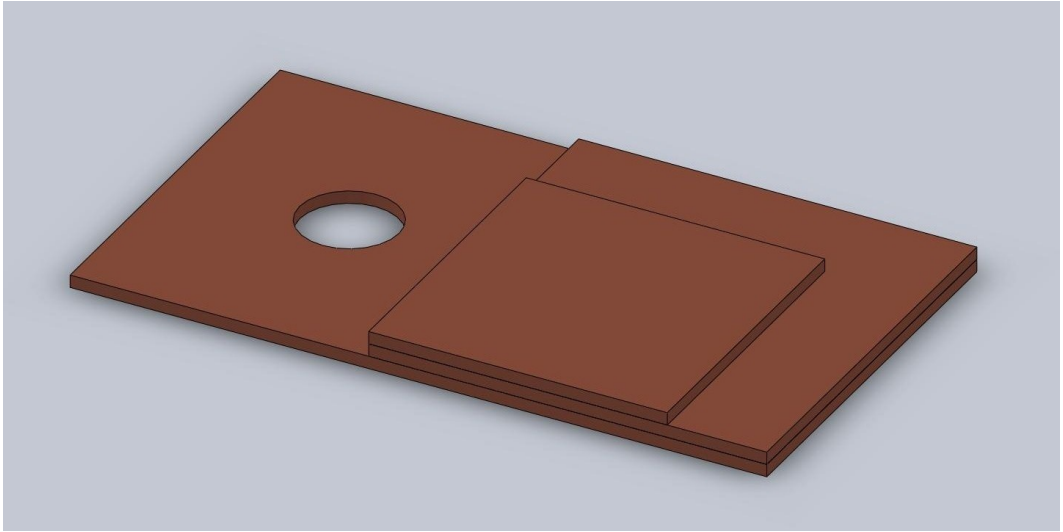

Figure 3.1: A solid model of the third iteration tab. Reproduced from [52]

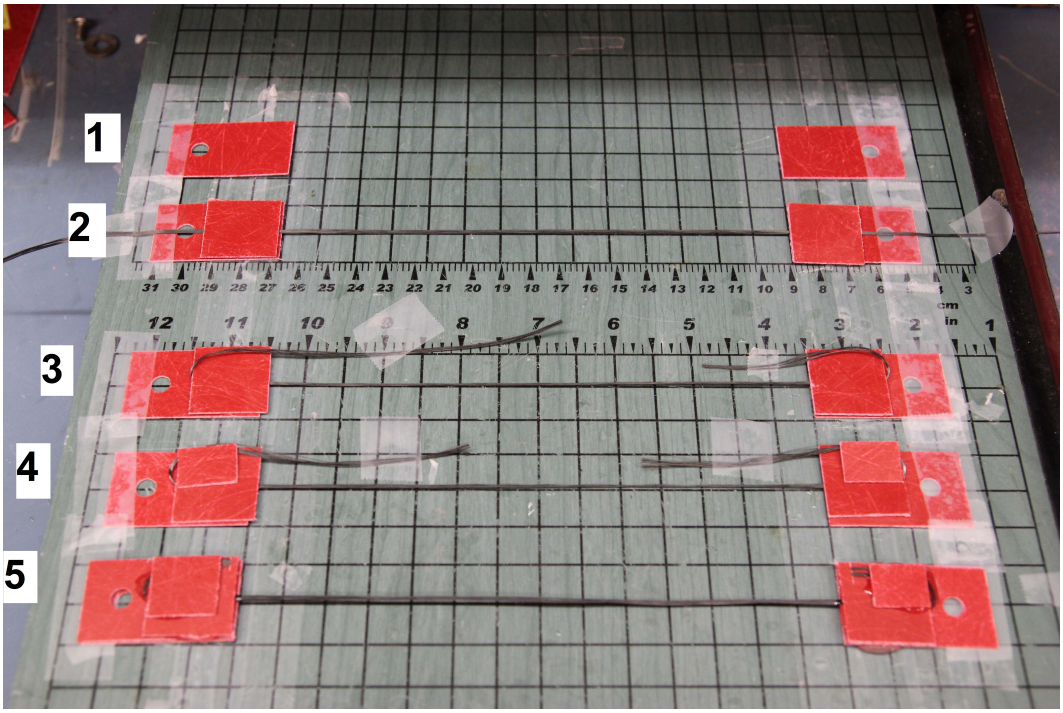

Figure 3.2: Preparation of the fiber tow test specimen, using the three tab system. Numbers on the left refer to the specimen preparation steps described above

IV. Experimental Arrangements and Procedures

4.1 Parameters

The experimental facility for testing fiber tows at elevated temperature in air and in steam environment was designed and built by Major Clinton Armani in the Mechanics of Advanced Aerospace Materials Laboratory of the Department of Aeronautics and Astronautics at the Air Force Institute of Technology. Methods for testing ceramic fiber tows under monotonic tension or in creep at elevated temperature in air and in steam environments were also by Major Clint Armani [2].

It is recognized that the tensile strength of ceramic fiber tows is generally less than the mean strength of single filaments [9, 13, 40]. Nevertheless, because composites are reinforced with fiber tows, the experiments conducted on fiber tows were more representative of the actual service conditions than those conducted on single filaments [9, 15] . Based on these observations, the present research focused on investigating the creep response of fiber tows rather than that of the single filaments.

The creep performance of Hi-Nicalon S fiber tows was investigated in air and in steam at 800°C, 900°C, 1000°C and 1100°C. Creep experiments were performed at stresses ranging from 154 to 1250 MPa in order to establish dependence of creep behavior on the applied stress. Creep run-out was set to 100 h. In order to evaluate the effects of steam environment on creep behavior, all creep tests were performed in air and in steam. In each test, load-displacement data were recorded during the initial heating, during loading to the creep stress level, and during the actual creep period. Thus applied stress, thermal strain, the total mechanical strain, and the creep strain could be calculated and examined. In all tests, a heating rate of 1.0°C/s was used, and the targeted temperature was maintained for a minimum of 45 min before each test in order to achieve thermal equilibrium of the test specimen. During heat-up and heat-soak each specimen was subjected to a small weight of

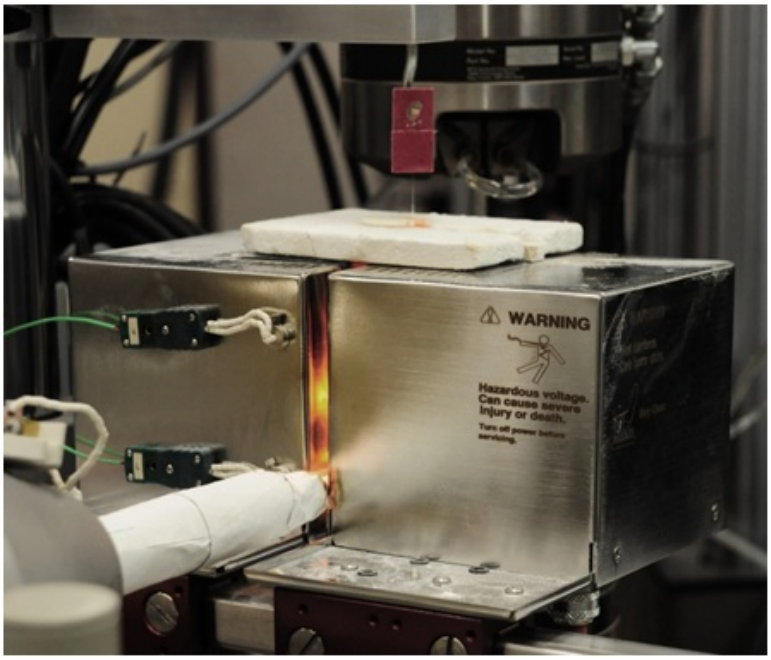

Figure 4.1: MTS 653.03A two-zone furnace used for fiber tow testing. Reproduced from [2]

10 to 20 g in order to keep the fiber tow taut. It is noteworthy that in all tests the failures occurred in the heated gauge section of the specimen. Analysis of the experimental data provided insight into the creep and the environmental degradation occurring in the fiber tows at elevated temperatures.

A compact two-zone resistance-heated furnace shown in Fig. 4.1 was used in all tests. The furnace had SiC heating elements and was equipped with two R-type control thermocouples, which supplied feedback to two MTS 409.83 temperature controllers. The furnace had a 3.5 inch (90 mm) hot zone. An MTS FlexTest 40 digital controller was employed for data acquisition. Temperature profiles were measured throughout the length of the furnace using an R-type thermocouple. Once the temperature profile throughout the length of the furnace was established, an effective gauge length of the fiber tow specimen was calculated, which enabled the calculation of engineering strain from recorded

displacement measurements. This technique is discussed in detail in Section 4.3. All tests on fiber tows employed an alumina test chamber (ceramic tube with end caps) designed to fit inside the furnace. The use of the test chamber resulted in a more uniform and

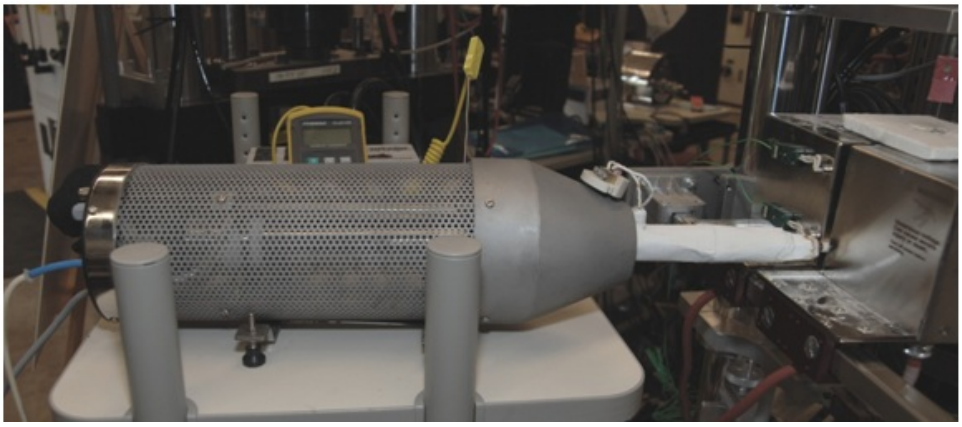

Figure 4.2: MHI model HGA-H steam generator. Reproduced from [2]

repeatable temperature distribution along the fiber tow specimen. The gauge section of the fiber tow specimen was located inside the test chamber with the ends of the fiber tow specimen passing through slots in the test chamber end caps.

A model HGA-H (MHI) steam generator (see Figure 4.2) was utilized to generate steam. De-ionized water was pumped into the steam generator using a medical grade pump at a rate of 2 ml/min. Variac was employed to control the power input to the steam generator. Accurate power control was needed to ensure that the steam generator maintained constant temperature at a low water flow rate. For testing in steam, steam is introduced into the test chamber (through a feeding tube) in a continuous stream with a slightly positive pressure, expelling the dry air and creating a near 100% steam environment inside the susceptor.

Figure 4.3 shows the alumina test chamber set in one half of the furnace with the steam feeding tube entering the test chamber at the bottom and a fiber tow specimen suspended from an extendable fixture of the creep testing facility.

Figure 4.3: Experimental setup for creep testing of fiber tows with alumina test chamber and steam feeding tube. Reproduced from [2]

Previous creep testing of SiC fiber tows at elevated temperature in air [52] produced satisfactory results. However, results of creep tests on SiC fiber tows performed at elevated temperature in steam [52] revealed problems associated with steam delivery into test chamber. Fiber tow specimens tested at 800°C in air failed at different location within the hot zone (red lines in Fig. 4.4). In contrast, in the case of fiber tow specimens tested at 800C in steam all failures were localized at the point of steam entry into the test chamber (blue line in Fig. 4.5). Careful analysis of the steam delivery system revealed that the

temperature and water input settings for the steam generator used in prior work did not result in a continuous flow of steam. Instead, the pressure within the steam generator would periodically drop causing the steam flow to stop completely. Then after a short period of time the pressure within the generator

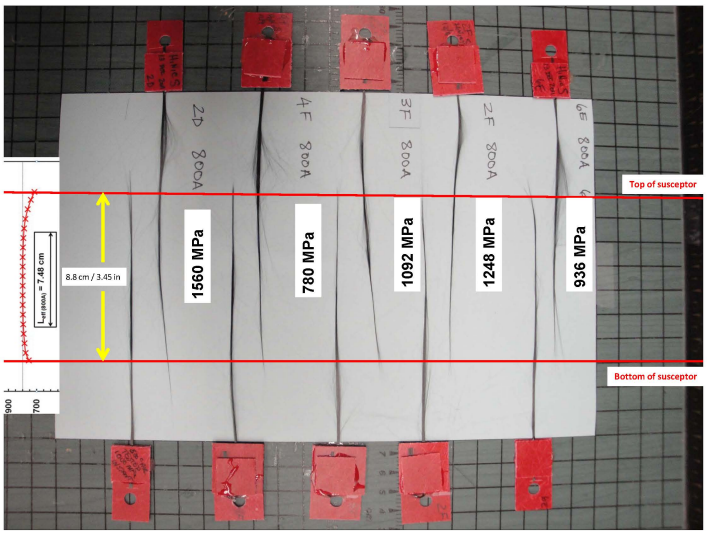

Figure 4.4: Hi-Nicalon S fiber tow specimens tested at 800°C in air. Note that fiber tows fail throughout the hot zone (marked with red lines). Reproduced from [52]

would build up and expel water droplets out at high speed. Such steam delivery was clearly unacceptable. It was concluded that the flow rate of water into the steam generator was too low. Additionally, the insulation at the generator tip connecting with the feeding tube was found to be inadequate allowing water condensation at the generator tip. As the water condensed the feeding tube became effectively plugged which resulted in the pressure buildup and subsequent high-speed ejection of water. SiC fibers are inherently brittle. It is believed that continual impingement by water droplets at high speed was a primary cause of localized failures in the fiber tow specimens. It was also recognized that

steam entering the test chamber is at a much lower temperature than the test specimen. Continuous stream of "cold" steam entering the "hot" test chamber caused a discontinuity in the temperature profile within the hot zone, as was reported in prior work [52]. The temperature gradient within the hot zone likely also contributed to localized failures at the steam port. Several steps were taken in order to correct these problems. The flow rate of

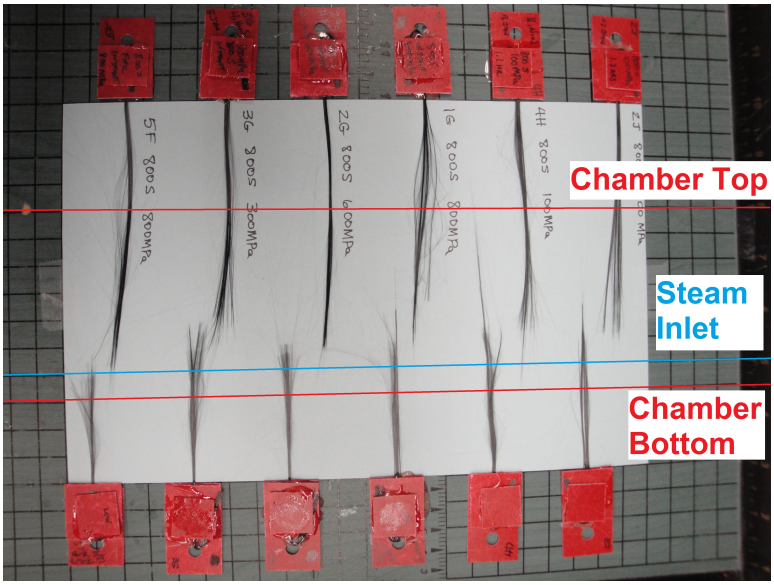

Figure 4.5: Hi-Nicalon S fiber tow specimens tested at 800°C in steam. Note that all failures are localized at the point of steam entry into the test chamber. Reproduced from [52]

water into steam generator was increased from 0.8 ml/min specified in prior work [52] to 2 ml/min. The steam generator tip was replaced and reinsulated to prevent condensation. Most importantly, a new design of the steam feeding tube was developed and implemented. In prior work steam was delivered via a simple open-ended alumina tube. In the new design, steam enters the test chamber though a capped alumina tube with a circumferential slot cut halfway through (see Fig. 4.6). The feeding tube is installed into the test chamber with the circumferential slot pointing downward, directing the flow of steam towards the bottom of

the chamber. As a result, steam is diverted and no longer impinges directly on the fiber tow specimen.

The new steam generator settings and the new design of the feeding tube proved to be successful. Fiber tow specimens tested at elevated temperature in steam in the present effort fail throughout the hot zone as seen in Fig. 4.7

The elongation of the fiber tow specimen was measured with an LVDT (Schaevitz M12-30). For tensile creep testing fiber tow specimen were suspended from an extendable fixture. The LVDT was connected to the bottom tab of the fiber tow specimen. The

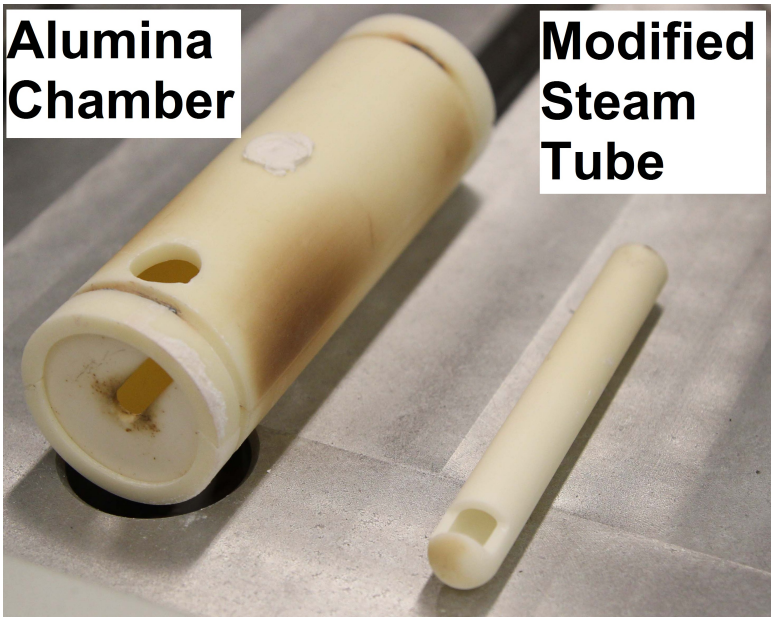

Figure 4.6: Alumina test chamber with steam port and alumina steam feeding tube with slot to divert steam away from directly impacting the fiber tow specimen

rod extending from the bottom of the LVDT core held the dead weight. Because slow application of the creep load is critical to preventing damage to the tow specimen during initial loading, a hand-driven screw elevator was used to apply the load to the fiber tow

specimen. Figure 4.8 shows a fiber tow specimen mounted in the dead weight creep testing facility.

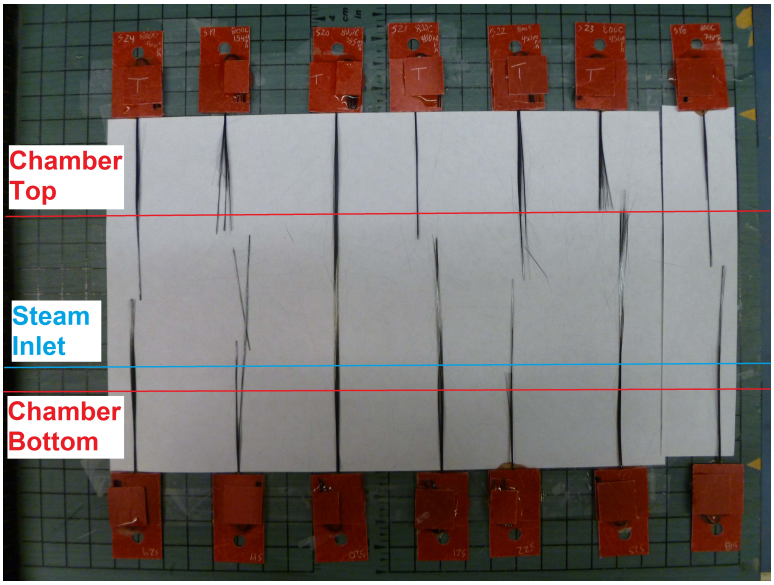

Figure 4.7: Hi-Nicalon S fiber tow specimens tested at 800°C in steam. Note that fiber tows fail throughout the hot zone(marked with red lines)

A detailed description of the specimens mounting procedure and of the creep test procedures is given elsewhere [2, 52]. A stress-weight index for the stackable weights is given in Table 7.1 of Appendix A. The settings for the steam generator are summarized in Table 7.2 of Appendix B.

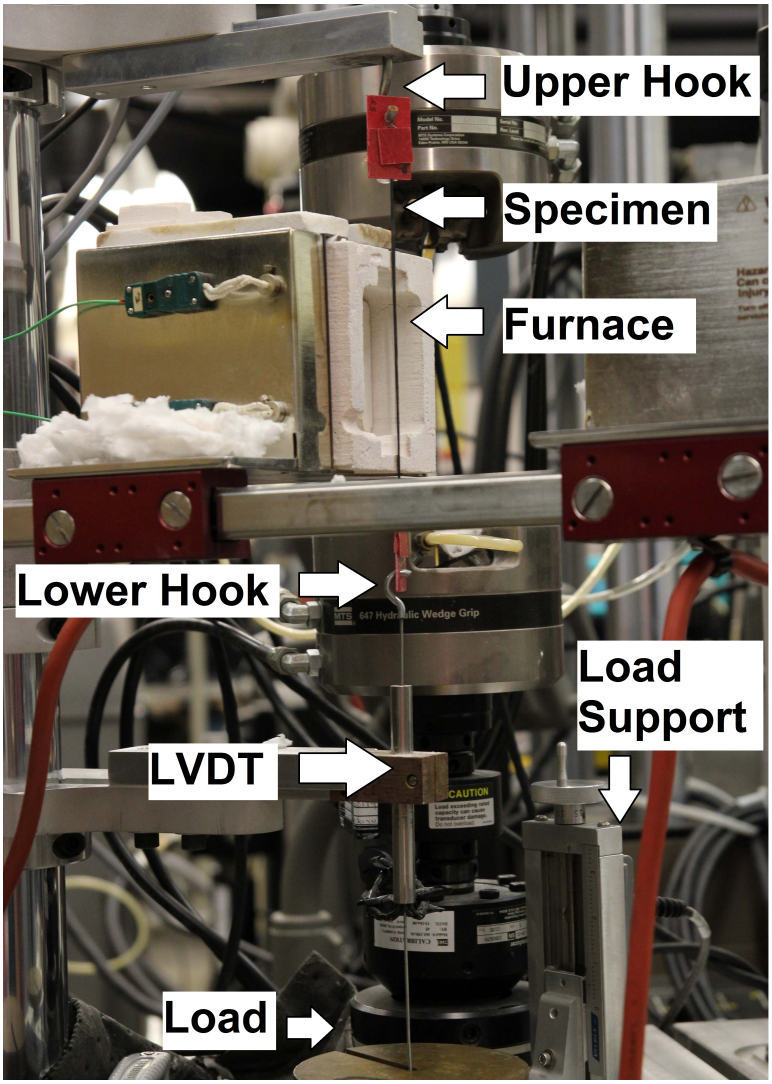

Figure 4.8: Fiber tow specimen mounted in the dead weigh creep testing facility

4.2 Temperature Profiles

Temperature profiles for fiber tow testing were obtained using same the procedure as in prior work [2, 52]. Temperature profiles for fiber tow testing were determined by measuring the temperature vertically along the centerline of the furnace with an R-type thermocouple. The 12 in. long R-type thermocouple was a Platinum-Rhodium alloy accurate up to 1200°C. A CL3515R model thermometer was used for temperature readings.

The accuracy was 1.5°C for the R-type thermocouple and 1.5°C for the thermometer. During the temperature measurements, the thermocouple was attached to a magnetic v-block fixture, which was attached to the ram of the servo-hydraulic machine. This allowed for controlled probing throughout the length of furnace.

In order to improve thermal insulation of the furnace and to shield the upper grip and the specimen tab, a 0.5-in. thick piece of oxide insulation board was placed on top of the furnace. To determine the setpoints of the temperature controller, the thermocouple was positioned in the center of the furnace as the temperature was increased. To obtain the desired temperature setpoints of the upper and lower temperature controllers, the thermocouple was moved up and down from the center point of the furnace while adjusting the setpoints. The heating elements and furnace control thermocouples were approximately 6 cm apart vertically. Therefore, initial observations of the temperature profile were obtained in the vertical region located within 3 cm from the center of the furnace. Once the desired setpoints for the temperature controllers were determined, a detailed temperature profile was obtained by taking measurements every 5 mm along the vertical axis of the furnace starting at the bottom inner surface of the alumina test chamber and ending at the top inner surface of the test chamber. Temperature profiles obtained in air and in steam are shown in Figures 4.9 and 4.10, respectively. Temperature profiles obtained in prior work [52] are shown in Figures 4.9 and 4.10 for comparison. Note that the temperature profiles obtained in air are consistent with those reported by Steffens [52]. In contrast, temperature profiles obtained in steam show marked improvement compared to those produced in prior work [52]. The temperature profiles from [52] show discontinuities (or "dips"), which correspond to the location of steam entry. Conversely, the temperature profiles obtained in the present effort are smooth.

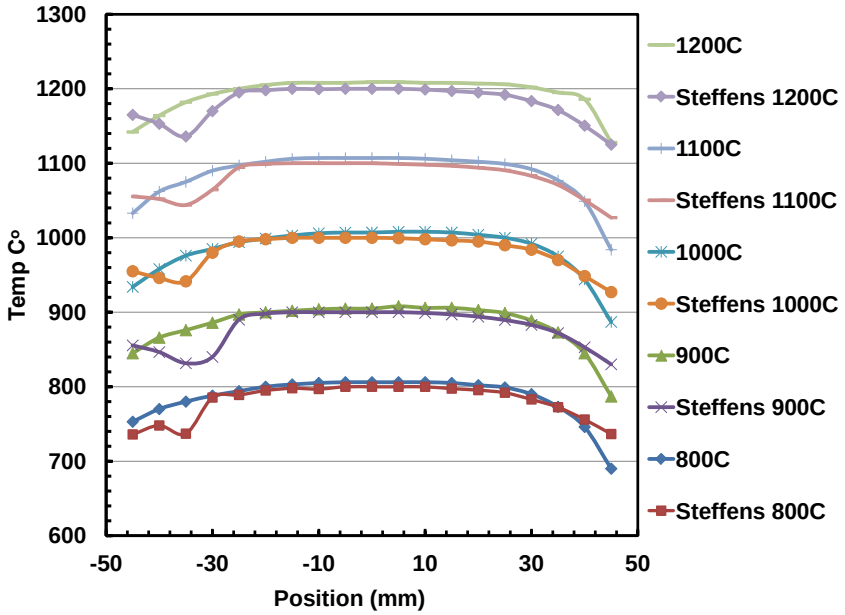

Figure 4.9: Temperature profile obtained for Hi-Nicalon S fiber tow specimen in steam. Temperature profiles from Steffens [52] are included for comparison.

.

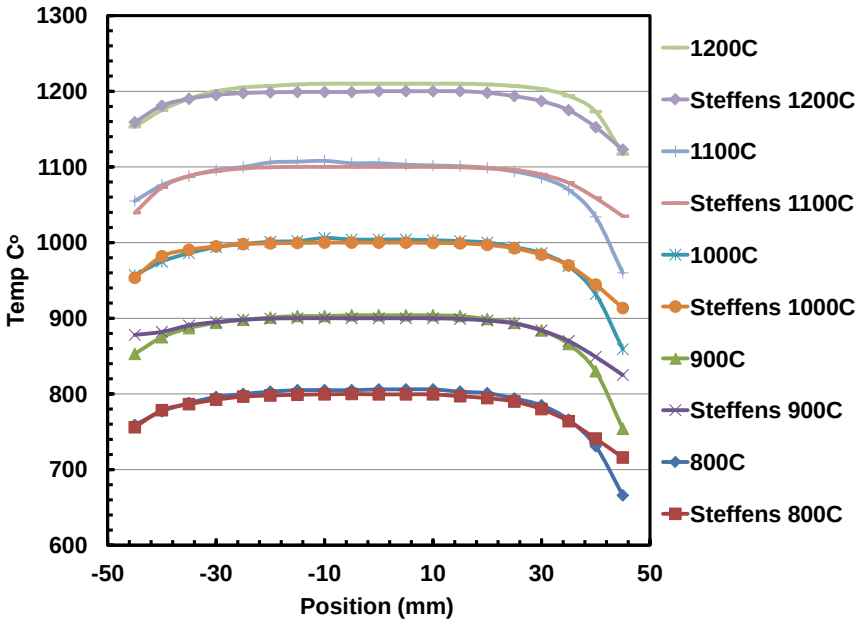

Figure 4.10: Temperature profile obtained for Hi-Nicalon S fiber tow specimen in air. Temperature profiles from Steffens [52] are included for comparison.

4.3 Strain Measurement

Because a strain measurement device could not be placed directly on a bundle of fibers inside a furnace, an indirect method of obtaining strain measurements detailed by Armani [2] was employed. Extension of the fiber tow specimen was measured by an LVDT outside the furnace. The initial strain measurements were calculated using the effective gauge length described below and the average displacement value of the fiber tow length upon thermal equilibrium during the heat-soak. Machine compliance correction was accomplished for each test during post-processing by subtracting the strain value immediately upon the load application from the subsequent strain data. An indirect method detailed by Armani [2] was also utilized in this research to calculate strain and the strain rate of the specimen in the hot test section. Because the cold gripping method was used in all tests, specimen elongation was measured outside the furnace. Thus the total recorded specimen elongation was the sum of contributions from parts of the specimen located in different temperature zones: the hot zone (at uniform test temperature), the temperature gradient zone and the cold zone. In order to convert the LVDT measurement into a representative strain at the desired test temperature, the amount of displacement along the length of the test specimen subjected to the temperature profile must be determined. Consider that the section of a fiber tow specimen subjected to a specific load at a higher temperature would displace more than another section of the same fiber tow specimen subjected to the same load but at a lower temperature in the temperature profile. In order to convert the overall displacement of the fiber tow specimen to strain at the desired temperature, the distribution of displacement along the temperature profile must be established. The method for calculating strain and strain rate from displacement measurements proposed below is similar to that of Morrell [43], Kandil and Dyson [31], and DiCarlo [16].

The calculation of the effective gauge length takes into account the varying compliance along the fiber tow subjected to a temperature profile. Steady-state creep can be described by the power-law creep as:

$$\dot{\epsilon} = A\sigma^n exp\left(\frac{-Q}{RT}\right) \tag{4.1}$$

Consider a test specimen of constant cross section with a length 2L. From the center of the specimen gauge section, creep occurs over a total length -L to L. Beyond these boundaries creep can be considered negligible. Therefore, the total measured strain and total measured strain rate are:

$$\epsilon_m = \frac{\Delta l}{2L} = \int_0^t \dot{\epsilon}_m \, \mathrm{d}t \tag{4.2}$$

$$\dot{\epsilon}_m = \frac{\text{measured extension rate}}{2L} = \frac{1}{2L}\int_{-L}^{L} \dot{\epsilon} \, \mathrm{d}l \tag{4.3}$$

Note that the total measured strain and strain rate account for variations in strain and strain rate along the specimen subject to a temperature profile. At the hottest sections, the amount of strain or strain rate will be greater than at a lower temperature.

Consider the strain and strain rate at the desired maximum temperature at the center of the furnace. Let subscript O denote quantities obtained at the center of the specimen gauge section. The strain at the center of the furnace can be calculated as the time integral of the strain rate at the center of the furnace. It can also be described by the same overall change in length of the entire specimen divided by a hypothetical length called the effective gauge length, $(2L)_{eff}$. The effective gauge length can also be thought of as the gauge length obtained under a hypothetical step-function temperature profile, in which all the strain was accumulated under the peak temperature and zero strain is achieved under the lower temperature.

$$\epsilon_o = \int_0^t \dot{\epsilon}_o \, \mathrm{d}t = \frac{\Delta L}{(2L)_{eff}} \tag{4.4}$$

Similarly, the strain rate at the maximum temperature (i.e. strain rate at the center of the furnace) can be expressed by using the effective gauge length as:

$$\dot{\epsilon}_o = \frac{\text{measured extension rate}}{(2L)_{eff}} = \frac{1}{(2L)_{eff}} \int_{-L}^{L} \dot{\epsilon} \, \mathrm{d}l \tag{4.5}$$

Taking the ratio of Equations 4.3 and 4.5 obtain:

$$\frac{\dot{\epsilon}_m}{\dot{\epsilon}_o} = \frac{(2L)_{eff}}{2L} \tag{4.6}$$

Using Equations 4.1, 4.3, and 4.6, the ratio of the measured strain rate to the actual strain rate becomes only a function of temperature, given by:

$$\frac{\dot{\epsilon}_m}{\dot{\epsilon}_o} = \frac{1}{2L} \int_{-L}^{L} \exp\left\{ \frac{-Q}{R} \left(\frac{1}{T(l)} - \frac{1}{T_o} \right) \right\} \mathrm{d}l \tag{4.7}$$

Utilizing a numerical summation of increments of length h, such that L = kh where k is an integer, the ratio of the measured strain rate to the actual strain rate is:

$$\frac{\dot{\epsilon}_m}{\dot{\epsilon}_o} = \frac{1}{2k} \sum_{i=-k}^{k} \exp\left\{ \frac{-Q}{R} \left(\frac{1}{T_i} - \frac{1}{T_o} \right) \right\} \mathrm{d}l \tag{4.8}$$

As a result, an effective gauge length can be calculated such that:

$$(2L)_{eff} = 2L \left(\frac{\dot{\epsilon}_m}{\dot{\epsilon}_o} \right) \tag{4.9}$$

The effective gauge length can be used to calculate strain as well as strain rate from displacement measurements made outside the hot zone of the furnace. Using this approach together with the temperature profiles established in Section 4.2 and creep activation energy of 177 kJ/mol from literature [23], effective gauge lengths were calculated for Hi-Nicalon S fiber tow specimens at temperatures of interest in air and in steam. The effective gauge

lengths calculated for the Hi-Nicalon S fiber tow specimens at 800-1200°C are summarized in Table 4.1.

Table 4.1: The effective lengths at each test condition. The nominal length of the specimen with-in the test chamber is 90mm.

Temperature(°C)	Effective Length in Air (mm)	Effective Length in Steam (mm)
800	80.44	79.83
900	78.27	80.46
1000	81.38	81.89
1100	83.60	83.60
1200	92.27	90.54

Hammond [25] and Yun et al. [54] assumed the main creep deformation occurred only in the hot zone of the furnace and approximated the gauge length by the flat portion of the temperature profile. This approach is subjective in defining the gauge length of the specimen and is dependent on how flat the maximum temperature profile was and how sharply the temperature drops at the edges of the furnace, the flatter and sharper, the better the estimate.

The calculated effective gauge lengths presented in Table 4.1 are physically representative of the flat portion of the temperature profile. Using this calculated effective gauge length is a more systematic approach to obtaining strain from extension measurements for a specimen subjected to a temperature profile regardless of the shape of the profile.

V. Results and Discussion

5.1 Creep of Hi-Nicalon S fiber tows at elevated temperature

Hi-Nicalon S fiber tows were subjected to tensile creep at 800°C, 900°C, 1000°C and 1100°C in laboratory air and in steam. Results of the creep-rupture tests performed at 800°C, 900°C, 1000°C and 1100°C are summarized in Tables 5.1 and 5.2.

Table 5.1: Summary of creep results for Hi-Nicalon S ceramic fiber tows at 800°C in laboratory air and in steam

Specimen ID	Test Environment	Creep Stress (MPa)	Creep Lifetime (h)	Steady-State Creep Rate (s^{-1})	Creep Strain (%)
800C					
A41	Air	10	291†	1.71E-10	0.590
A1	Air	798	100†	1.37E-09	0.109
A4	Air	937	0.09	5.81E-06	1.040
A6	Air	937	0.02	1.56E-05	0.188
A13	Air	937	1.52	1.34E-07	0.293
A14	Air	937	17.95	1.78E-09	0.102
A12	Air	1023	1.02	1.31E-07	0.280
A15	Air	1023	0.18	5.09E-09	0.023
A16	Air	1023	96.99	2.29E-09	0.347
A17	Air	1023	35.32	3.52E-09	0.097
A3	Air	1103	B.O.L		
A2	Air	1250	B.O.L		
S19	Steam	154	37.89	5.51E-10	0.030
S24	Steam	154	71.69	2.97E-09	0.108
S49	Steam	255	6.71	6.18E-09	0.079
S50	Steam	353	8.23	2.12E-08	0.121
S21	Steam	400	8.66	5.68E-09	0.069
S23	Steam	450	B.O.L		
S22	Steam	450	B.O.L		
S18	Steam	798	B.O.L		

†Runout defined as 100h at creep stress. Failure of specimen did not occur when the test was terminated.

B.O.L–Broke on loading

Table 5.2: Summary of creep results for Hi-Nicalon S ceramic fiber tows at 900°C-1100°C in laboratory air and in steam

Specimen ID	Test Environment	Creep Stress (MPa)	Creep Lifetime (h)	Steady-State Creep Rate (s^{-1})	Creep Strain (%)
900C					
A34	Air	1023	1.66	9.17E-08	0.140
A37	Air	937	57.44	4.72E-09	0.239
A54	Air	798	20.45	6.20E-10	0.096
S56	Steam	154	118.55†	1.07E-09	0.067
S48	Steam	255	101.64	4.12E-10	0.458
S40	Steam	353	17.88	1.82E-09	0.080
S38	Steam	400	B.O.L		
1000C					
A42	Air	700	71.18	2.26E-09	0.123
A43	Air	937	0.81	2.37E-07	0.107
S47	Steam	255	23.99	3.70E-09	0.063
S44	Steam	353	29.43	3.29E-09	0.100
S45	Steam	400	3.21	2.85E-08	0.125
1100C					
A27	Air	154	116.9†	5.31E-10	0.042
A30	Air	255	118.6†	8.52E-10	0.057
A35	Air	353	105.45†	1.32E-09	0.093
A28	Air	450	20.90	2.64E-09	0.076
A57	Air	650	1.50	3.55E-08	0.087
S25	Steam	154	63.25	6.26E-09	0.216
S26	Steam	255	38.00	7.62E-09	0.171
S33	Steam	353	8.27	1.49E-08	0.126
S32	Steam	400	B.O.L		
S31	Steam	450	B.O.L		
S29	Steam	450	B.O.L		

†Runout defined as 100h at creep stress. Failure of specimen did not occur when the test was terminated.

B.O.L–Broke on loading

Hi-Nicalon S Fiber tows were tested at temperatures 800°C, 900°C, 1000°C, and 1100°C in air and steam. The stress levels were adjusted at each temperature and environment to induce stress rupture times throughout the 100 hr time frame of interest. After 100 hrs the fiber was considered functional at that stress level and environment and

the test was stopped. The results of the fibers tested can be seen in the Tables 5.1 and 5.2. Since 800°C was the first temperature that was tested, the appropriate response of the fiber was not known so more testing was done at this temperature. At the conclusion of testing it was recognized that at 800°C there was a large amount of scatter in the data taken on specimen tested in air. There are a number of possible reasons for this scatter. It is only a conjecture at this point but since the tests in air at 800°C were conducted first, fibers on the exterior of the spool were utilized to create the specimens. The fibers on the exterior of the spool could have been damaged due to prior handling of the spool. In addition, as these were the first specimens, inconsistent methods could have been used in the creation and testing of these specimens.

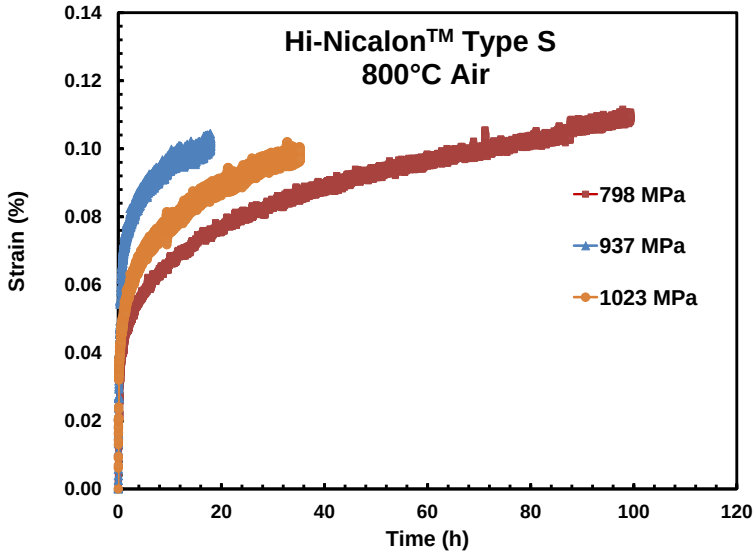

Figure 5.1: Representative creep strain vs time curves obtained for Hi-Nicalon S fiber tows at 800°C in laboratory air.

Representative creep curves obtained at 800°C in laboratory air and in steam are shown in Figures 5.1 and 5.2, respectively. It is seen that creep curves produced in all tests conducted at 800°C exhibit primary and secondary creep regimes, but no tertiary creep.

Transition from primary to secondary creep occurred fairly early in the creep life. At 800°C in air, creep stresses ranged from 798 MPa to 1023 MPa. All creep strains accumulated in tests performed in air remained below 0.12%. Creep run-out of 100 hours was achieved at 798 MPa.

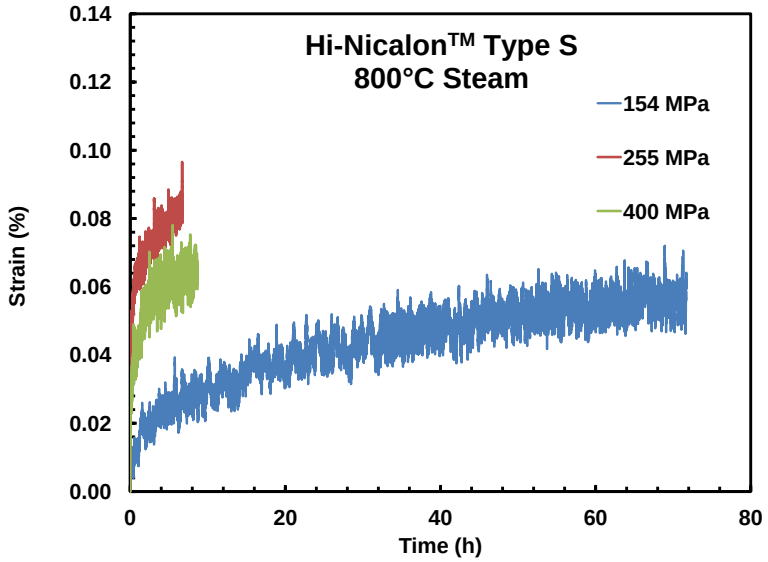

Figure 5.2: Representative creep strain vs time curves obtained for Hi-Nicalon S fiber tows at 800°C in steam

At 800°C the presence of steam had a dramatic effect on creep performance of Hi-Nicalon S fiber tows. Creep stress levels used at 800C in air could not be reached in steam. Fiber tow specimens failed during loading once the stress exceeded 400 MPa. Therefore in steam creep tests were performed at lower stress levels of 150, 255 and 400 MPa. All creep strains accumulated in steam were below 0.11%. The presence of steam drastically reduced creep lifetimes at 800°C. Even at lower stress levels, creep run-out was not achieved in steam. The longest creep lifetime in steam was 72 h (produced at 154 MPa). It is recognized that when subjected to creep at 800°C in oxidizing environments (such as steam or air) Hi-

Nicalon S fibers suffer oxidation, which promotes subcritical crack growth on the surface leading to degradation of creep resistance.

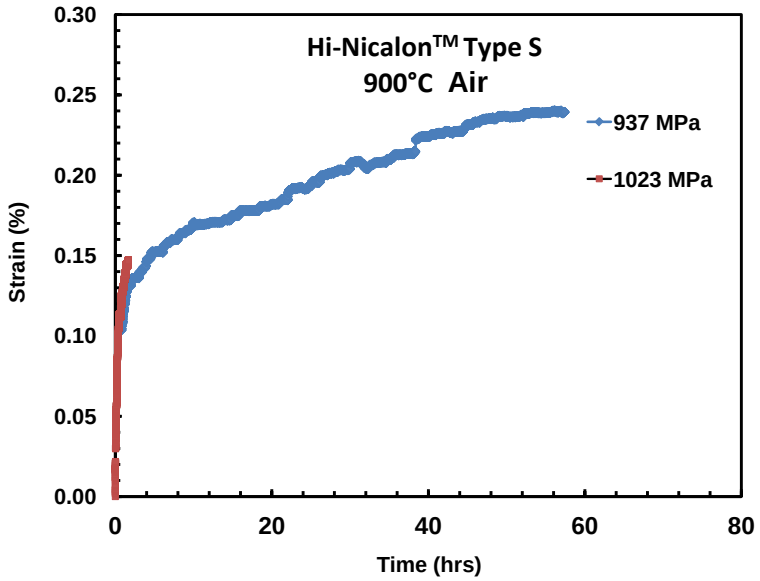

Figure 5.3: Representative creep strain vs time curves obtained for Hi-Nicalon S fiber tows at 900°C in laboratory air.

Creep curves obtained at 900°C in laboratory air and in steam are shown in Figures 5.3 and 5.4, respectively. It is seen that creep curves produced in all tests conducted in air exhibit primary and secondary creep regimes, but no tertiary creep. At 900°C in air, creep stresses were 937 MPa and 1023 MPa. Creep strain accumulated at 937 MPa reached 0.24%. In air creep run-out of 100 hours was not achieved.

As was the case at 800°C the presence of steam had a significant effect on creep performance of Hi-Nicalon S fiber tows at 900°C. Creep stress levels used in tests performed at 900°C in air could not be achieved in steam. Thus, lower creep stresses of 154MPa, 255 MPa and 353 MPa were used for testing in steam. While only primary and secondary creep regimes were observed at 154 and 353 MPa, all three creep regimes were

noted at 255 MPa. Surprisingly, creep strain of nearly 0.4% was accumulated at 255 MPa in steam. Creep run-out of 100 h was achieved at 255 MPa in steam.

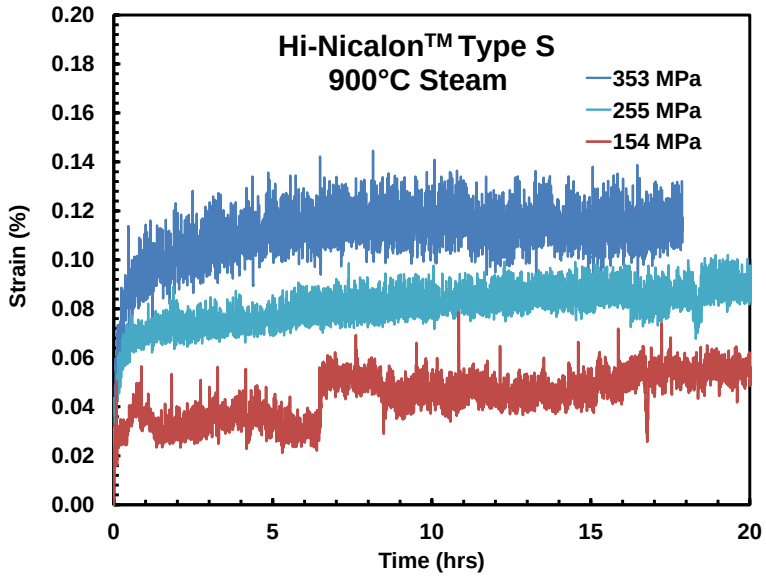

Figure 5.4: Representative creep strain vs time curves obtained for Hi-Nicalon S fiber tows at 900°C in steam. The x-axis was reduced to better compare the secondary creep regime. A full scale chart can be seen in Appendix C

Creep curves obtained at 1000C in laboratory air and in steam are shown in Figures 5.5 and 5.6, respectively. It is noteworthy that the temperature increase from 800°C to 1000°C had only slight influence on creep performance in air. At 1000°C in air, creep stress levels had to be reduced; creep tests were performed at 700 MPa and 937 MPa. Creep curves obtained at 1000°C in air were qualitatively similar to those produced at 800°C and 900°C. Creep strains accumulated in air did not exceed 0.12%. In air creep run-out of 100 hours was not achieved. Specimen tested at 700 MPa failed after 71 h of creep.

At 1000°C the effects of steam were similar to those noted at 800°C and at 900°C. At 1000°C in steam creep stress range was reduced to 255-400 MPa. Creep curves obtained at

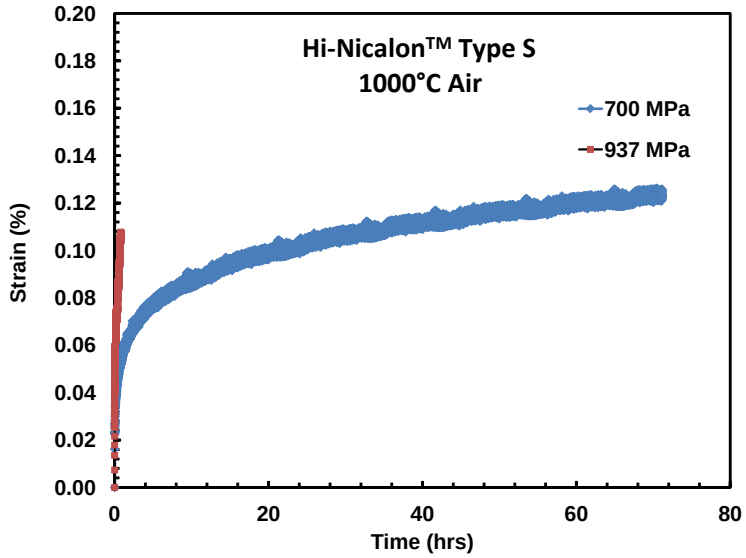

Figure 5.5: Representative creep strain vs time curves obtained for Hi-Nicalon S fiber tows at 1000°C in laboratory air.

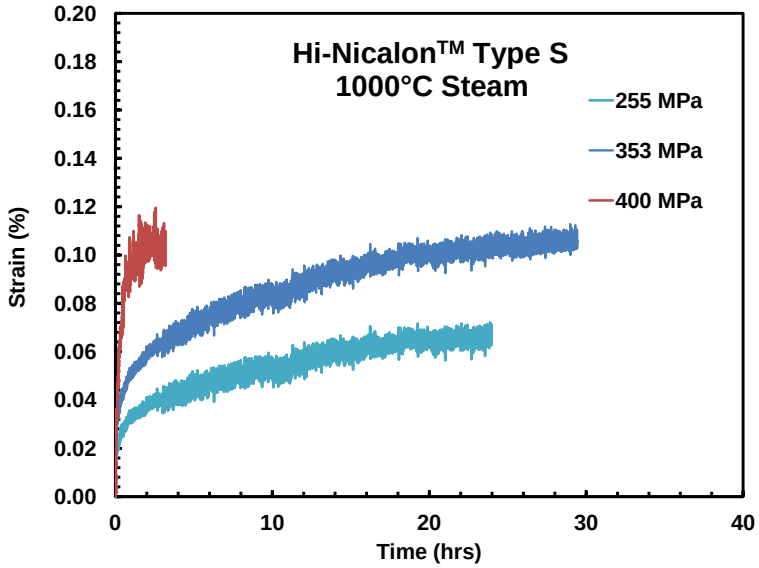

Figure 5.6: Representative creep strain vs time curves obtained for Hi-Nicalon S fiber tows at 1000°C in steam.

1000°C in steam exhibited primary and secondary creep. Tertiary creep was not observed. Creep strains accumulated in steam did not exceed 0.12%. Creep lifetimes obtained in steam were substantially shorter than those produced at higher creep stress levels in air. In steam creep run-out was not achieved.

As noted earlier, the temperature increase from 800°C to 1000°C had negligible effect on creep performance of Hi-Nicalon S fibers in air. While steam had a strong influence on creep performance at 800-1000°C, results reveal that creep performance in air was minimally affected by temperature rise from 800°C to 1000°C. In contrast, temperature increase to 1100°C had a significant effect on creep performance of Hi-Nicalon S fibers in air.

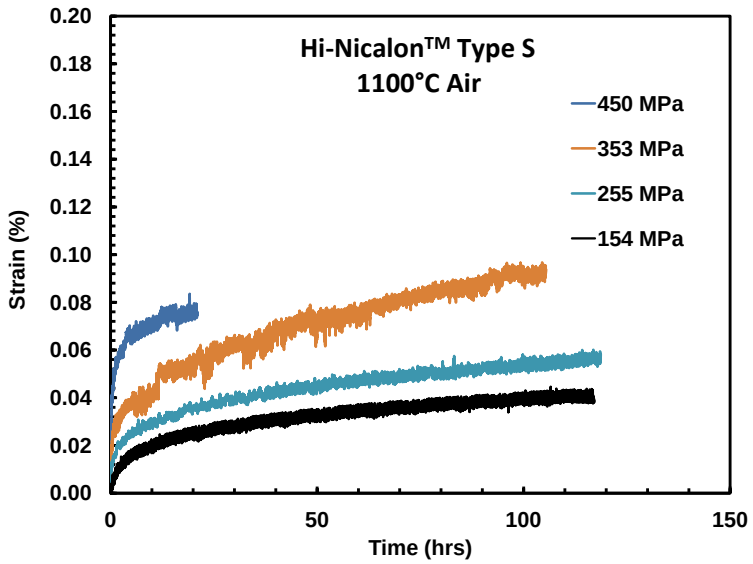

Figure 5.7: Representative creep strain vs time curves obtained for Hi-Nicalon S fiber tows at 1100°C in laboratory air.

Creep curves of Hi-Nicalon S fiber tows obtained at 1100°C in air are presented in Fig. 5.7. Results in Fig. 5.7 and in Table 5.2 reveal a dramatic effect of temperature increase to 1100°C on creep in air. Creep stresses of 700 MPa and above could not be reached

at 1100°C in air. To avoid instantaneous failures during load-up, creep stress range was reduced to 154-650 MPa. Recall that at 800-1000C in air creep tests were conducted at 700-1023 MPa. Creep curves obtained 1100°C in air exhibit primary and secondary creep regimes, but not tertiary creep. Creep run-out was achieved at 353 MPa. Creep strains did not exceed 0.1%.

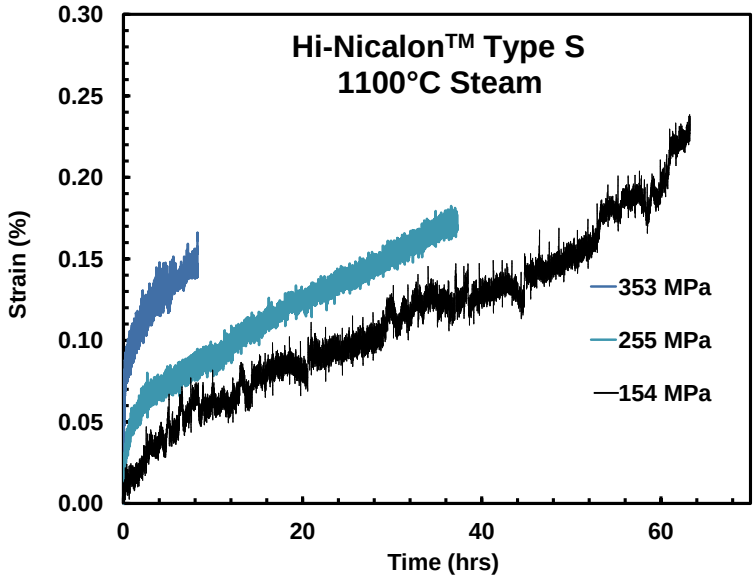

Figure 5.8: Representative creep strain vs time curves obtained for Hi-Nicalon S fiber tows at 1100°C in steam.

While creep performance at 800-1000°C was dramatically affected by the presence of steam, creep performance at 1100°C was only moderately influenced by steam. Creep curves obtained 1100°C in steam are shown in Fig. 5.8. Once again, only primary and secondary creep regimes are observed in all tests. Creep stress range employed in steam (150-353 MPa) is somewhat reduced compared to that used in air (154-650 MPa). Note, however, that at 1100C the reduction in creep stress range due to steam is much less drastic than that observed at lower temperatures. Whereas at 1100°C in air creep run-out was

achieved at 353 MPa, in steam creep run-out was not achieved even at the low stress of 154 MPa. Moreover, creep strains accumulated at 1100°C in steam (≤0.22%) were considerably larger than those accumulated in air (0.04% - 0.09%).

Analysis of creep results obtained at 800°C in air and in steam reveals significant degradation in fiber strength due to steam. Creep stress levels used at 800°C in air ranged from 800 MPa to 1023 MPa. In contrast creep stress levels used at 800°C in steam were significantly lower with the highest creep stress being only 450 MPa. Results obtained at 900°C and at 1000°C show similar strength degradation due to steam. It is noteworthy that at 1100°C fiber strength is not nearly as degraded by the presence of steam as at lower temperatures. Recall that similar creep stress levels (150-650 MPa) were employed in tests conducted at 1100°C in air and in steam.

Steady-state creep rate was reached in all tests. Creep rate as a function of applied stress is shown in Eq. 5.1.

$$\dot{\epsilon} = A\sigma^n \tag{5.1}$$

Here $\dot{\epsilon}$ is the minimum creep rate, A is a temperature-dependent coefficient that accounts for the activation energy, grain size and other variables in the full form of the power law, and σ is the applied stress. Using a log-log plot of the creep rate as a function of stress, the stress exponent n was determined for Hi-Nicalon S fiber tows at each temperature investigated in air and in steam by linear regression. The results however were inconclusive. Per Figure 5.9 there is quite a bit of scatter in the data. A power fit to the data generated results that were not meaningful and were subsequently removed from the chart.

It is recognized that the controlling creep mechanism can be identified from the analysis of experimental creep data. Different creep mechanisms have been correlated with different values of the stress exponent n, obtained from the experimental creep data [3, 20]. In order to generate meaningful values for n, between 2-5, more data would have to be generated. Generating additional data points would further isolate outlying data points. In

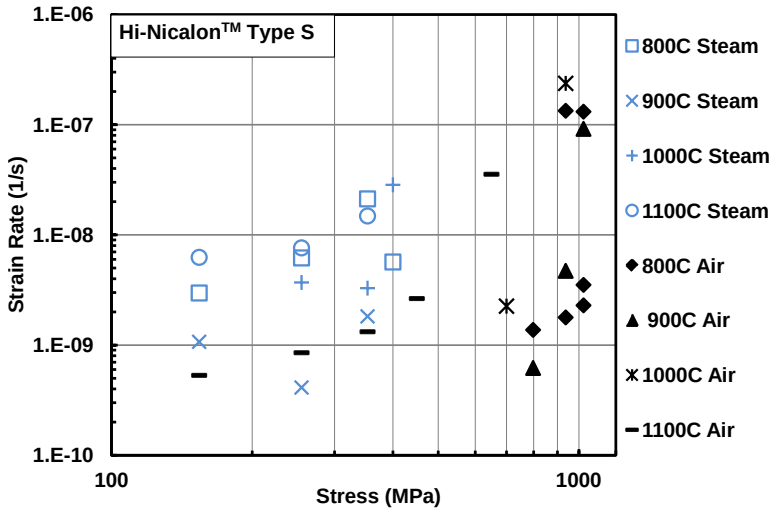

Figure 5.9: Steady-state creep rate vs applied stress for Hi-Nicalon S fiber tows at 800°C, 900°C, 1000°C, and 1100°C in laboratory air and in steam.

addition, it is recognized that in the full form of Equation 5.2 the steady-state creep rate is proportional to the applied stress σ raised to a stress exponent, n, and inversely proportional to the grain size d raised to a grain size exponent, m:

$$\dot{\epsilon} \propto \frac{\sigma^n}{d^m} \tag{5.2}$$

Therefore the grain size of the tested fiber tows would also have to be determined before a conclusion regarding creep mechanisms could be reached.

However, results in Figure 5.9 reveals that at 800°C-1000°C the presence of steam significantly accelerated creep rates for stress levels. It is noteworthy that the creep rate produced at 154 MPa in steam is very close to that produced at a higher stress of 800 MPa in air. Recall that creep run-out was not achieved at 154 MPa in steam while a 100-h runout was achieved at 800 MPa in air.

Increase in temperature from 800°C to 1000°C appeared to have a moderate effect on creep rates obtained in laboratory air. Creep rates accelerate dramatically as the temperature

increases to 1100°C. Creep rate produced at 700 MPa at 1000°C is roughly an order of magnitude less then that obtained at a similar stress of 650 MPa at 1100°C.

The stress-rupture behavior of Hi-Nicalon S fiber tows at 800°C, 900°C, 1000°C and 1100°C in air and in steam is summarized in Figure 5.10. As expected, the creep lifetime decreases with increasing applied stress at all temperatures investigated. At 800°C in air, creep run-out of 100 h was achieved at 780 MPa. As noted earlier, presence of steam severely degraded strength of Hi-Nicalon S fibers at 800°C. Furthermore, the presence of steam had a dramatic effect on creep lifetimes at 800°C. Creep run-out was not achieved at 800°C in steam. The longest lifetime produced at 800°C in steam was 71 h at a low stress of 154 MPa.

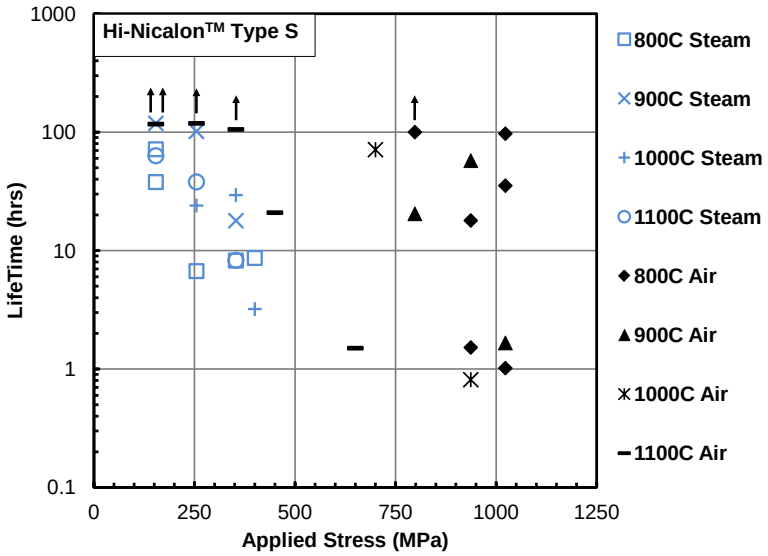

Figure 5.10: Stress Rupture data for Hi-Nicalon Type S fiber tows tested at 800°C-1100°C in air and steam environments.

Creep lifetimes in air decreased slightly as the temperature increased from 800°C to 900°C and to 1000°C. At 900°C and at 1000°C in air creep run-out was not achieved. The longest lifetime produced at 900°C in air was 60 h at 937 MPa. At 1000°C in air the longest

creep lifetime of 71 h was obtained at 700 MPa. At 900°C and at 1000°C both fiber strength and creep performance were significantly affected by steam. At 900°C creep stresses used in steam were much lower than those used in air. At 900°C in steam creep run-out was achieved at 154 MPa and at 255 MPa. Likewise, at 1000°C creep stresses in steam were much lower than those in air. At 1000°C creep lifetimes deteriorated in the presence of steam. At 1000°C in steam the longest creep lifetime of only 29 h was reached at 353 MPa.

Fiber strength and creep performance in air decreased significantly as the temperature increased from 1000°C to 1100°C. Note that at 1100°C in air creep stresses were much lower than those used at 800-1000°C. Creep lifetimes produced at 1100°C in air were also much reduced compared to those obtained at higher stress levels at 800-1000°C. At 1100°C in air creep run-out was achieved at 353 MPa. At 1100°C fiber strength was only moderately degraded due to steam. At 1100°C the effect of steam on creep performance was appreciable, albeit not quite as drastic as at 800-1000°C. Still, at 1100C in steam creep run-out was not achieved. At 1100C in steam the longest creep lifetime of 63 h was produced at 154 MPa.

In the figure 5.10 the performance of each fiber tow at a specific loading can also be compared with other fiber tows tested at different temperatures and environments. Comparing steam data across the four test temperatures between 150 and 450 MPa indicates that fibers in steam environments at 800C consistently have the shortest lifetimes. The fibers at 900C and 1000C generally survived longer under similar stress levels then those tested at 800C. At 1100C, the rupture time of the fibers were similar to the fibers tested at 800C and in one case, at 250MPa , significantly outperformed the fibers tested at 800C in steam. These results supports the claim that at higher temperatures in an highly oxidizing environment,such as steam, a silica scale forms on the surface of the fiber protecting the fiber from the deleterious environment.

5.2 Fiber Microstructure

Microstructure of the tested fiber tow specimens was analyzed using scanning electron microscopy (SEM). In addition, energy dispersive X-ray diffraction (EDX) was also conducted to identify the elemental composition of the tested fibers. The EDX system can identify the elements that are present but not their exact ratios. The relative size of the peak obtained via EDX can however be an indicator of the thickness and or composition of the elements under inspection. For comparison a fiber was placed in the test chamber for 40 minutes at 800°C. This procedure burned off the fiber coating used for sizing but minimized any potential oxidation. The virgin fiber can be seen in Fig. 5.11. The surface has a few small particles which could be left over inorganic particulates from the sizing but are most likely contaminants from the SEM preparation. No glassy oxide layer can be seen and the fibers are uniform in size and texture.

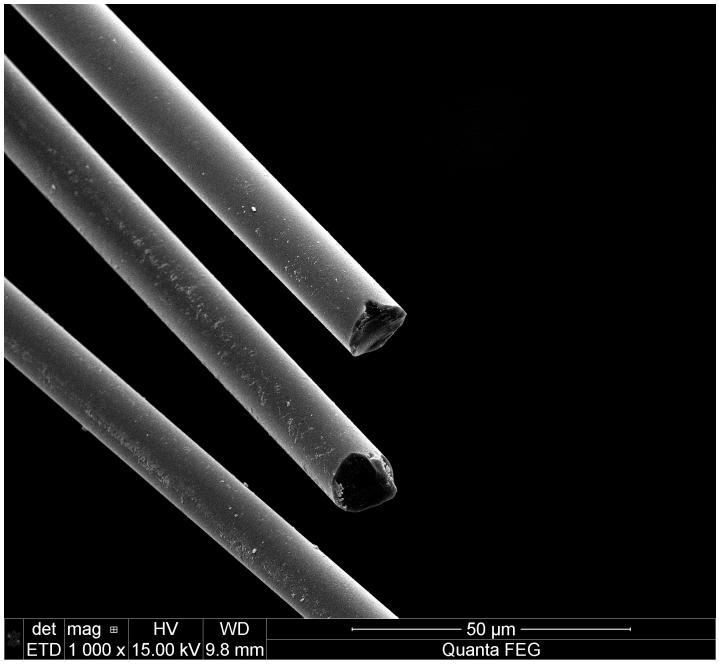

Figure 5.11: Fiber sizing was burned off at 800°C for 40 minutes in order to expose the virgin fiber surface.The magnification was 1000X for this micrographs

The micrographs of the fibers tested in steam from 800°C to 1100°C show variability in the oxidation mechanism present. On some fibers a thick SiO_2 layer can be seen. This indicates that the primary oxidation mechanism is passive oxidation in that SiO_2 is created and deposited on the fiber as seen in Eq. 5.3. Within the same fiber tow pitting and erosion can also be seen due to active oxidation represented by Eq. 5.4. The variability in oxidation mechanisms within fiber tows is due to localized environmental variations. These reactions are represented by the equations below:

$$\text{Passive} \quad SiC + 2H_2O(g) = SiO_2(s) + CH_4(g) \tag{5.3}$$

$$\text{Active} \quad SiO_2 + 2H_2O(g) = Si(OH)_4(g) \tag{5.4}$$

Both of these reactions are temperature dependent. At lower temperatures the creation of SiO_2 dominates but as the temperature increases the volatilization of the SiO_2 increases. Ultimately, at higher temperatures this results in a steady state environment with SiO_2 and $Si(OH)_4$ being created and volatilized at the same rate. Fig. 5.12 show fibers tested in steam at 800°C next to fibers tested at 1100°C at 5000X magnification. The specimen tested at 800°C in steam show a thick SiO_2 scale. This is consistent with the work done by Opila in studying the oxidation and volatilization of silica [48].

When comparing micrographs taken of specimens tested at differing temperature the effects of how temperature alters the growth and volatilization of SiO_2 at different temperatures is apparent. By visually inspecting Fig. 5.13 it is clear that as the temperature increases, the deposited SiO_2 remaining on the fiber decreases. A close look at the fibers tested at 800°C in Fig. 5.13 show erosion of the fiber due to active oxidation. A complete compilation of all fibers analyzed under SEM is located in Appendix D. By comparing each fiber a better picture can be generated as to the variability of the oxidation mechanism inter and intra specimen.

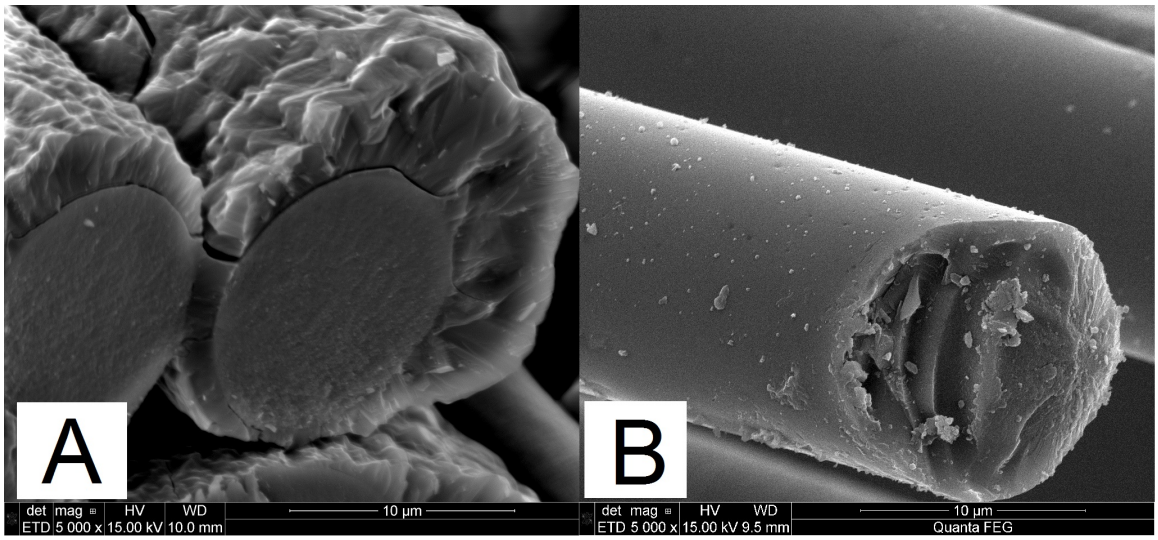

Figure 5.12: Both fibers shown were tested in steam. Fibers in picture A were tested at 800°C and fibers in picture B were tested at 1100°C under similar loading conditions. Both specimens were taken at or near the fracture surface. The magnification was 1000X for both micrographs

Initially, the fibers tested in steam at higher temperatures, mainly 1100°C, the surface of the fiber looked devoid of activity. When EDX was used to analyze the surface, a surprisingly strong oxygen peak was present as seen in Fig. 5.14. This supports the idea that the bulk SiO_2 growth deposited on the surface is being volatilized but oxygen is still diffusing into the fiber.

Another interesting formation due to the variability in oxidizing mechanism can be seen in several fibers tested at 800°C as well as 900°C shown in figure 5.15. The fibers displayed areas of gross erosion. When this area was analyzed for its elemental composition there were only peaks at silicon, carbon and oxygen which was to be expected. The unexpected result was the absence of a large oxygen peak which is what would be expected in a passive oxidative environment. The fiber adjacent to the fiber shown in figure 5.16 shows a completely different picture. In less than 5μm the oxidation mechanism

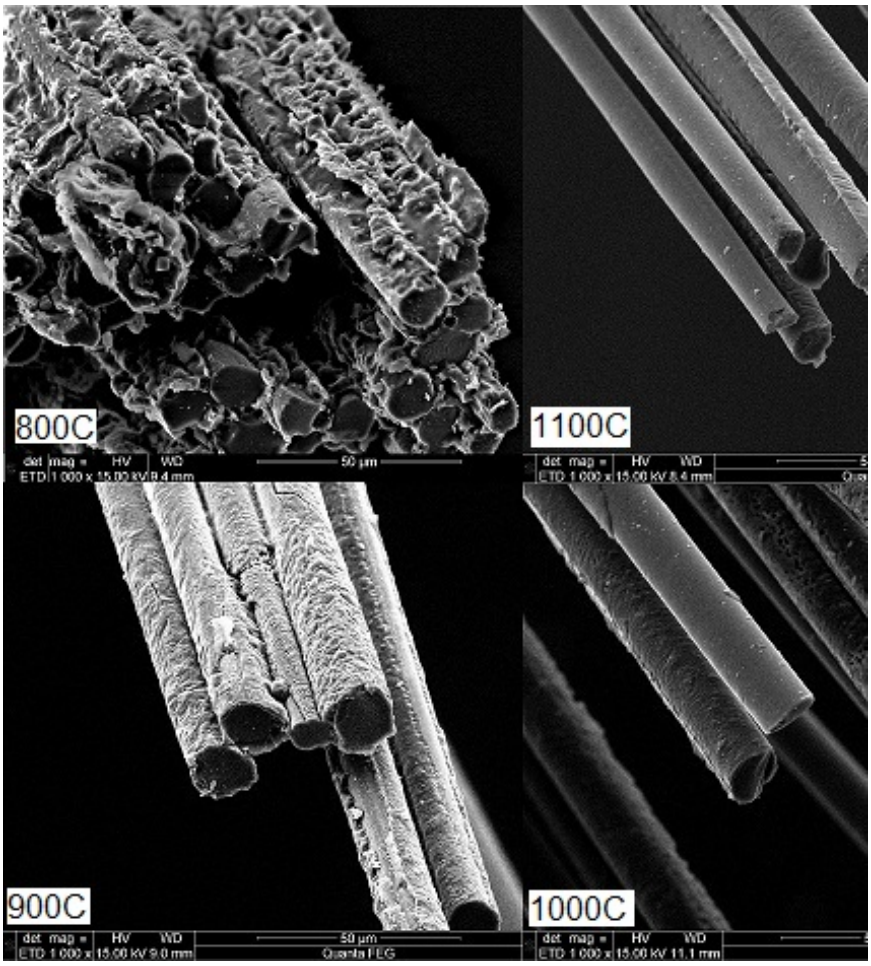

Figure 5.13: Hi-Nicalon Type S fibers tested in steam at 800°C for 71hrs, 900°C for 100hrs , 1000°C for 24hrs, and 1100°C for 63hrs. With the same flow rate of steam in each. Fibers were taken at or near fiber tow fracture location. The magnification was 1000X for each micrographs

changes and now SiO_2 is being deposited on the fiber surface rather than the volatilization of the SiC fiber itself. In the same fiber bundle, though not directly adjacent to the fibers seen in 5.15 and 5.16, a third growth mechanism can be seen. Fig. 5.17 shows a large bulk formation of SiO_2. The generation of these nodules is due to the generation of gaseous Si species due to active oxidation which redeposit on the fiber. Variations of SiO_2 of growth

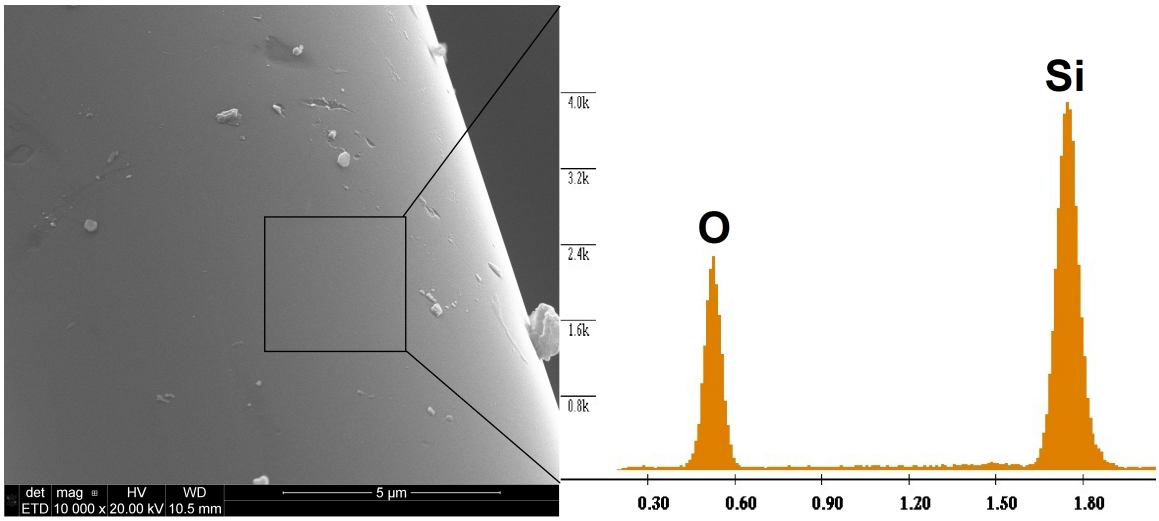

Figure 5.14: Hi-Nicalon Type S fiber tested in steam at 1100°C in steam at 154MPa for approximately 60hrs.

within each fiber tow was apparent in all the fibers viewed. A low magnification micrograph showing the variability of oxidation mechanisms along a single fiber tow can be seen in Appendix C.

At 1100°C, as seen in figure 5.18, additional types of formations were created due to the oxidative environment. It is hypothesized that the variability in growth is due to different degrees of reduction reactions. Depending on how the oxygen bonds with the silicon atoms will dictate what growth pattern the silicate preferentially chooses. Up to this point it has been assumed that the silicate formation both on the surface of the fiber or into the fiber has been SiO_2. At this point due to the lack of quantitative results it would be better said that SiO_x is forming. These different growths manifest themselves as wire, sheet and bulk growth formations. It is supposed that the variation of SiO_x growth across a seemingly small distance at assumed similar test conditions is a result of variability in the

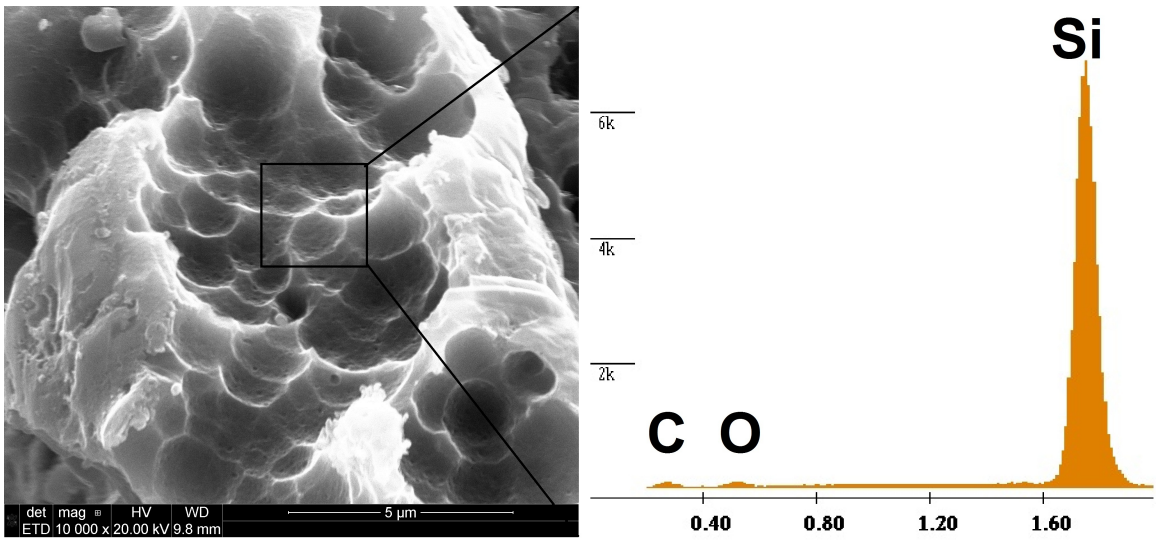

Figure 5.15: Hi-Nicalon Type S fiber tested at 800°C in steam at 154 MPa for 71hrs. The Carbon and Oxygen peak are minimal

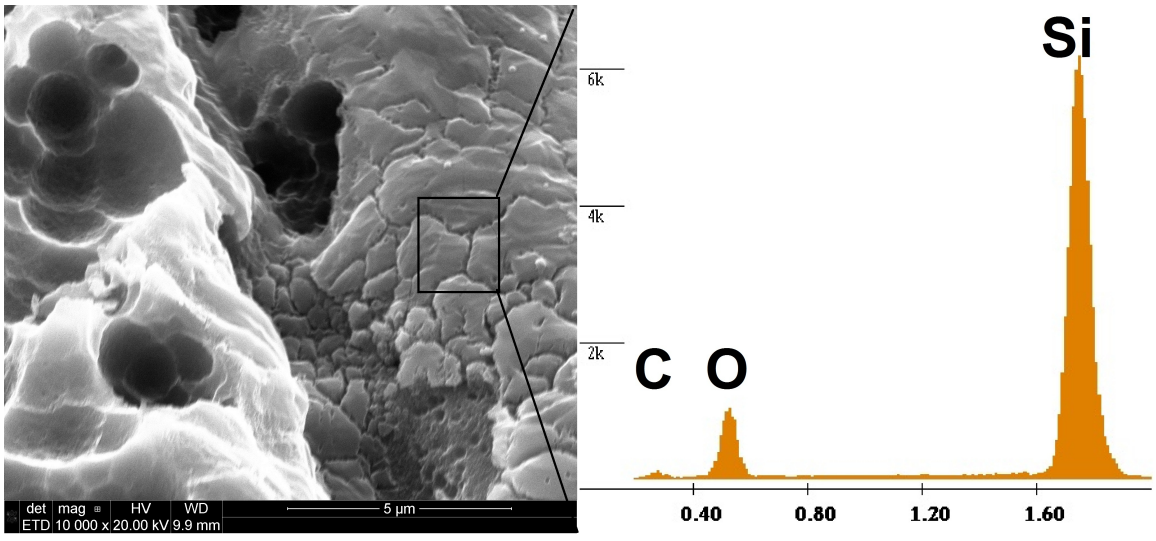

Figure 5.16: Hi-Nicalon Type S fiber tested at 800°C in steam at 154MPa for 71 hrs. Pronounced oxygen peak indicate thick SiO_2 scale.

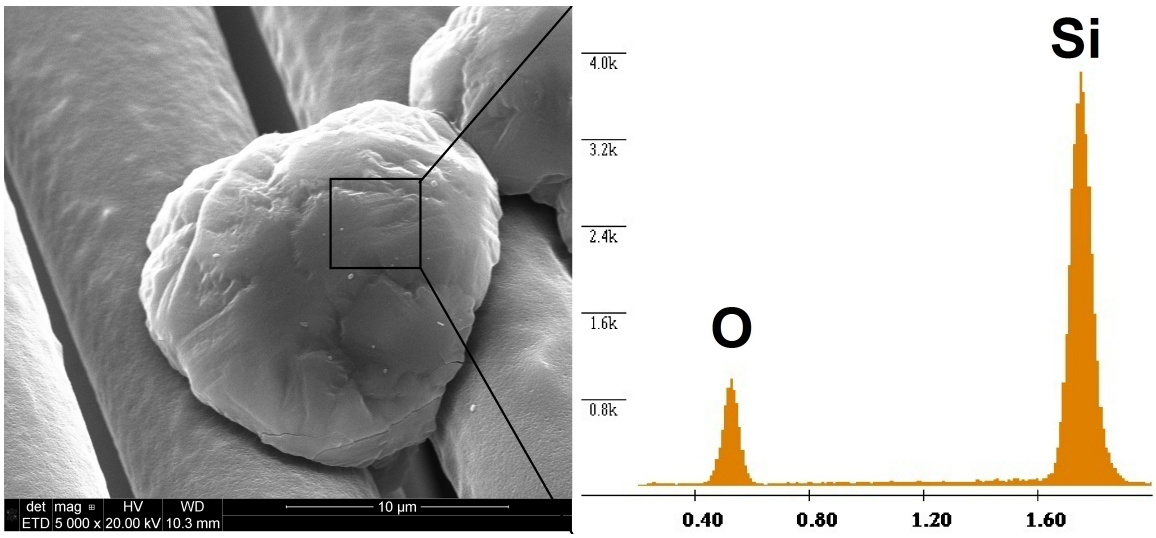

Figure 5.17: Hi-Nicalon Type S fiber tested at 800°C in steam at 154MPa for 71 hrs. The oxygen peak indicates SiO_2 and can be seen as the large bulbous formation on the fiber

fiber surface. The fiber surface at one location due to surface defects or contaminants may preferentially oxidize in a manner distinctly different then a neighboring fiber.

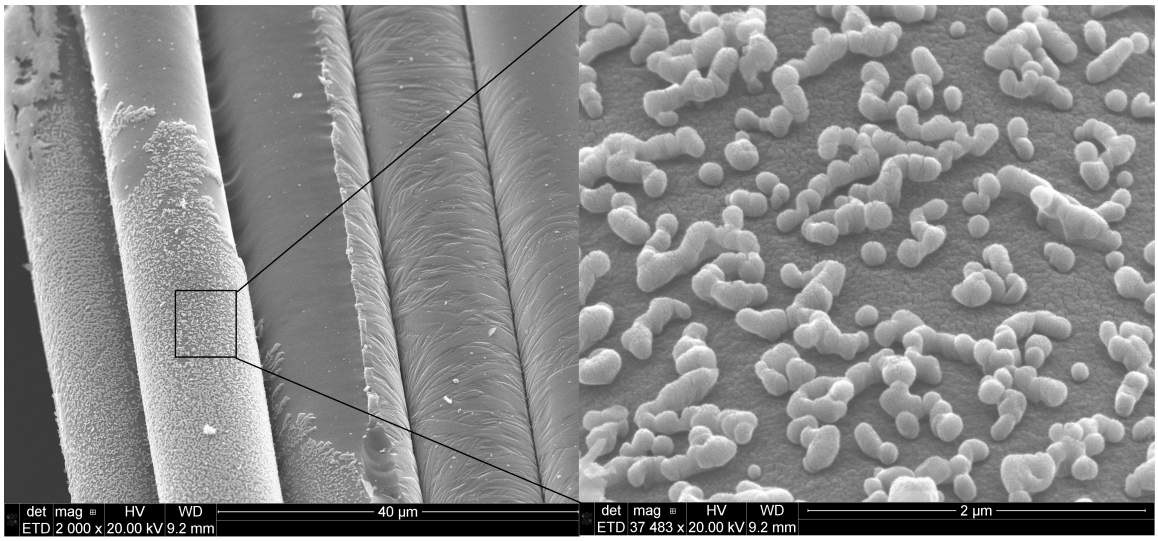

Figure 5.18: Hi-Nicalon Type S fiber tested at 1100°C in steam at 255MPa for 38 hrs.

During the analysis of the fiber tows several interesting crystal formations where noticed. These formations were consistent enough across several fibers to be deemed noteworthy. Figure 5.19 shows glassy rings with spherical particulates in the middle. This fiber was tested in steam at 800°C the specimen broke upon load up. The fiber was subjected to 45 minutes of temperature and steam soak. An elemental analysis was done using the Quanta II and the results are shown in figure 5.20. The elemental analysis of both the small spheres and the glassy ring indicate a large silicon and small carbon, oxygen and sodium peaks. The silicon, carbon and oxygen are expected as this is SiC in an oxidative environment. The sodium source however is unknown. The sodium impurity was however present in several of the 800°C fiber tests and only in the steam environments. The sodium impurities were only seen on tests that failed early due to high loading. The sodium impurity could have possibly been a catalyst for some of the oxidative effects on fibers tested for a longer duration. The water vapor is thought to enhance the transport of impurities to the test article via the formation of gaseous hydroxide species which subsequently increases the oxidation of the SiC test article [47]. Tunneling electron microscopy (TEM) would need to be utilized to see if sodium impurities are present in the heavily oxidized fibers. The presence of sodium impurities could have led to the large scatter seen in the fibers tested at 800°C.

At 1100°C small spherical formations were noted as in Fig. 5.21. These formations were identified as aluminum impurites. Once again the source of the impurities is unknown. It is known however that the PVA sizing that is used on these Hi-Nicalon S fiber contains trace amounts of inorganic elements. The amount present on the fibers in Fig. 5.21 would indicate that some sort of contamination was present during testing or SEM sample prep.

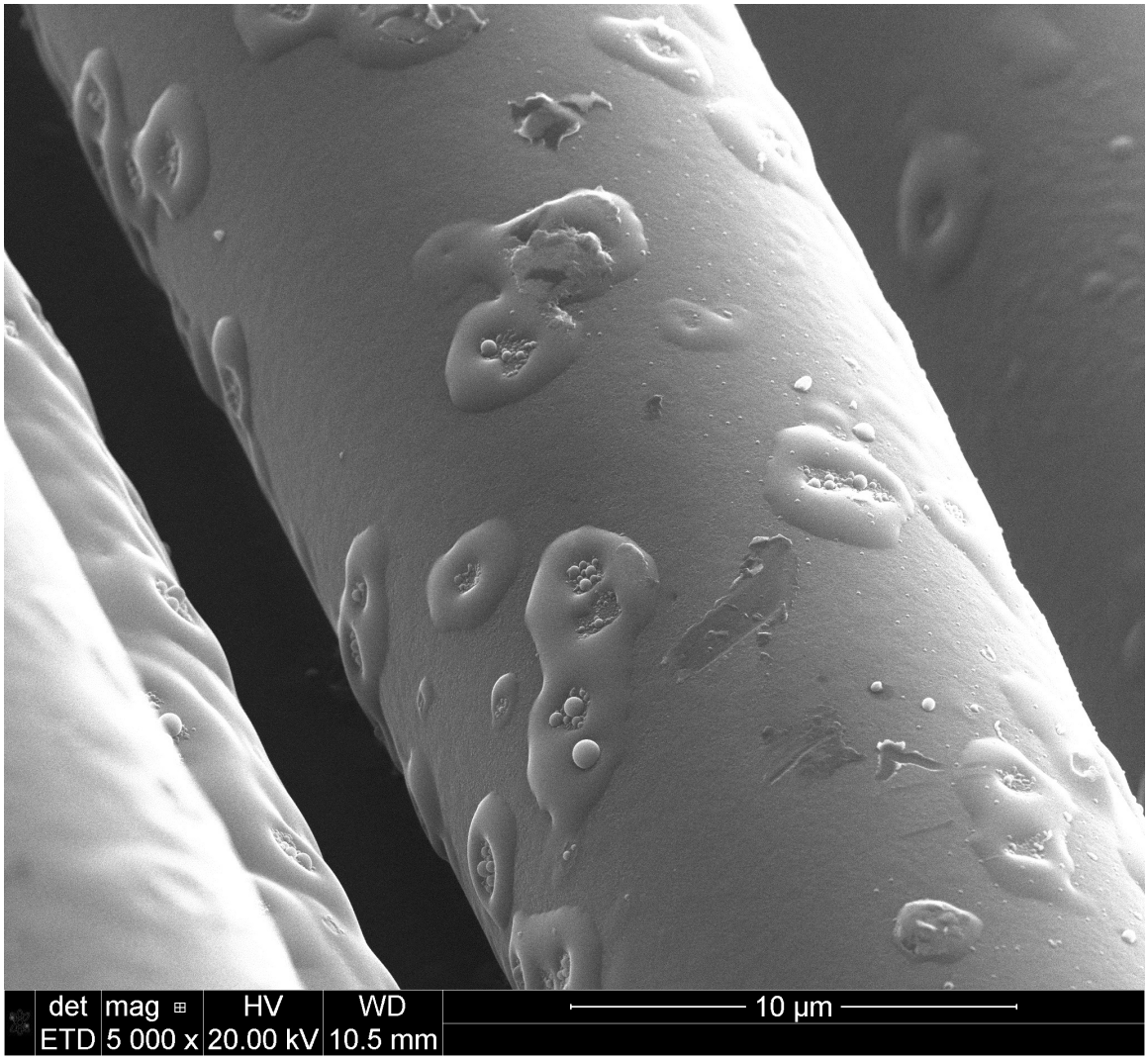

Figure 5.19: Hi-Nicalon Type S fiber tested at 800°C in steam for 45 minutes.

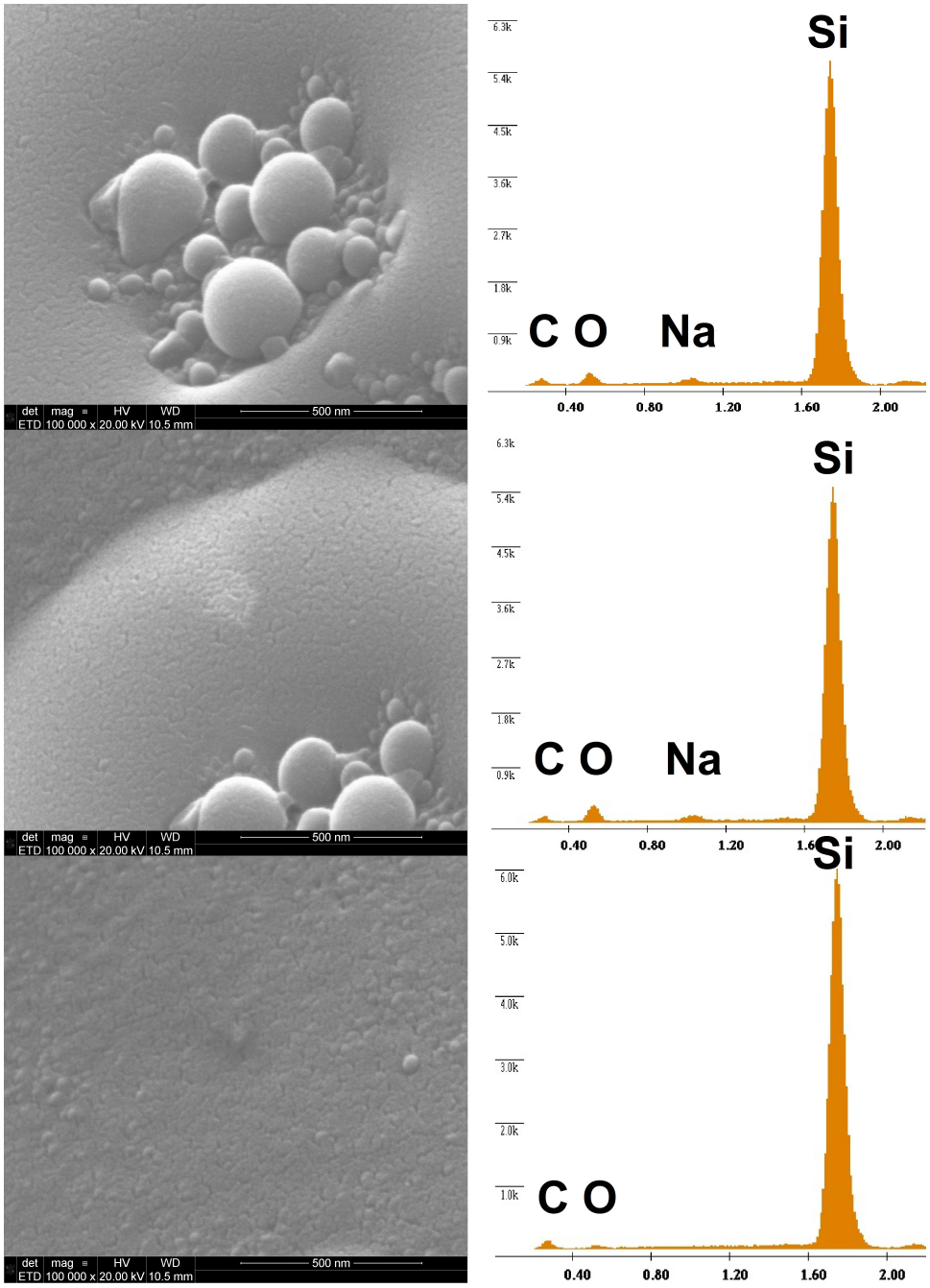

Figure 5.20: Elemental analysis of spherical impurities on a fiber tow tested at 800°C in steam. The elemental analysis of each location is located to the right of the picture. The absence of sodium in the barren region indicates that, though small, the sodium impurity is indeed present.

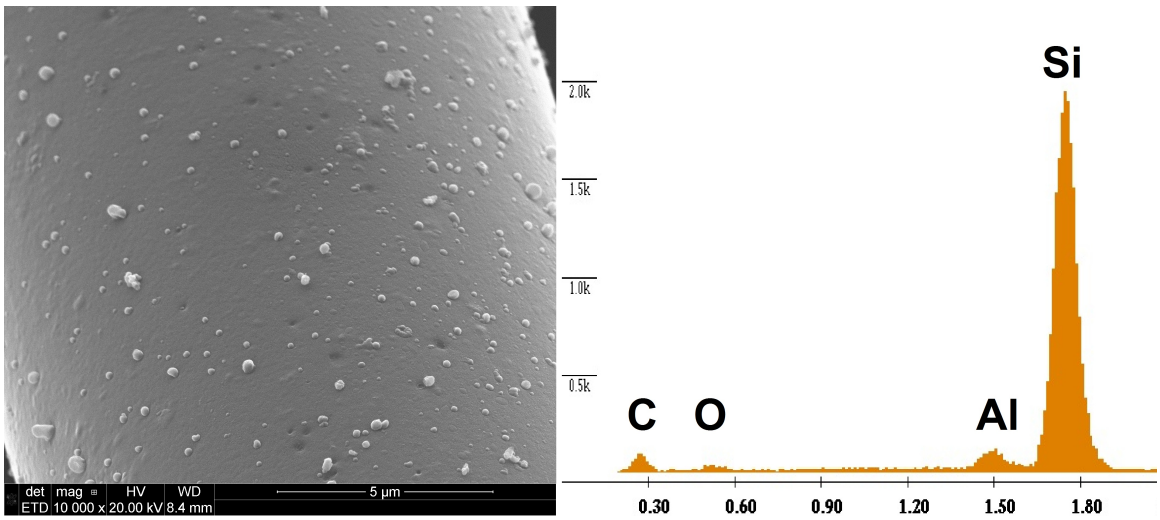

Figure 5.21: Elemental analysis of spherical impurities on a fiber tow tested at 1100°C in steam at 400Mpa. The test article failed upon loading. The impurities showed peaks for aluminum when analyzed using the EDX system.

VI. Conclusion and Recommendations

6.1 Conclusion

Like most materials as the temperature and stress increase the creep performance of Hi-Nicalon S decreases in both air and steam. At 1100°C, in air, the creep performance is significantly affected relative to the three lower temperatures. Interestingly, the negative effects of steam on creep performance diminish as temperature increases. At 1100°C the creep performance in steam environments is lower yet comparable to creep performance in air. The accumulation of creep strain during testing in steam is positively correlated with temperature and the converse is true for creep strain accumulated in air environments. In agreement with Steffens and Opila, there appears to be a protective silica formed on the Hi-Nicalon S fibers as the test temperature is increased from 800°C to 1100°C [52] [48]. The steam environment causes various SiO_x formations on the fiber and as Opila predicts there is a relationship between the growths of SiO_x and the volitalization of SiO_x. At higher temperatures the oxide thickness reaches an equilibrium thickness and can be seen by the mostly uniform fiber surfaces in any of the micrographs taken at 1100°C in steam. The affects of impurities on the fiber is known and were seen in this study but too what extent the impurities affected the results is unknown.

6.2 Recommendation

To further solidify these results more testing needs to be conducted at 700°C and 1200°C in both air and steam. Through testing at higher and lower temperatures, the temperature dependence of Hi-Nicalon S in creep and associated oxidation mechanisms could be further refined. In addition, the tests conducted in this research effort contained a number of anomalies, namely, fiber contamination and results inconsistent with values obtained from fibers tested at similar loads and environmental conditions. This resulted

in a failure to predict the creep mechanisms present. To identify the creep mechanisms present additional testing at all temperatures should be performed. Further tests would allow for these anomalies to be discounted as just that, or proved to be an actual property of Hi-Nicalon S fibers. The effects of impurities on the creep performance should also be conducted by comparing data taken in known clean environments versus data taken in "dirty" environments.

VII. Appendices

7.1 Appendix A- Weight Chart

Table 7.1: Stress-weight index table and equations

Engineering Stress = Force / Cross-sectional Area Total

Force = (Mass)kg x (Gravity)m/s^2

Hi-Nicalon S Fiber Data

Avg filament diameter (m) =	0.000013
# filaments per tow =	500

Engineering Stress = $\frac{\text{Mass(kg) x Gravity(9.81 m/s^2)}}{\text{Cross-sectional Area Total(m^2)}}$

Cross-sectional Area = n * Cross-sectional Area of filament

Area of filament = 1.32732E-10 m^2

Area Total = 6.63661E-08 m^2

Engineering Stress		Sequence of Weights	Mass of Sequence	
52.26	MPa	M, N, O, (LT)	0.35355	kg
102.52	MPa	H, M, N, (LT)	0.69355	kg
154.25	MPa	F, M, (LT)	1.04355	kg
255.51	MPa	F, G, M, N, O, (LT)	1.72855	kg
353.36	MPa	D, E, H, R, (LT)	2.391	kg
400.37	MPa	C, M, N, O, V, W, X, (LT)	2.70855	kg
450.63	MPa	C, G, M, O, V, W, X, (LT)	3.049	kg
650.92	MPa	C, D, F, M, N, V, W, (LT)	4.40355	kg
700.73	MPa	C, D, E, G, N, V, W, (LT)	4.741	kg
798.73	MPa	A,G,O,M,N,T,X,Y,(LT)	5.40355	kg
937.24	MPa	A, D, E, (LT)	6.34055	kg
1023.71	MPa	A, C, O, (LT)	6.92555	kg
1103.53	MPa	A, C, H, R, S, (LT)	7.46555	kg
1249.87	MPa	A, C, D, H, N, O, T, (LT)	8.45555	kg
1552.89	MPa	A, B, H, I, J, N, (LT)	10.50555	kg

A-F weighed on Acculab SV-30 (+/- .005 kg)
G-Z weighed on Voyager Pro (+/- .001 kg)

Weight Cross-Reference Chart

	(kg)		(kg)		(kg)		(kg)
A=	4.505	H=	0.455	O=	0.115	V=	0.020
B=	4.51	I=	0.455	P=	0.115	W=	0.020
C=	2.295	J=	0.455	Q=	0.115	X=	0.020
D=	0.91	K=	0.455	R=	0.100	Y=	0.020
E=	0.915	L=	0.455	S=	0.100	Z=	0.010
F=	0.92	M=	0.113	T=	0.050	LT (Load Train)=	0.01055
G=	0.455	N=	0.115	U=	0.050		

7.2 Appendix B- Furnace and Generator Settings

Table 7.2: Temperature set-points and steam generator settings

Furnace Temperature Settings

		Air	Steam
800°C	upper	789	788
	lower	789	808
900°C	upper	893	898
	lower	899	914
1000°C	upper	1002	1002
	lower	1012	1035
1100°C	upper	1110	1110
	lower	1131	1152
1200°C	upper	1215	1206
	lower	1250	1265

Steam Generator Settings

Variac	45%
Pump	2ml/min

7.3 Appendix C- Supporting Charts and Micrographs

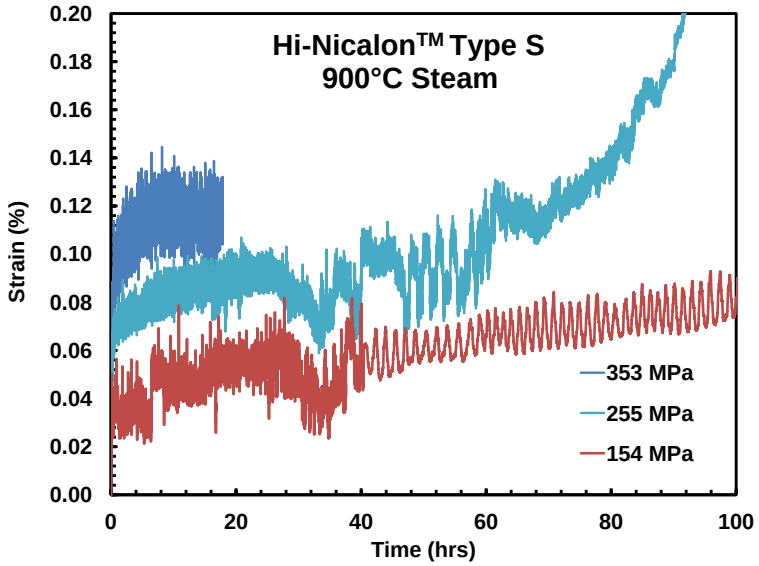

Figure 7.1: Representative creep strain vs time curves obtained for Hi-Nicalon S fiber tows at 900°C in steam. This chart reflects the entire creep to failure. The tertiary creep is atypical.

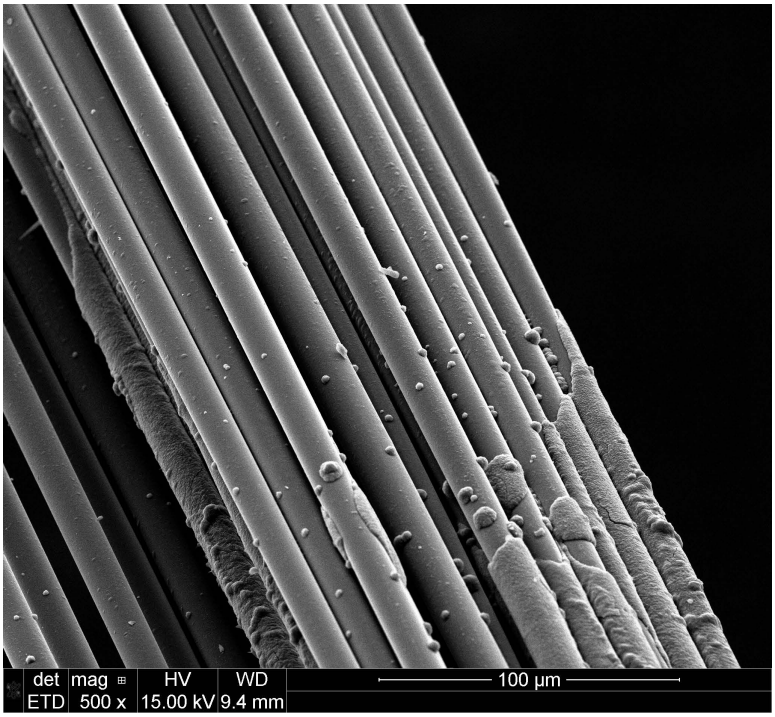

Figure 7.2: Low magnification of a fiber tested at 800°C in steam for 8 hrs at 350MPa. The oxidation mechanism varies along the axis of the fiber.

7.4 Appendix D- SEM Micrographs

7.4.1 Fibers tested at 800°C.

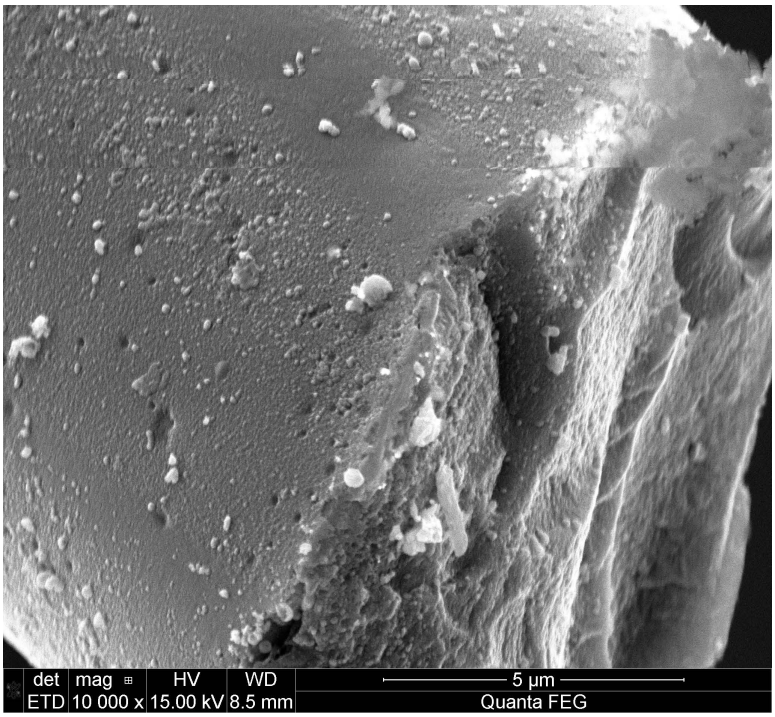

Figure 7.3: Hi-Nicalon S fiber specimen A1, tested in air at 800°C at 798MPa

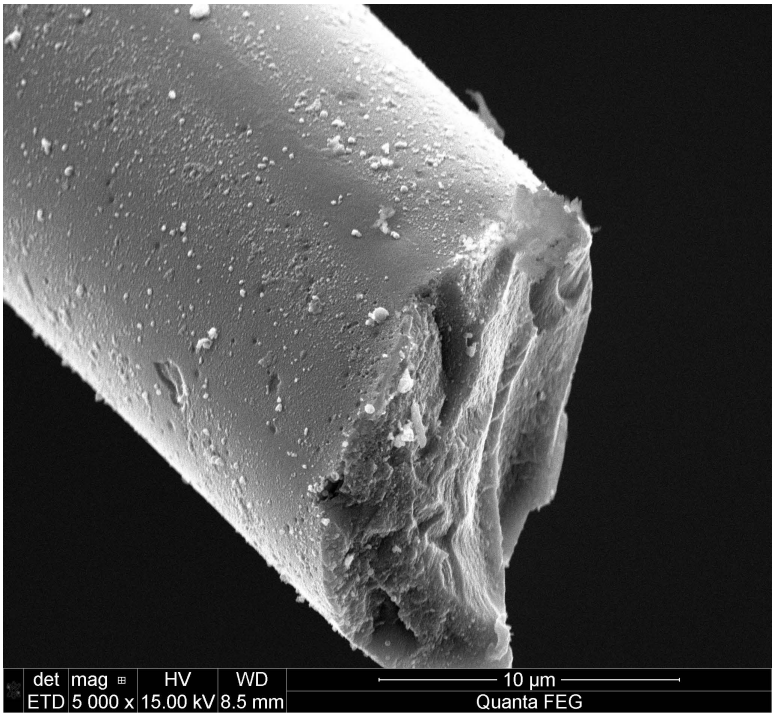

Figure 7.4: Hi-Nicalon S fiber specimen A1, tested in air at 800°C at 798MPa

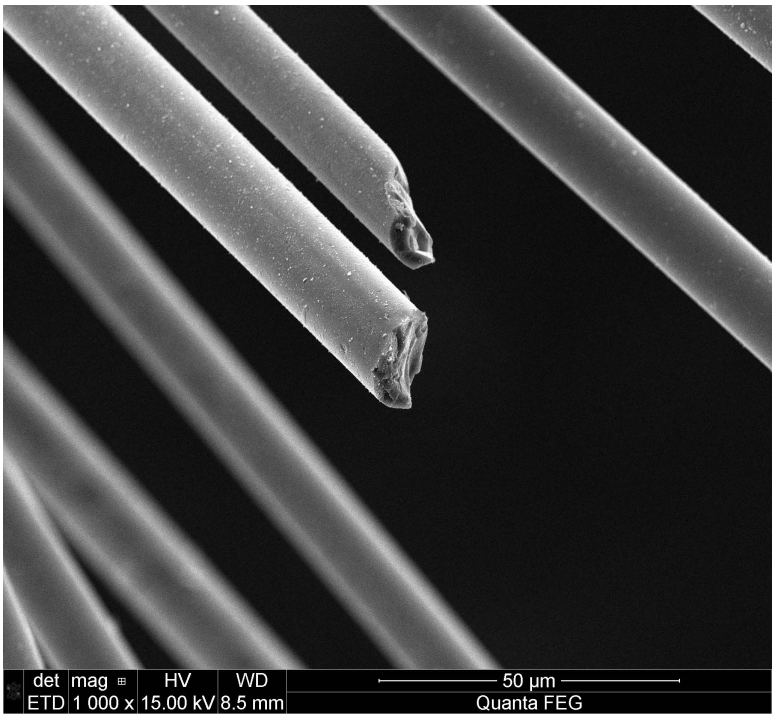

Figure 7.5: Hi-Nicalon S fiber specimen A1, tested in air at 800°C at 798MPa

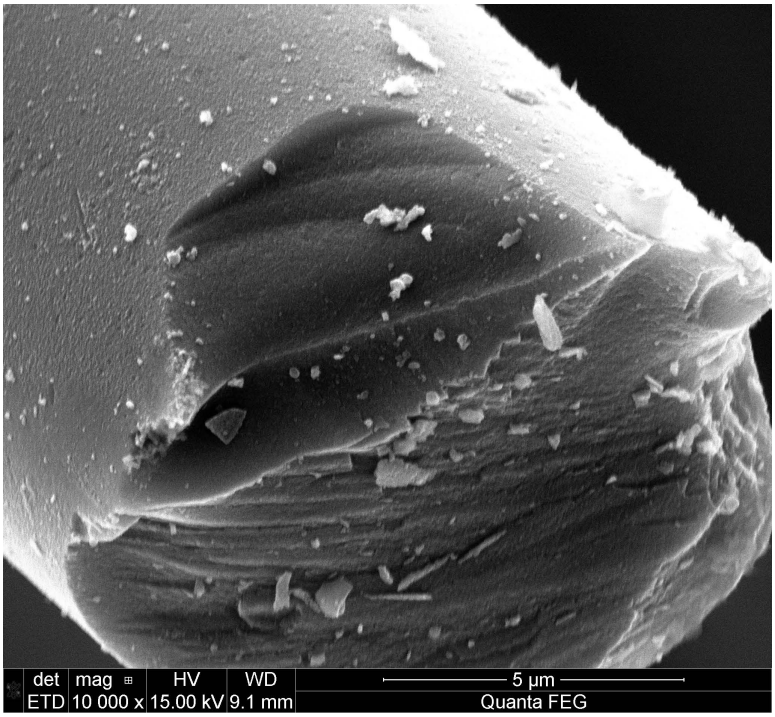

Figure 7.6: Hi-Nicalon S fiber specimen A1, tested in air at 800°C at 798MPa

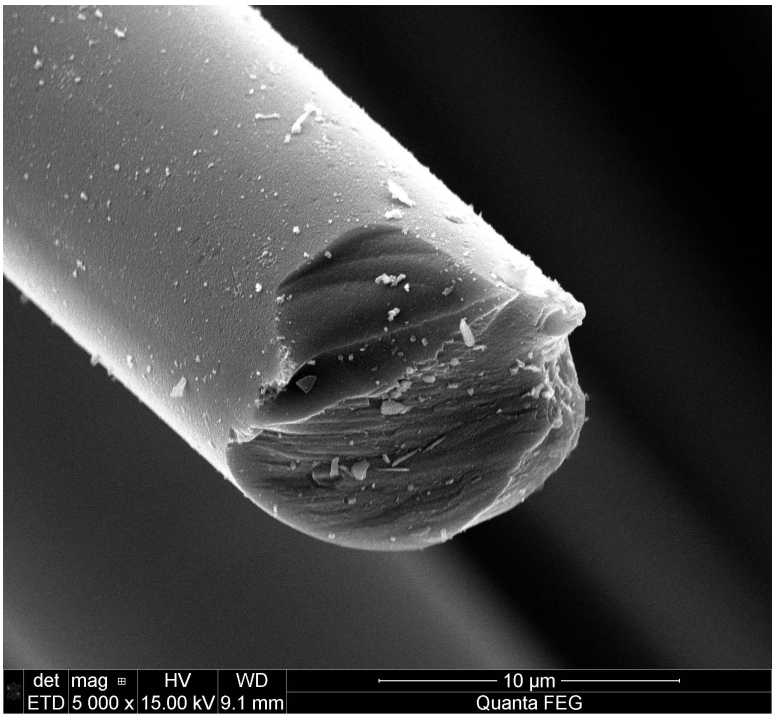

Figure 7.7: Hi-Nicalon S fiber specimen A1, tested in air at 800°C at 798MPa

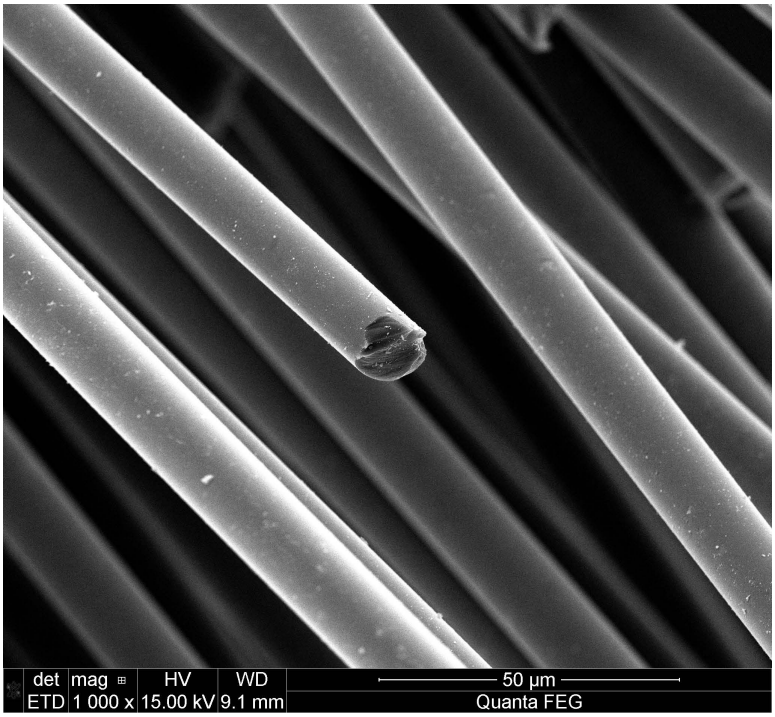

Figure 7.8: Hi-Nicalon S fiber specimen A1, tested in air at 800°C at 798MPa

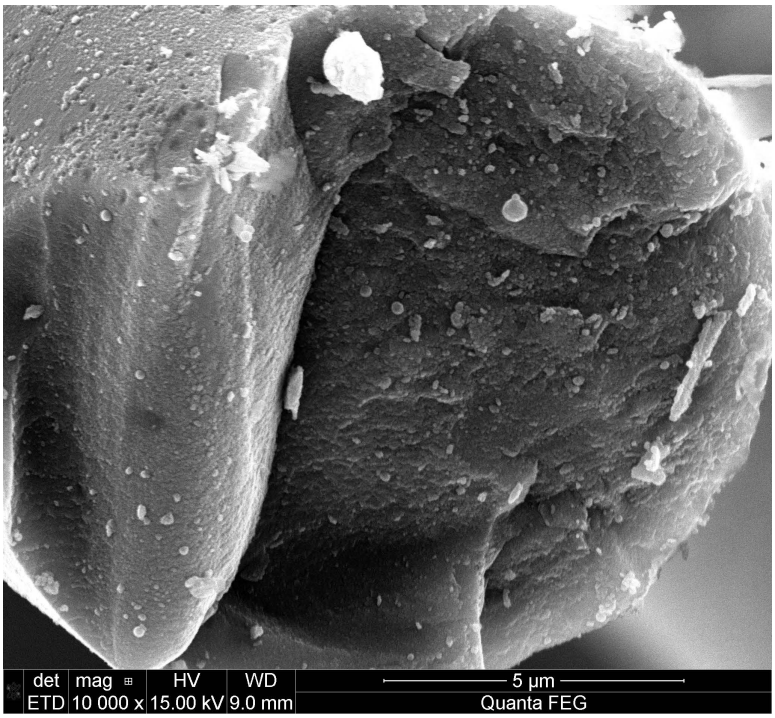

Figure 7.9: Hi-Nicalon S fiber specimen A1, tested in air at 800°C at 798MPa

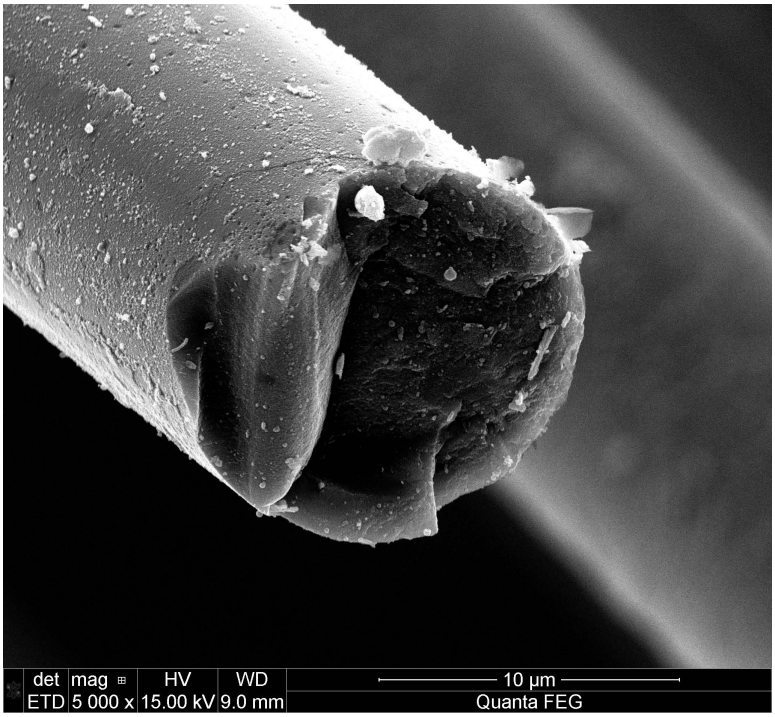

Figure 7.10: Hi-Nicalon S fiber specimen A1, tested in air at 800°C at 798MPa

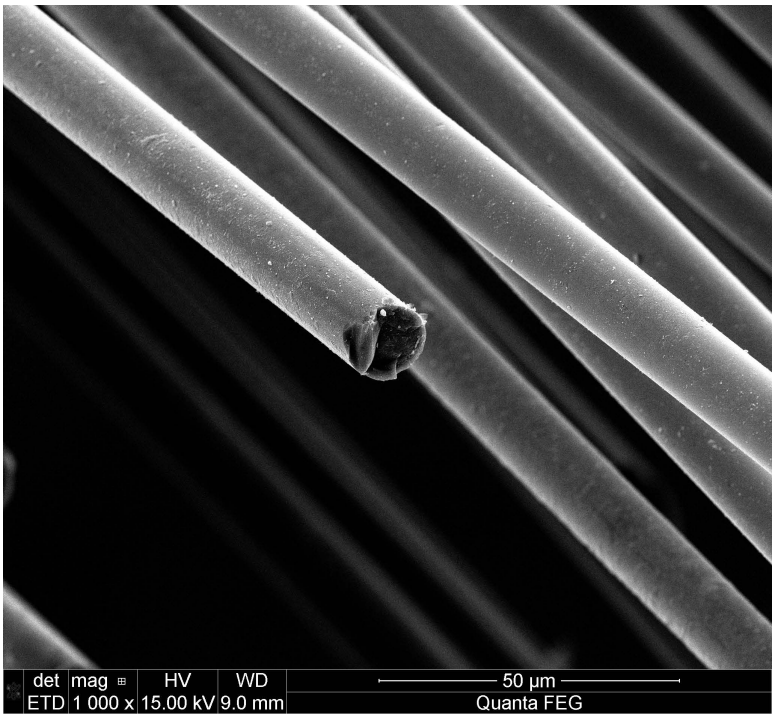

Figure 7.11: Hi-Nicalon S fiber specimen A1, tested in air at 800°C at 798MPa

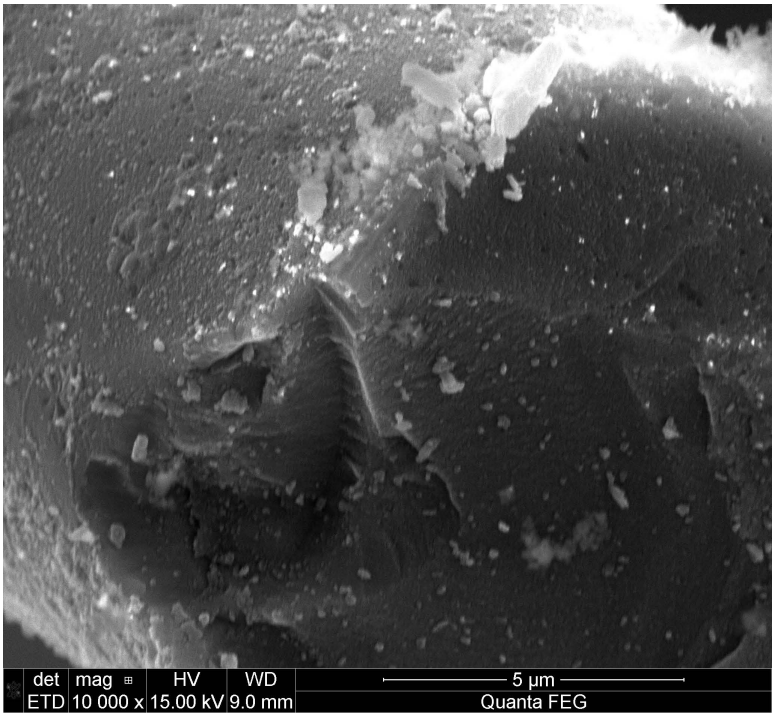

Figure 7.12: Hi-Nicalon S fiber specimen A1, tested in air at 800°C at 798MPa

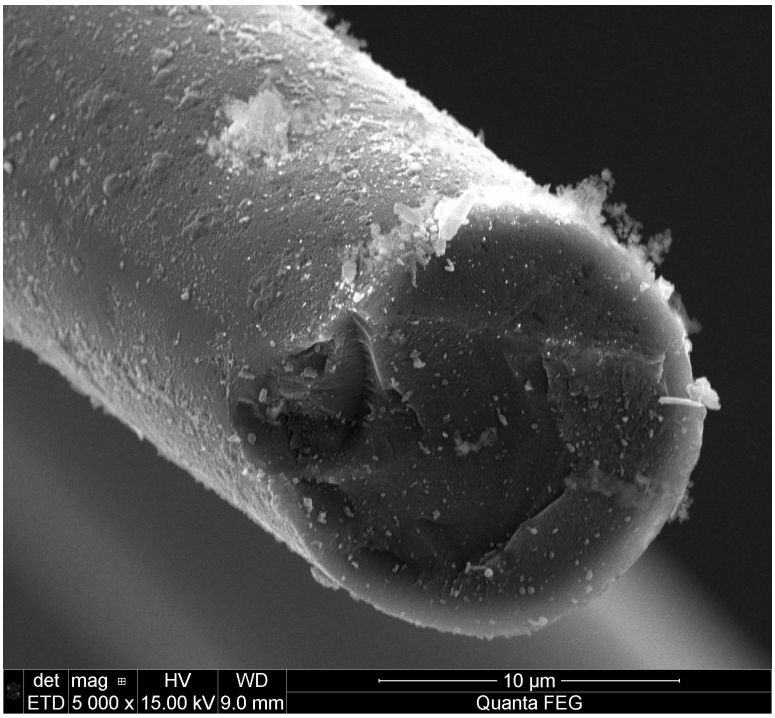

Figure 7.13: Hi-Nicalon S fiber specimen A1, tested in air at 800°C at 798MPa

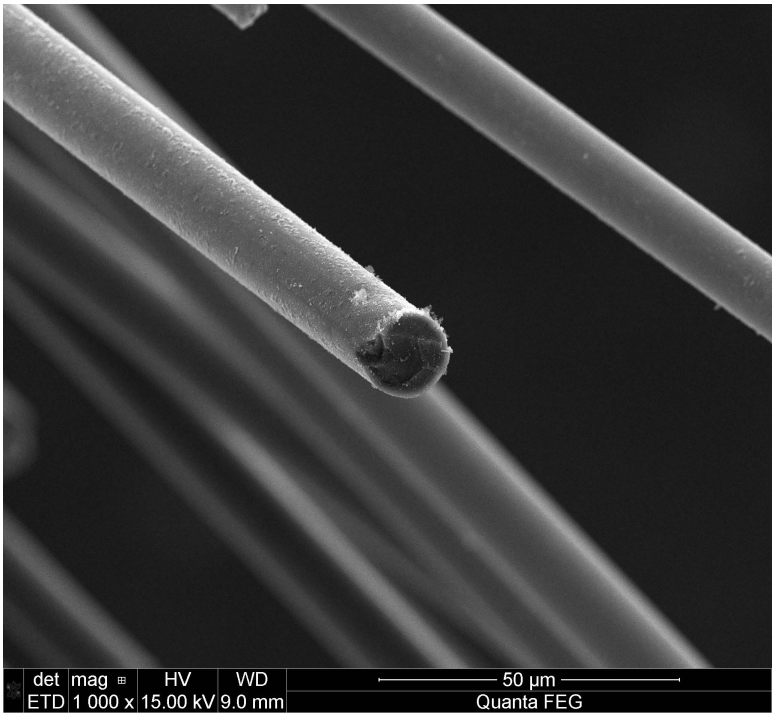

Figure 7.14: Hi-Nicalon S fiber specimen A1, tested in air at 800°C at 798MPa

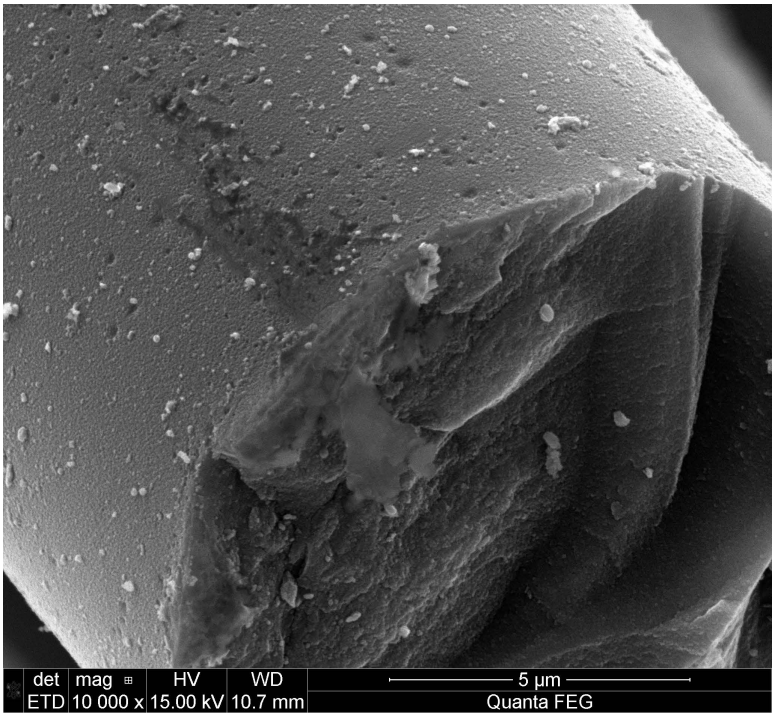

Figure 7.15: Hi-Nicalon S fiber specimen A13, tested in air at 800°C at 937MPa

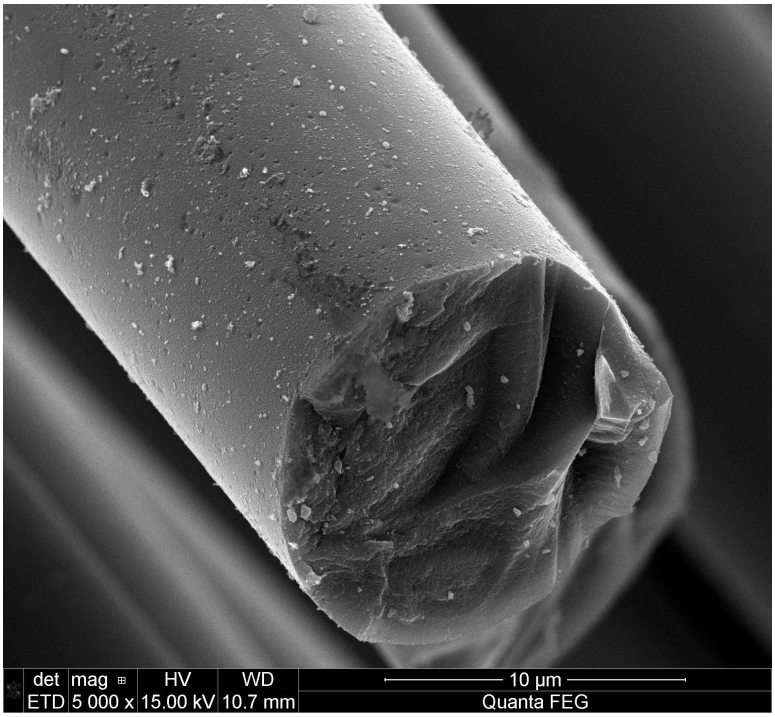

Figure 7.16: Hi-Nicalon S fiber specimen A13, tested in air at 800°C at 937MPa

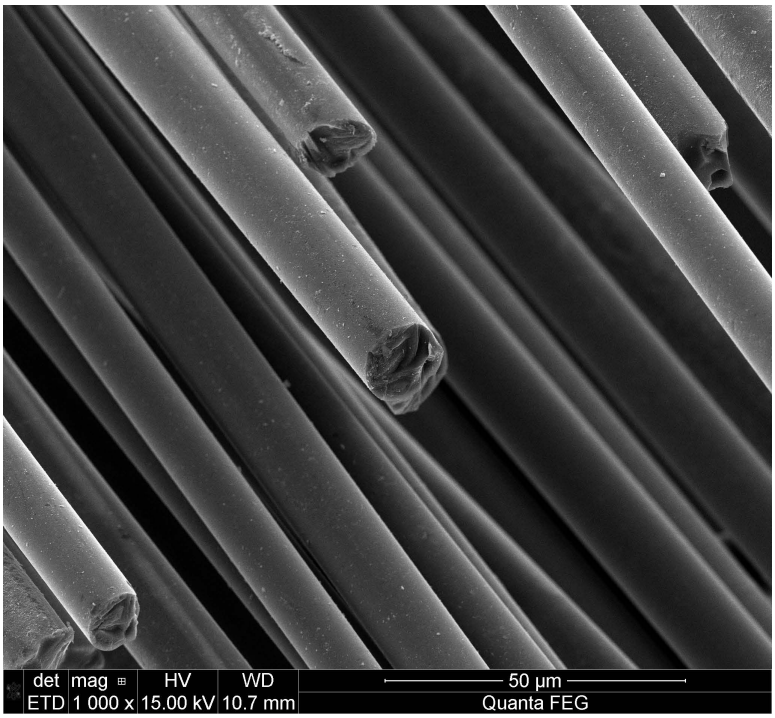

Figure 7.17: Hi-Nicalon S fiber specimen A13, tested in air at 800°C at 937MPa

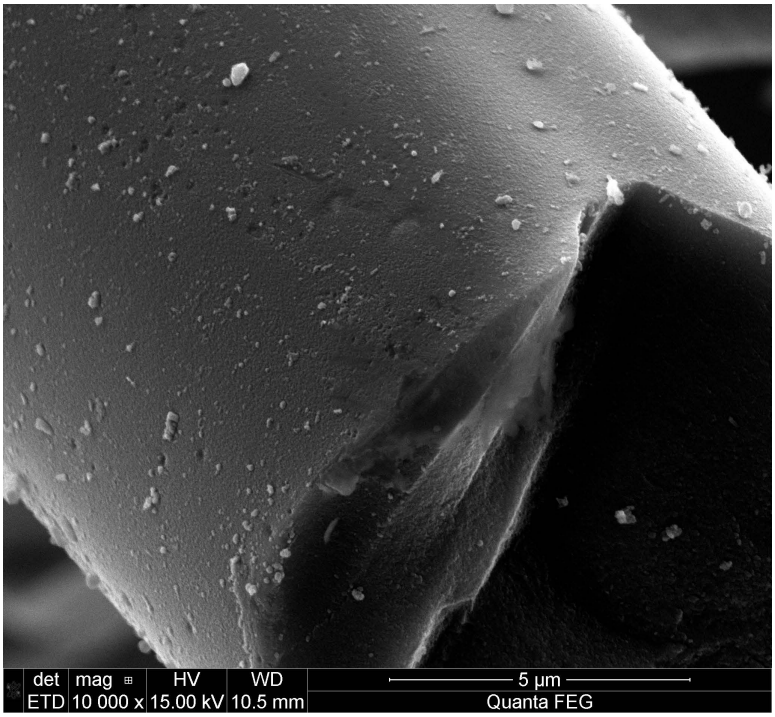

Figure 7.18: Hi-Nicalon S fiber specimen A13, tested in air at 800°C at 937MPa

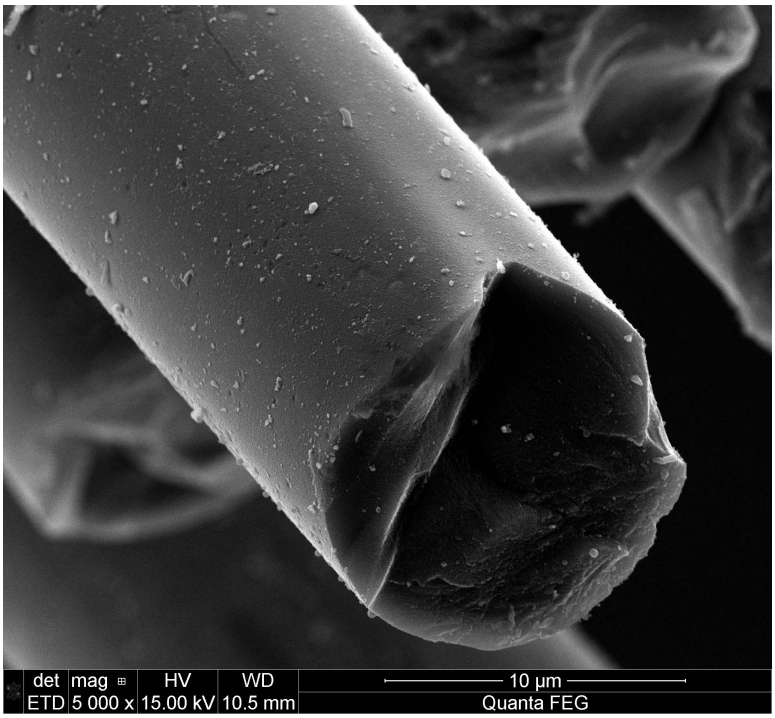

Figure 7.19: Hi-Nicalon S fiber specimen A13, tested in air at 800°C at 937MPa

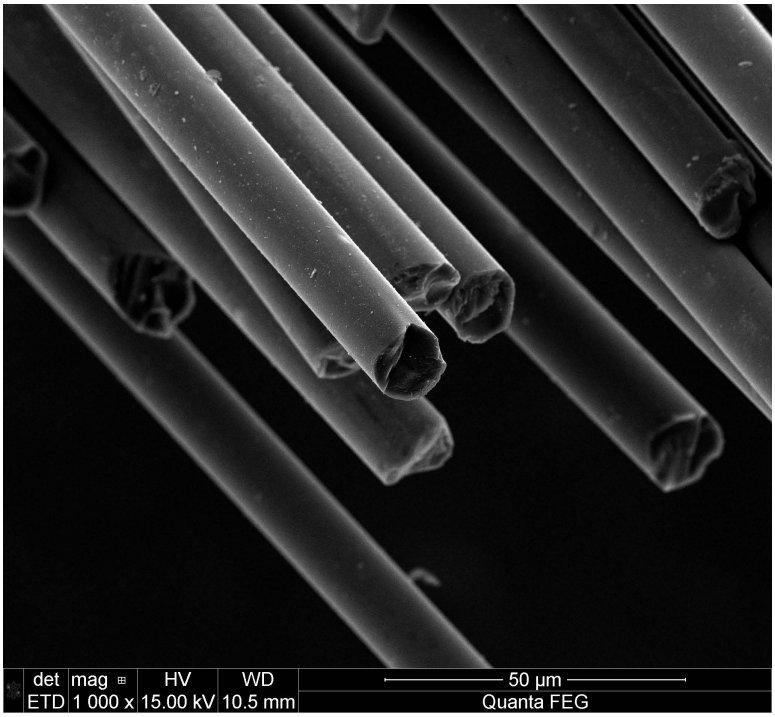

Figure 7.20: Hi-Nicalon S fiber specimen A13, tested in air at 800°C at 937MPa

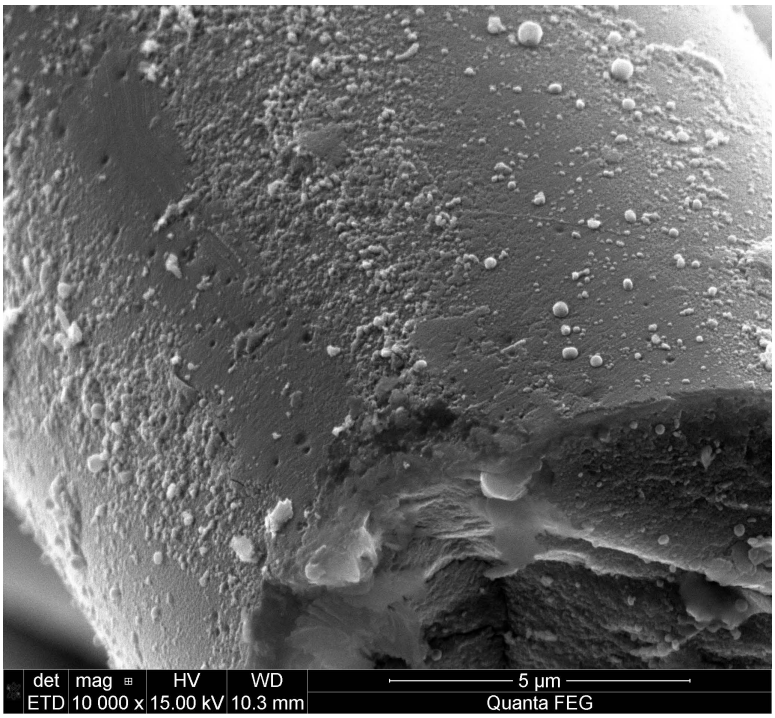

Figure 7.21: Hi-Nicalon S fiber specimen A13, tested in air at 800°C at 937MPa

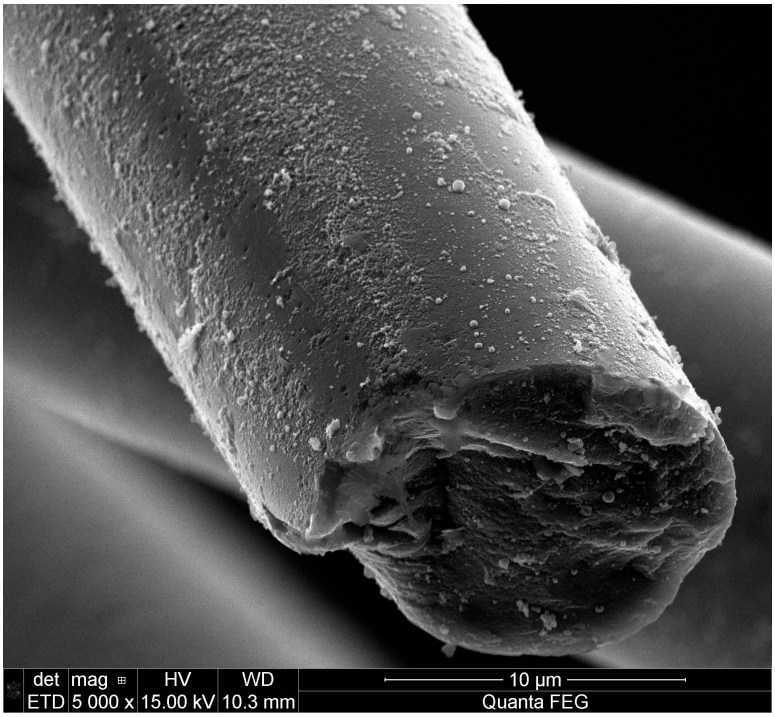

Figure 7.22: Hi-Nicalon S fiber specimen A13, tested in air at 800°C at 937MPa

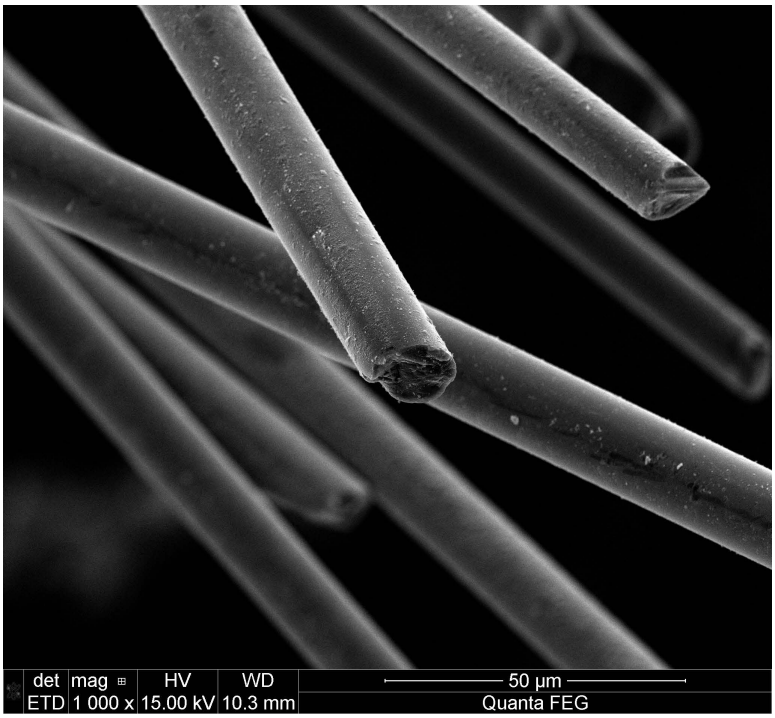

Figure 7.23: Hi-Nicalon S fiber specimen A13, tested in air at 800°C at 937MPa

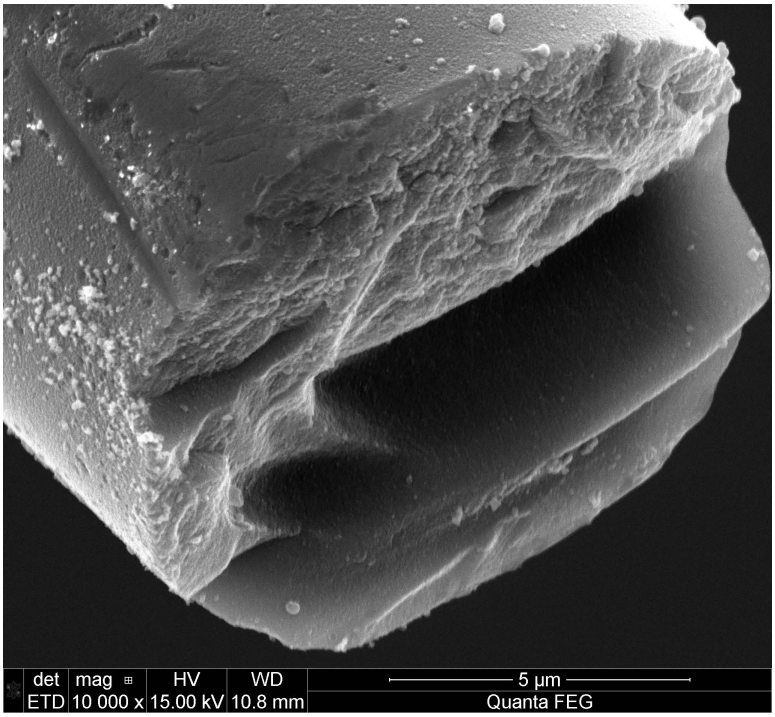

Figure 7.24: Hi-Nicalon S fiber specimen A14, tested in air at 800°C at 937MPa

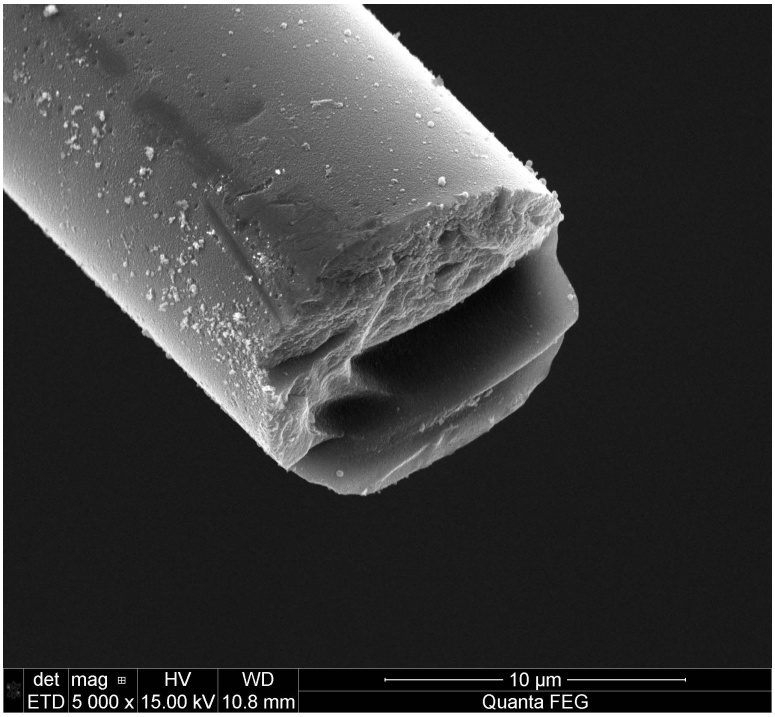

Figure 7.25: Hi-Nicalon S fiber specimen A14, tested in air at 800°C at 937MPa

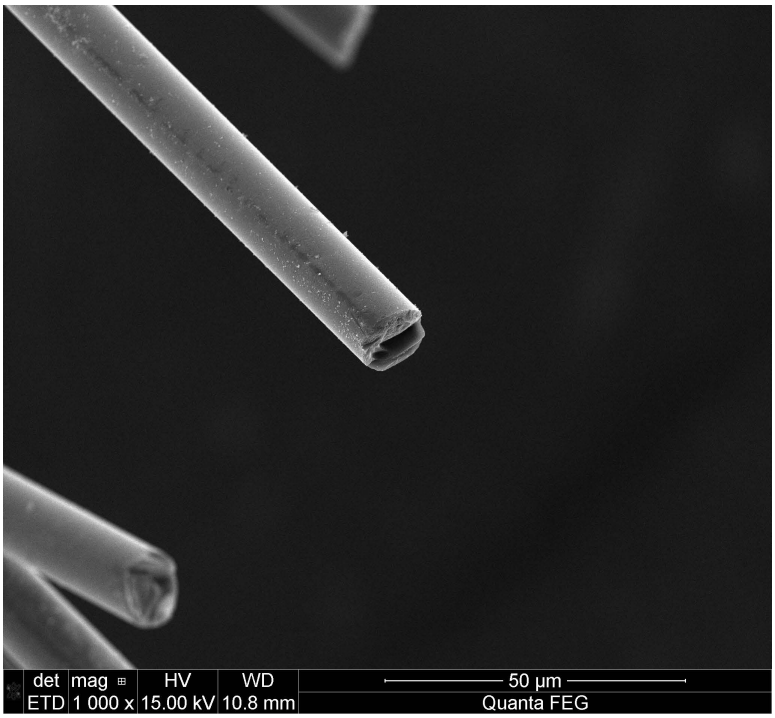

Figure 7.26: Hi-Nicalon S fiber specimen A14, tested in air at 800°C at 937MPa

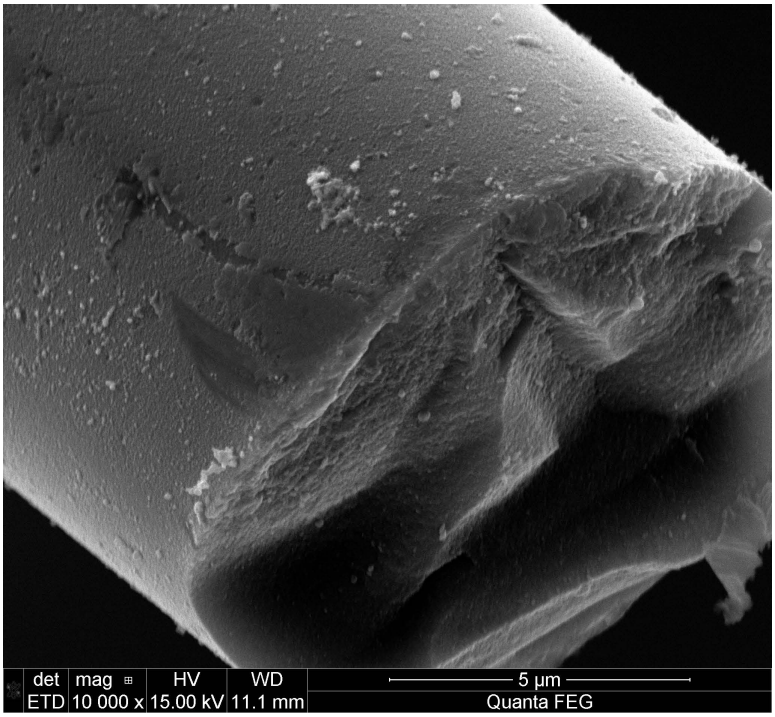

Figure 7.27: Hi-Nicalon S fiber specimen A14, tested in air at 800°C at 937MPa

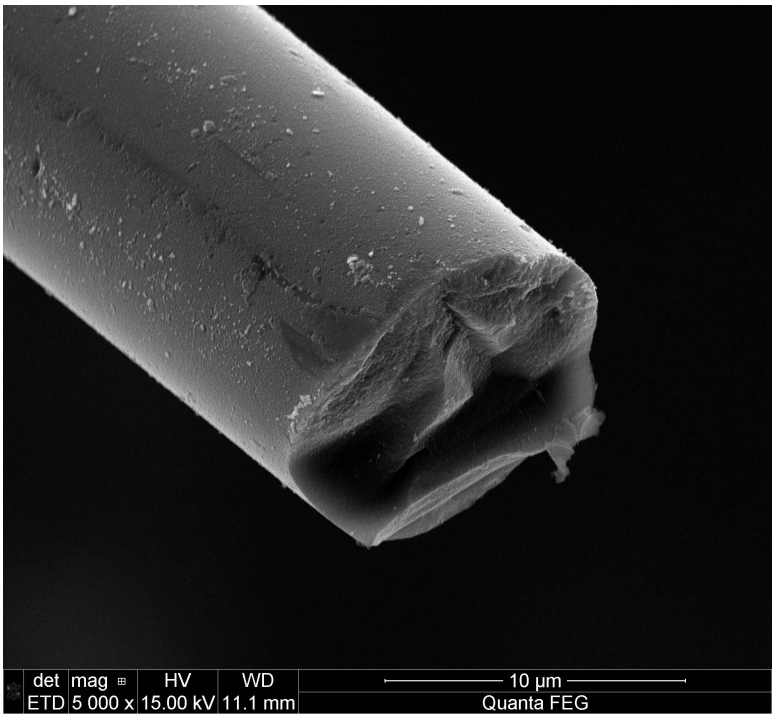

Figure 7.28: Hi-Nicalon S fiber specimen A14, tested in air at 800°C at 937MPa

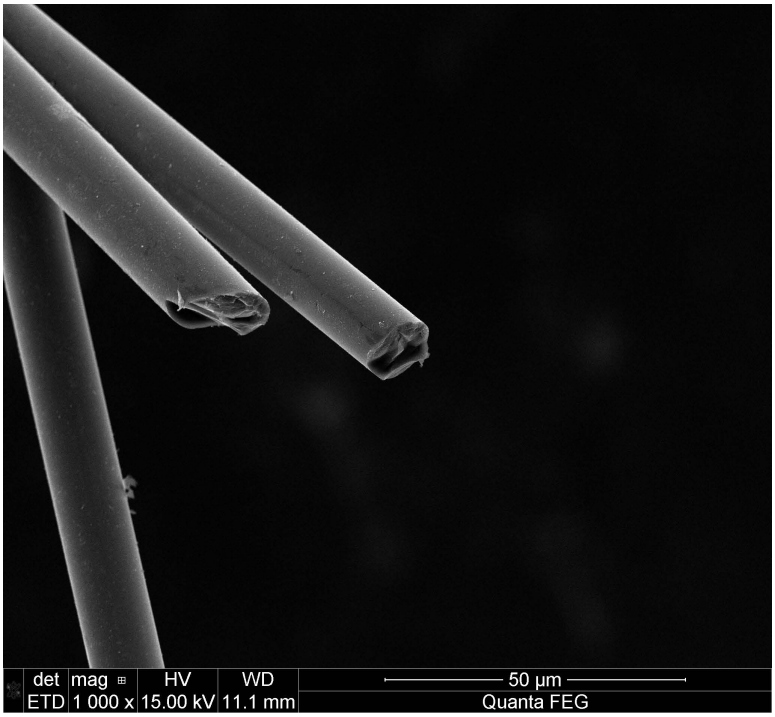

Figure 7.29: Hi-Nicalon S fiber specimen A14, tested in air at 800°C at 937MPa

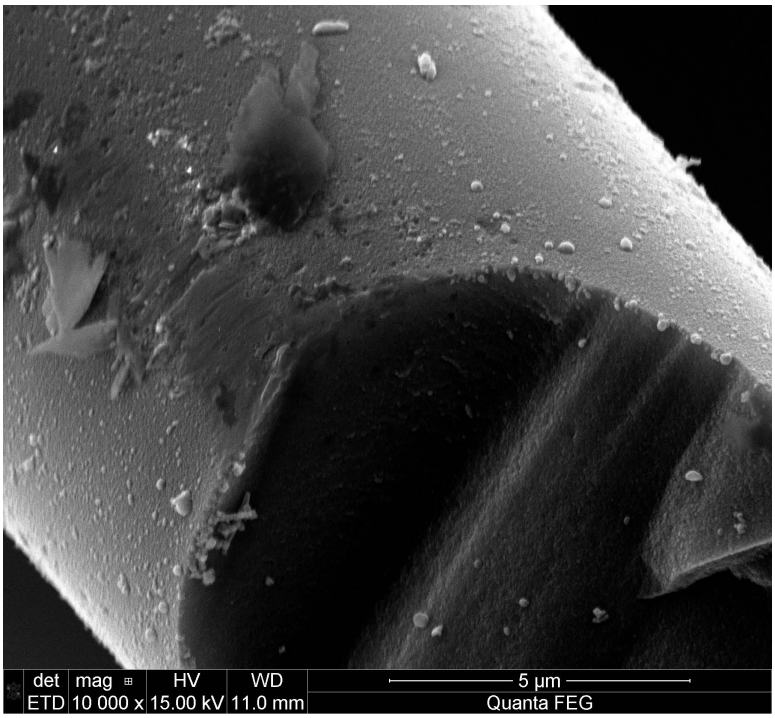

Figure 7.30: Hi-Nicalon S fiber specimen A14, tested in air at 800°C at 937MPa

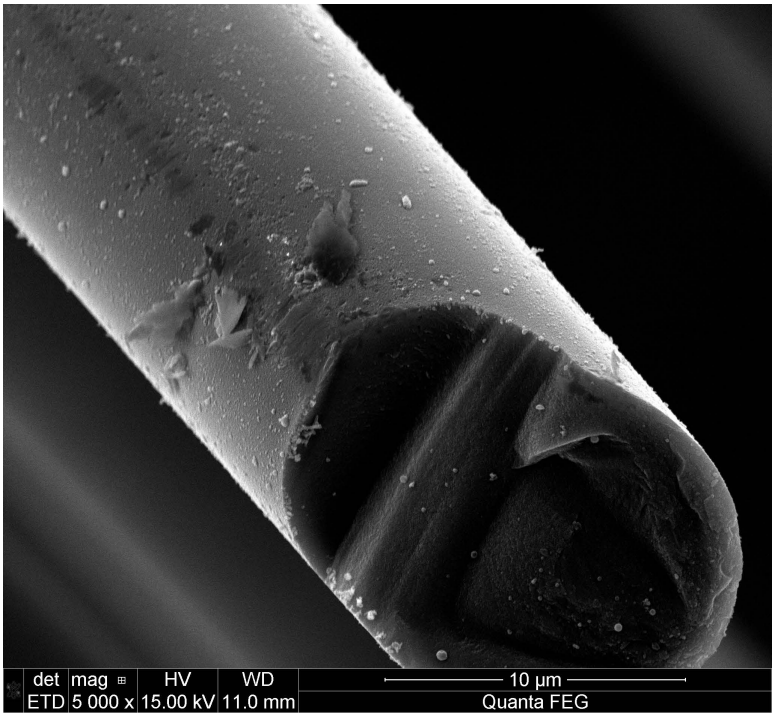

Figure 7.31: Hi-Nicalon S fiber specimen A14, tested in air at 800°C at 937MPa

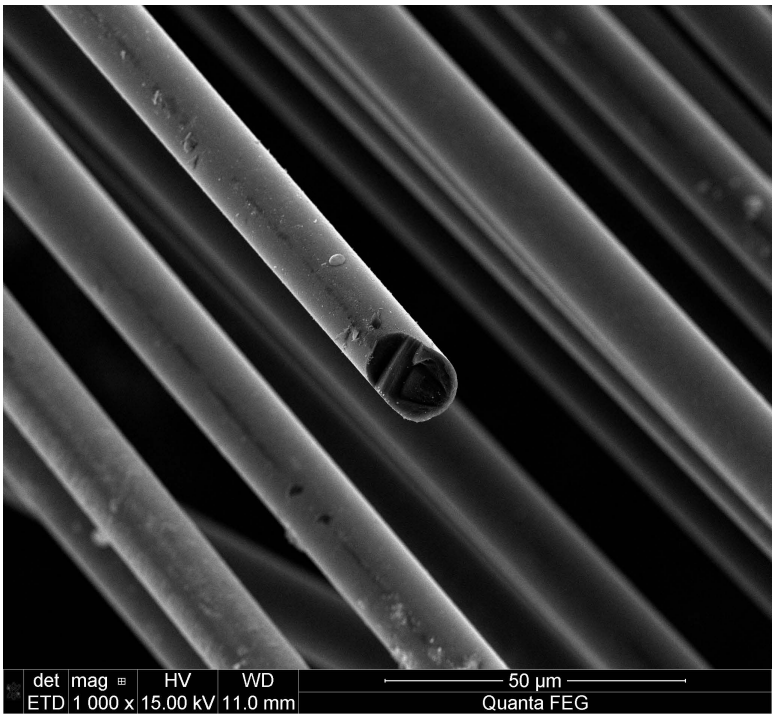

Figure 7.32: Hi-Nicalon S fiber specimen A14, tested in air at 800°C at 937MPa

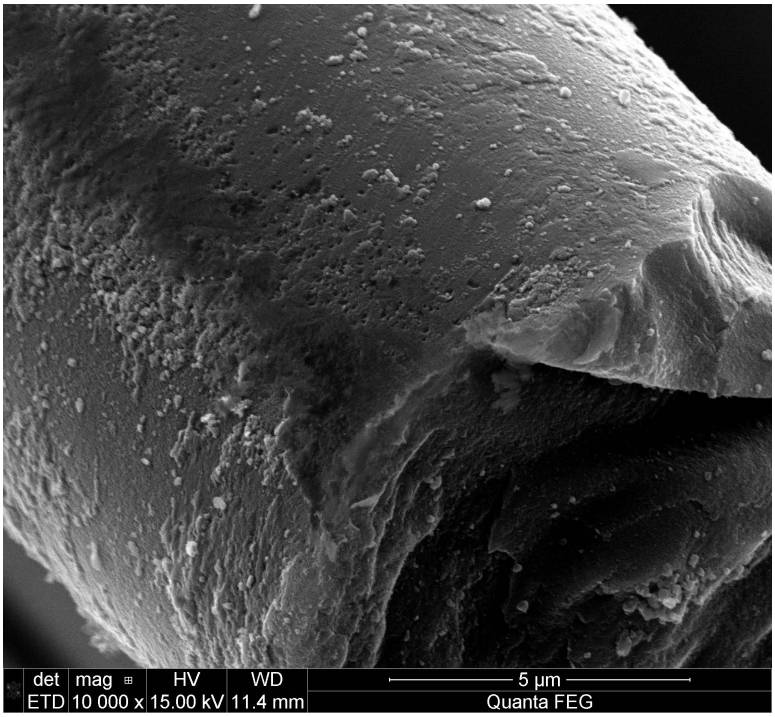

Figure 7.33: Hi-Nicalon S fiber specimen A14, tested in air at 800°C at 937MPa

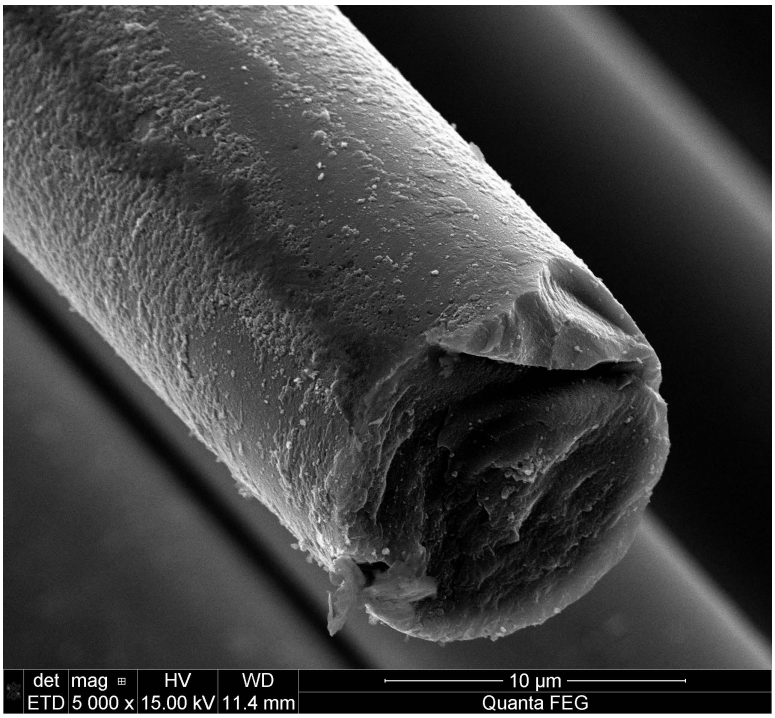

Figure 7.34: Hi-Nicalon S fiber specimen A14, tested in air at 800°C at 937MPa

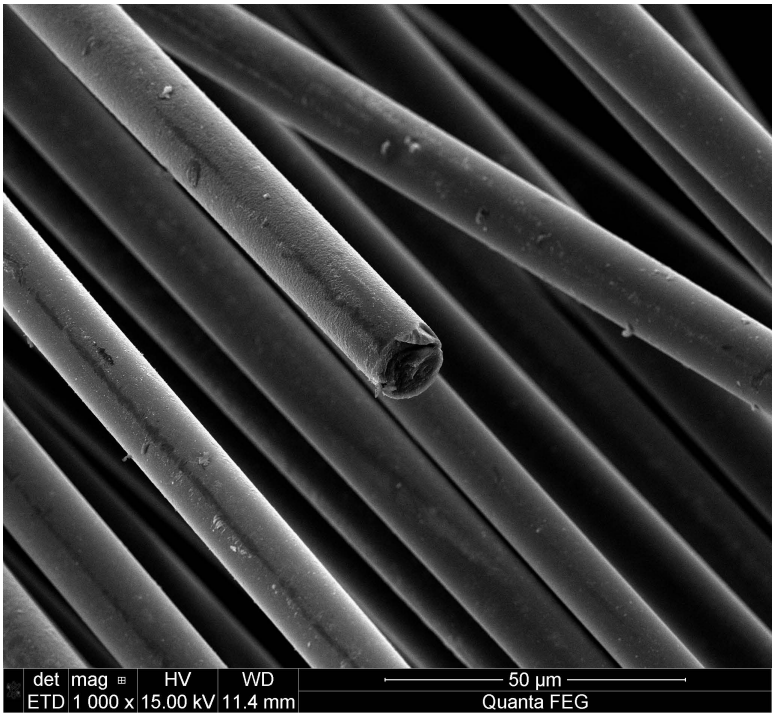

Figure 7.35: Hi-Nicalon S fiber specimen A14, tested in air at 800°C at 937MPa

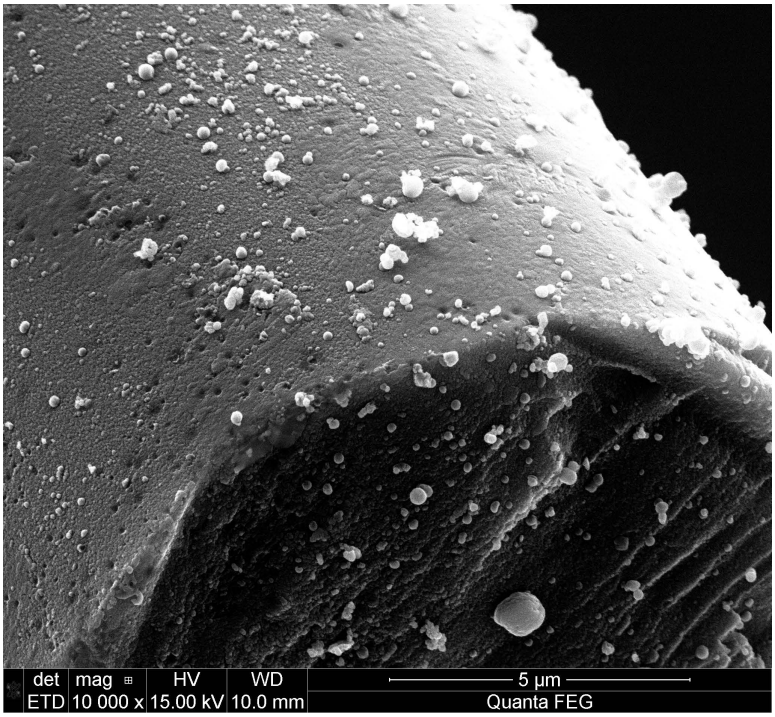

Figure 7.36: Hi-Nicalon S fiber specimen A16, tested in air at 800°C at 1032MPa

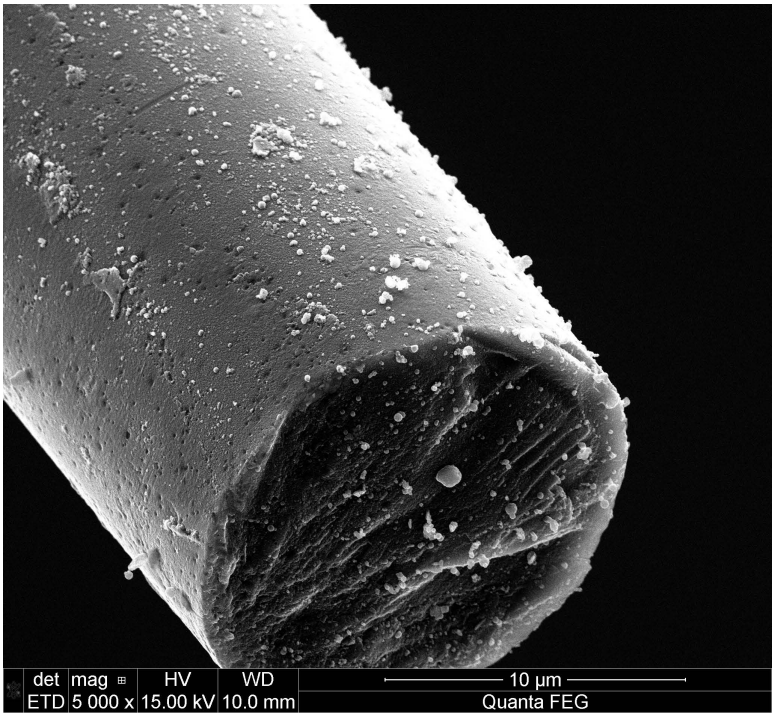

Figure 7.37: Hi-Nicalon S fiber specimen A16, tested in air at 800°C at 1032MPa

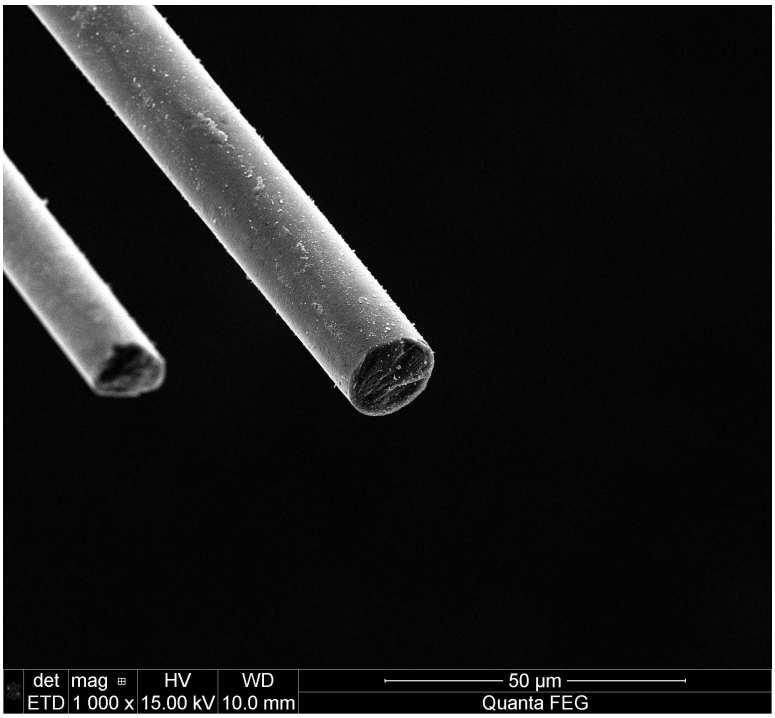

Figure 7.38: Hi-Nicalon S fiber specimen A16, tested in air at 800°C at 1032MPa

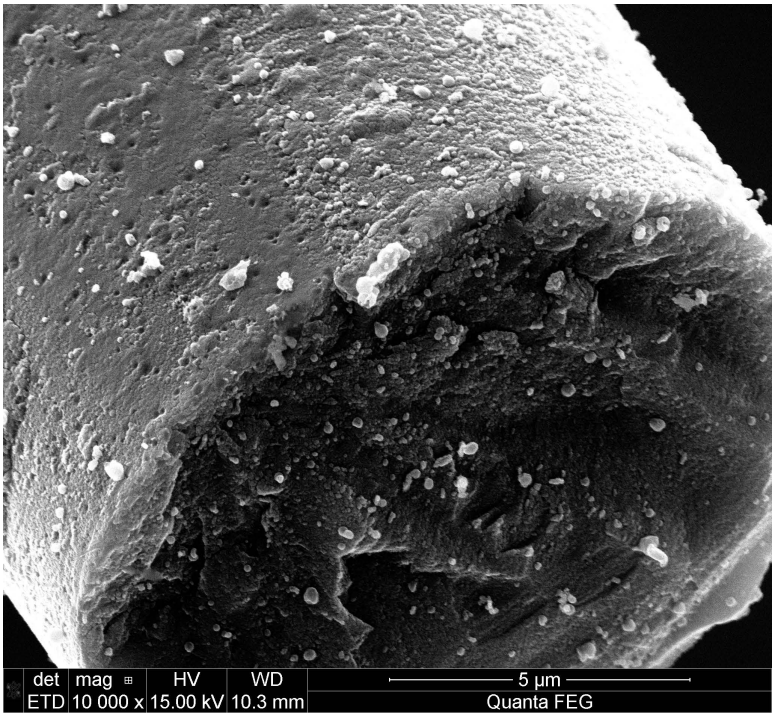

Figure 7.39: Hi-Nicalon S fiber specimen A16, tested in air at 800°C at 1032MPa

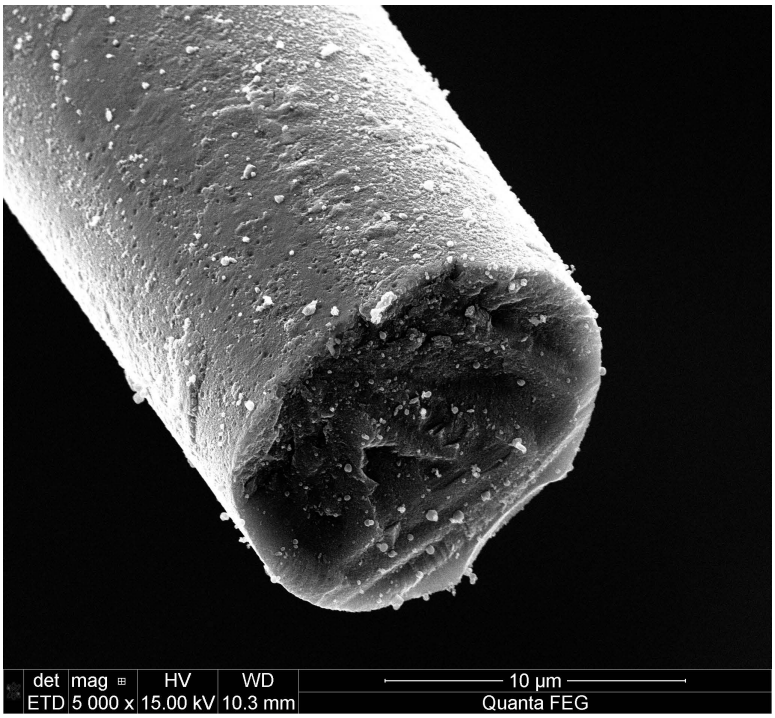

Figure 7.40: Hi-Nicalon S fiber specimen A16, tested in air at 800°C at 1032MPa

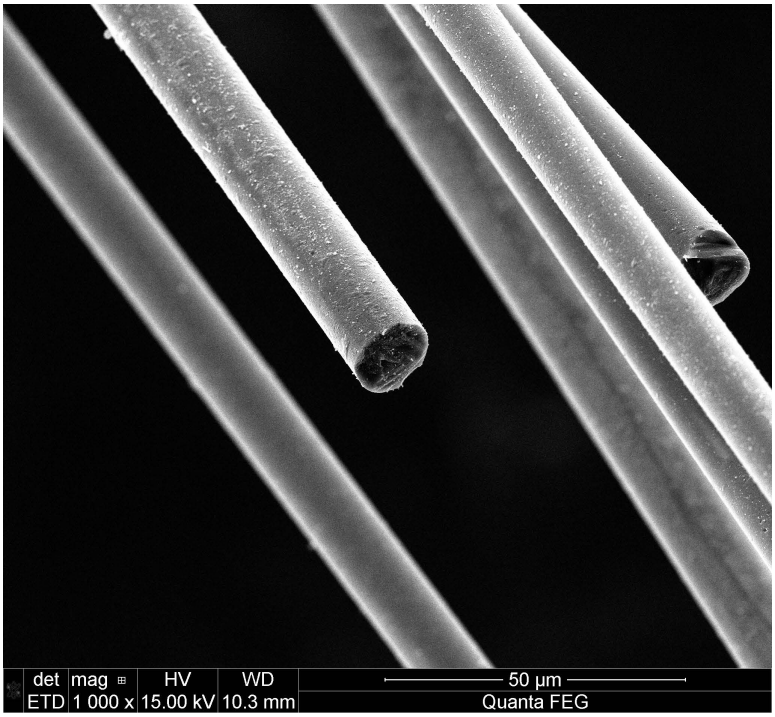

Figure 7.41: Hi-Nicalon S fiber specimen A16, tested in air at 800°C at 1032MPa

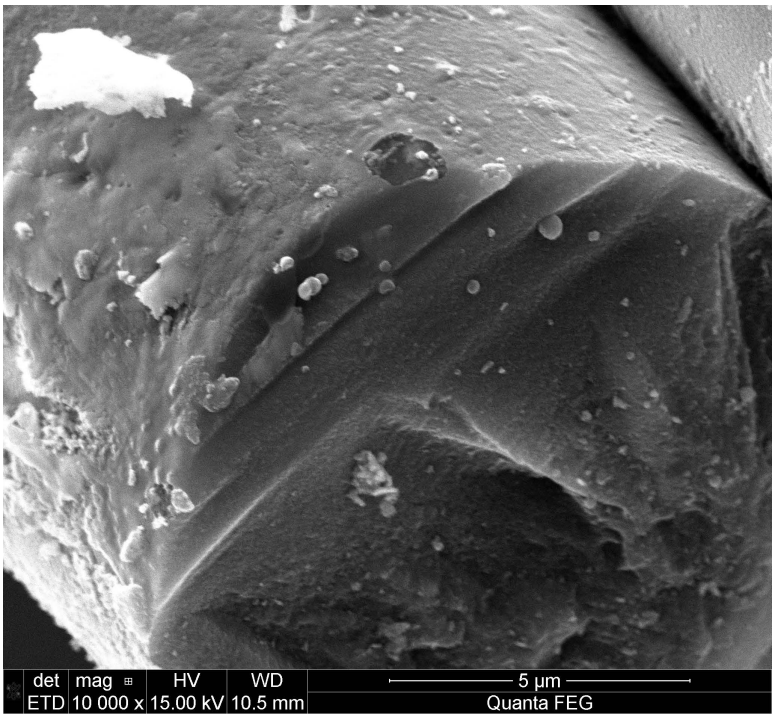

Figure 7.42: Hi-Nicalon S fiber specimen A16, tested in air at 800°C at 1032MPa

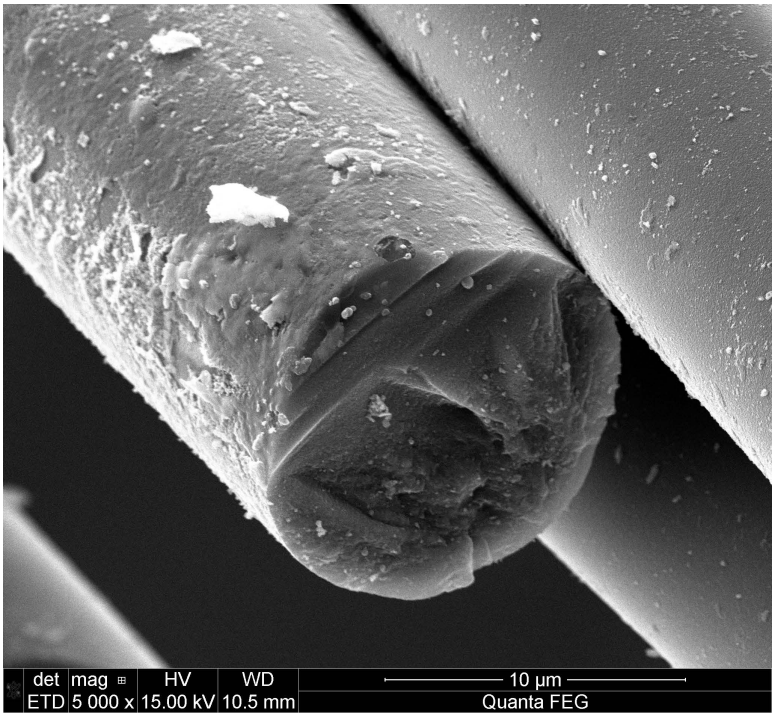

Figure 7.43: Hi-Nicalon S fiber specimen A16, tested in air at 800°C at 1032MPa

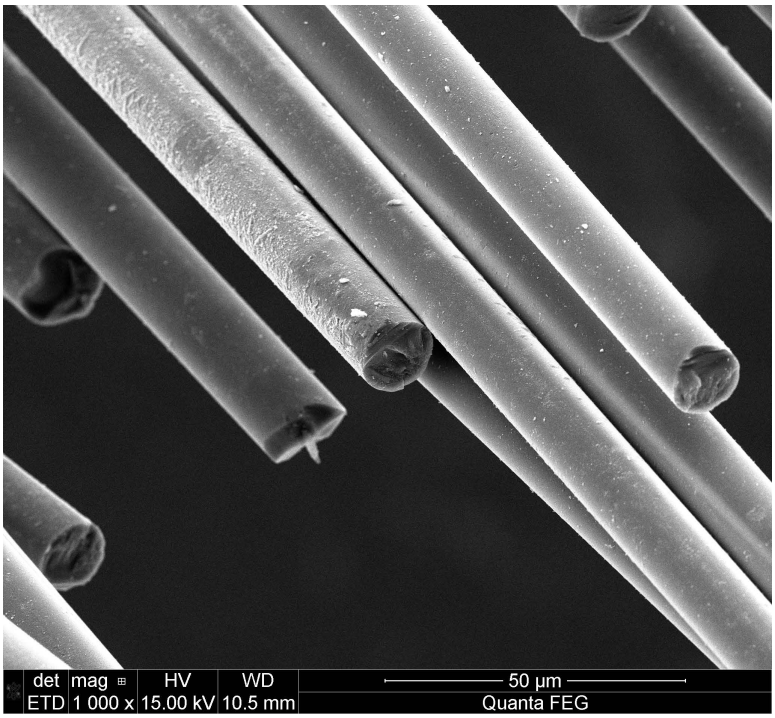

Figure 7.44: Hi-Nicalon S fiber specimen A16, tested in air at 800°C at 1032MPa

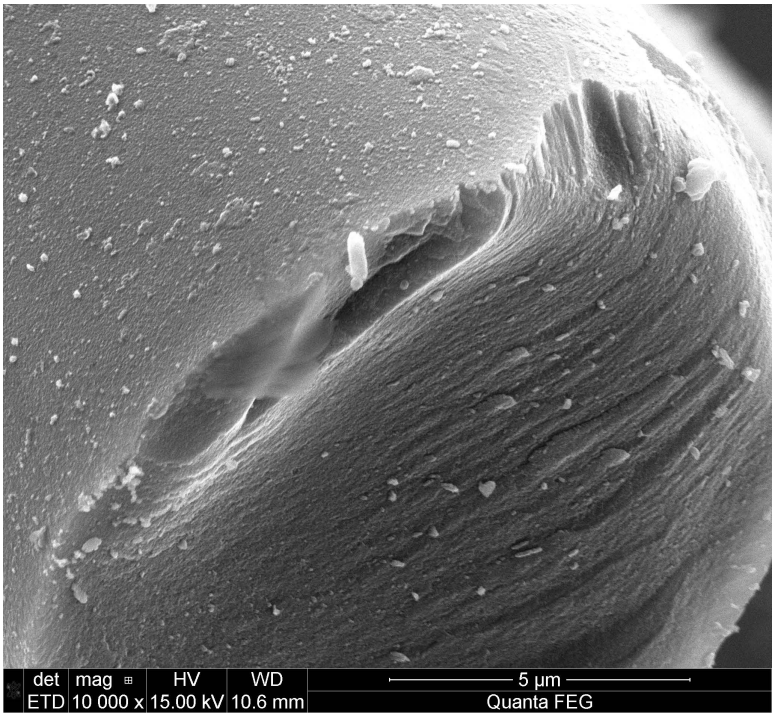

Figure 7.45: Hi-Nicalon S fiber specimen A16, tested in air at 800°C at 1032MPa

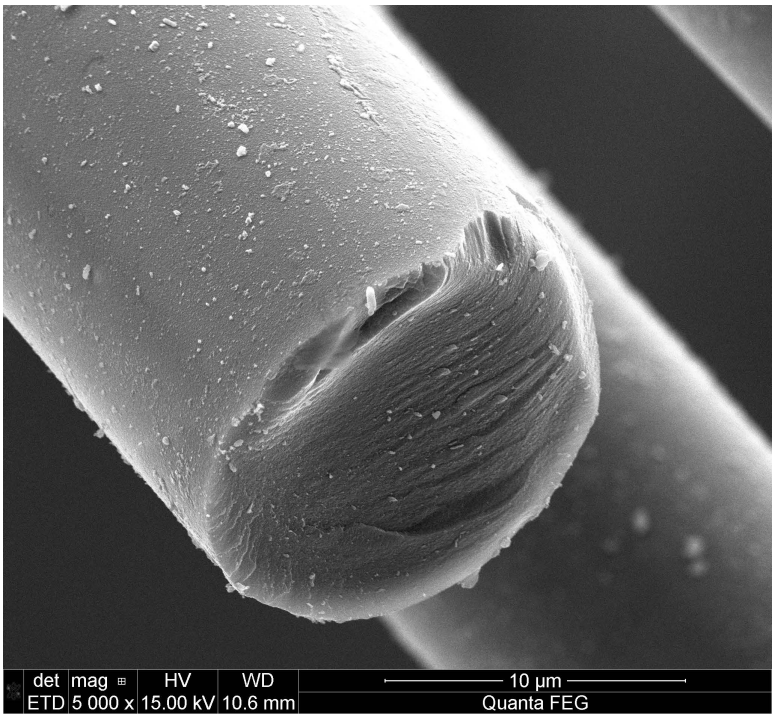

Figure 7.46: Hi-Nicalon S fiber specimen A16, tested in air at 800°C at 1032MPa

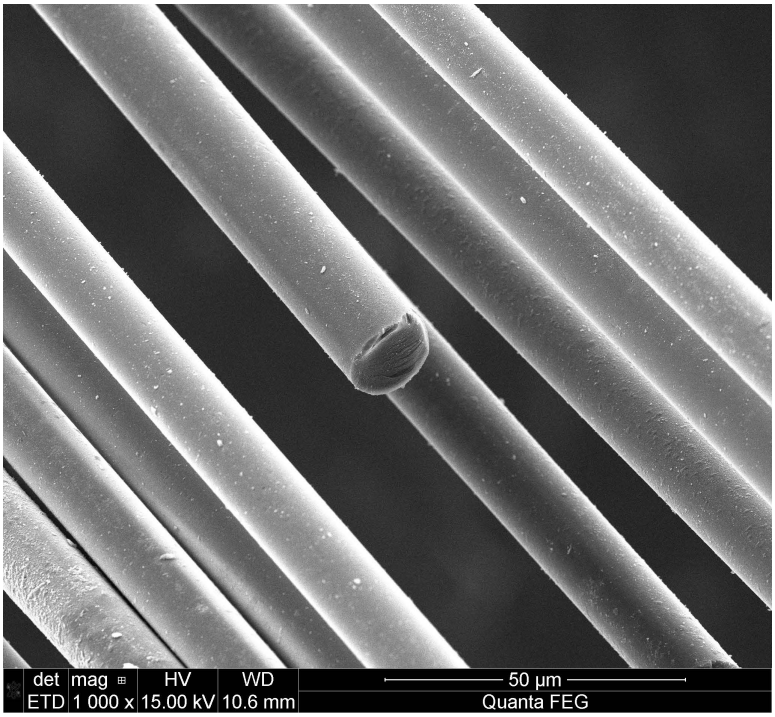

Figure 7.47: Hi-Nicalon S fiber specimen A16, tested in air at 800°C at 1032MPa

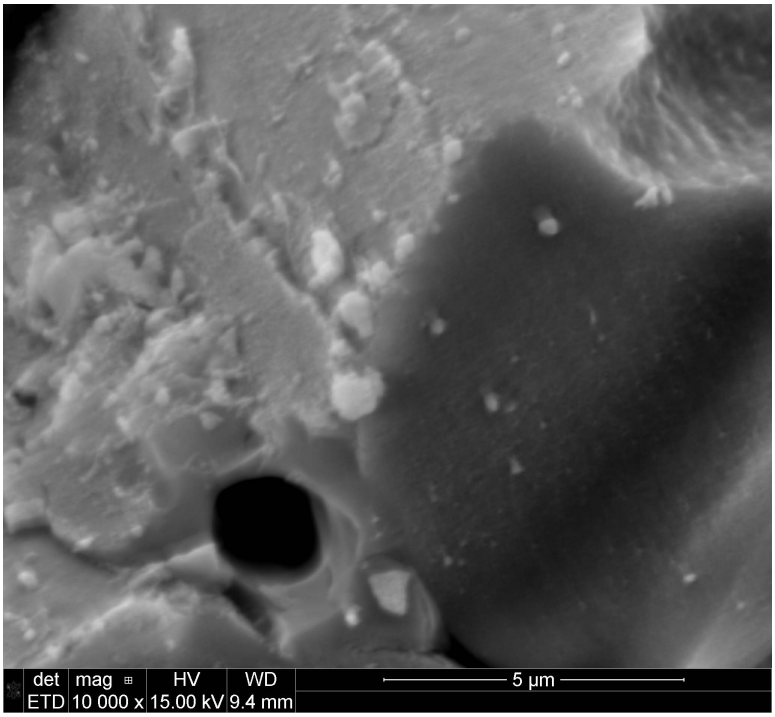

Figure 7.48: Hi-Nicalon S fiber specimen S19, tested in steam at 800°C at 154MPa

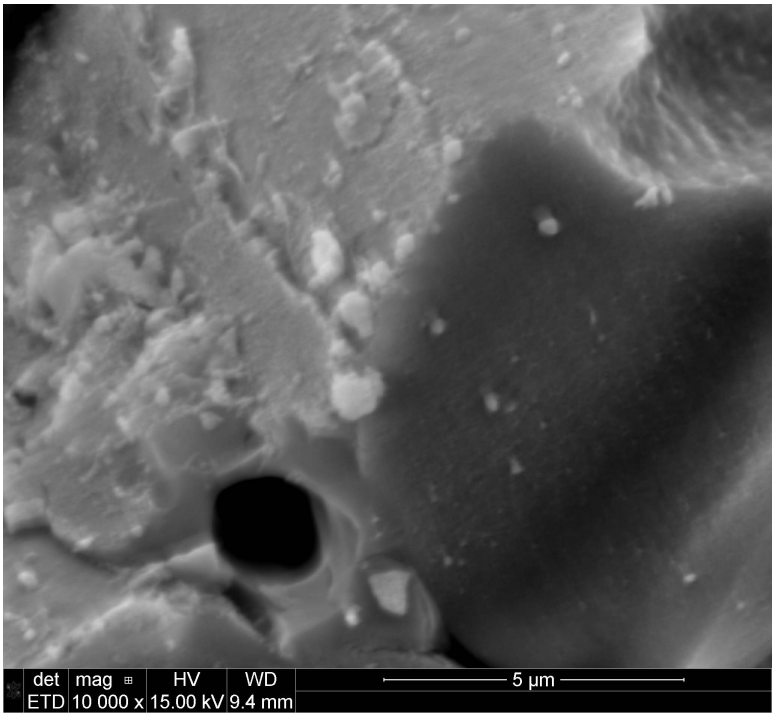

Figure 7.49: Hi-Nicalon S fiber specimen S19, tested in steam at 800°C at 154MPa

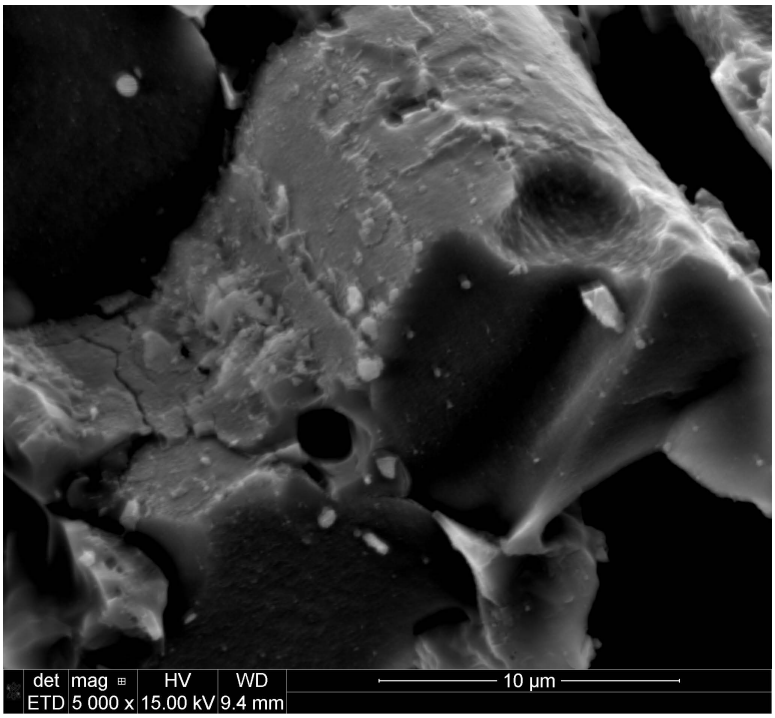

Figure 7.50: Hi-Nicalon S fiber specimen S19, tested in steam at 800°C at 154MPa

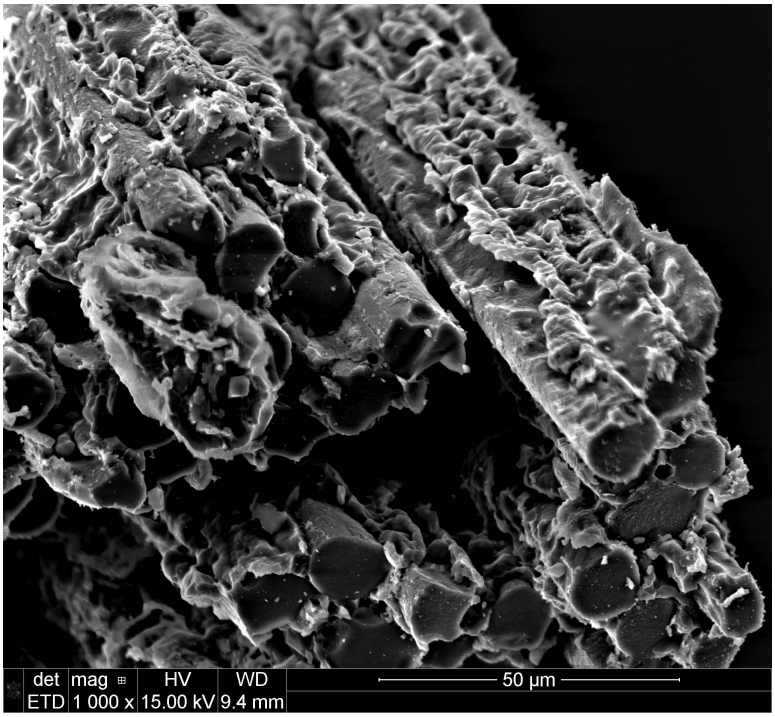

Figure 7.51: Hi-Nicalon S fiber specimen S19, tested in steam at 800°C at 154MPa

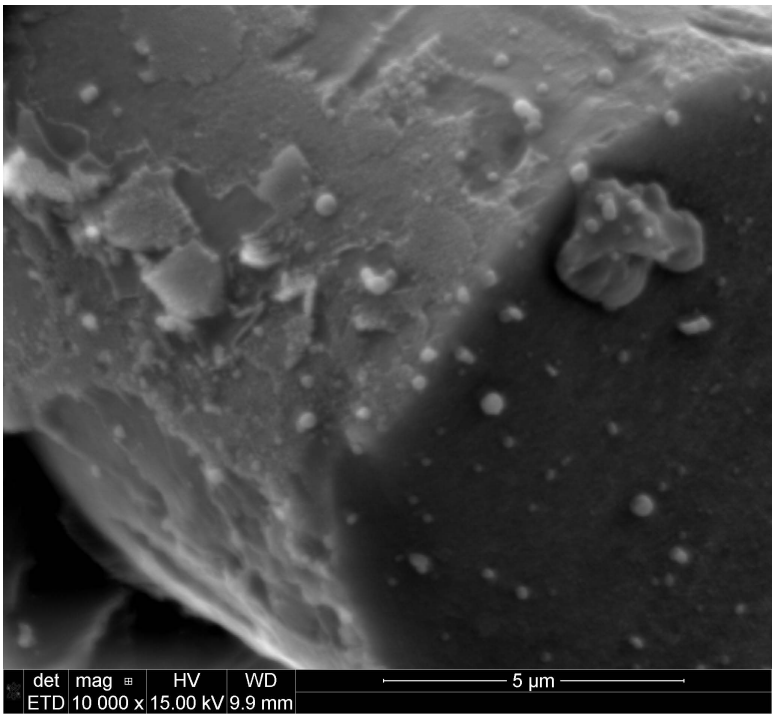

Figure 7.52: Hi-Nicalon S fiber specimen S19, tested in steam at 800°C at 154MPa

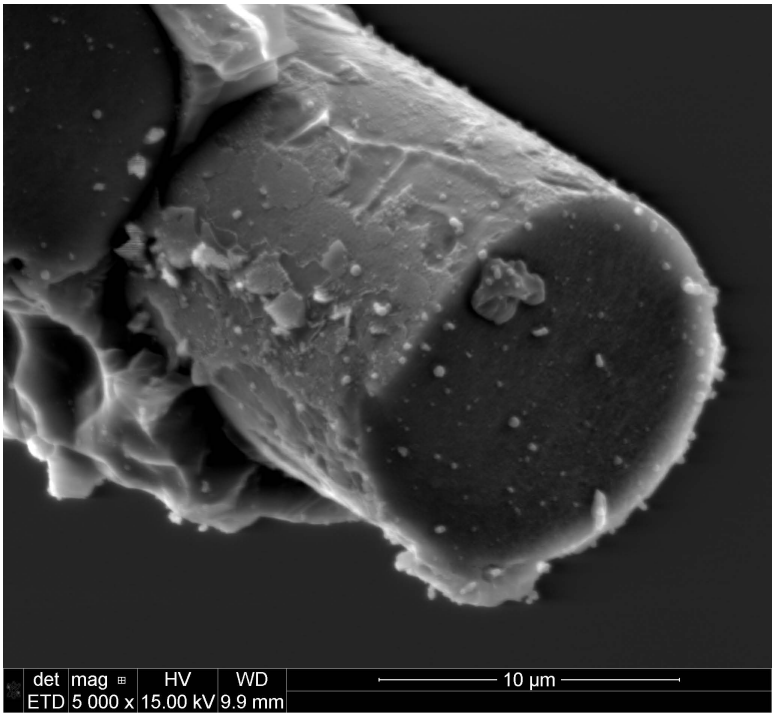

Figure 7.53: Hi-Nicalon S fiber specimen S19, tested in steam at 800°C at 154MPa

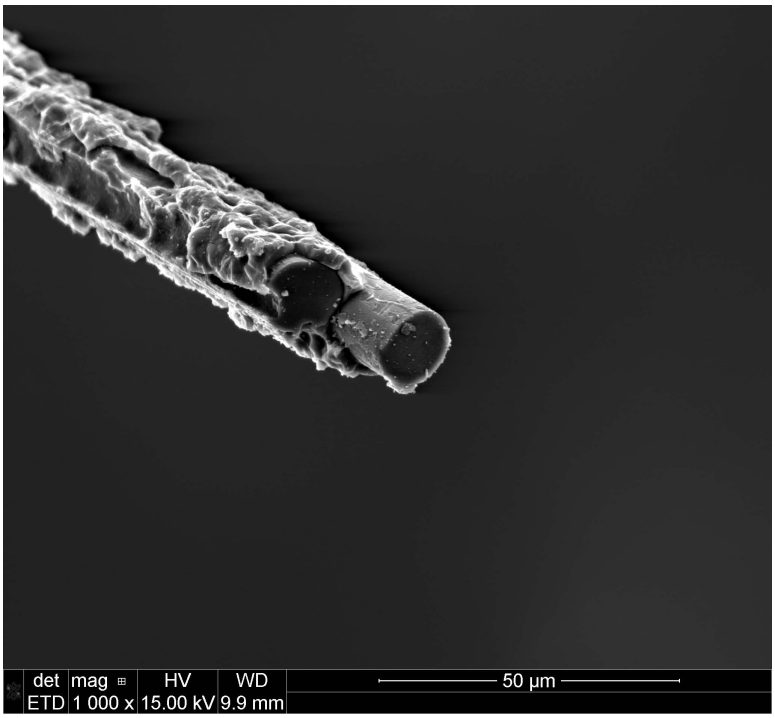

Figure 7.54: Hi-Nicalon S fiber specimen S19, tested in steam at 800°C at 154MPa

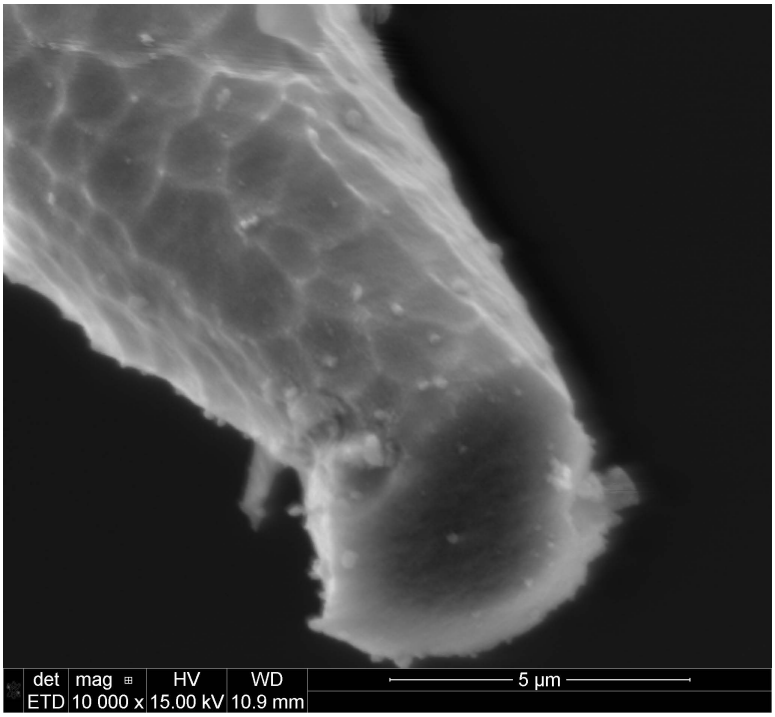

Figure 7.55: Hi-Nicalon S fiber specimen S19, tested in steam at 800°C at 154MPa

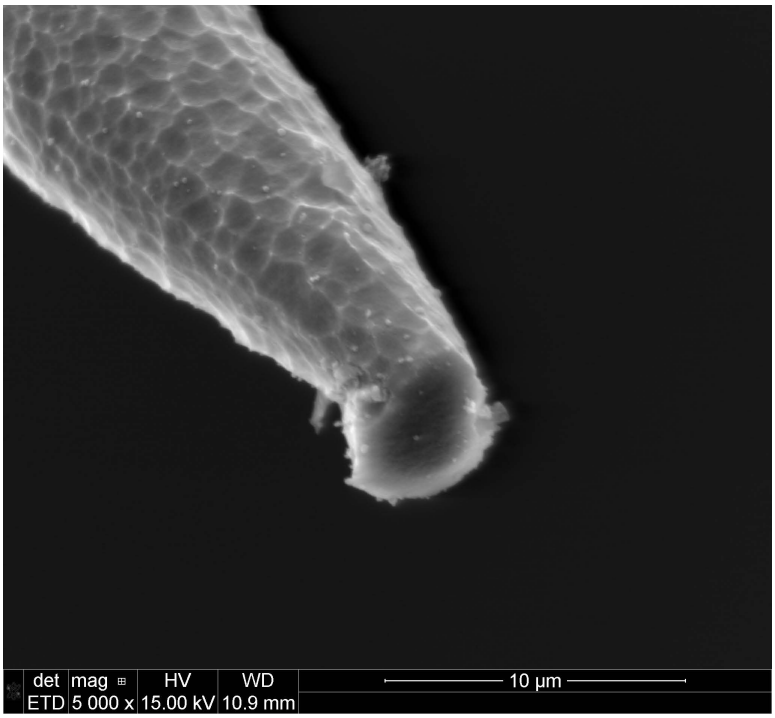

Figure 7.56: Hi-Nicalon S fiber specimen S19, tested in steam at 800°C at 154MPa

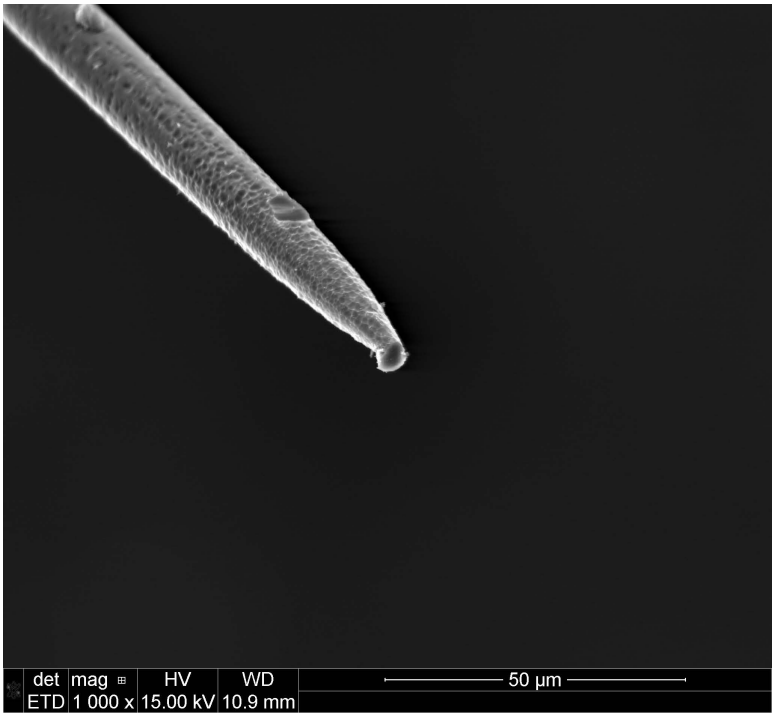

Figure 7.57: Hi-Nicalon S fiber specimen S19, tested in steam at 800°C at 154MPa

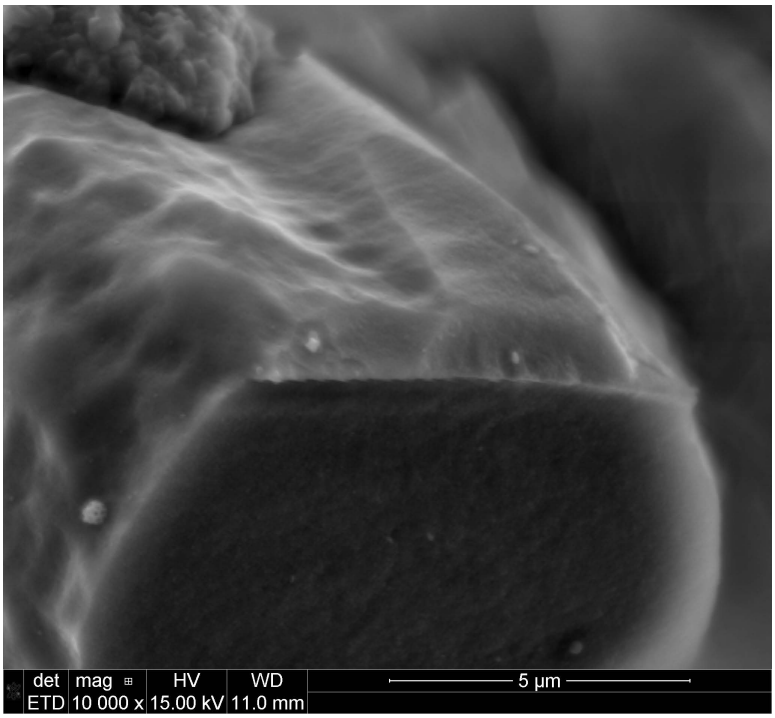

Figure 7.58: Hi-Nicalon S fiber specimen S19, tested in steam at 800°C at 154MPa

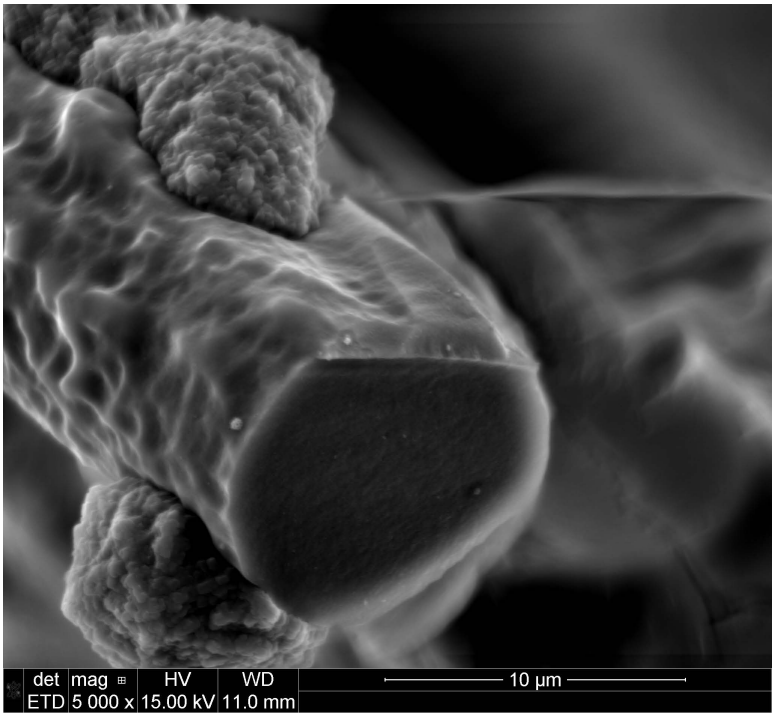

Figure 7.59: Hi-Nicalon S fiber specimen S19, tested in steam at 800°C at 154MPa

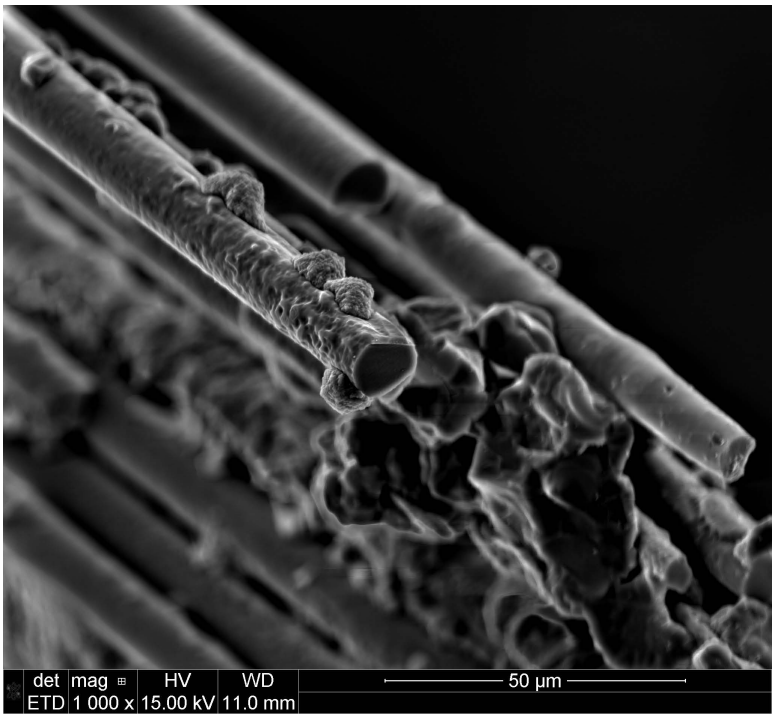

Figure 7.60: Hi-Nicalon S fiber specimen S19, tested in steam at 800°C at 154MPa

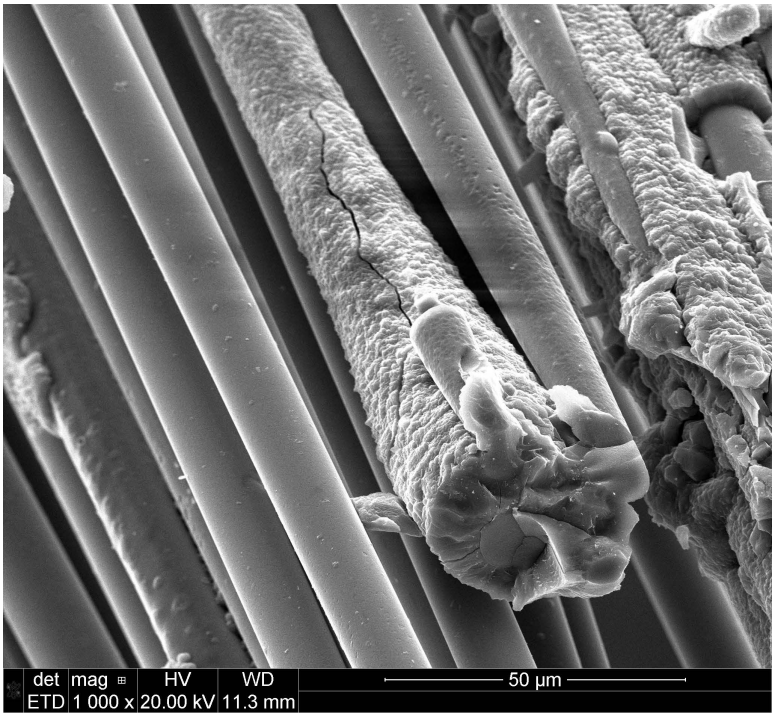

Figure 7.61: Hi-Nicalon S fiber specimen S19, tested in steam at 800°C at 154MPa

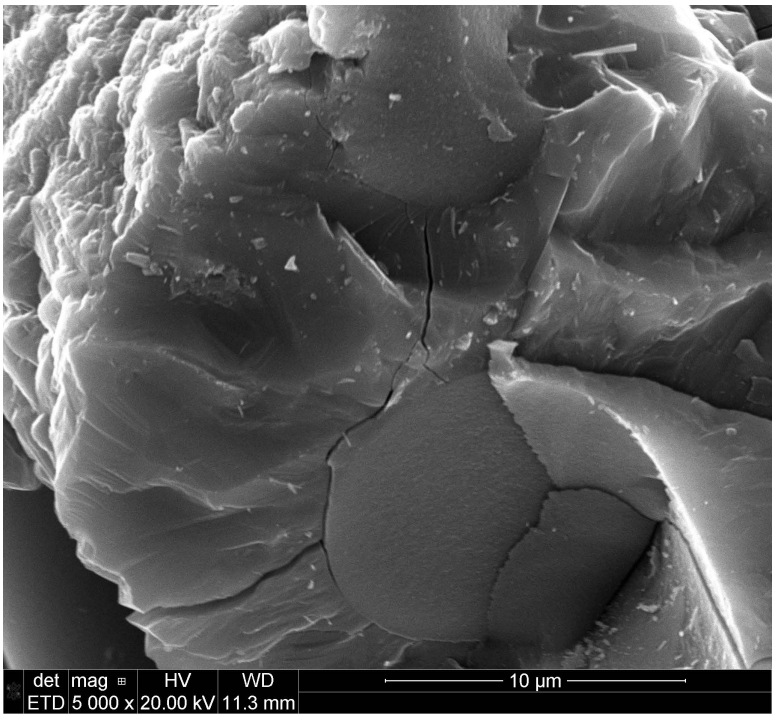

Figure 7.62: Hi-Nicalon S fiber specimen S19, tested in steam at 800°C at 154MPa

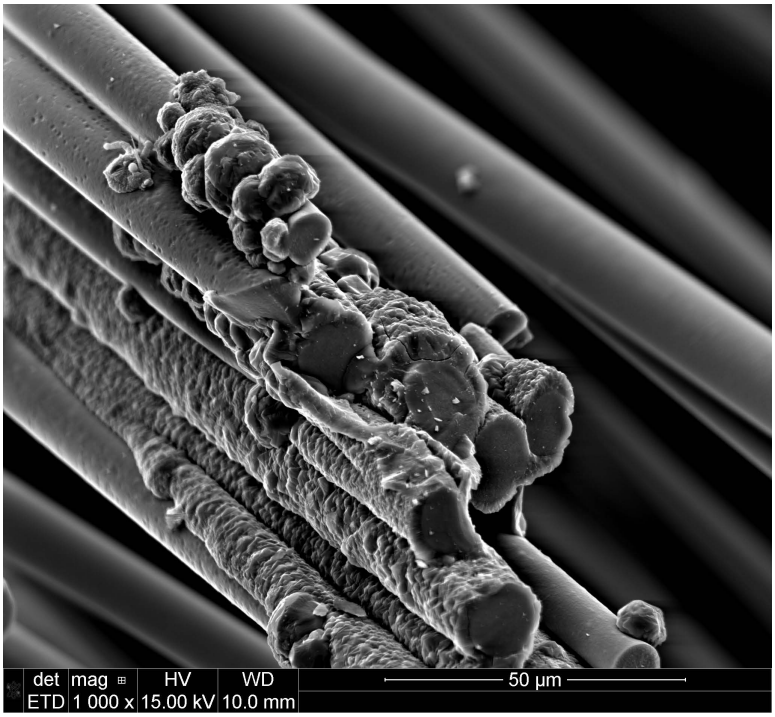

Figure 7.63: Hi-Nicalon S fiber specimen S24, tested in steam at 800°C at 154MPa

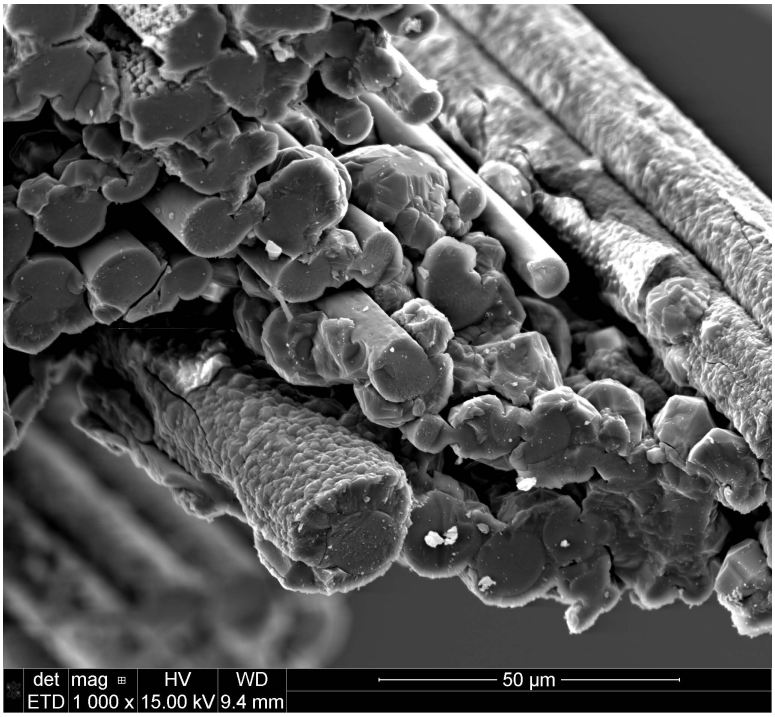

Figure 7.64: Hi-Nicalon S fiber specimen S24, tested in steam at 800°C at 154MPa

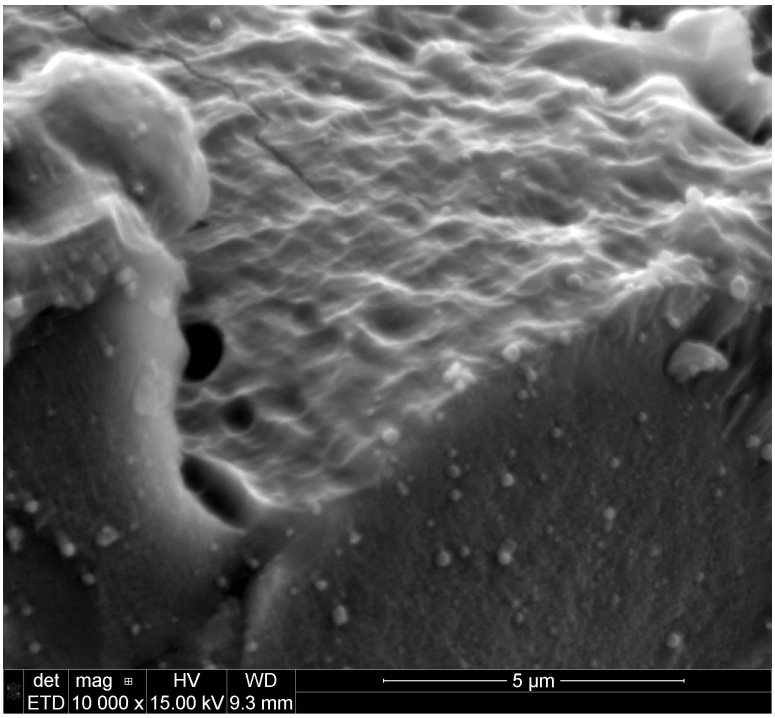

Figure 7.65: Hi-Nicalon S fiber specimen S24, tested in steam at 800°C at 154MPa

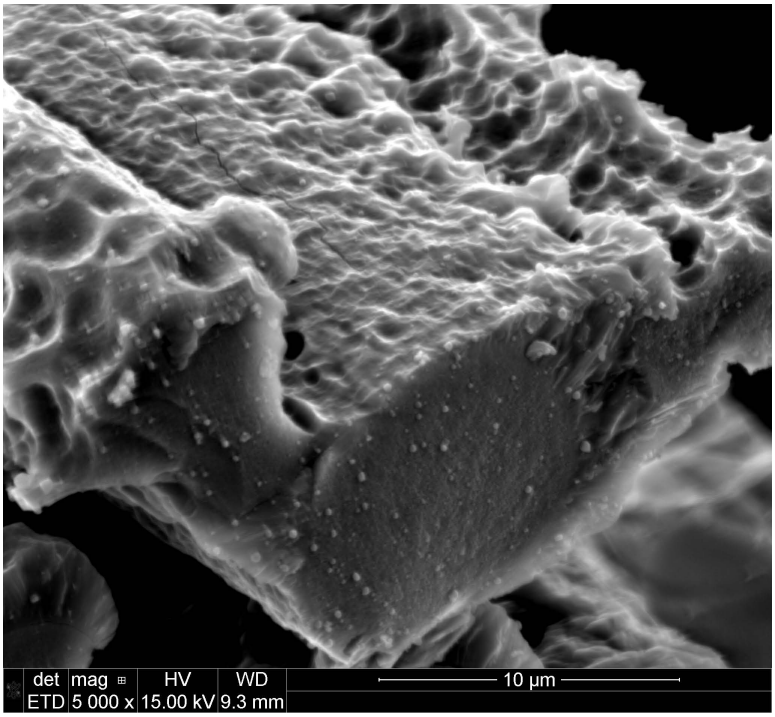

Figure 7.66: Hi-Nicalon S fiber specimen S24, tested in steam at 800°C at 154MPa

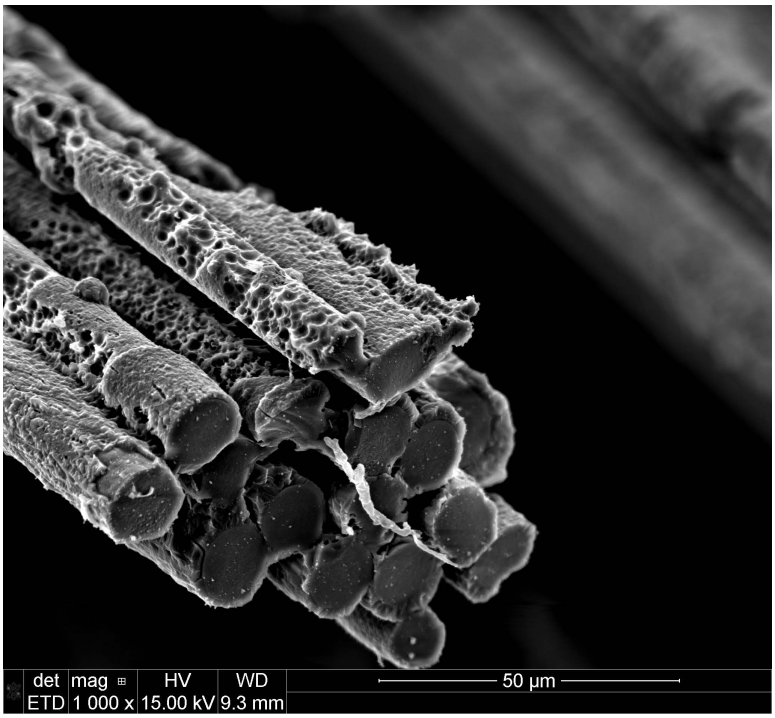

Figure 7.67: Hi-Nicalon S fiber specimen S24, tested in steam at 800°C at 154MPa

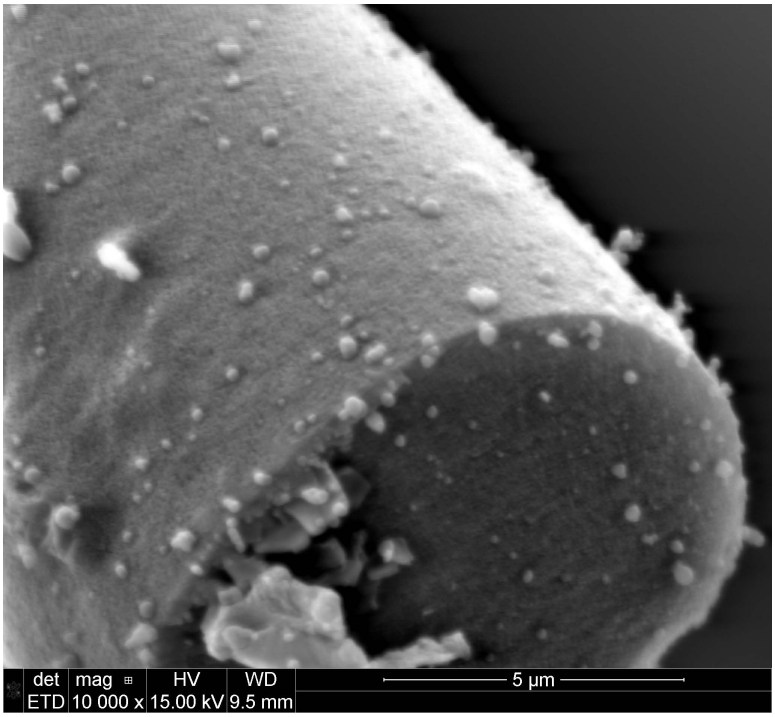

Figure 7.68: Hi-Nicalon S fiber specimen S24, tested in steam at 800°C at 154MPa

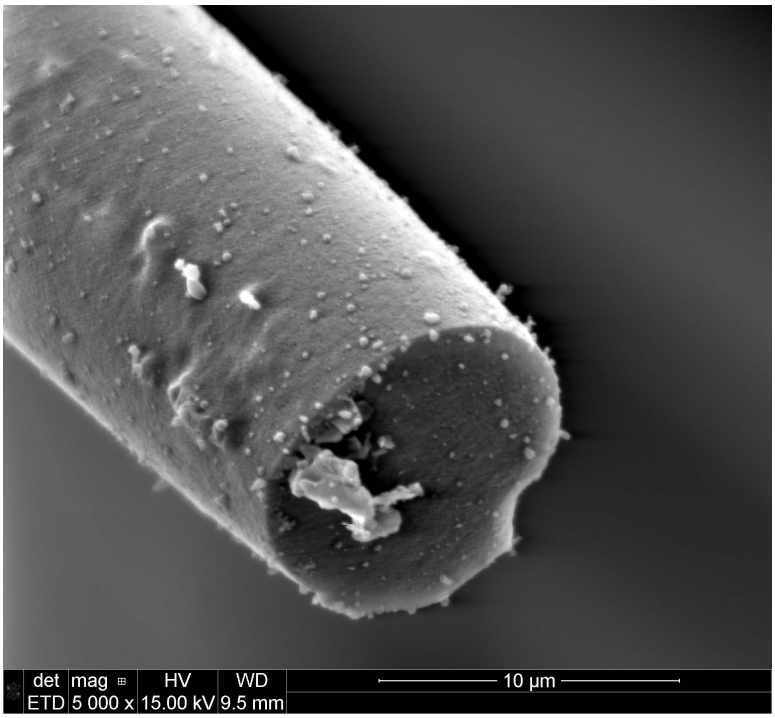

Figure 7.69: Hi-Nicalon S fiber specimen S24, tested in steam at 800°C at 154MPa

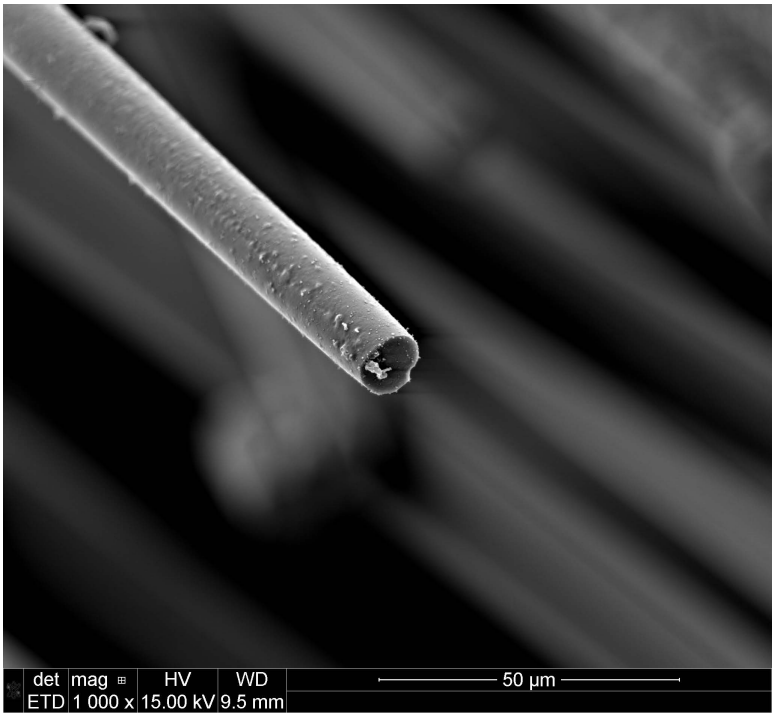

Figure 7.70: Hi-Nicalon S fiber specimen S24, tested in steam at 800°C at 154MPa

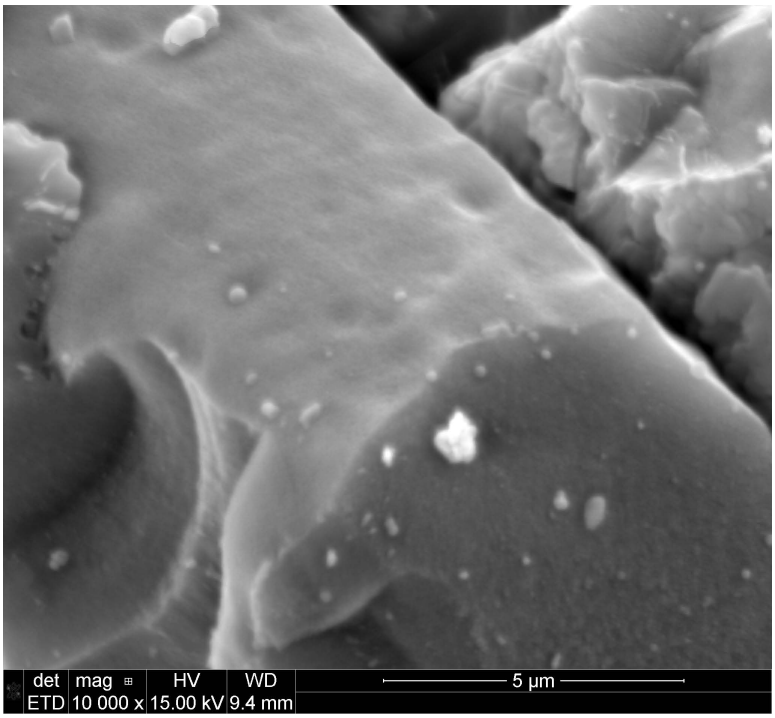

Figure 7.71: Hi-Nicalon S fiber specimen S24, tested in steam at 800°C at 154MPa

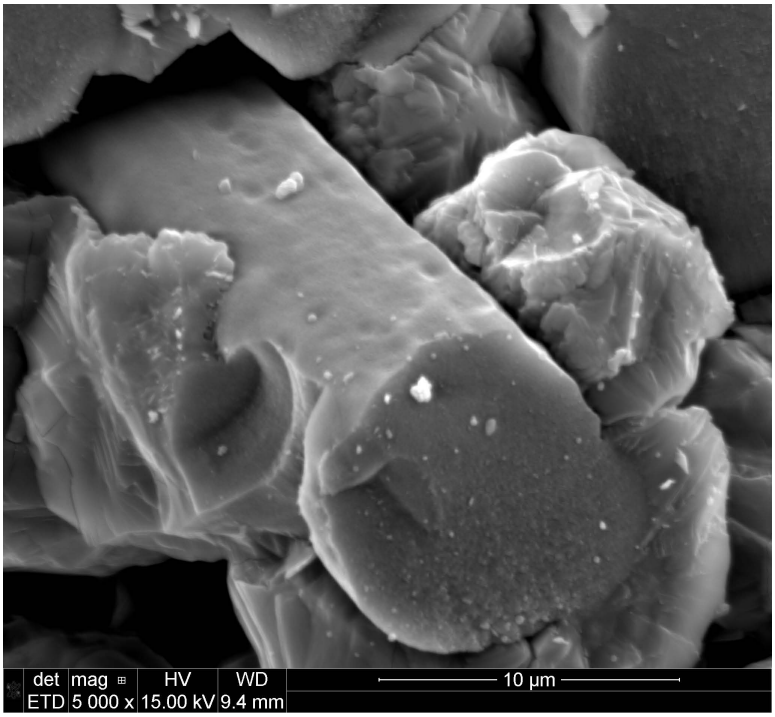

Figure 7.72: Hi-Nicalon S fiber specimen S24, tested in steam at 800°C at 154MPa

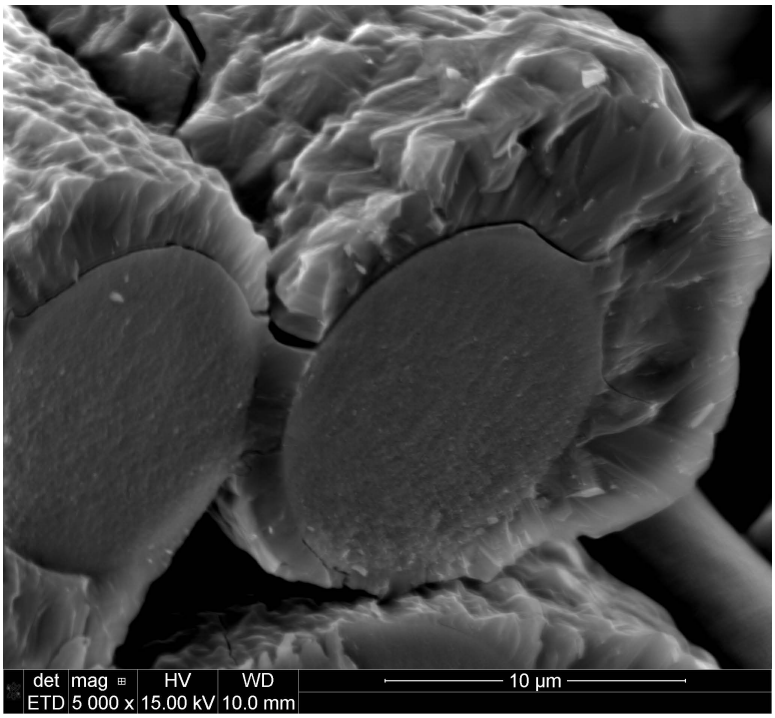

Figure 7.73: Hi-Nicalon S fiber specimen S24, tested in steam at 800°C at 154MPa

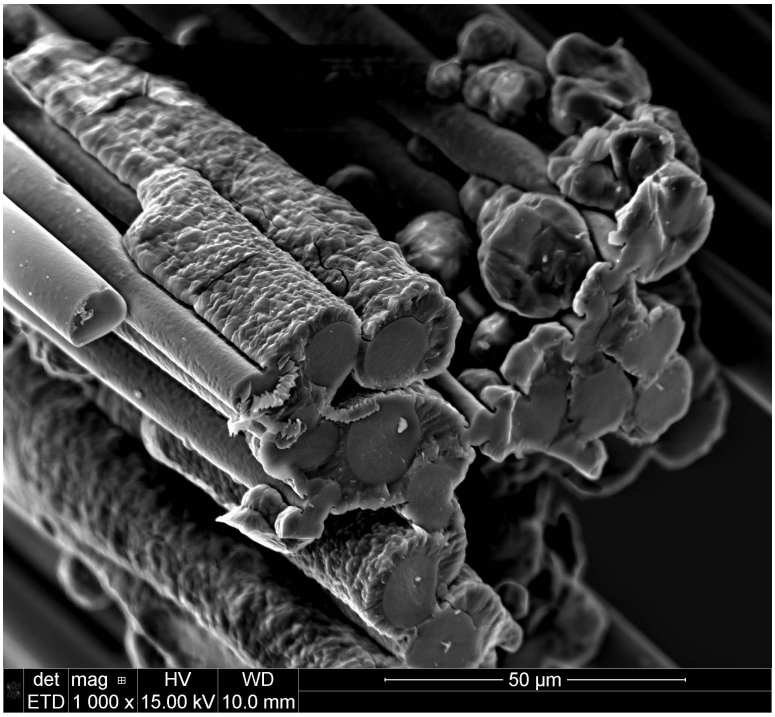

Figure 7.74: Hi-Nicalon S fiber specimen S24, tested in steam at 800°C at 154MPa

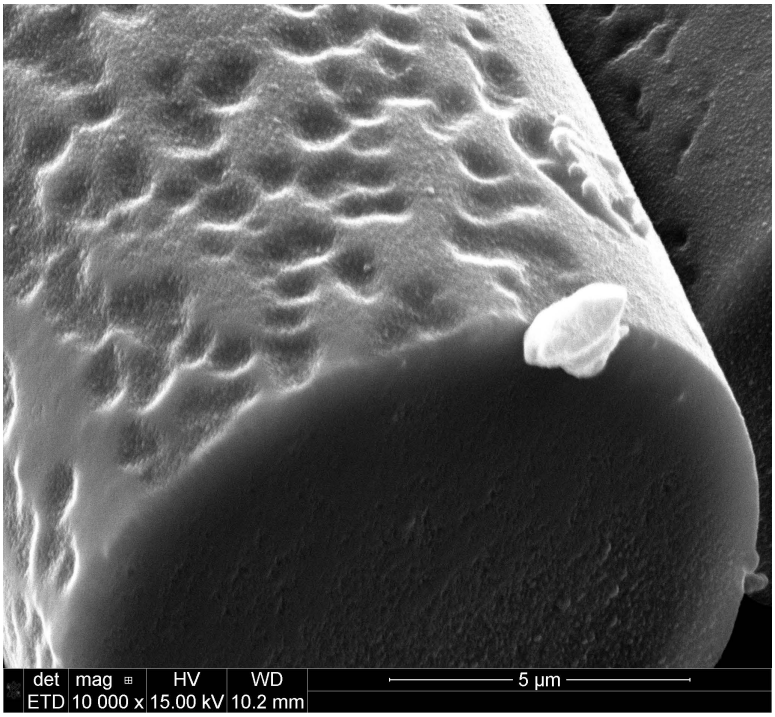

Figure 7.75: Hi-Nicalon S fiber specimen S49, tested in steam at 800°C at 255MPa

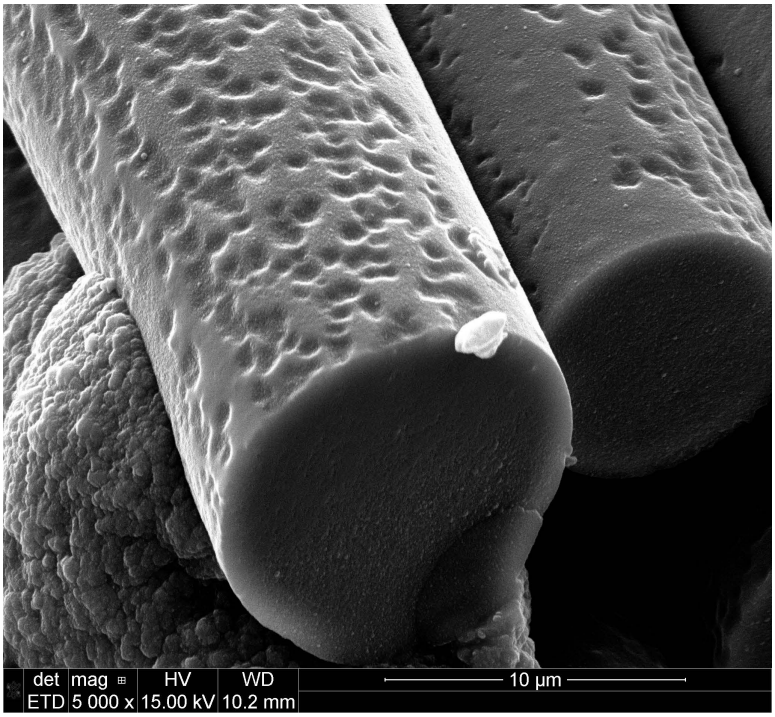

Figure 7.76: Hi-Nicalon S fiber specimen S49, tested in steam at 800°C at 255MPa

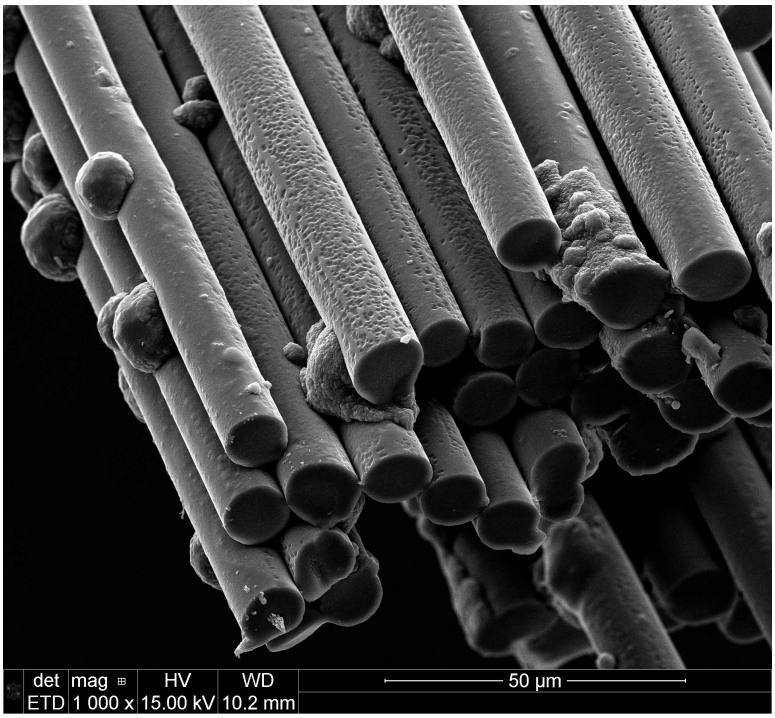

Figure 7.77: Hi-Nicalon S fiber specimen S49, tested in steam at 800°C at 255MPa

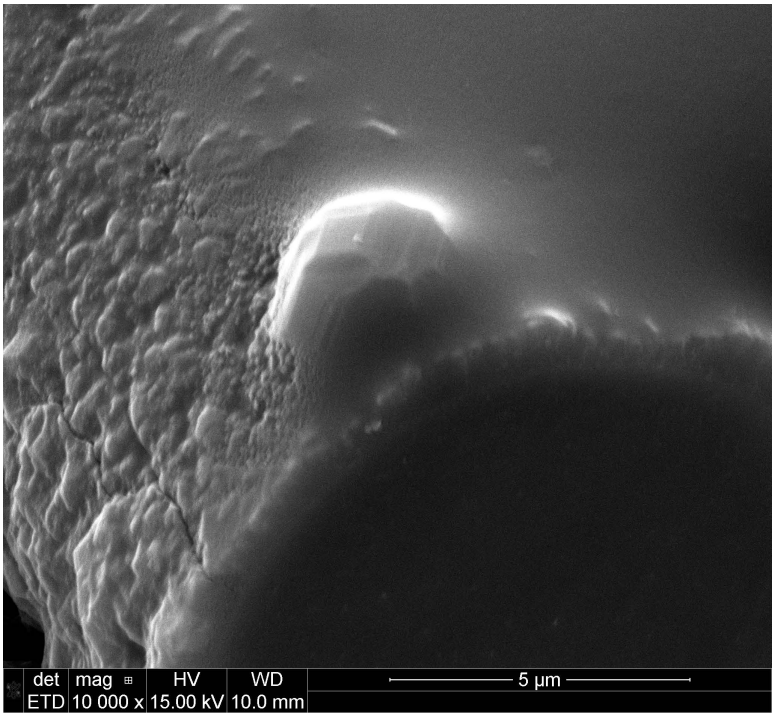

Figure 7.78: Hi-Nicalon S fiber specimen S49, tested in steam at 800°C at 255MPa

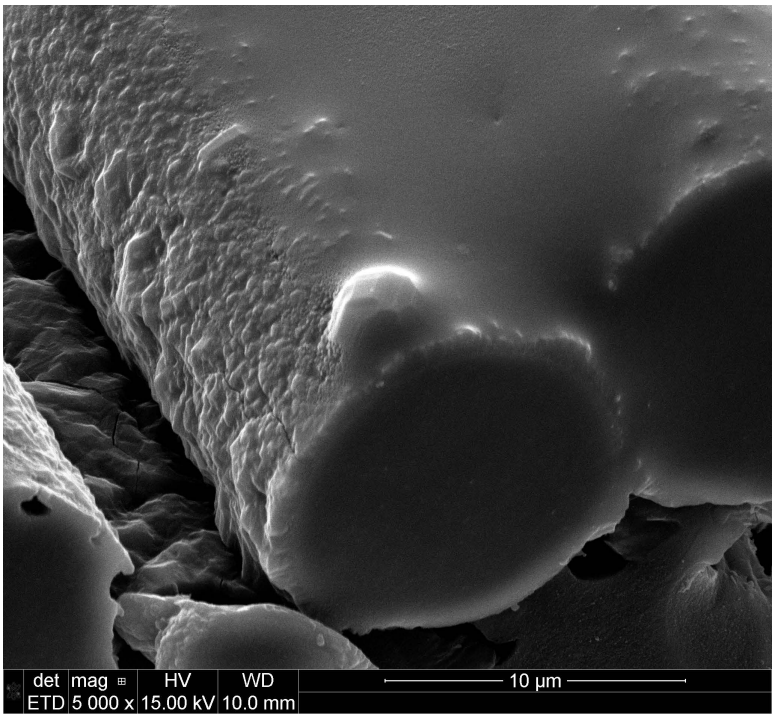

Figure 7.79: Hi-Nicalon S fiber specimen S49, tested in steam at 800°C at 255MPa

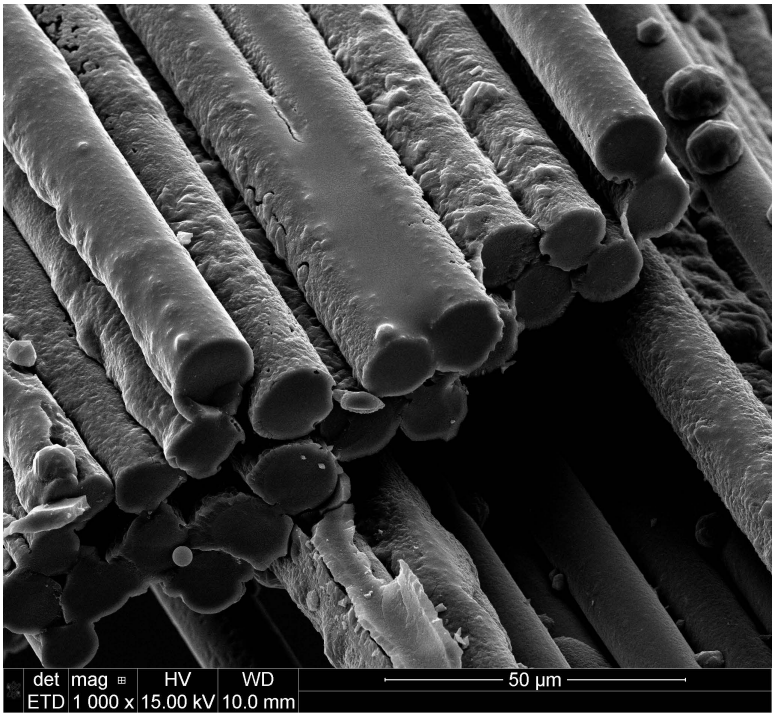

Figure 7.80: Hi-Nicalon S fiber specimen S49, tested in steam at 800°C at 255MPa

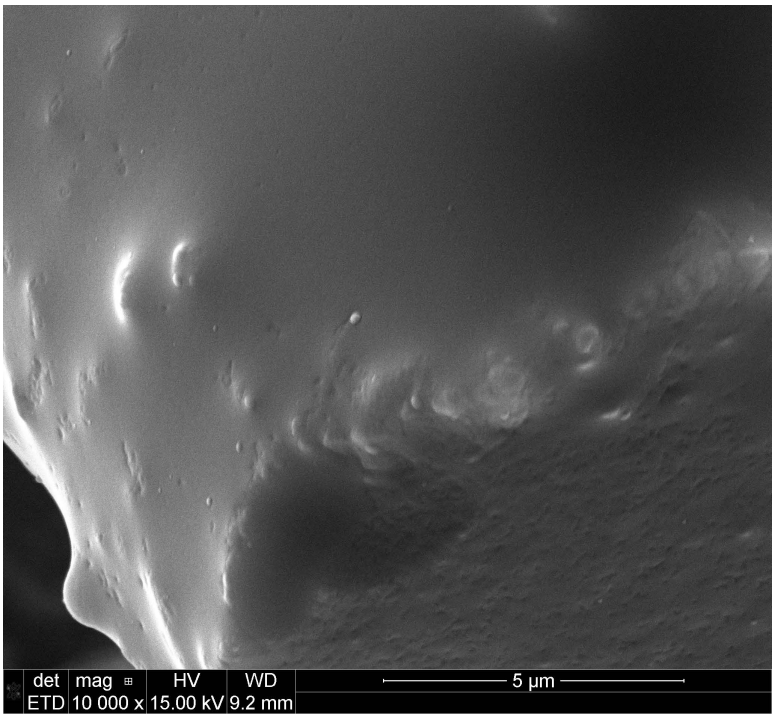

Figure 7.81: Hi-Nicalon S fiber specimen S49, tested in steam at 800°C at 255MPa

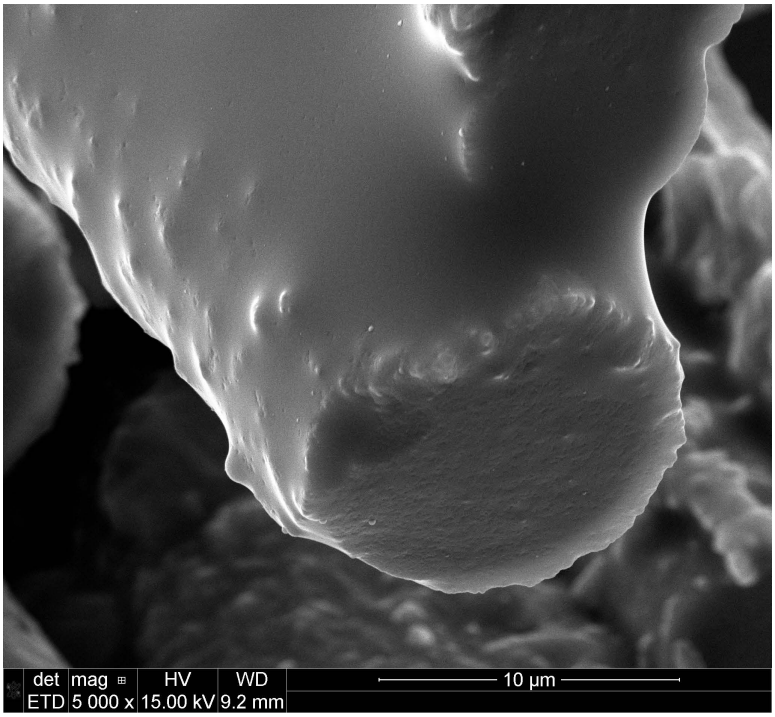

Figure 7.82: Hi-Nicalon S fiber specimen S49, tested in steam at 800°C at 255MPa

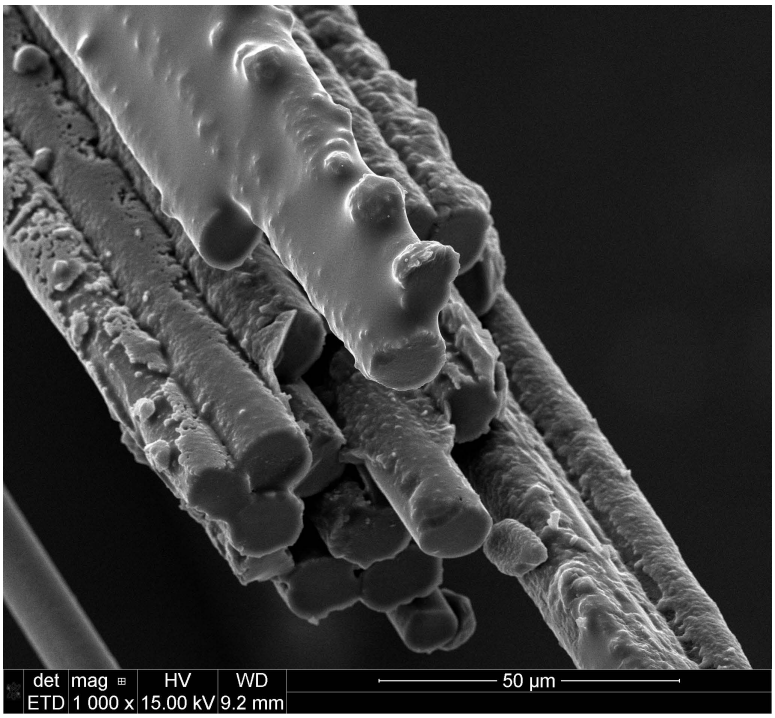

Figure 7.83: Hi-Nicalon S fiber specimen S49, tested in steam at 800°C at 255MPa

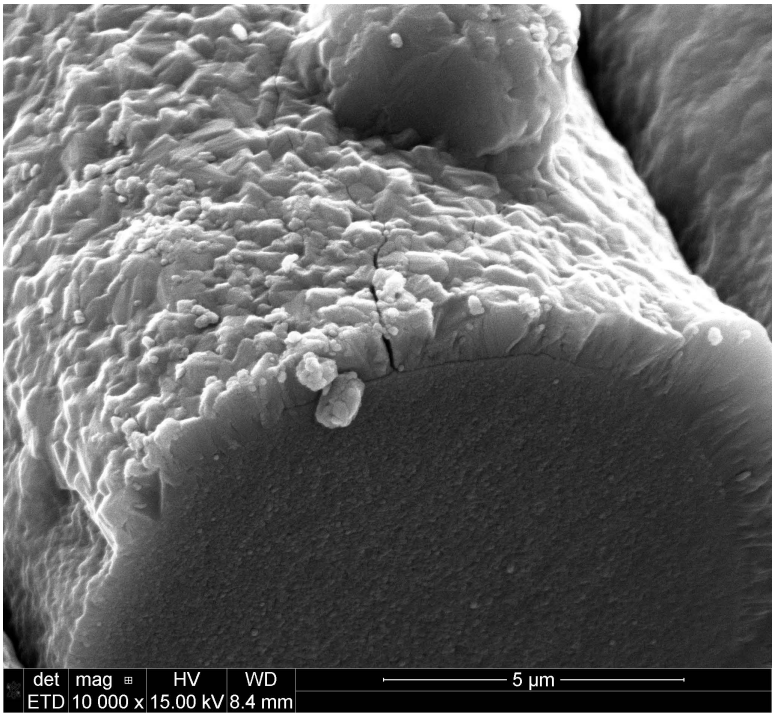

Figure 7.84: Hi-Nicalon S fiber specimen S50, tested in steam at 800°C at 353MPa

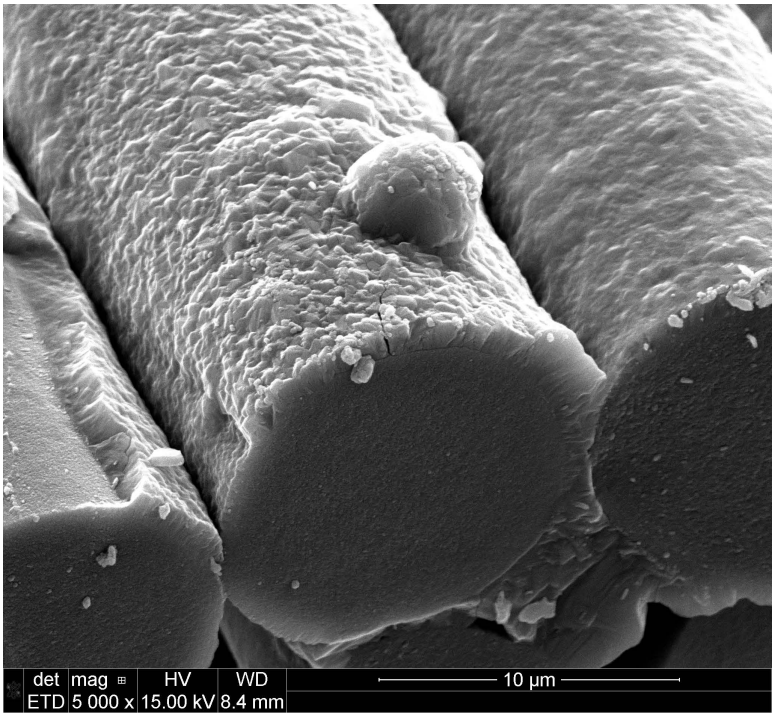

Figure 7.85: Hi-Nicalon S fiber specimen S50, tested in steam at 800°C at 353MPa

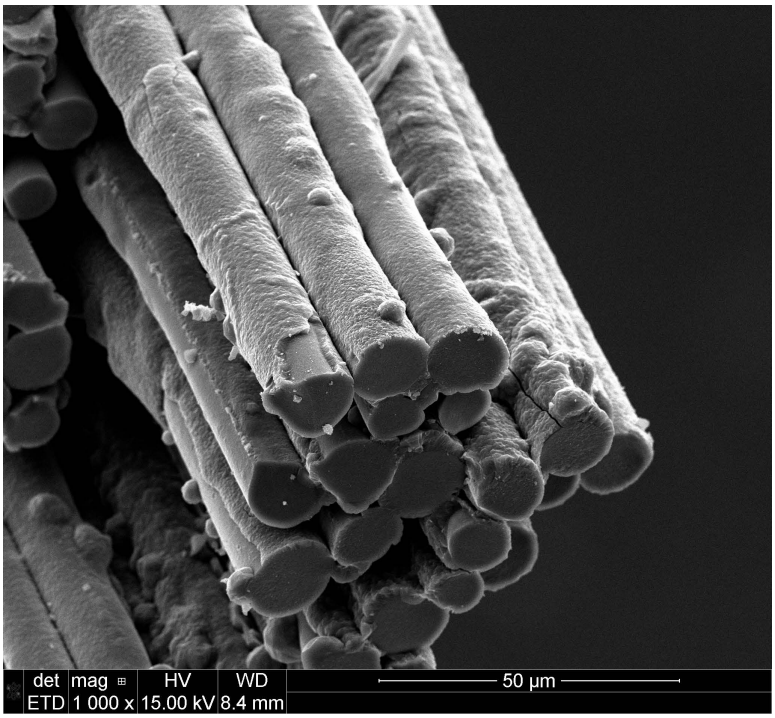

Figure 7.86: Hi-Nicalon S fiber specimen S50, tested in steam at 800°C at 353MPa

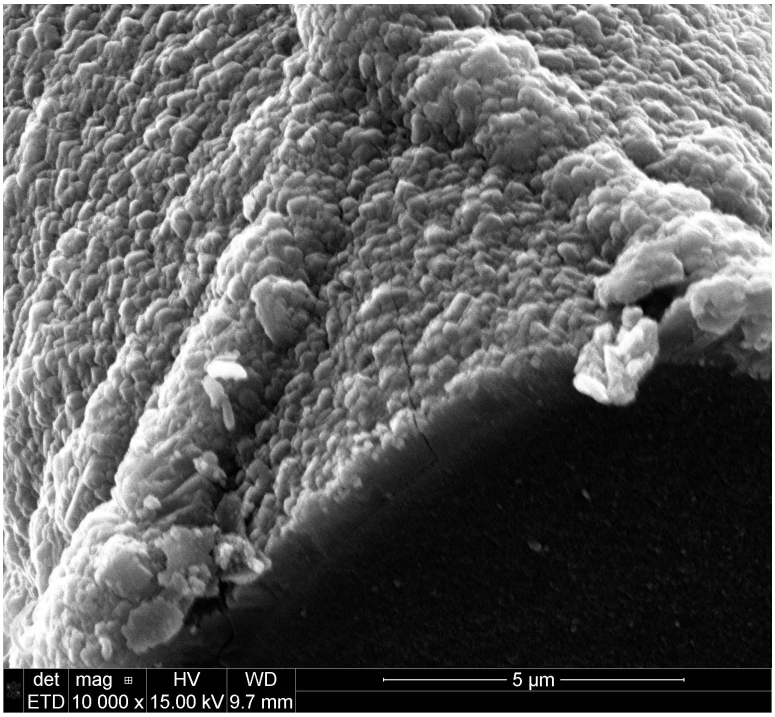

Figure 7.87: Hi-Nicalon S fiber specimen S50, tested in steam at 800°C at 353MPa

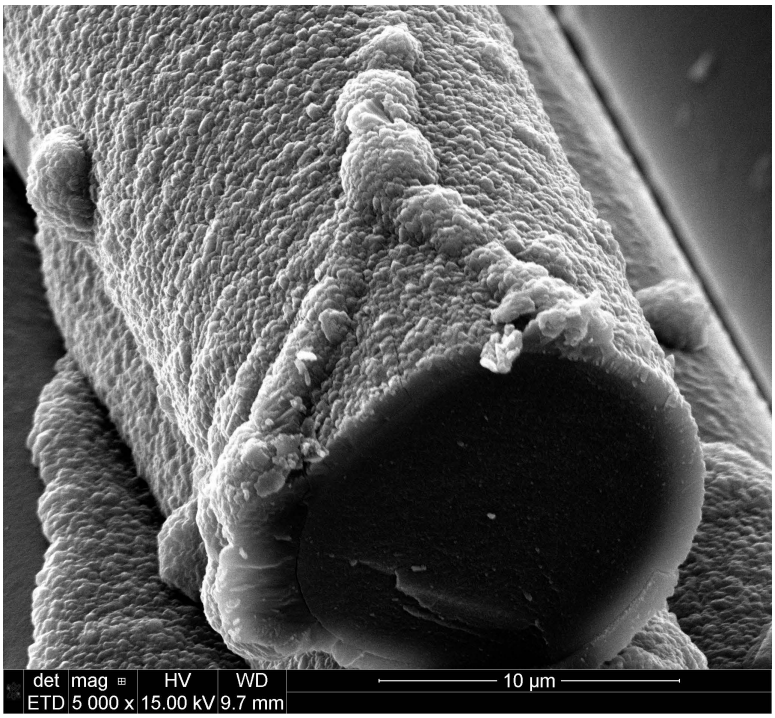

Figure 7.88: Hi-Nicalon S fiber specimen S50, tested in steam at 800°C at 353MPa

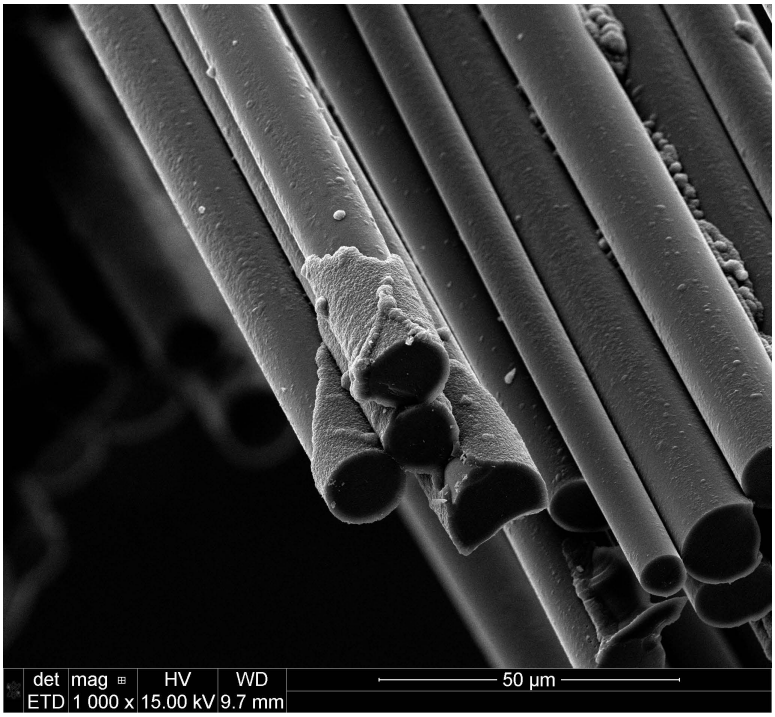

Figure 7.89: Hi-Nicalon S fiber specimen S50, tested in steam at 800°C at 353MPa

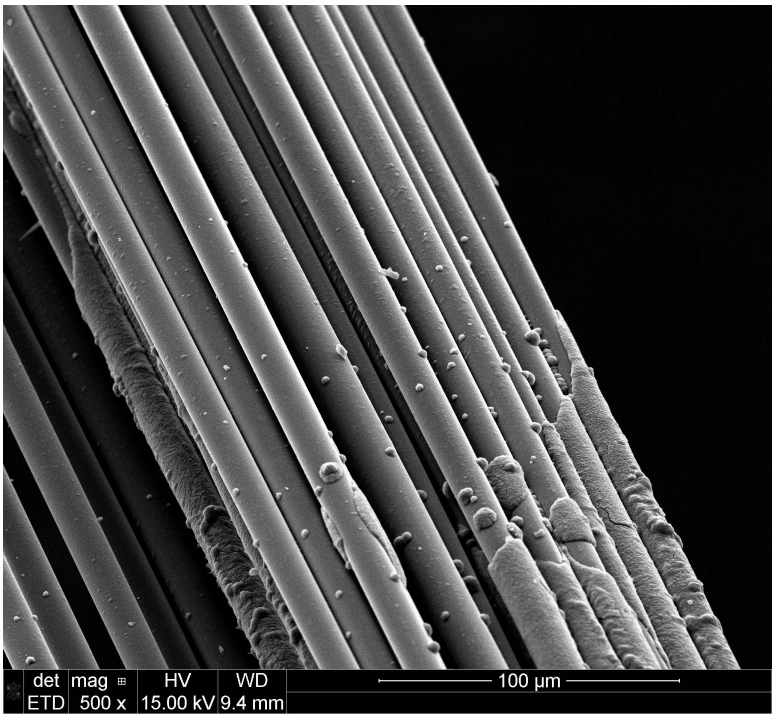

Figure 7.90: Hi-Nicalon S fiber specimen S50, tested in steam at 800°C at 353MPa

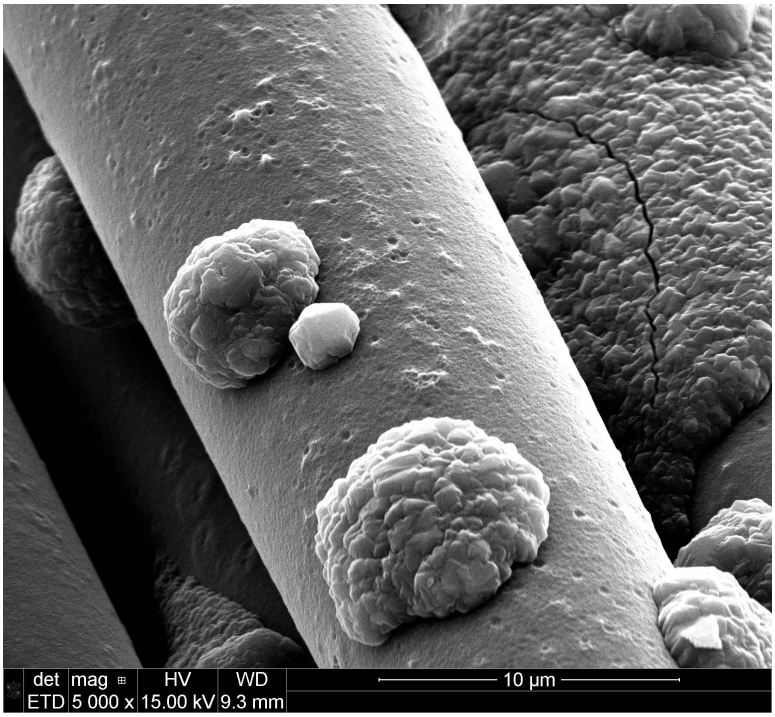

Figure 7.91: Hi-Nicalon S fiber specimen S50, tested in steam at 800°C at 353MPa

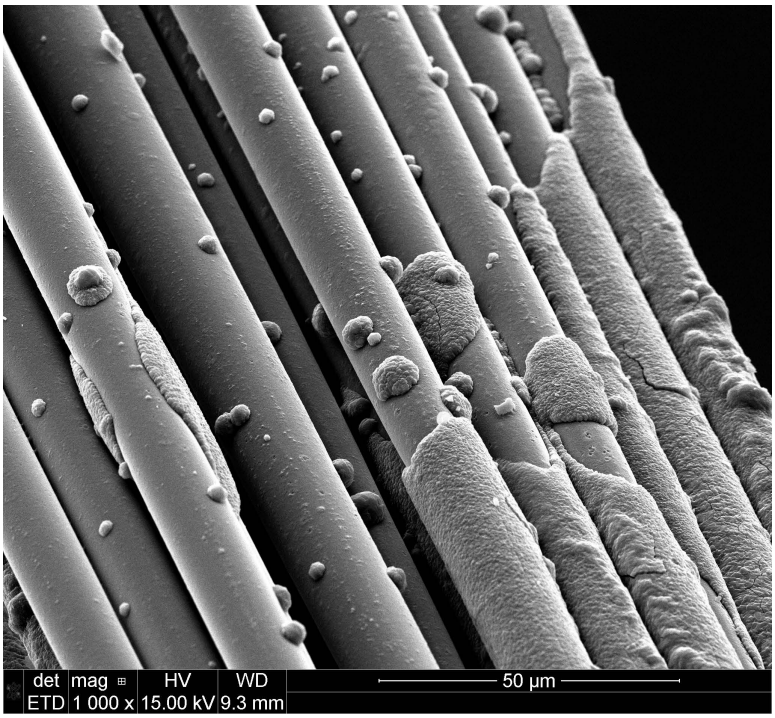

Figure 7.92: Hi-Nicalon S fiber specimen S50, tested in steam at 800°C at 353MPa

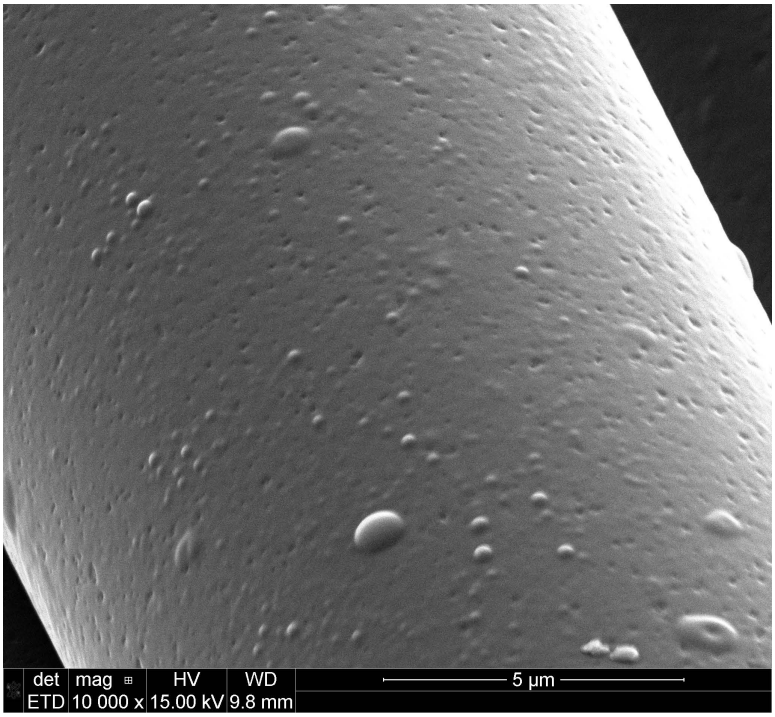

Figure 7.93: Hi-Nicalon S fiber specimen S50, tested in steam at 800°C at 353MPa

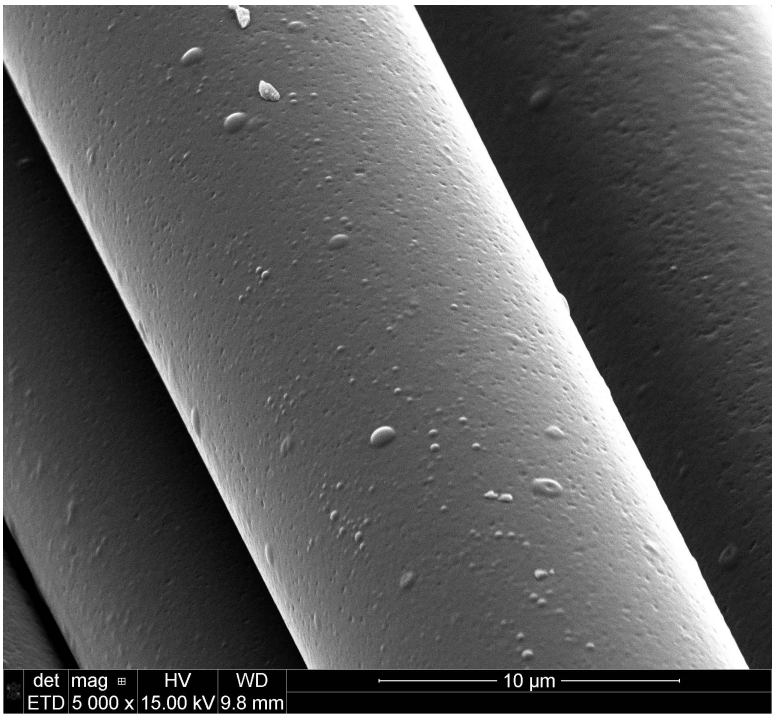

Figure 7.94: Hi-Nicalon S fiber specimen S50, tested in steam at 800°C at 353MPa

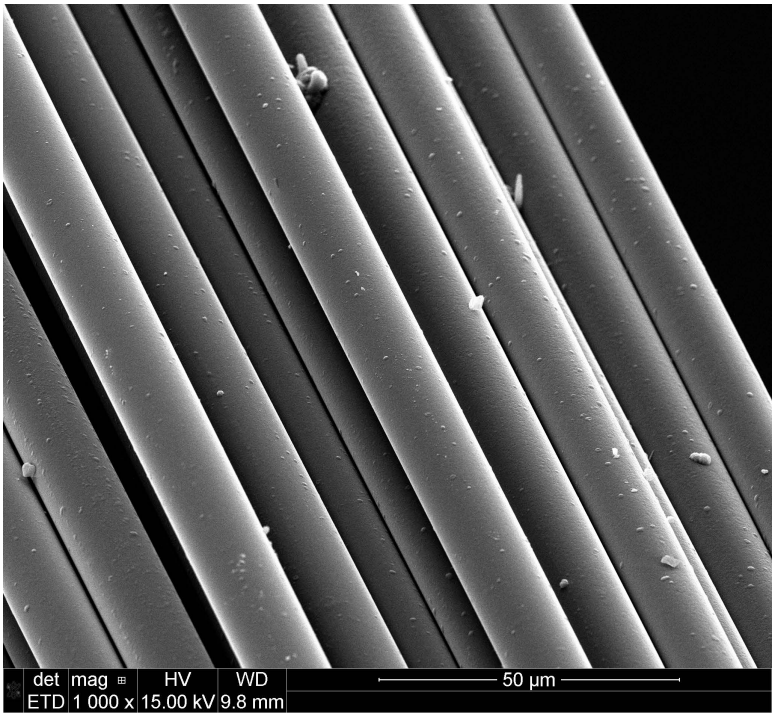

Figure 7.95: Hi-Nicalon S fiber specimen S50, tested in steam at 800°C at 353MPa

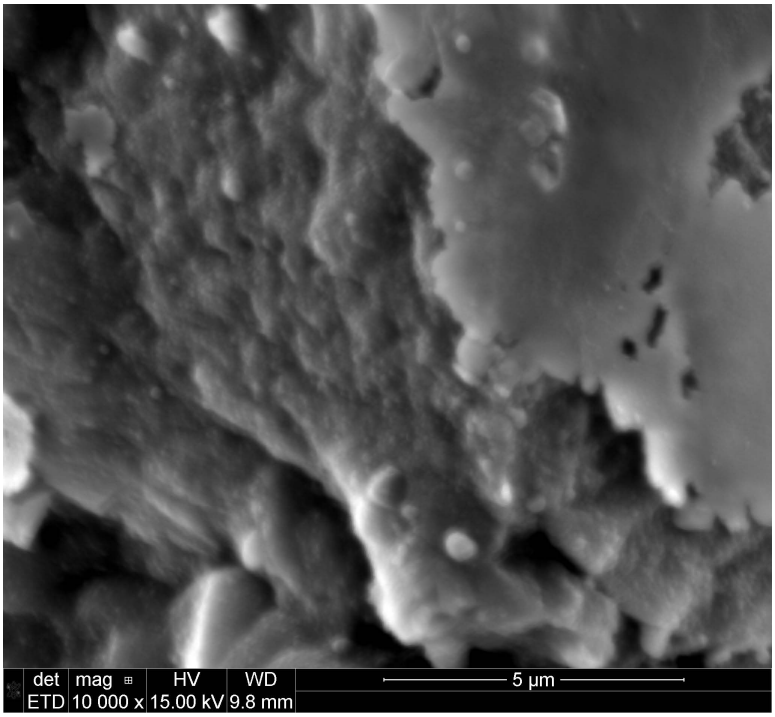

Figure 7.96: Hi-Nicalon S fiber specimen S21, tested in steam at 800°C at 400MPa

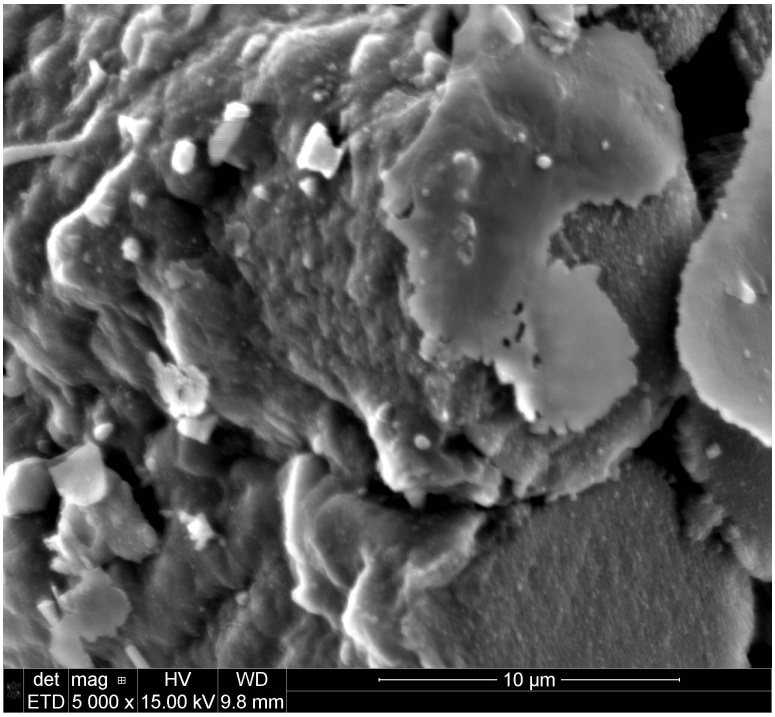

Figure 7.97: Hi-Nicalon S fiber specimen S21, tested in steam at 800°C at 400MPa

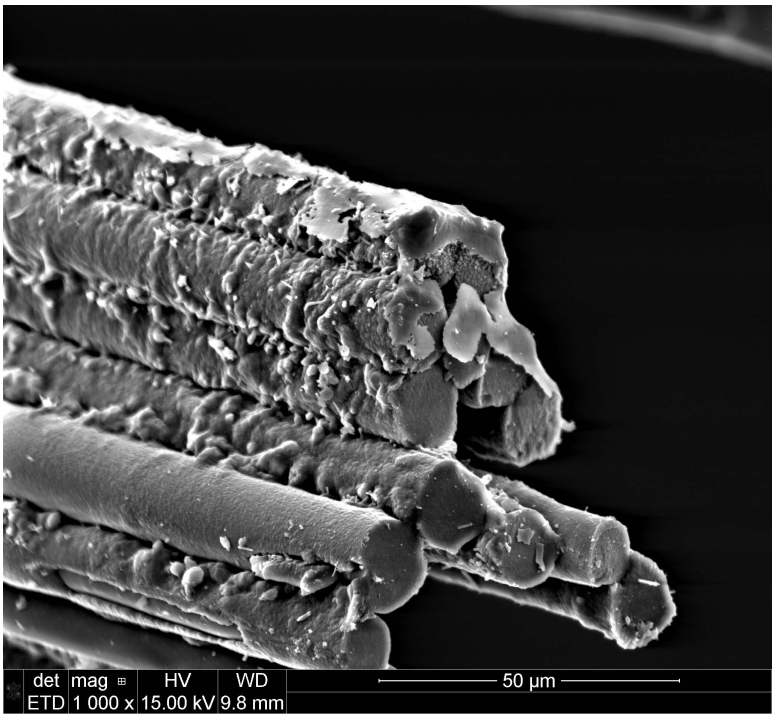

Figure 7.98: Hi-Nicalon S fiber specimen S21, tested in steam at 800°C at 400MPa

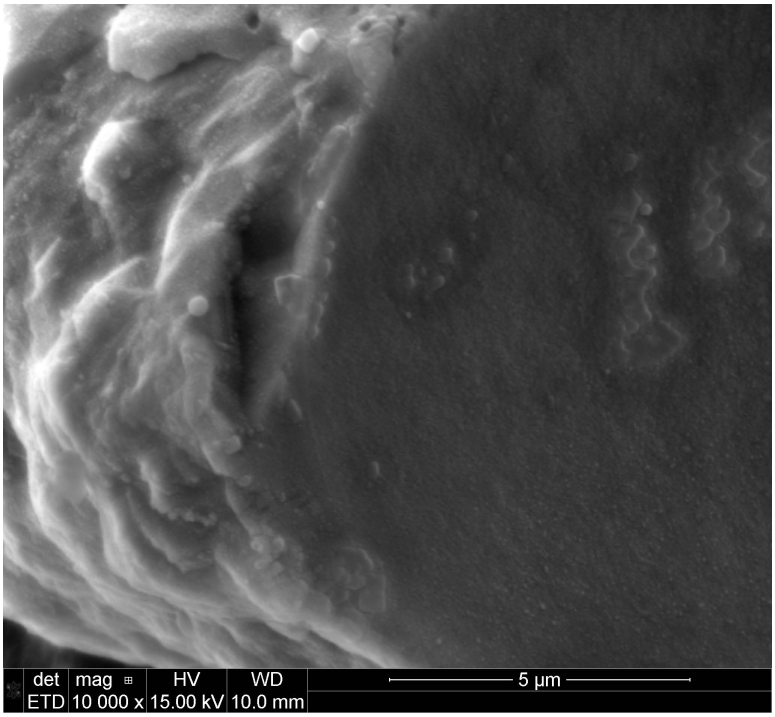

Figure 7.99: Hi-Nicalon S fiber specimen S21, tested in steam at 800°C at 400MPa

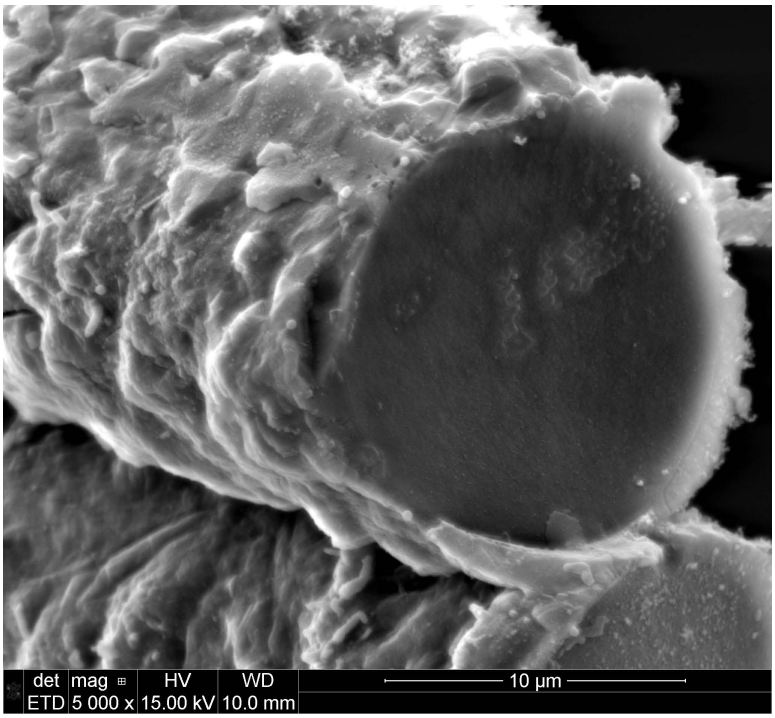

Figure 7.100: Hi-Nicalon S fiber specimen S21, tested in steam at 800°C at 400MPa

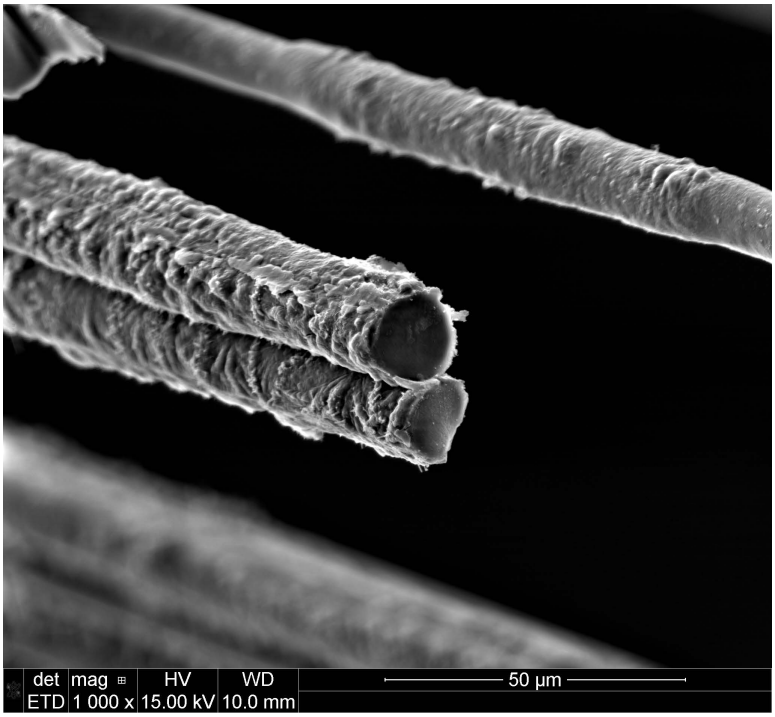

Figure 7.101: Hi-Nicalon S fiber specimen S21, tested in steam at 800°C at 400MPa

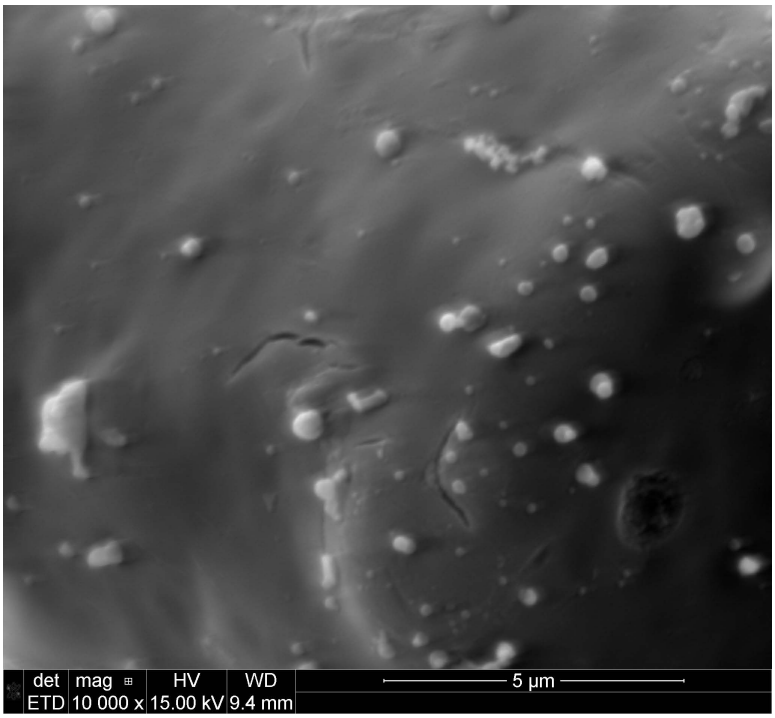

Figure 7.102: Hi-Nicalon S fiber specimen S21, tested in steam at 800°C at 400MPa

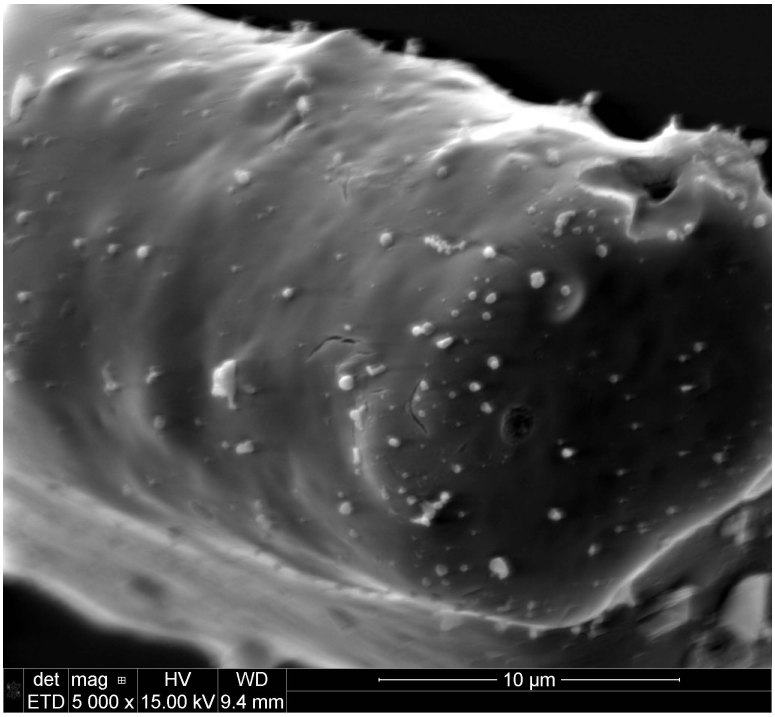

Figure 7.103: Hi-Nicalon S fiber specimen S21, tested in steam at 800°C at 400MPa

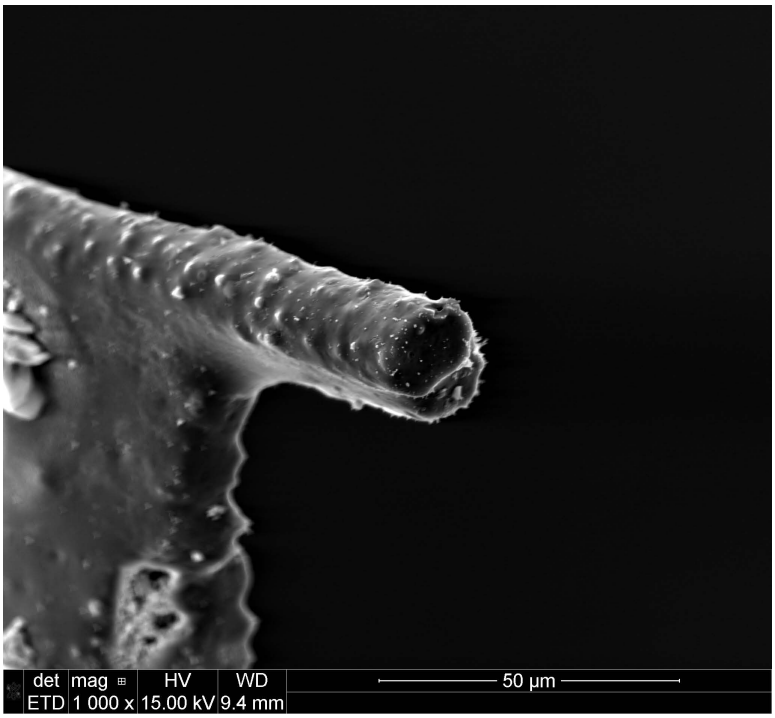

Figure 7.104: Hi-Nicalon S fiber specimen S21, tested in steam at 800°C at 400MPa

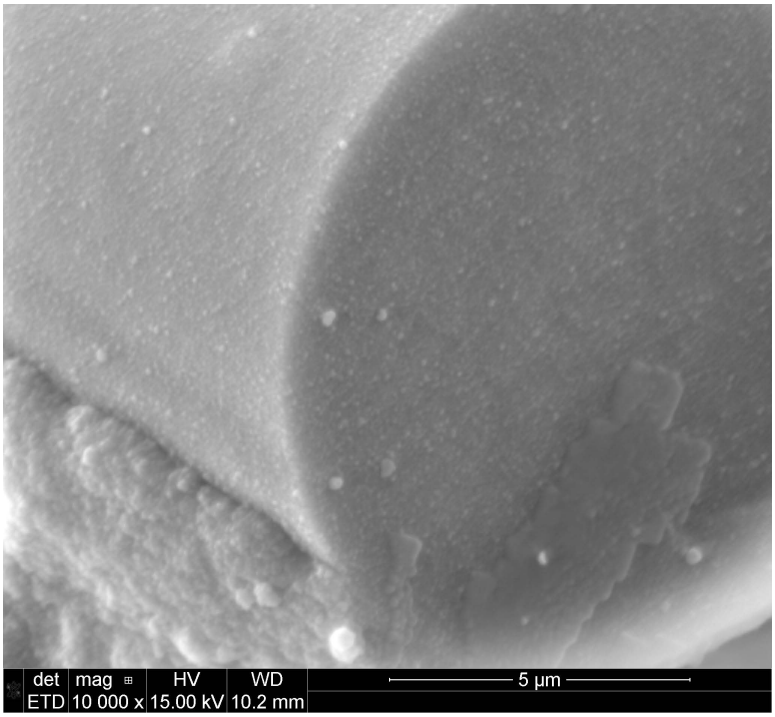

Figure 7.105: Hi-Nicalon S fiber specimen S21, tested in steam at 800°C at 400MPa

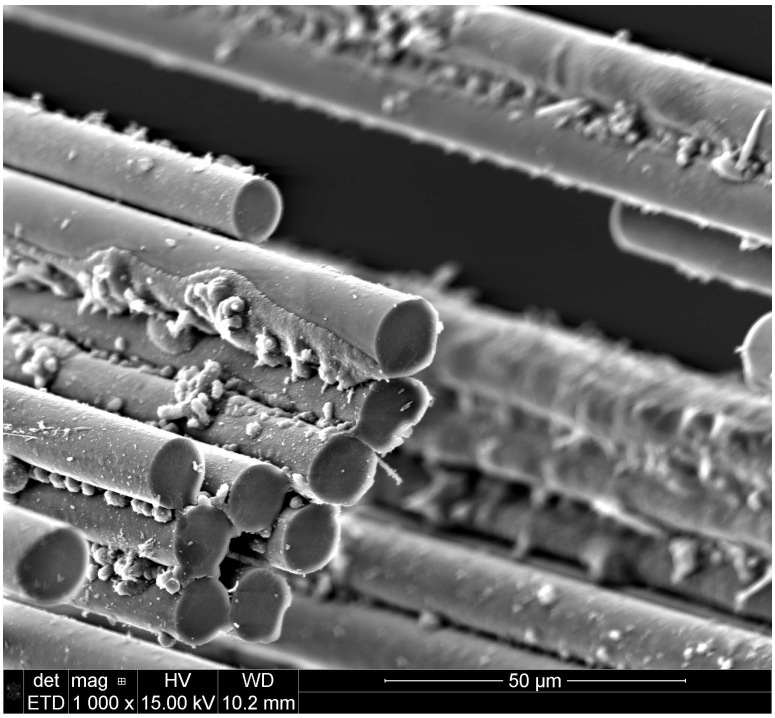

Figure 7.106: Hi-Nicalon S fiber specimen S21, tested in steam at 800°C at 400MPa

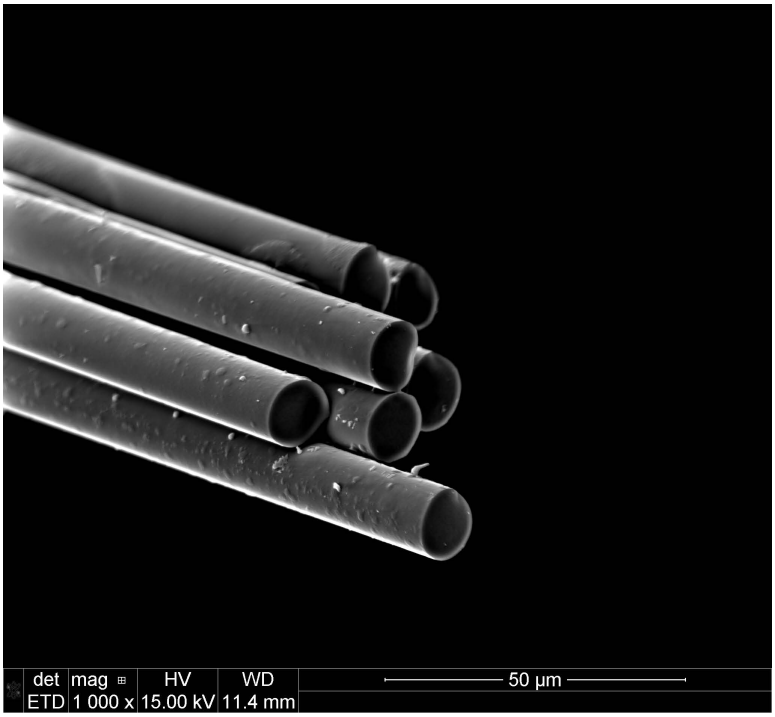

Figure 7.107: Hi-Nicalon S fiber specimen S21, tested in steam at 800°C at 400MPa

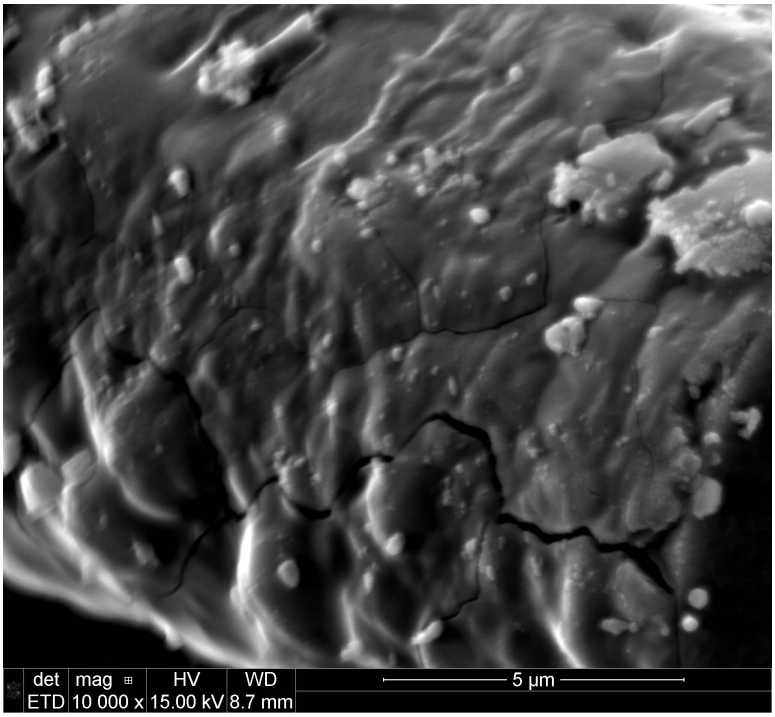

Figure 7.108: Hi-Nicalon S fiber specimen S23, tested in steam at 800°C at 450MPa

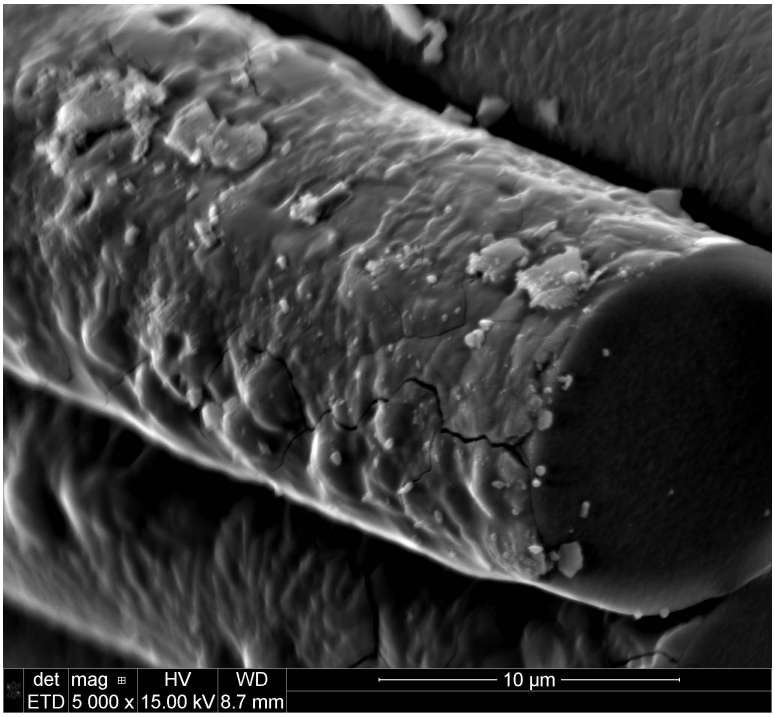

Figure 7.109: Hi-Nicalon S fiber specimen S23, tested in steam at 800°C at 450MPa

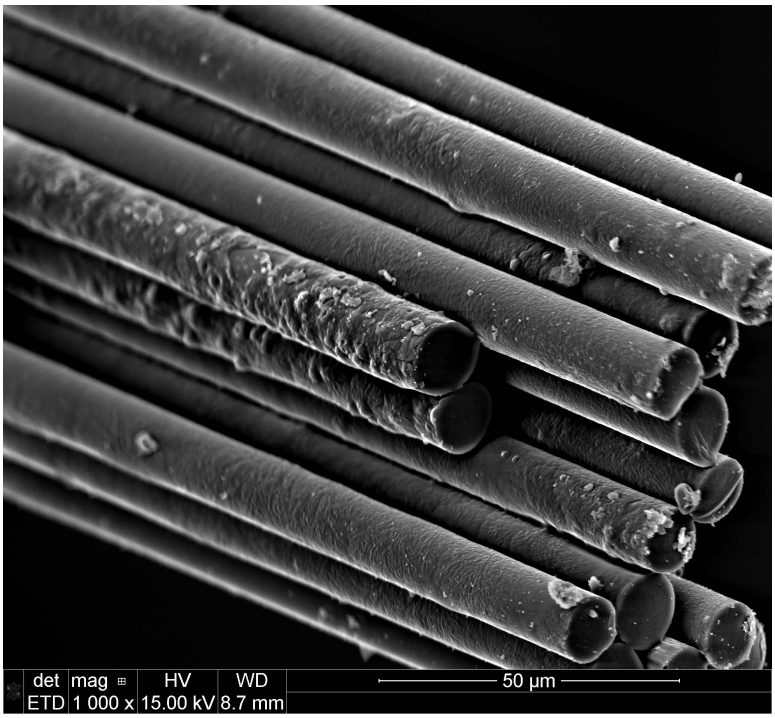

Figure 7.110: Hi-Nicalon S fiber specimen S23, tested in steam at 800°C at 450MPa

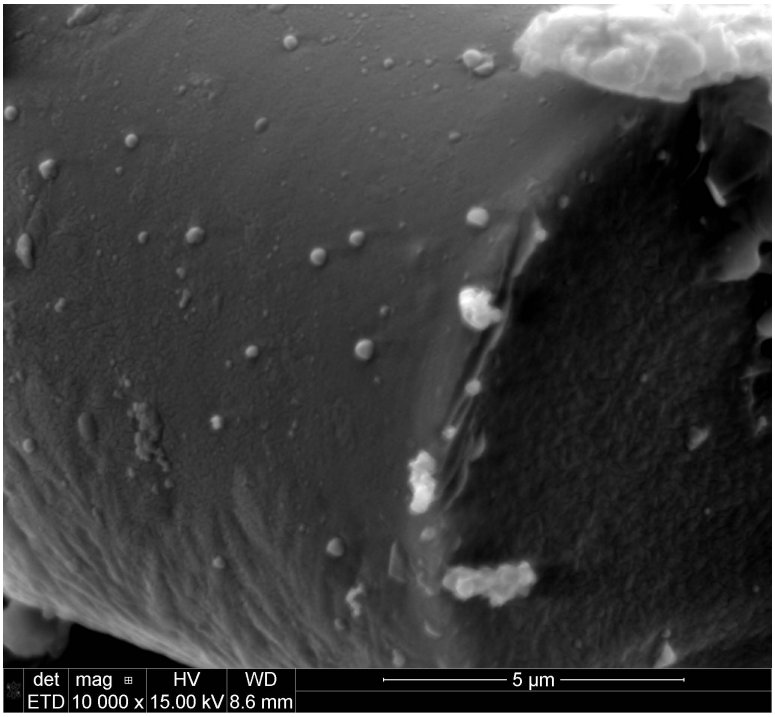

Figure 7.111: Hi-Nicalon S fiber specimen S23, tested in steam at 800°C at 450MPa

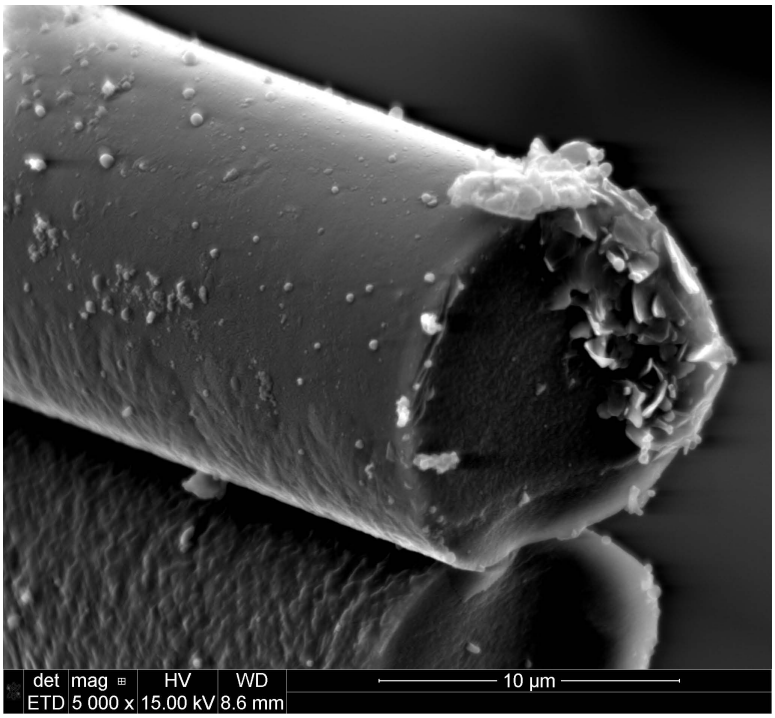

Figure 7.112: Hi-Nicalon S fiber specimen S23, tested in steam at 800°C at 450MPa

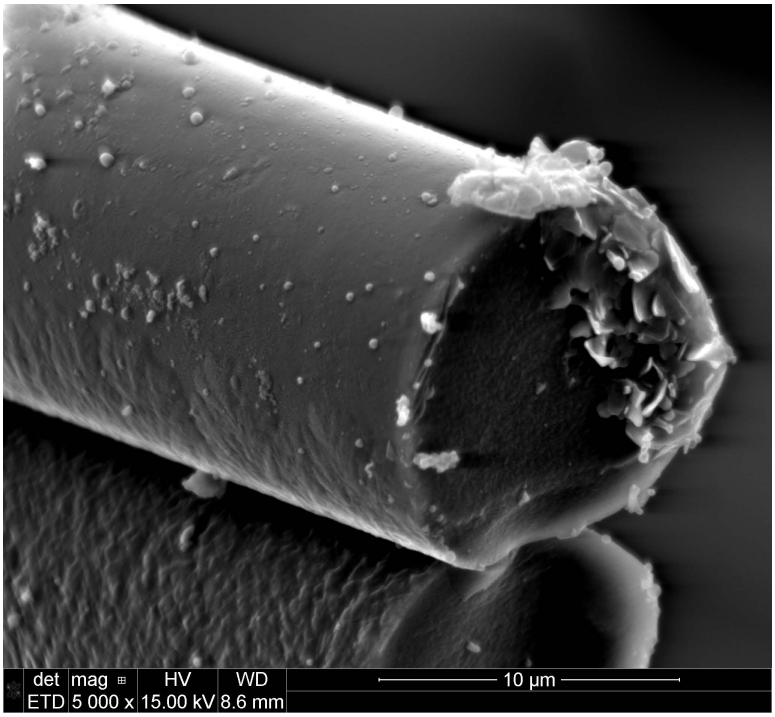

Figure 7.113: Hi-Nicalon S fiber specimen S23, tested in steam at 800°C at 450MPa

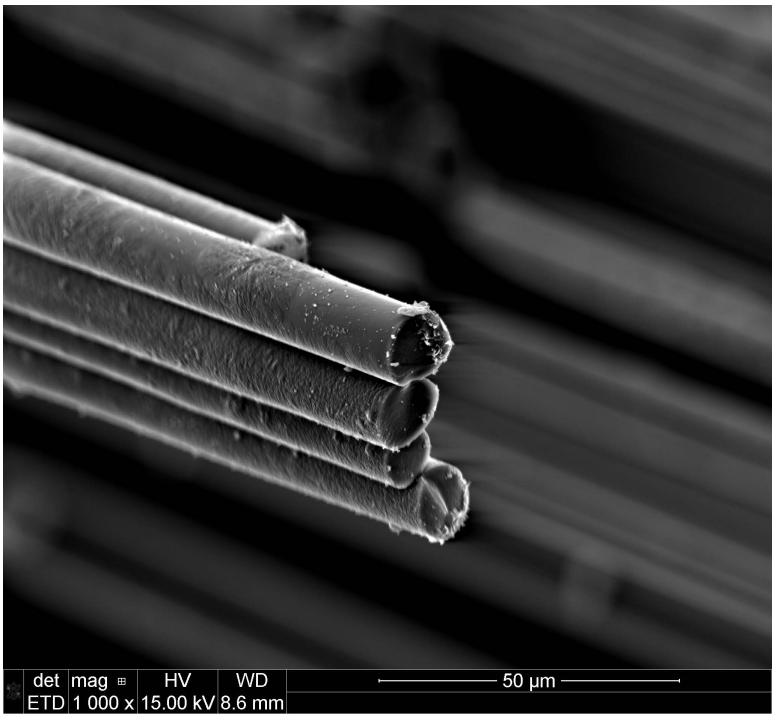

Figure 7.114: Hi-Nicalon S fiber specimen S23, tested in steam at 800°C at 450MPa

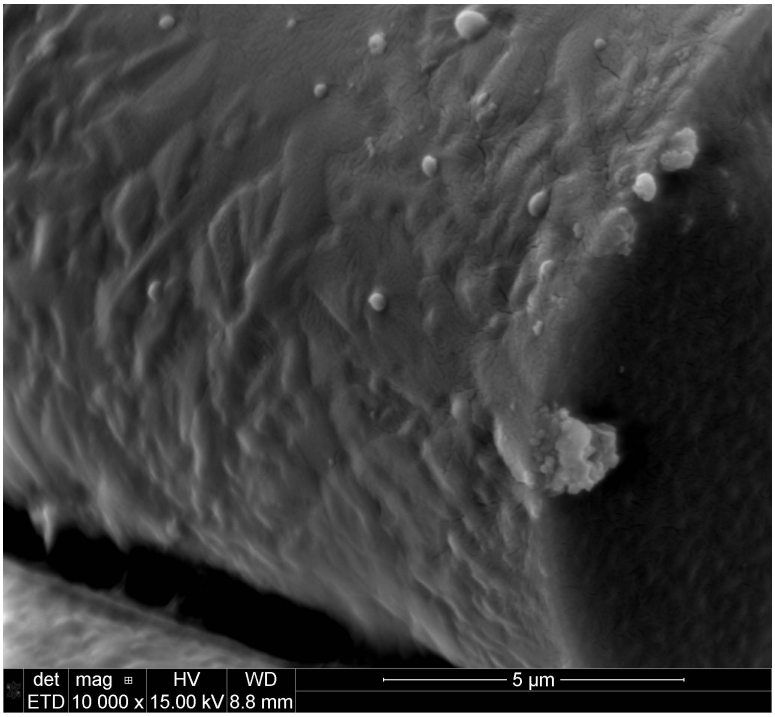

Figure 7.115: Hi-Nicalon S fiber specimen S23, tested in steam at 800°C at 450MPa

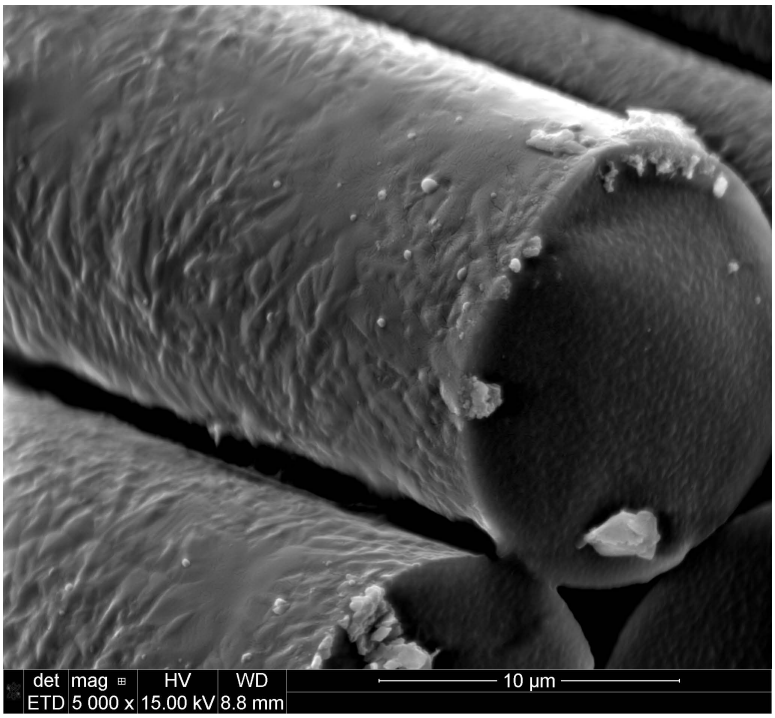

Figure 7.116: Hi-Nicalon S fiber specimen S23, tested in steam at 800°C at 450MPa

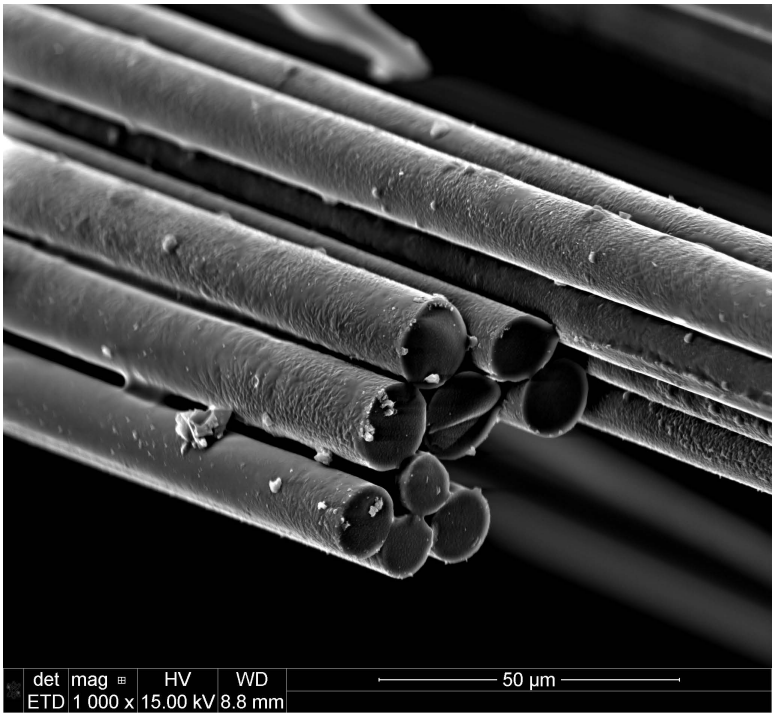

Figure 7.117: Hi-Nicalon S fiber specimen S23, tested in steam at 800°C at 450MPa

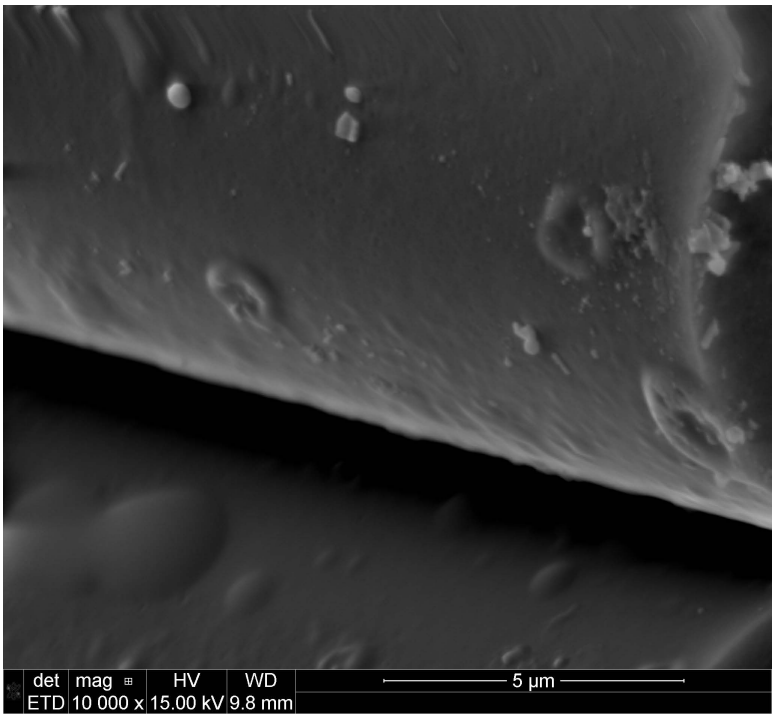

Figure 7.118: Hi-Nicalon S fiber specimen S23, tested in steam at 800°C at 450MPa

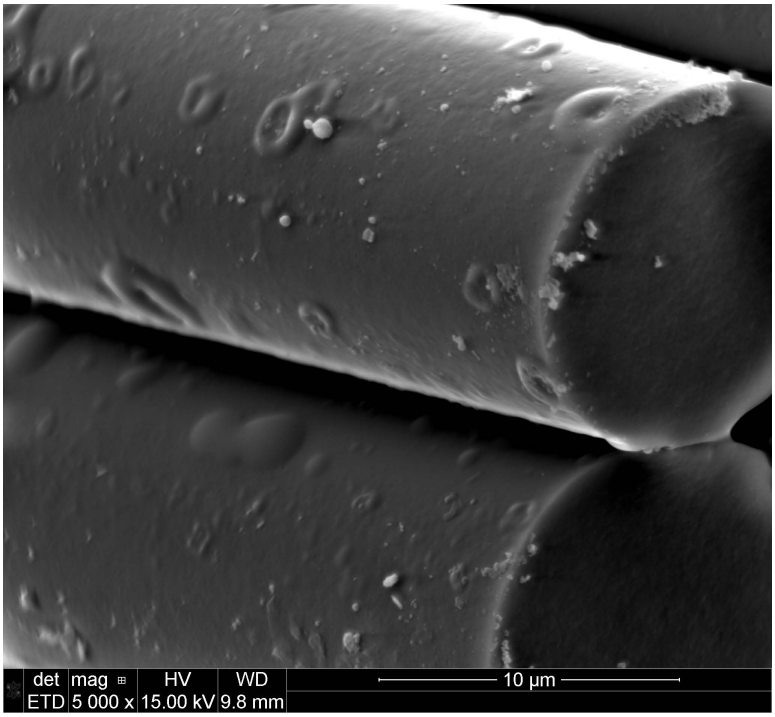

Figure 7.119: Hi-Nicalon S fiber specimen S23, tested in steam at 800°C at 450MPa

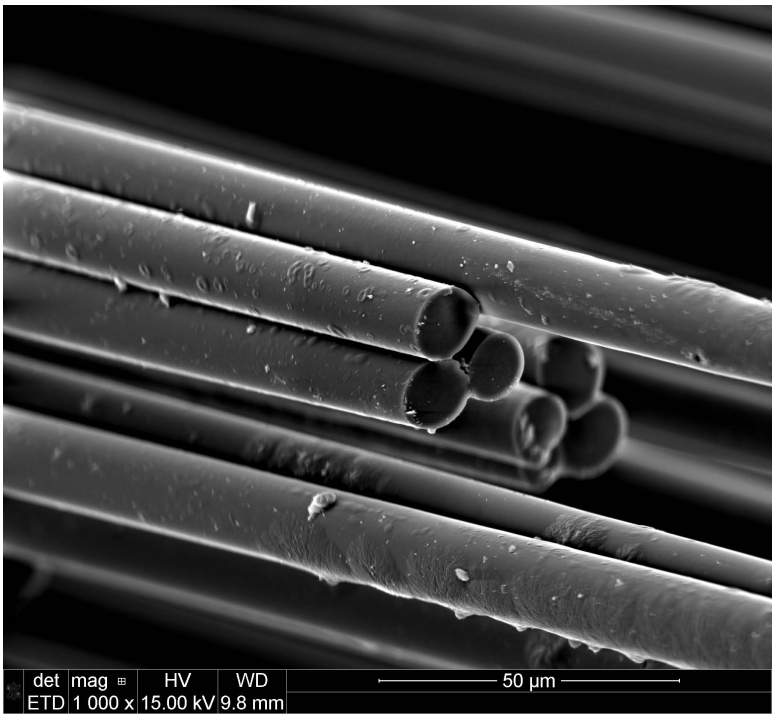

Figure 7.120: Hi-Nicalon S fiber specimen S23, tested in steam at 800°C at 450MPa

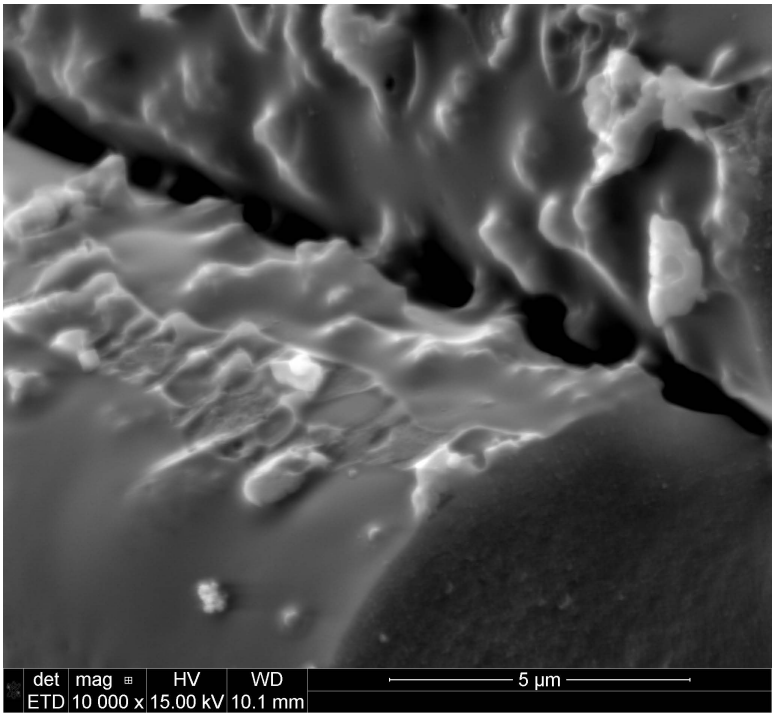

Figure 7.121: Hi-Nicalon S fiber specimen S22, tested in steam at 800°C at 450MPa

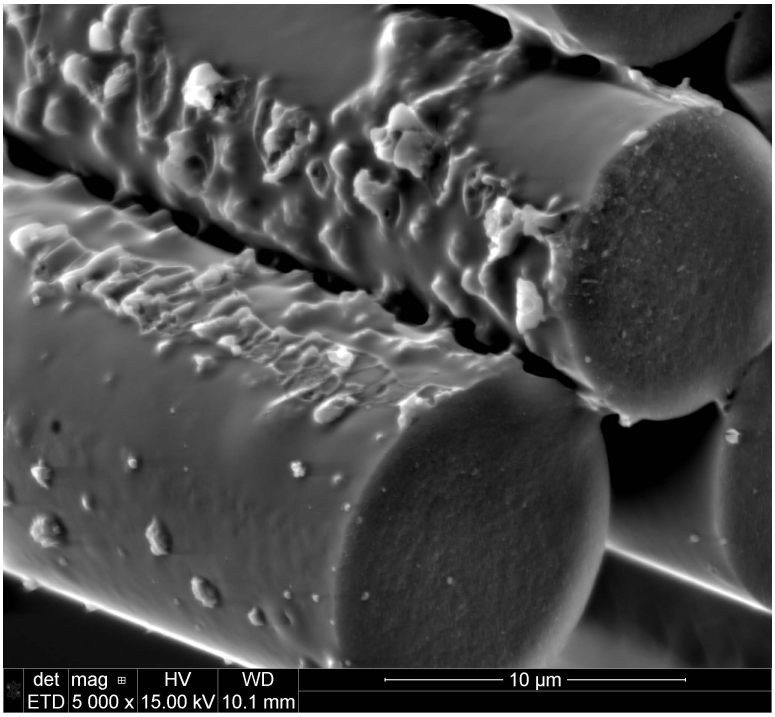

Figure 7.122: Hi-Nicalon S fiber specimen S22, tested in steam at 800°C at 450MPa

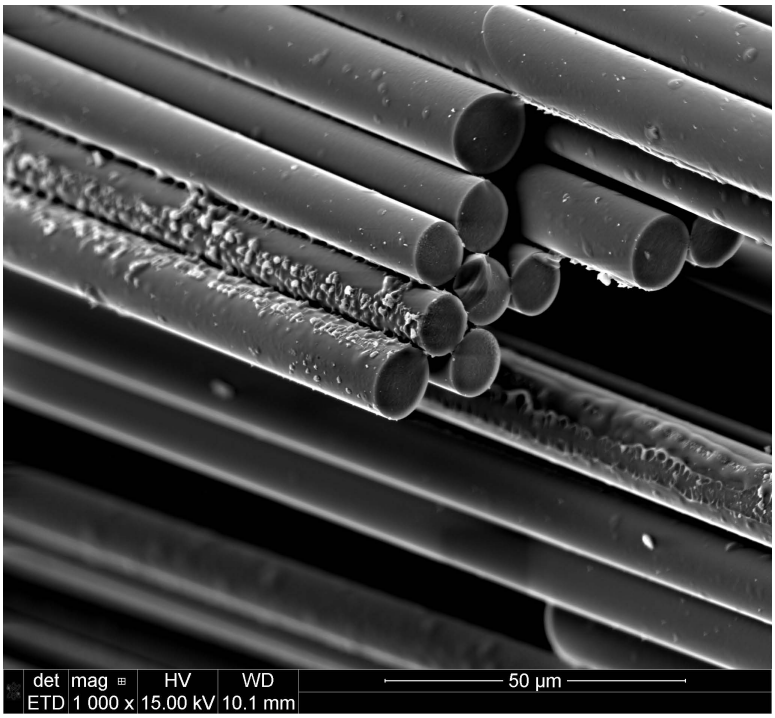

Figure 7.123: Hi-Nicalon S fiber specimen S22, tested in steam at 800°C at 450MPa

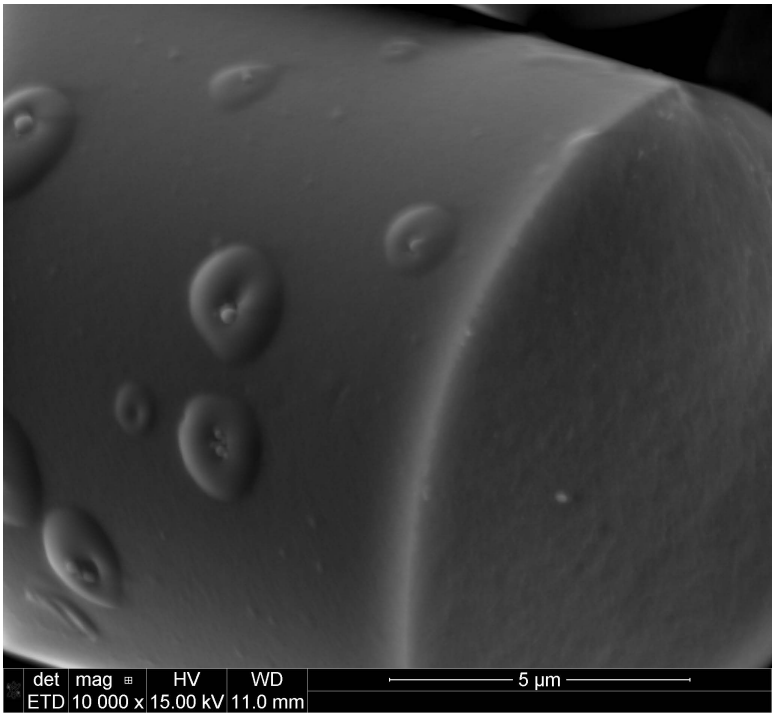

Figure 7.124: Hi-Nicalon S fiber specimen S22, tested in steam at 800°C at 450MPa

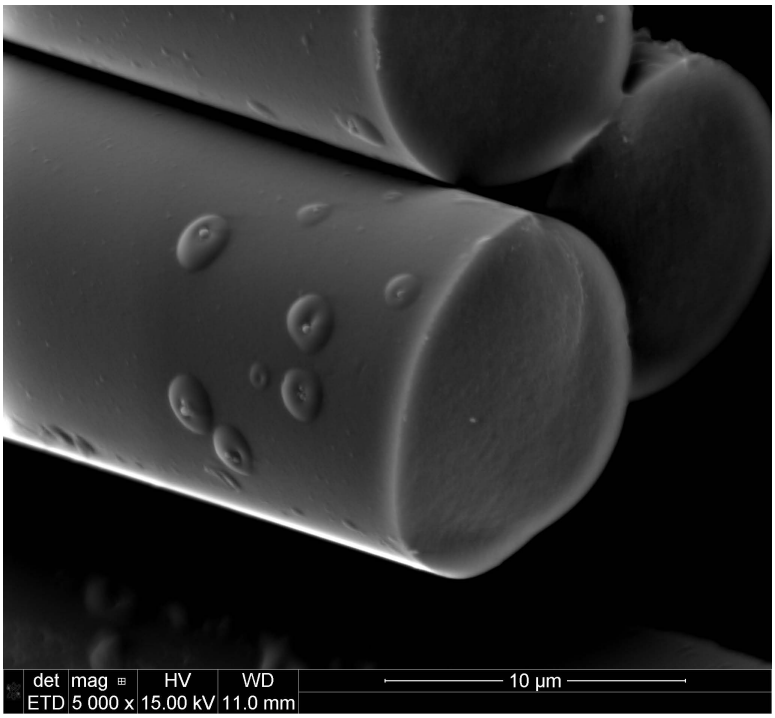

Figure 7.125: Hi-Nicalon S fiber specimen S22, tested in steam at 800°C at 450MPa

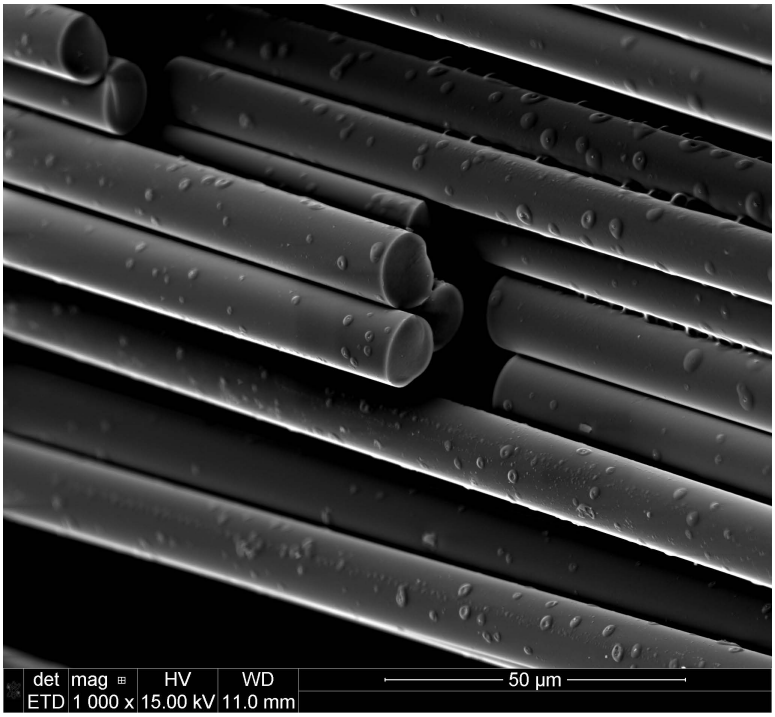

Figure 7.126: Hi-Nicalon S fiber specimen S22, tested in steam at 800°C at 450MPa

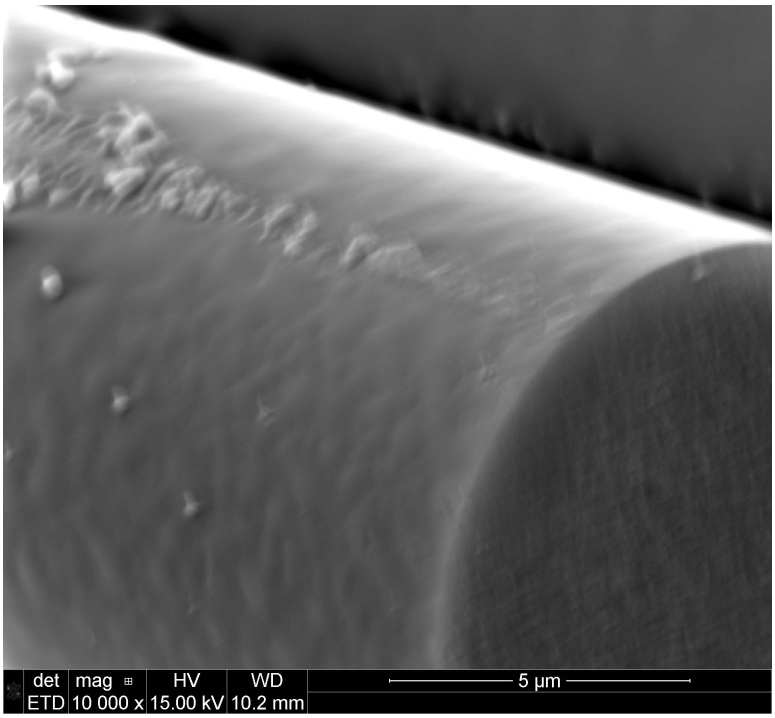

Figure 7.127: Hi-Nicalon S fiber specimen S22, tested in steam at 800°C at 450MPa

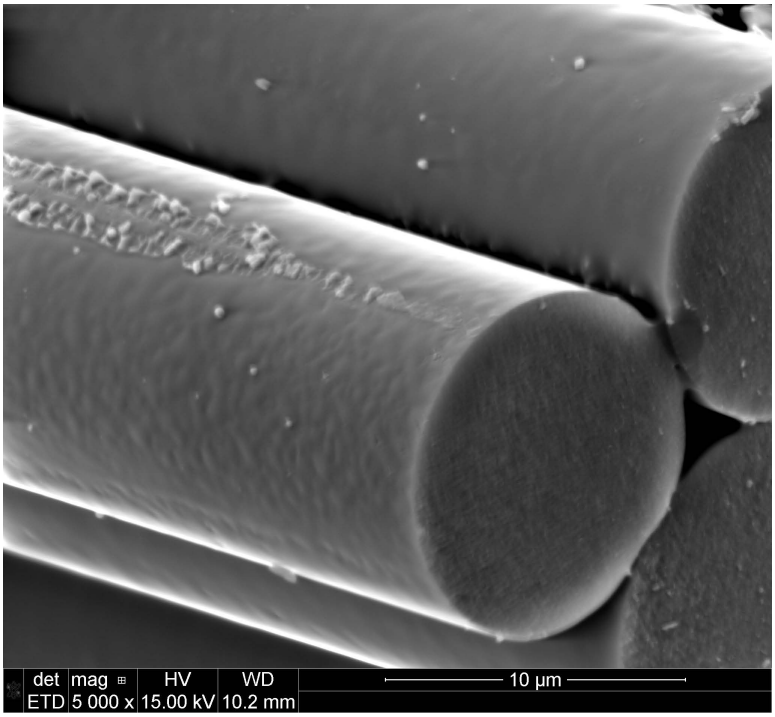

Figure 7.128: Hi-Nicalon S fiber specimen S22, tested in steam at 800°C at 450MPa

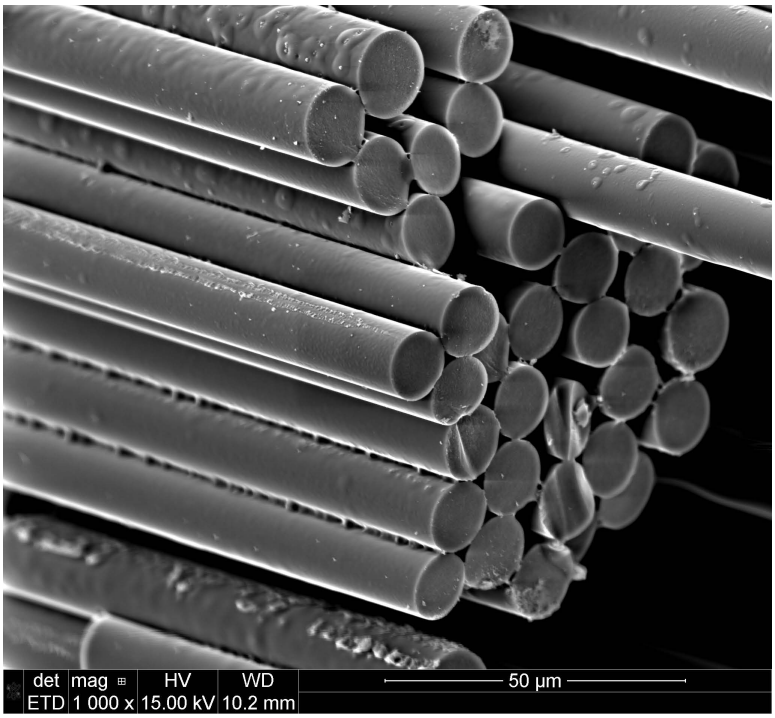

Figure 7.129: Hi-Nicalon S fiber specimen S22, tested in steam at 800°C at 450MPa

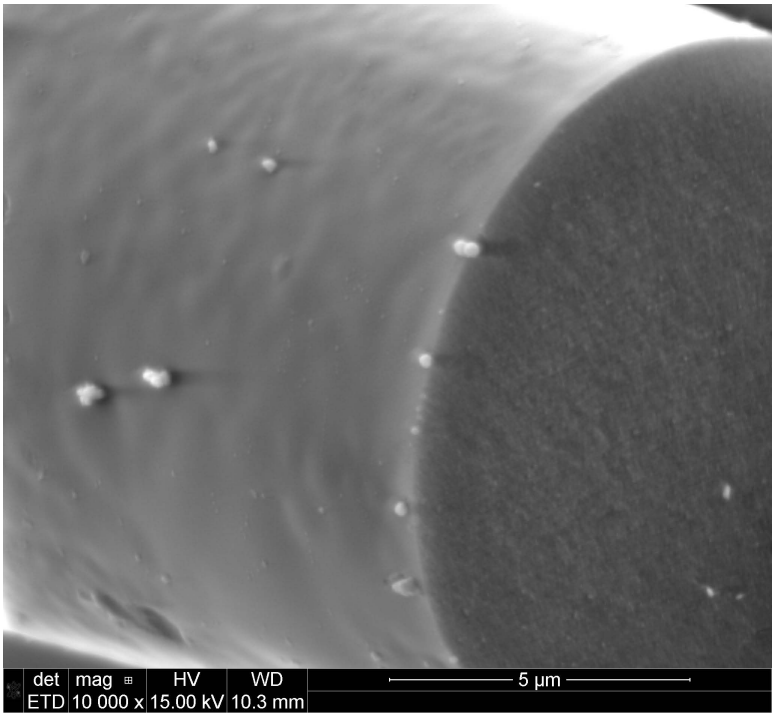

Figure 7.130: Hi-Nicalon S fiber specimen S22, tested in steam at 800°C at 450MPa

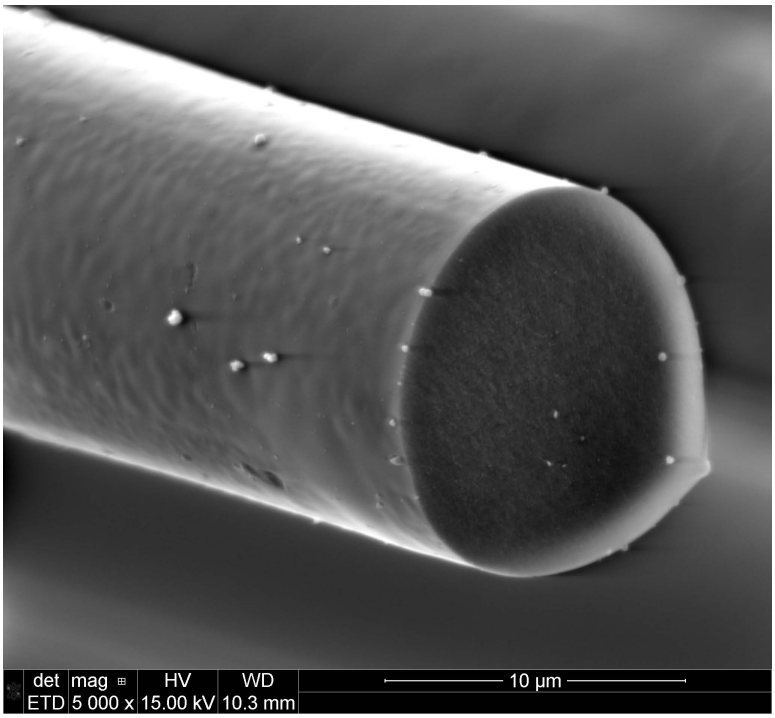

Figure 7.131: Hi-Nicalon S fiber specimen S22, tested in steam at 800°C at 450MPa

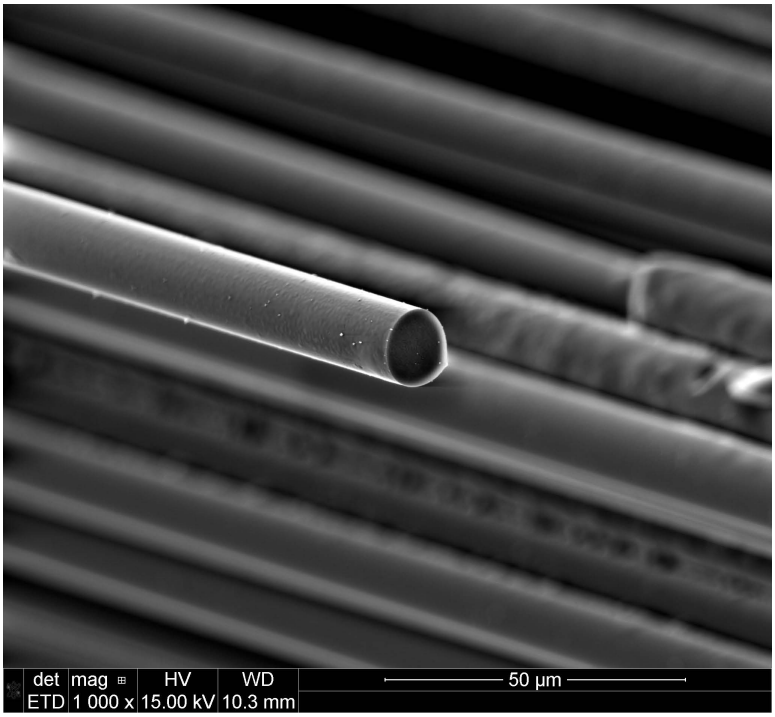

Figure 7.132: Hi-Nicalon S fiber specimen S22, tested in steam at 800°C at 450MPa

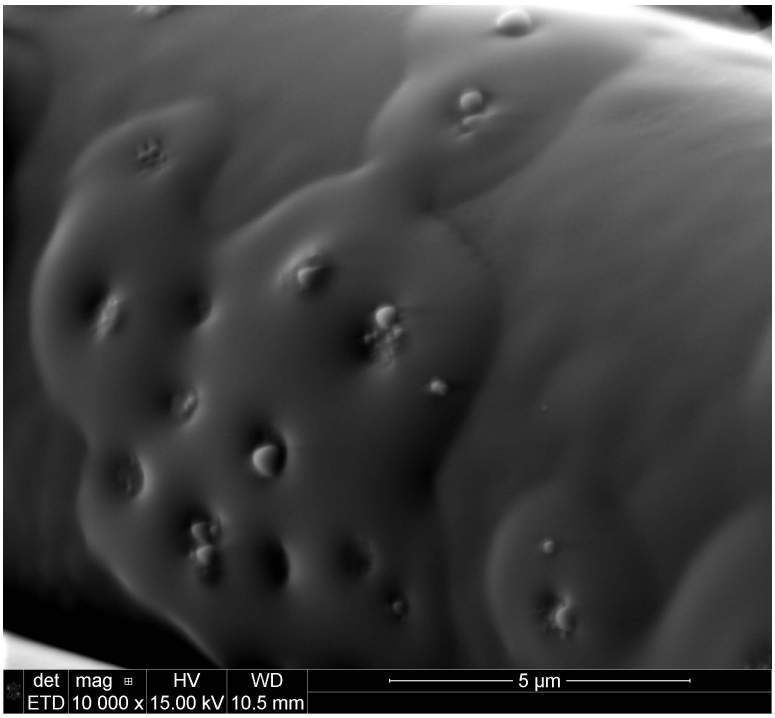

Figure 7.133: Hi-Nicalon S fiber specimen S22, tested in steam at 800°C at 450MPa

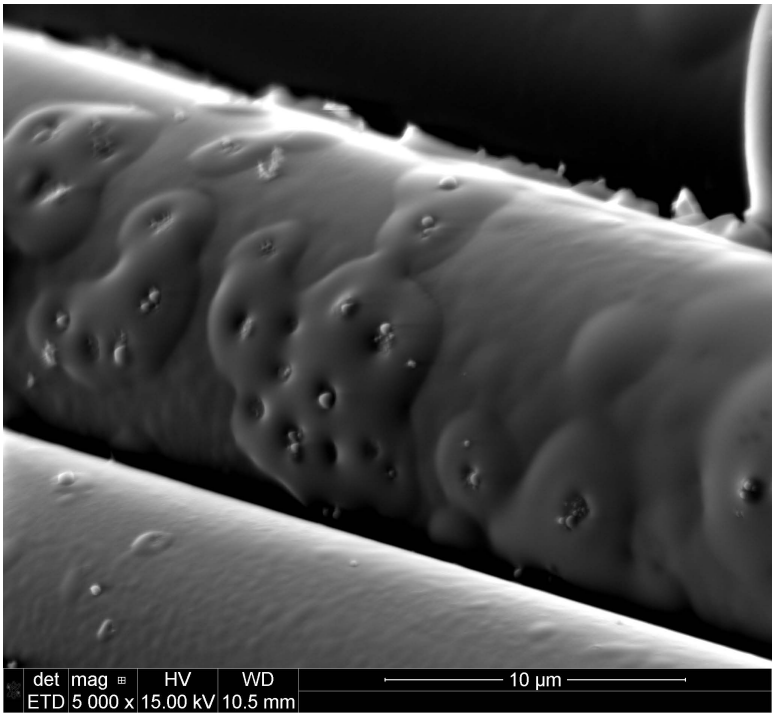

Figure 7.134: Hi-Nicalon S fiber specimen S22, tested in steam at 800°C at 450MPa

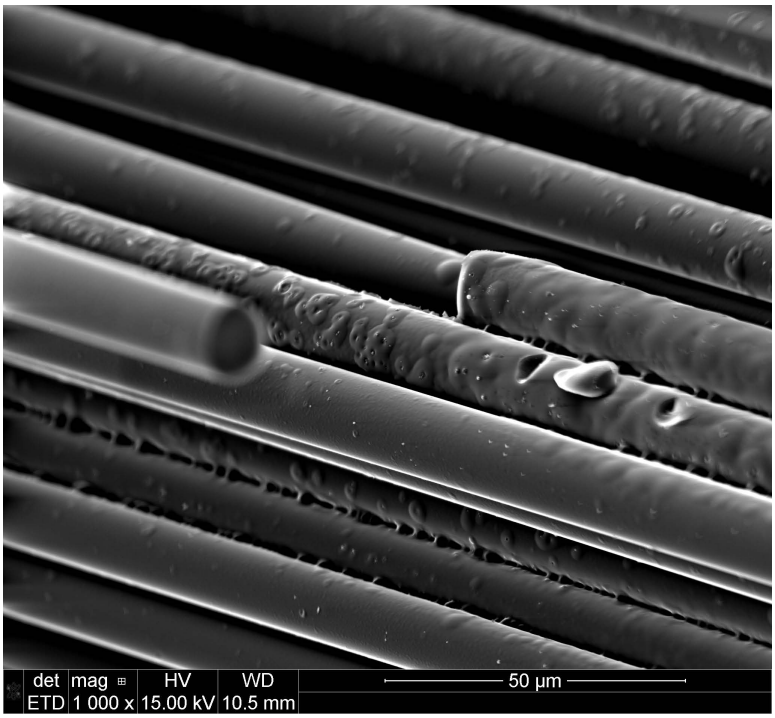

Figure 7.135: Hi-Nicalon S fiber specimen S22, tested in steam at 800°C at 450MPa

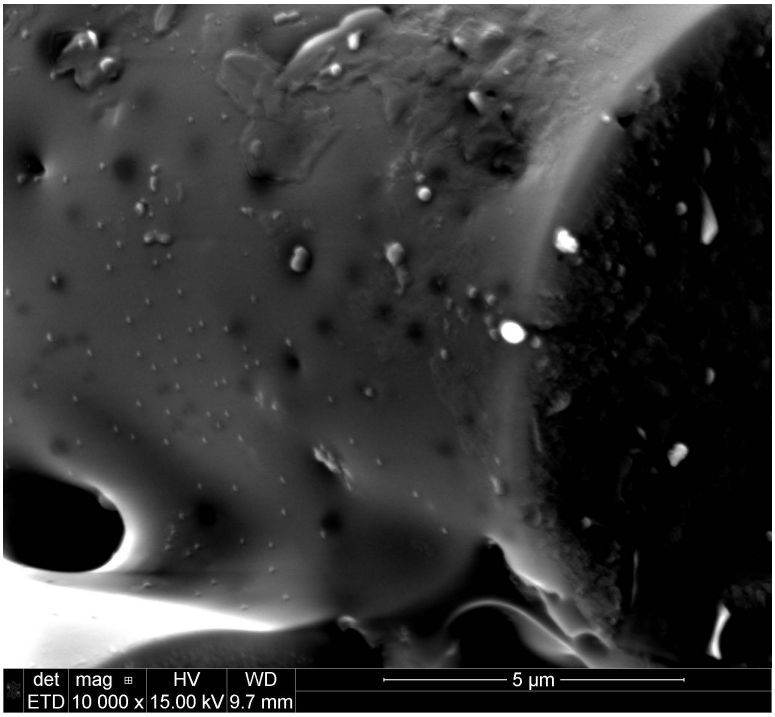

Figure 7.136: Hi-Nicalon S fiber specimen S18, tested in steam at 800°C at 798MPa

7.4.2 Fibers tested at 900°C.

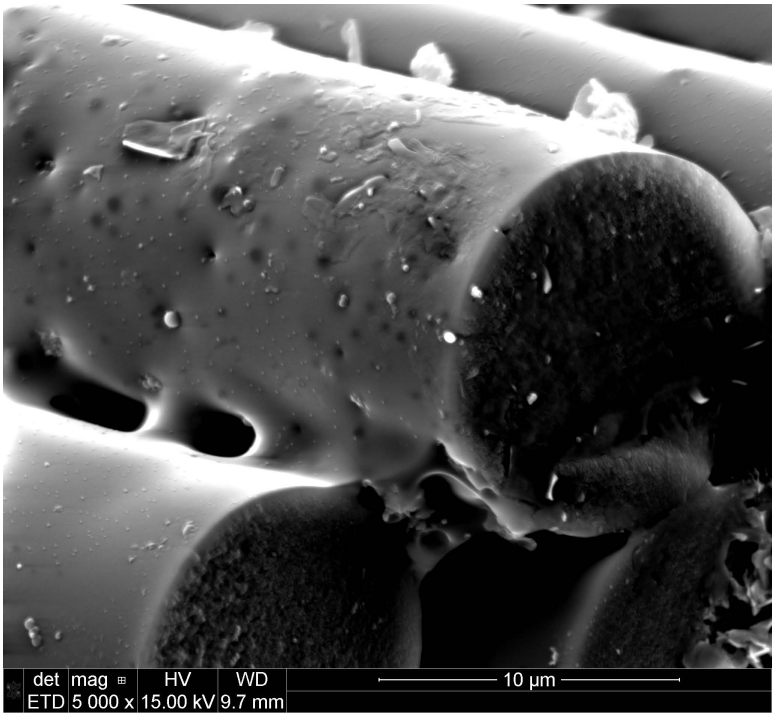

Figure 7.137: Hi-Nicalon S fiber specimen S18, tested in steam at 800°C at 798MPa

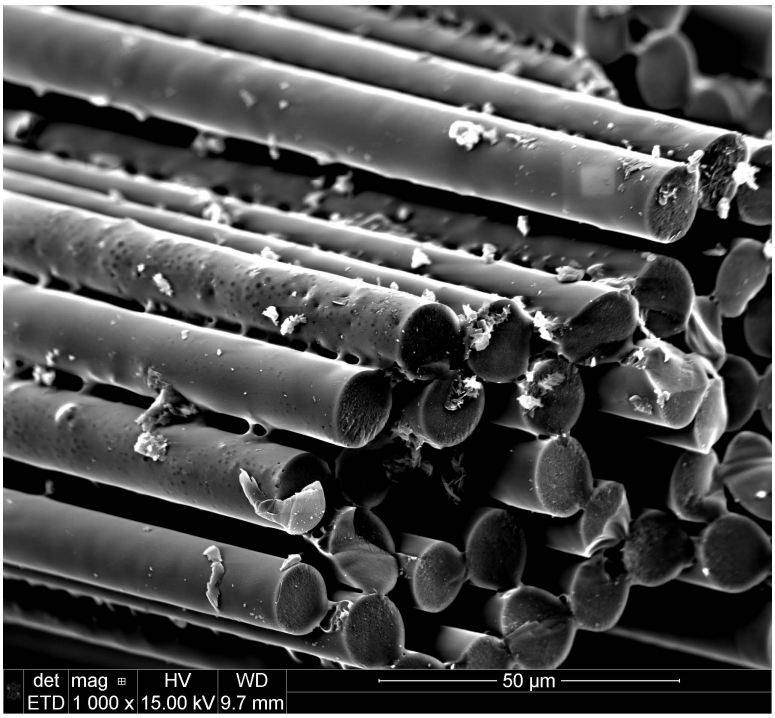

Figure 7.138: Hi-Nicalon S fiber specimen S18, tested in steam at 800°C at 798MPa

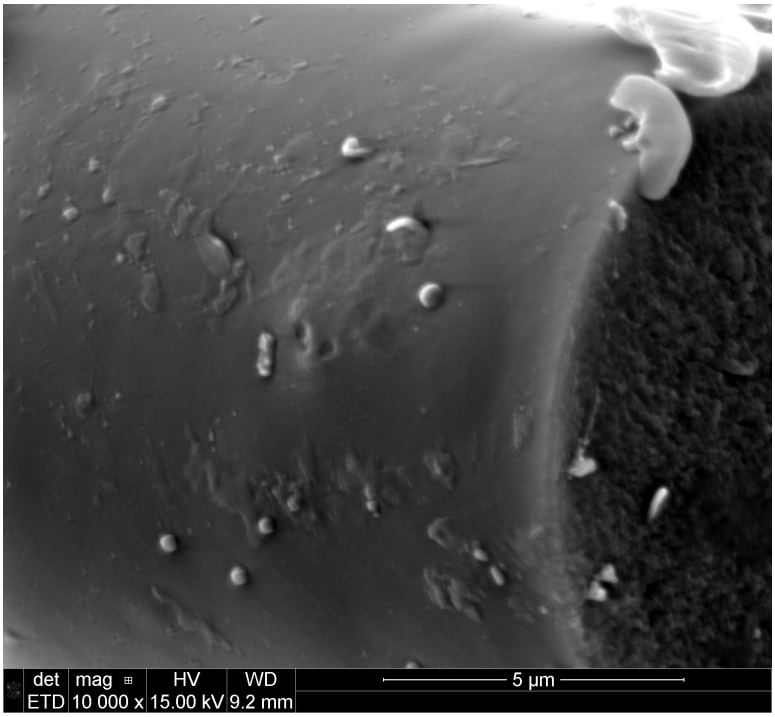

Figure 7.139: Hi-Nicalon S fiber specimen S18, tested in steam at 800°C at 798MPa

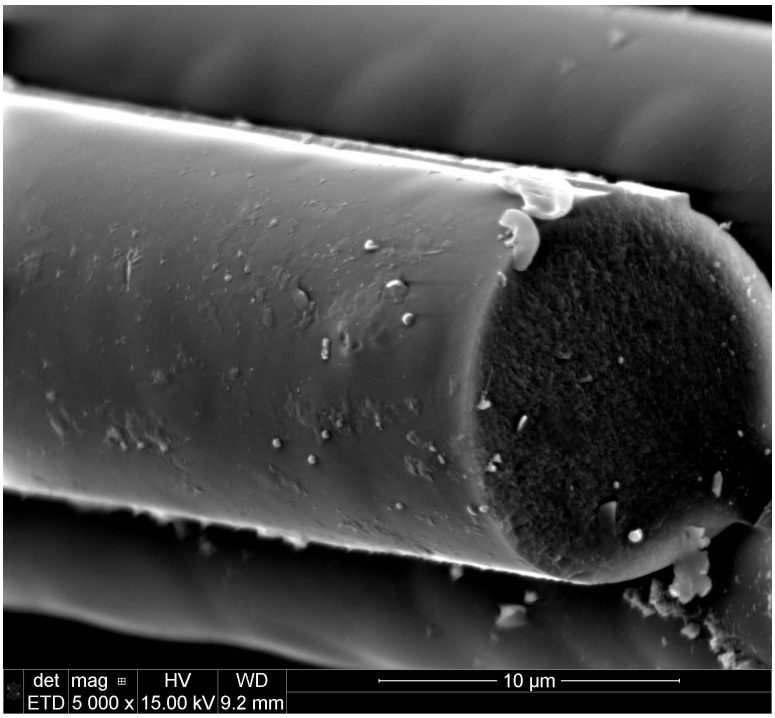

Figure 7.140: Hi-Nicalon S fiber specimen S18, tested in steam at 800°C at 798MPa

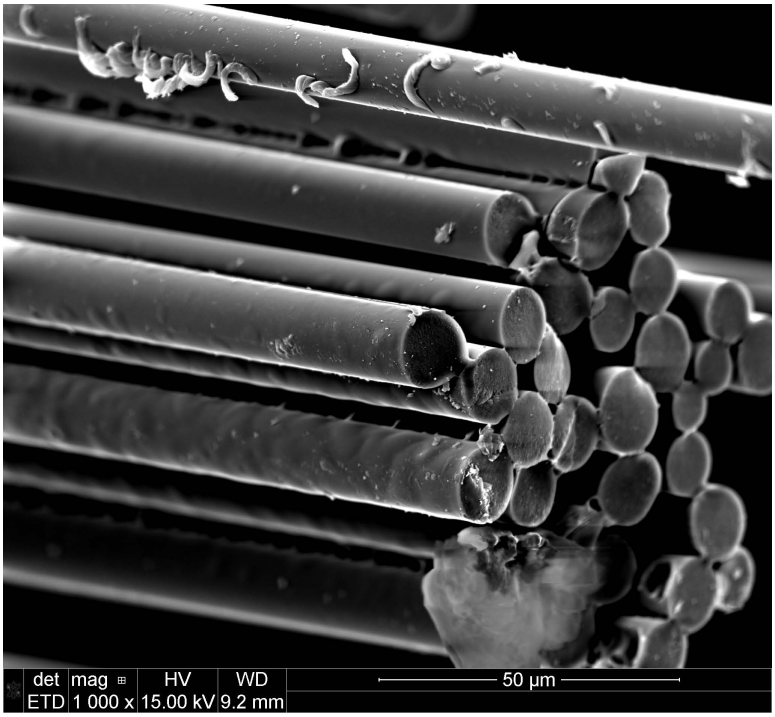

Figure 7.141: Hi-Nicalon S fiber specimen S18, tested in steam at 800°C at 798MPa

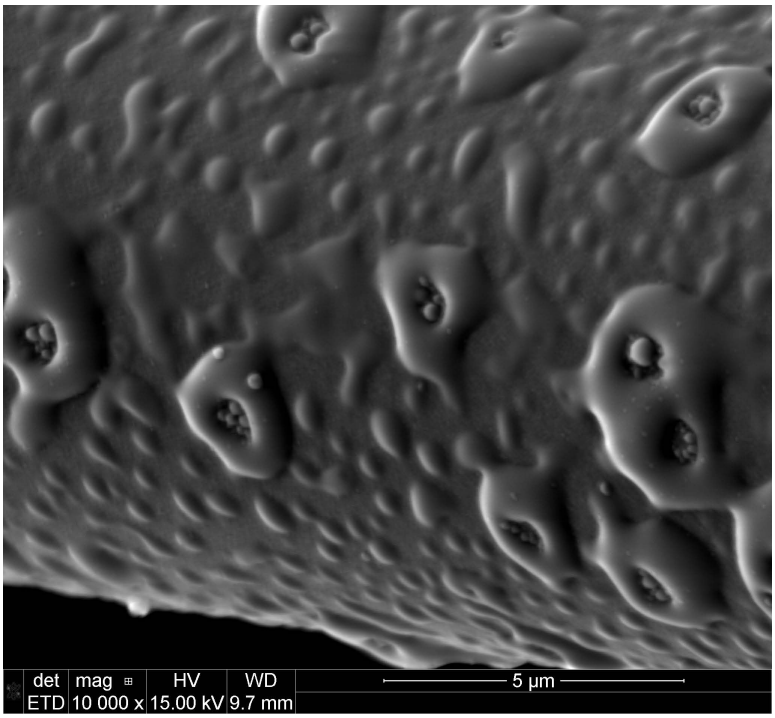

Figure 7.142: Hi-Nicalon S fiber specimen S18, tested in steam at 800°C at 798MPa

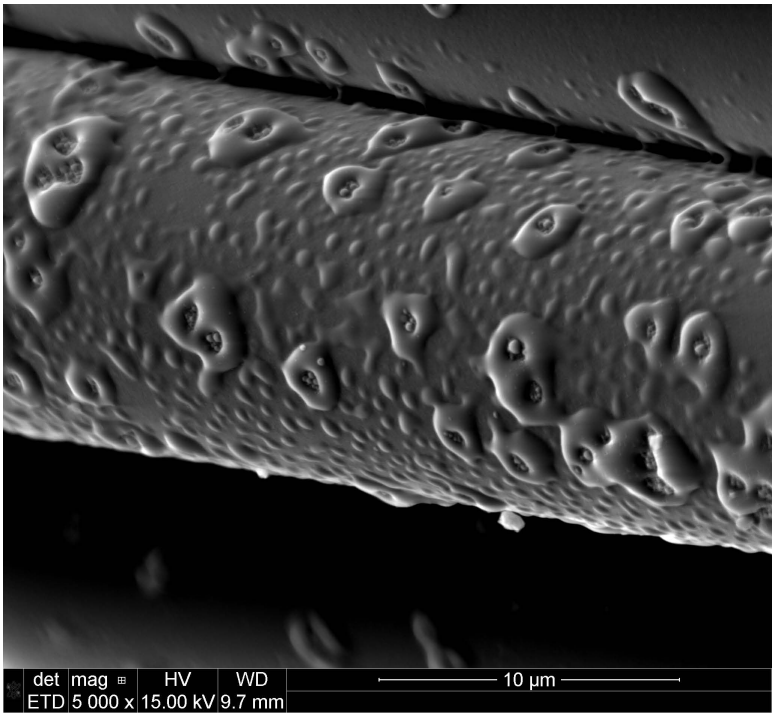

Figure 7.143: Hi-Nicalon S fiber specimen S18, tested in steam at 800°C at 798MPa

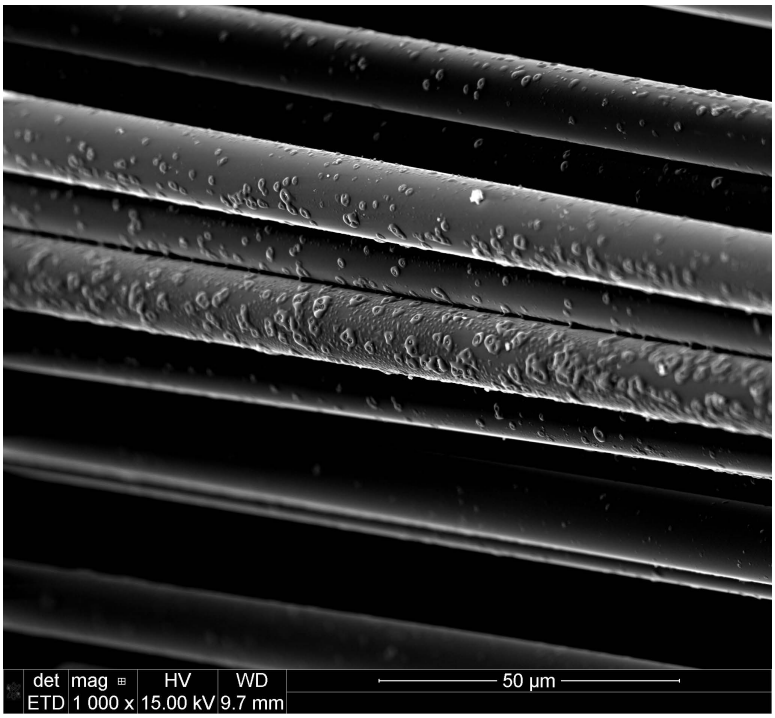

Figure 7.144: Hi-Nicalon S fiber specimen S18, tested in steam at 800°C at 798MPa

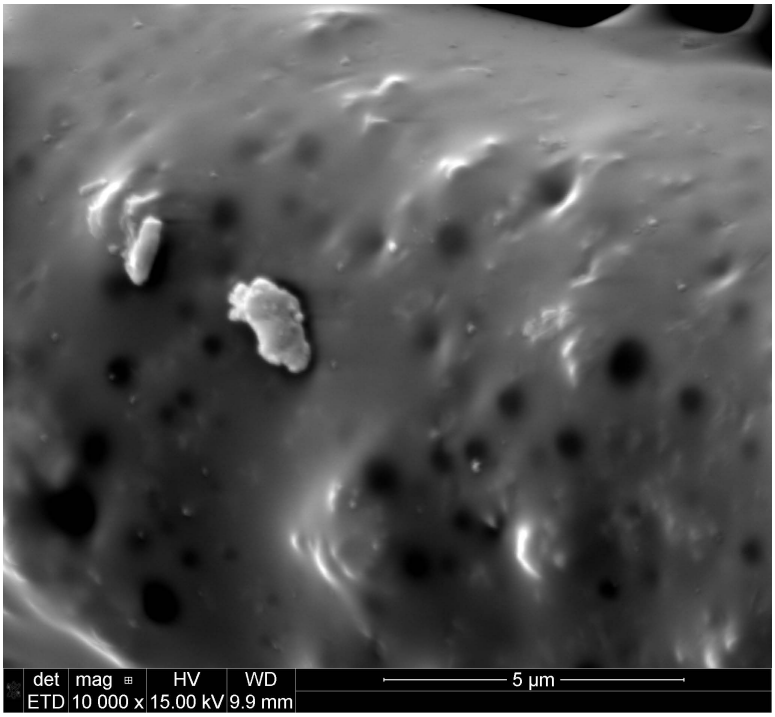

Figure 7.145: Hi-Nicalon S fiber specimen S18, tested in steam at 800°C at 798MPa

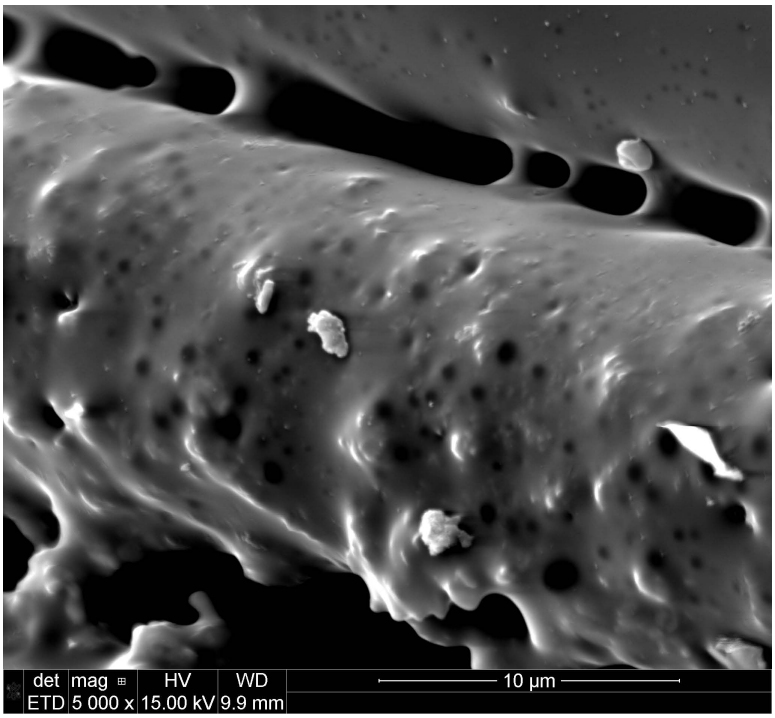

Figure 7.146: Hi-Nicalon S fiber specimen S18, tested in steam at 800°C at 798MPa

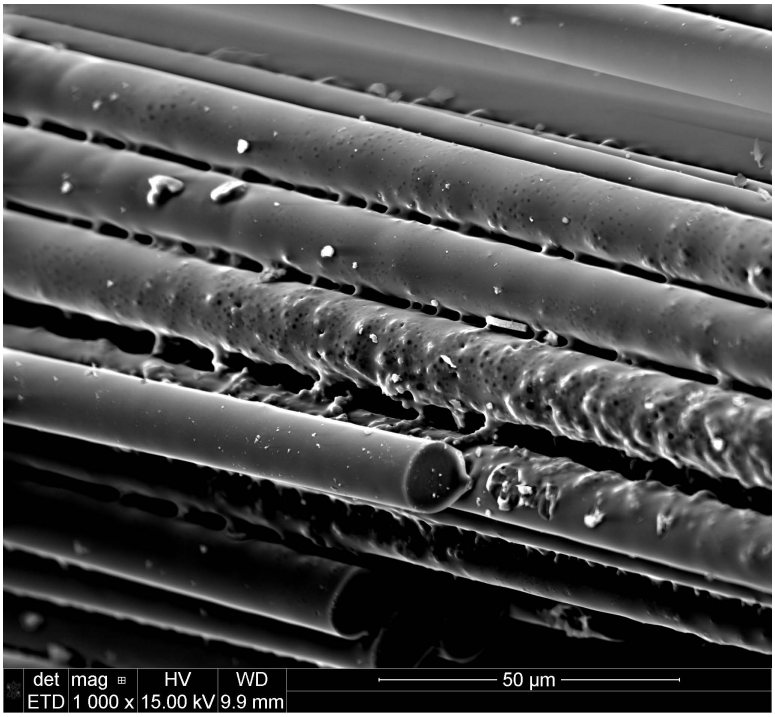

Figure 7.147: Hi-Nicalon S fiber specimen S18, tested in steam at 800°C at 798MPa

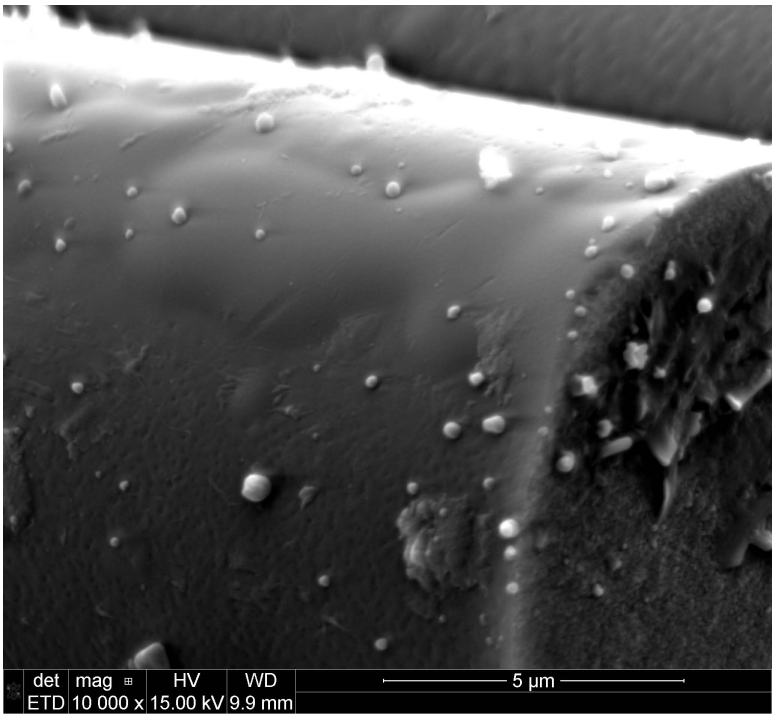

Figure 7.148: Hi-Nicalon S fiber specimen S18, tested in steam at 800°C at 798MPa

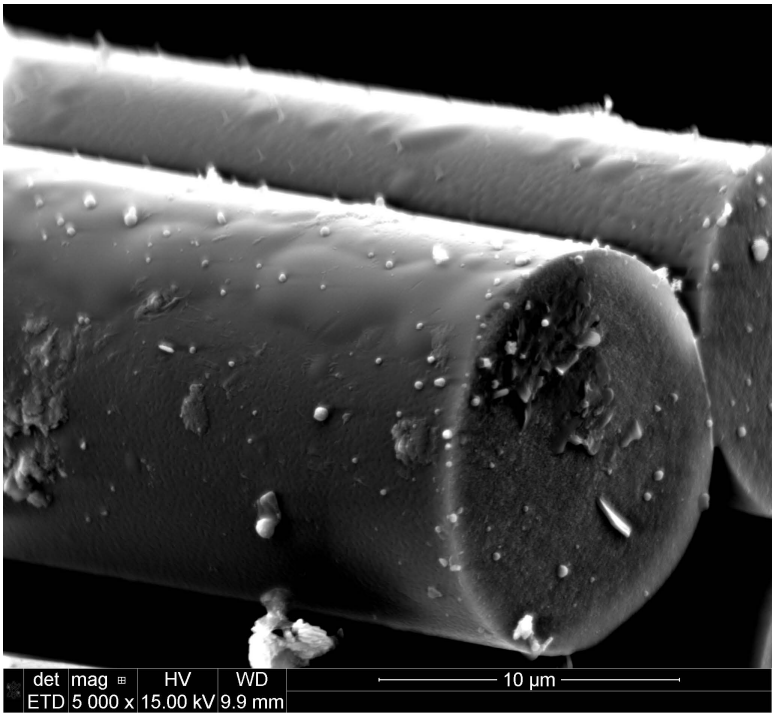

Figure 7.149: Hi-Nicalon S fiber specimen S18, tested in steam at 800°C at 798MPa

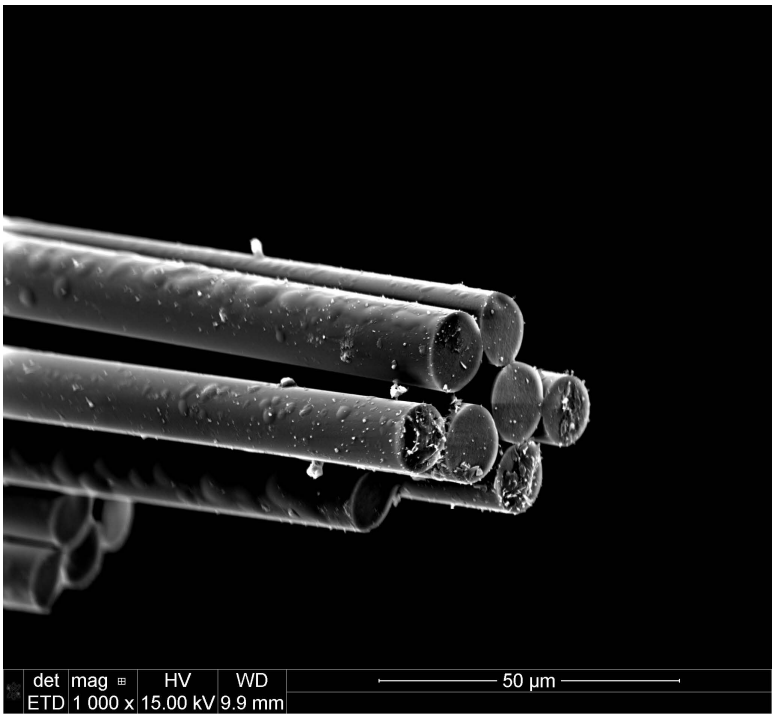

Figure 7.150: Hi-Nicalon S fiber specimen S18, tested in steam at 800°C at 798MPa

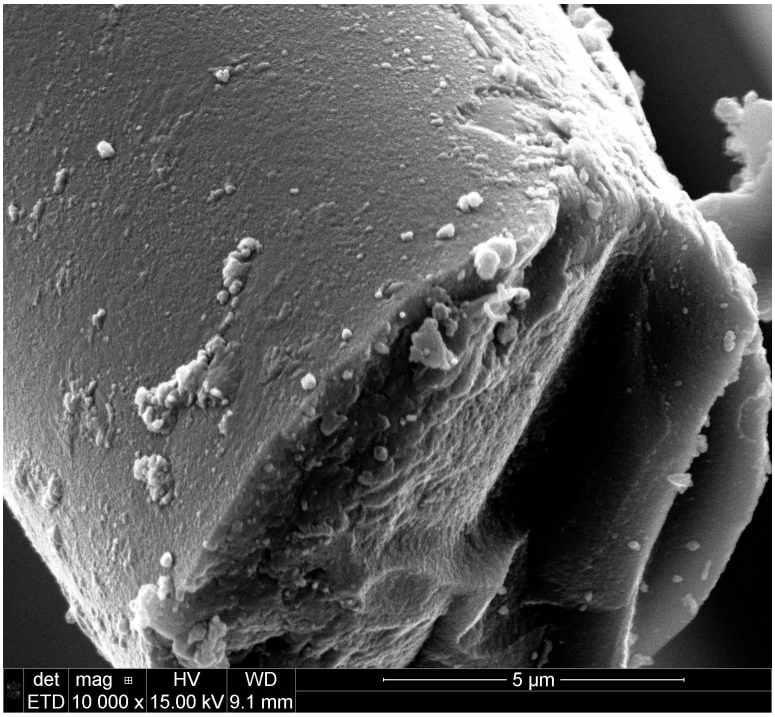

Figure 7.151: Hi-Nicalon S fiber specimen A37, tested in air at 900°C at 937MPa

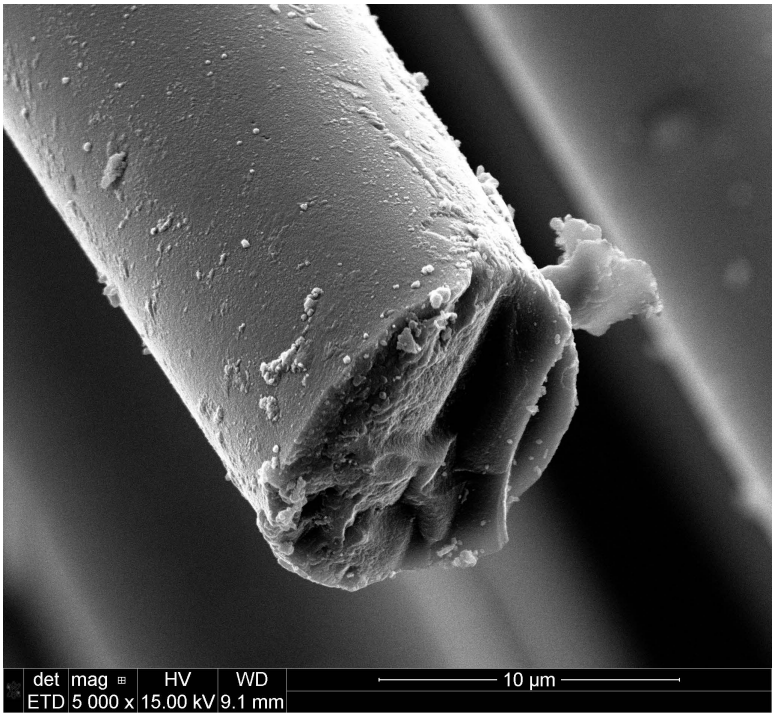

Figure 7.152: Hi-Nicalon S fiber specimen A37, tested in air at 900°C at 937MPa

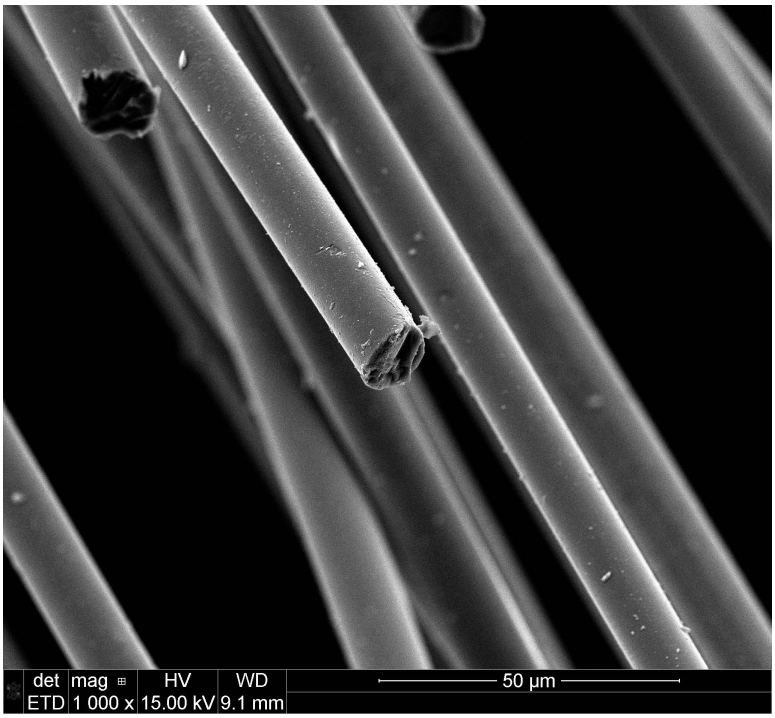

Figure 7.153: Hi-Nicalon S fiber specimen A37, tested in air at 900°C at 937MPa

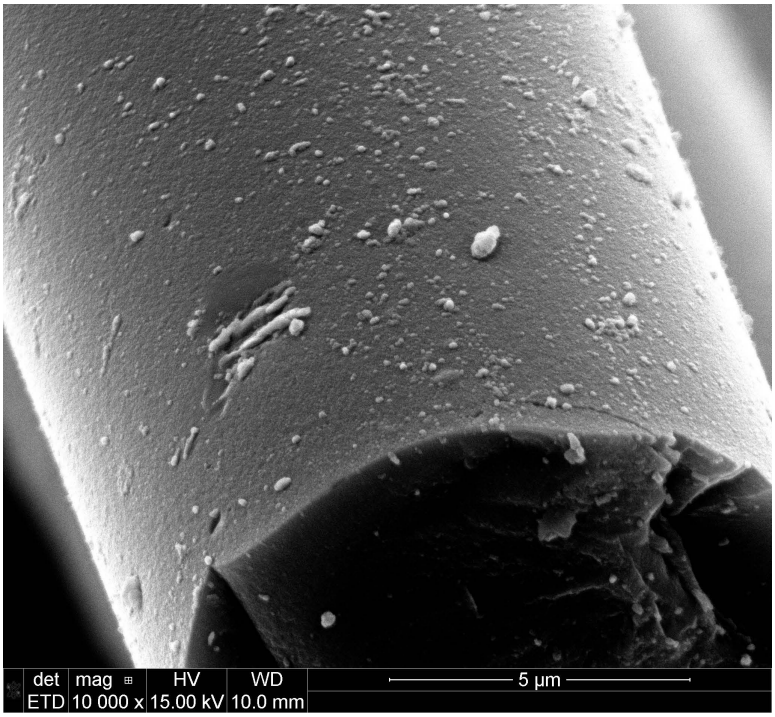

Figure 7.154: Hi-Nicalon S fiber specimen A37, tested in air at 900°C at 937MPa

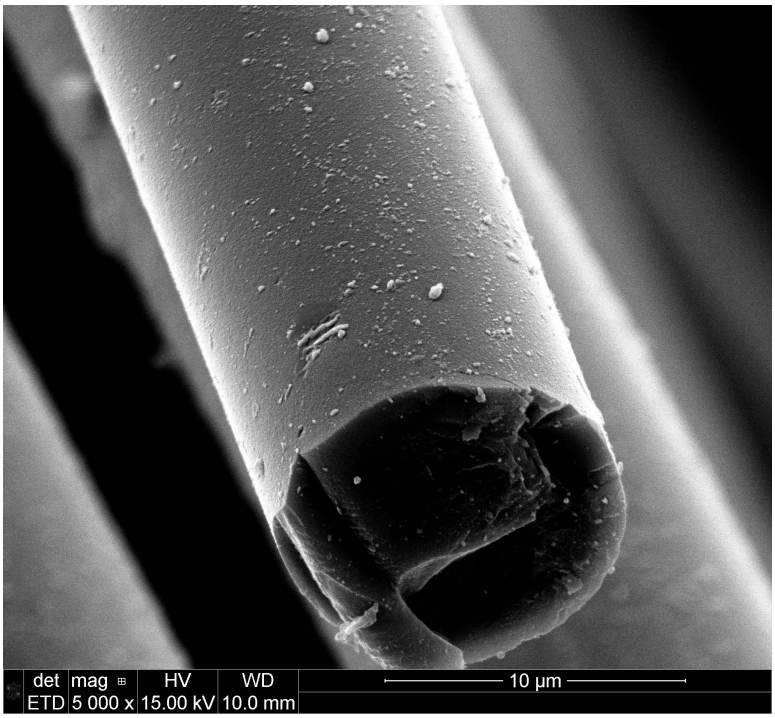

Figure 7.155: Hi-Nicalon S fiber specimen A37, tested in air at 900°C at 937MPa

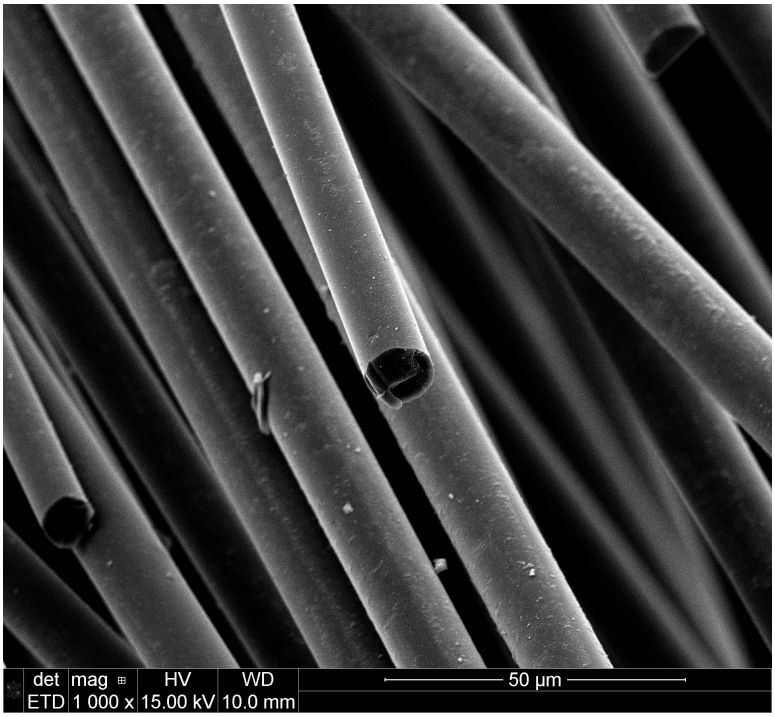

Figure 7.156: Hi-Nicalon S fiber specimen A37, tested in air at 900°C at 937MPa

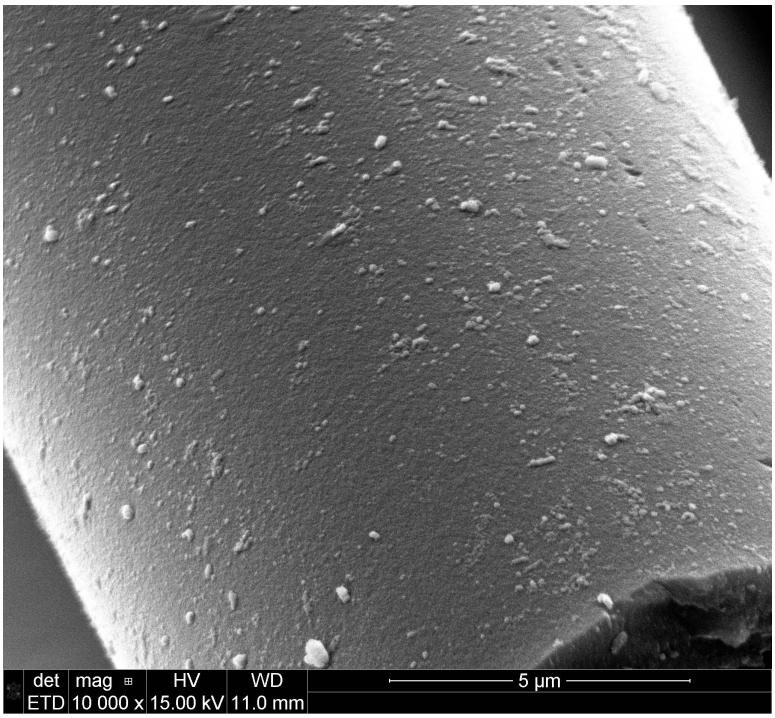

Figure 7.157: Hi-Nicalon S fiber specimen A37, tested in air at 900°C at 937MPa

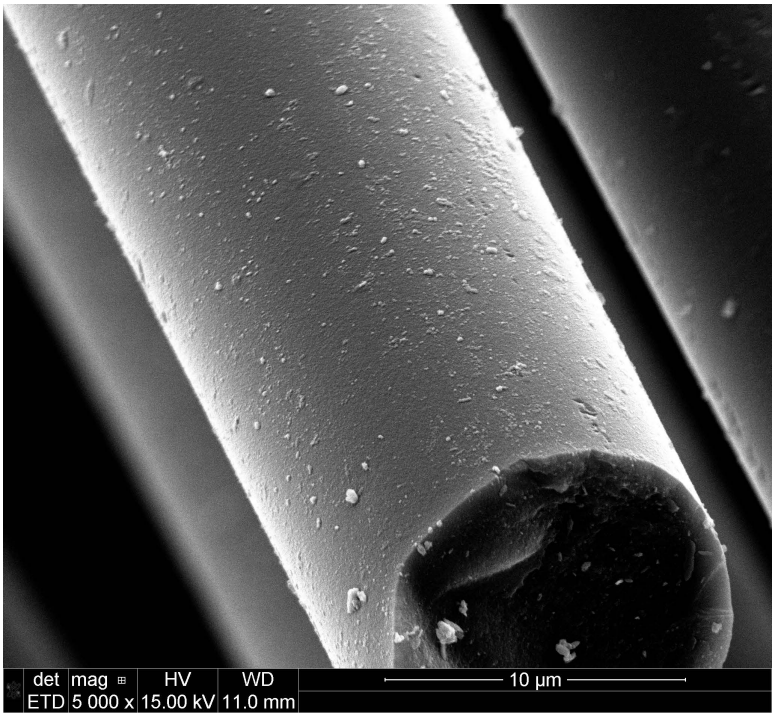

Figure 7.158: Hi-Nicalon S fiber specimen A37, tested in air at 900°C at 937MPa

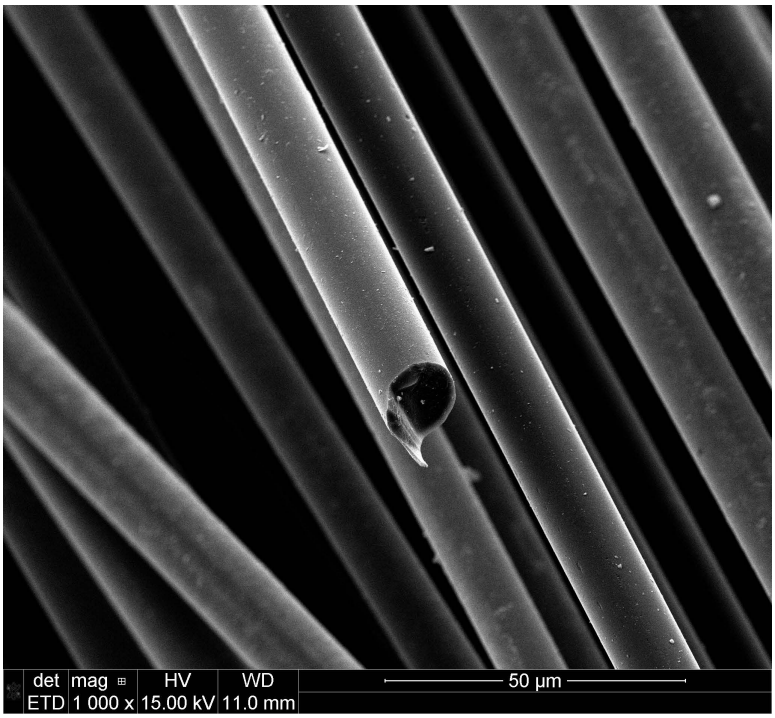

Figure 7.159: Hi-Nicalon S fiber specimen A37, tested in air at 900°C at 937MPa

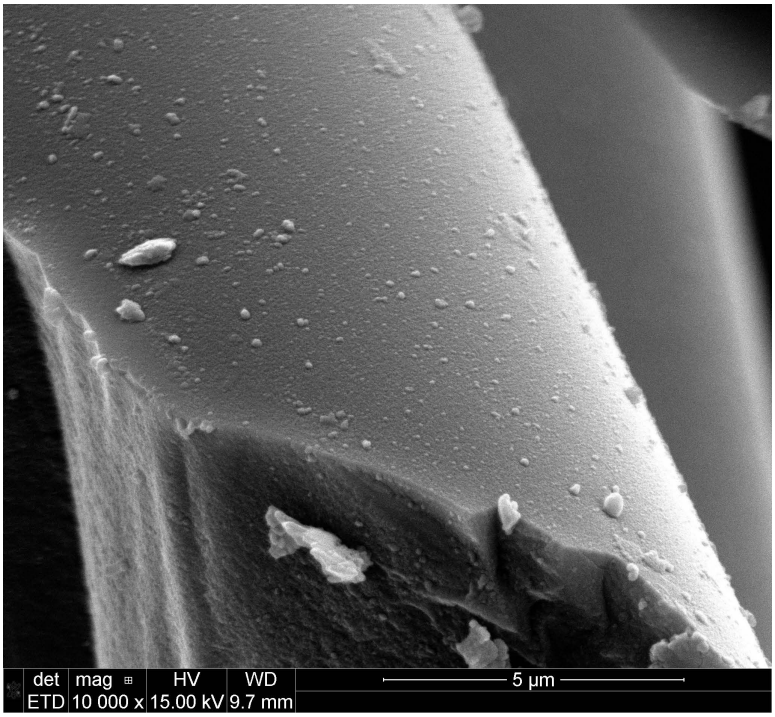

Figure 7.160: Hi-Nicalon S fiber specimen A34, tested in air at 900°C at 1023MPa

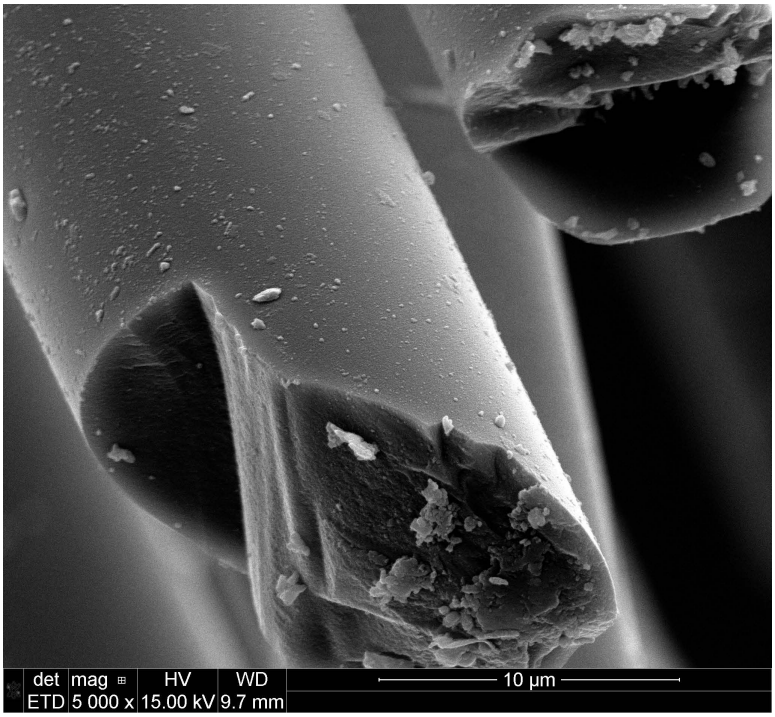

Figure 7.161: Hi-Nicalon S fiber specimen A34, tested in air at 900°C at 1023MPa

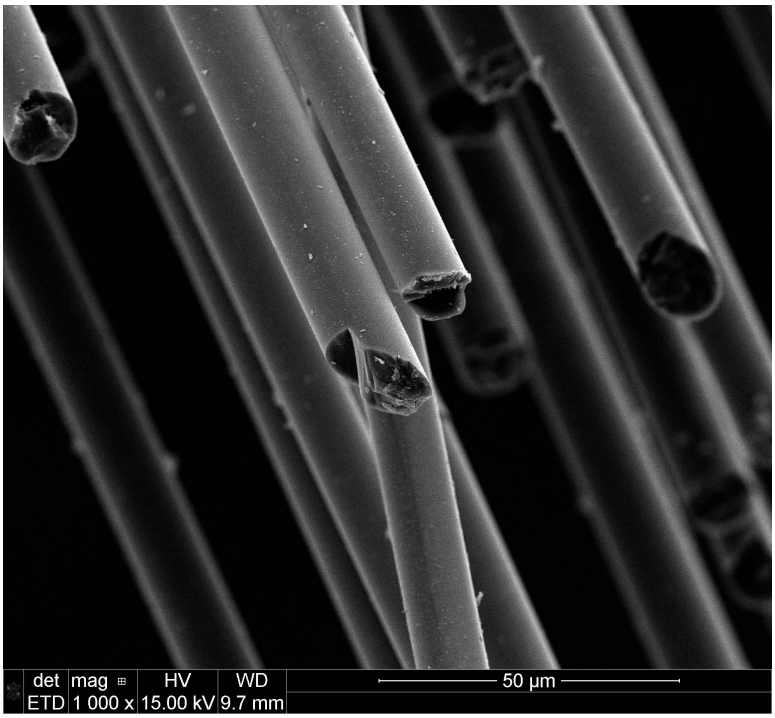

Figure 7.162: Hi-Nicalon S fiber specimen A34, tested in air at 900°C at 1023MPa

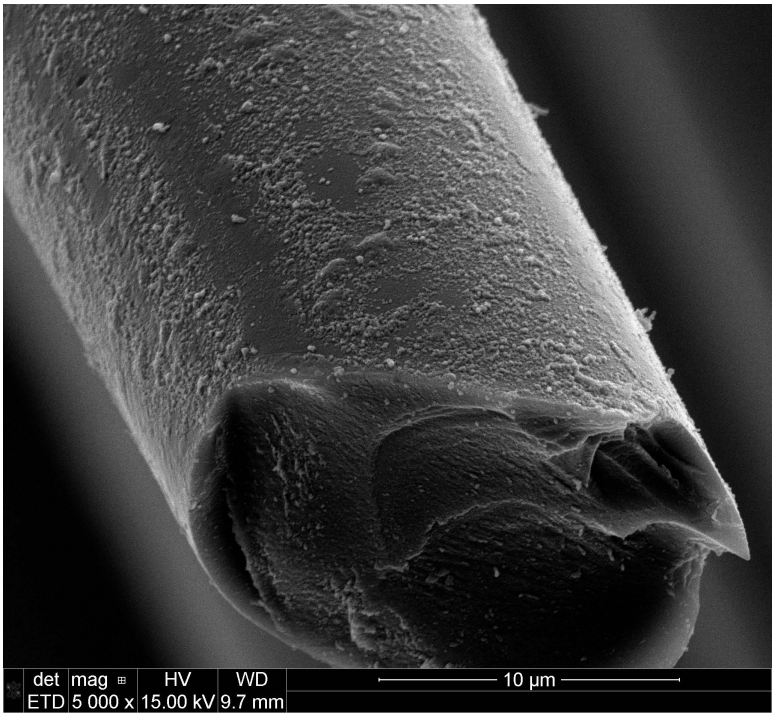

Figure 7.163: Hi-Nicalon S fiber specimen A34, tested in air at 900°C at 1023MPa

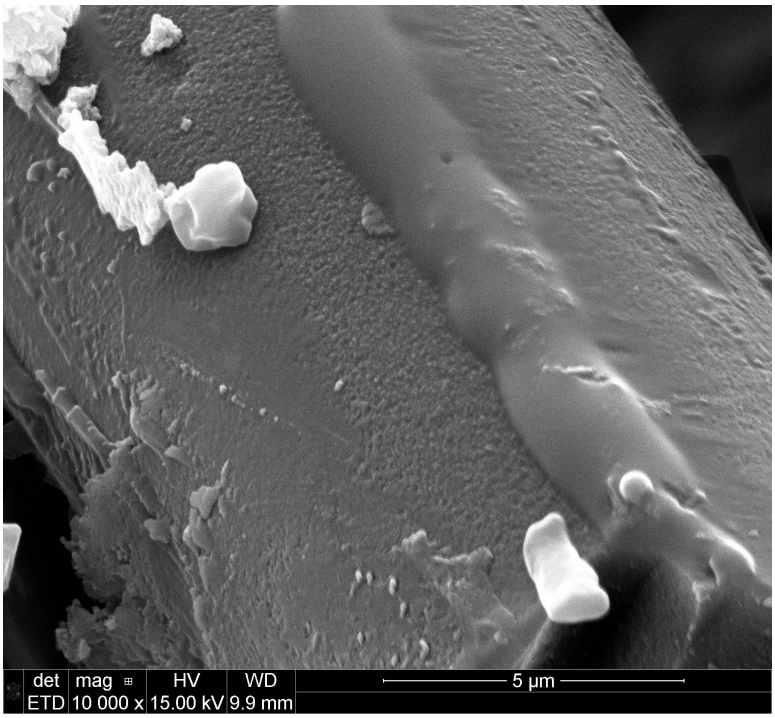

Figure 7.164: Hi-Nicalon S fiber specimen S48, tested in steam at 900°C at 255MPa

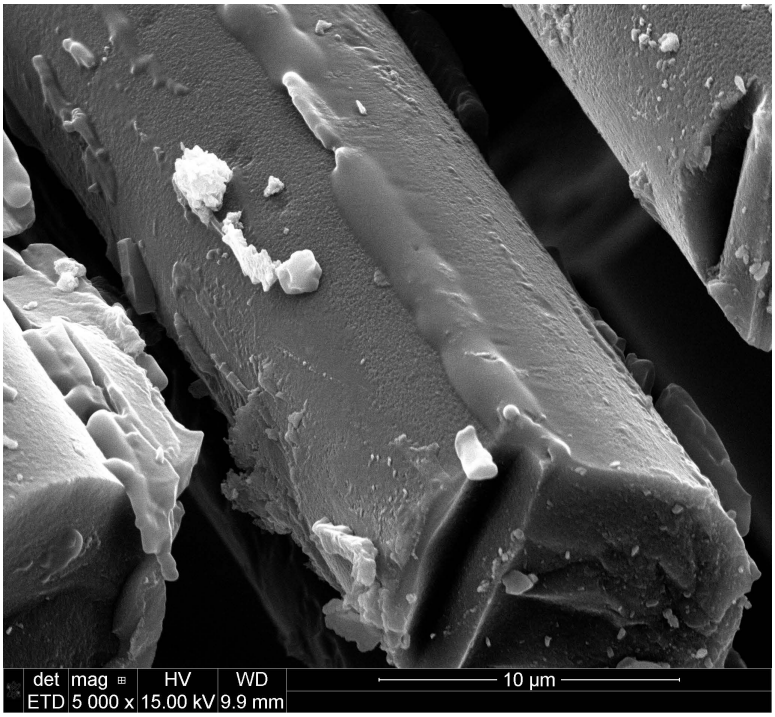

Figure 7.165: Hi-Nicalon S fiber specimen S48, tested in steam at 900°C at 255MPa

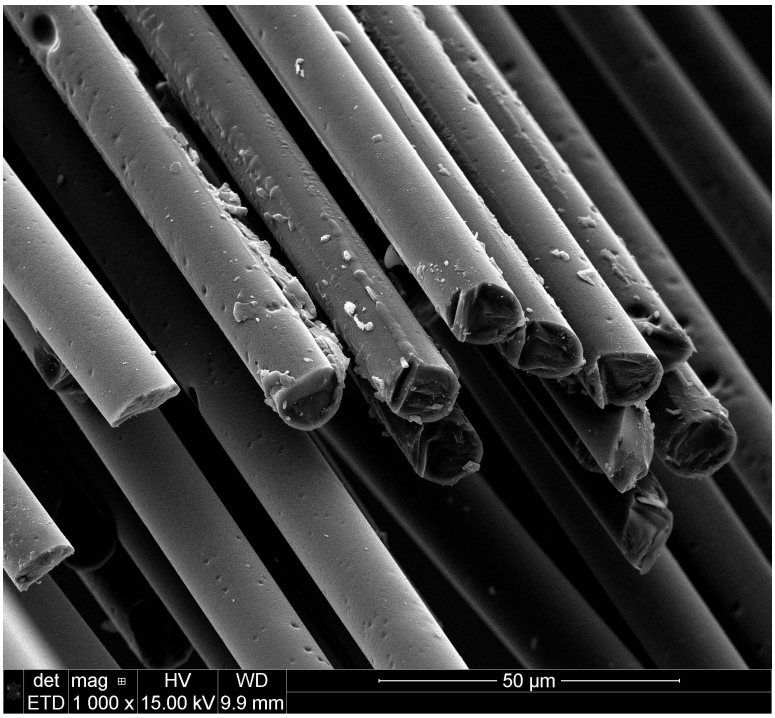

Figure 7.166: Hi-Nicalon S fiber specimen S48, tested in steam at 900°C at 255MPa

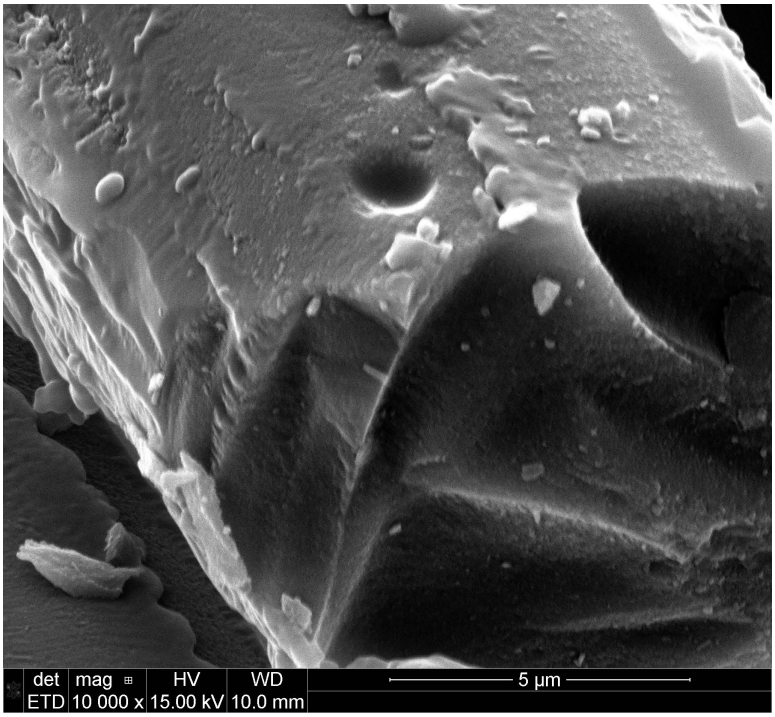

Figure 7.167: Hi-Nicalon S fiber specimen S48, tested in steam at 900°C at 255MPa

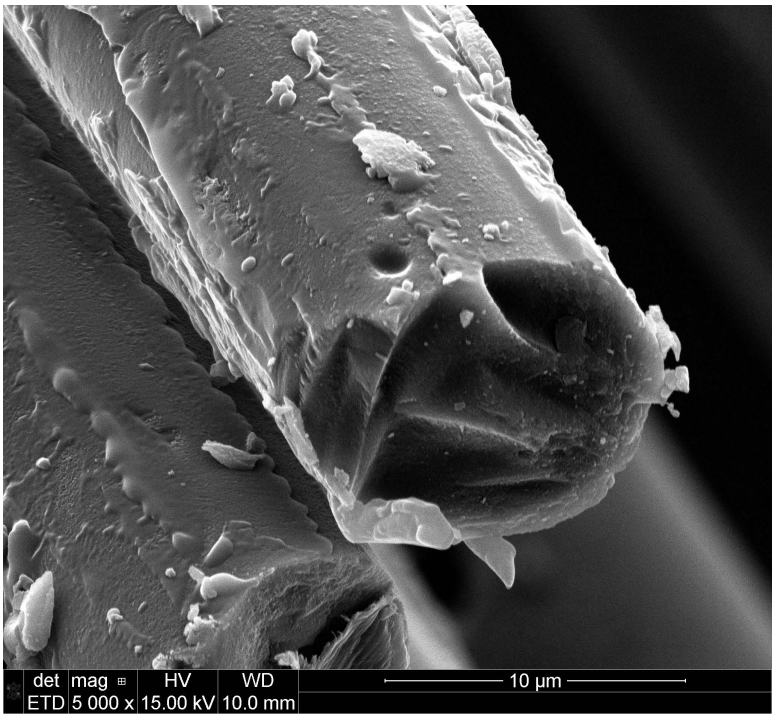

Figure 7.168: Hi-Nicalon S fiber specimen S48, tested in steam at 900°C at 255MPa

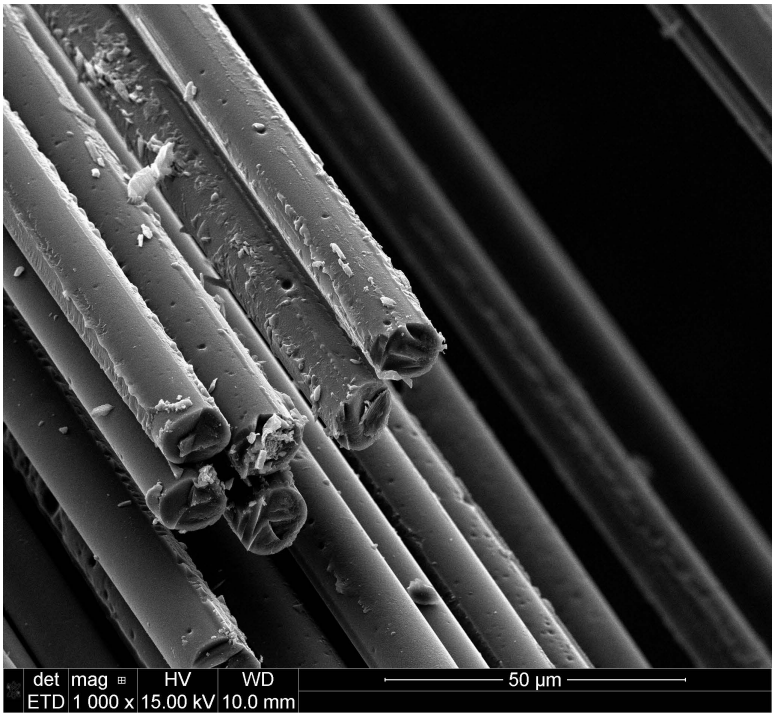

Figure 7.169: Hi-Nicalon S fiber specimen S48, tested in steam at 900°C at 255MPa

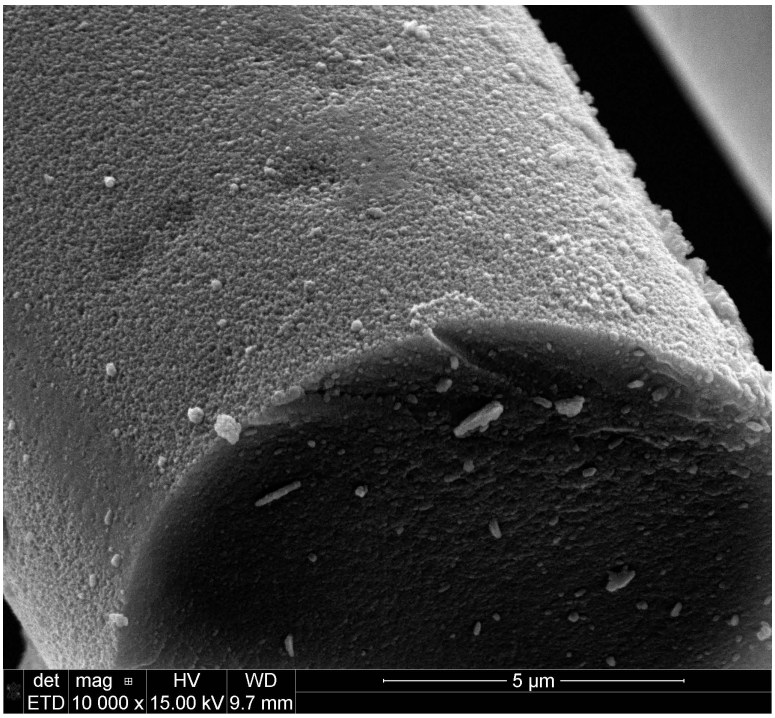

Figure 7.170: Hi-Nicalon S fiber specimen S48, tested in steam at 900°C at 255MPa

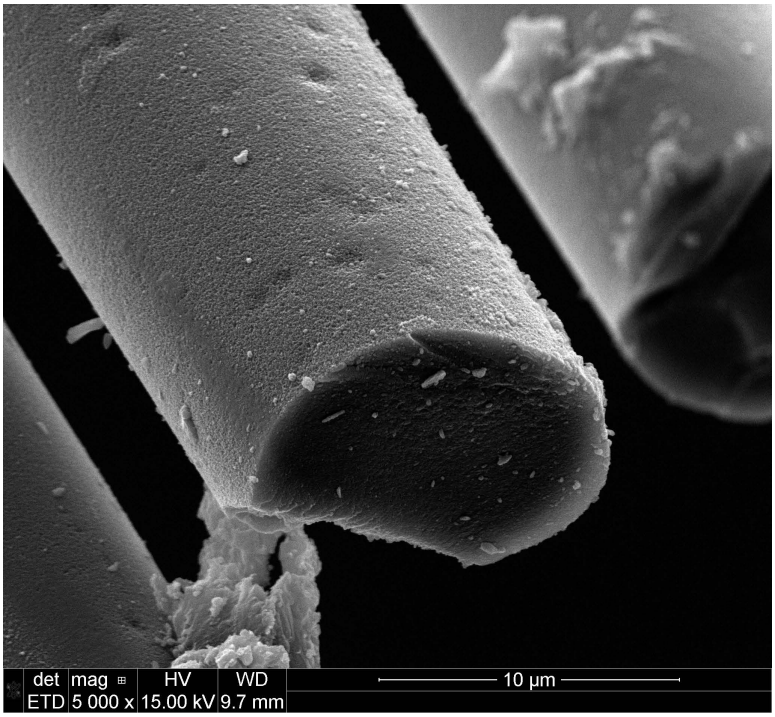

Figure 7.171: Hi-Nicalon S fiber specimen S48, tested in steam at 900°C at 255MPa

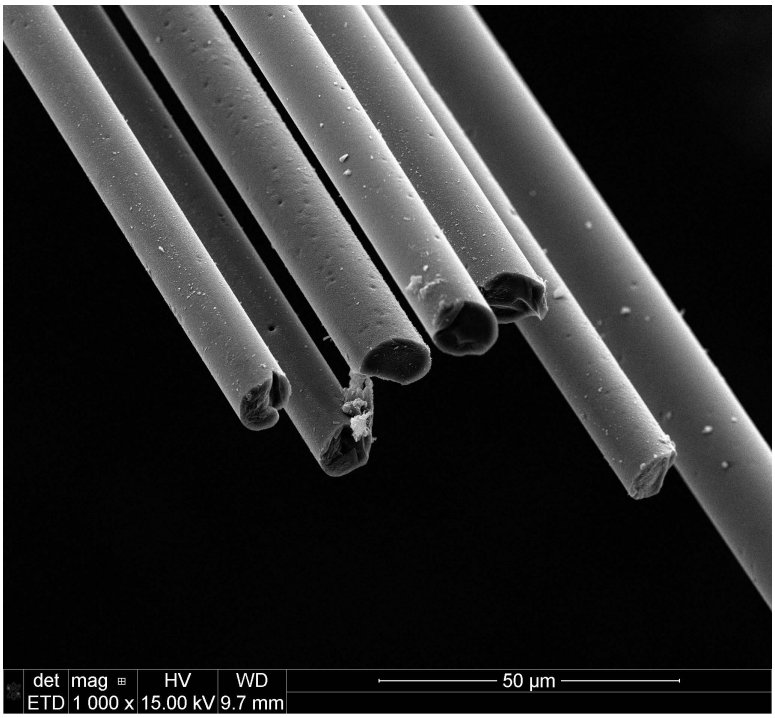

Figure 7.172: Hi-Nicalon S fiber specimen S48, tested in steam at 900°C at 255MPa

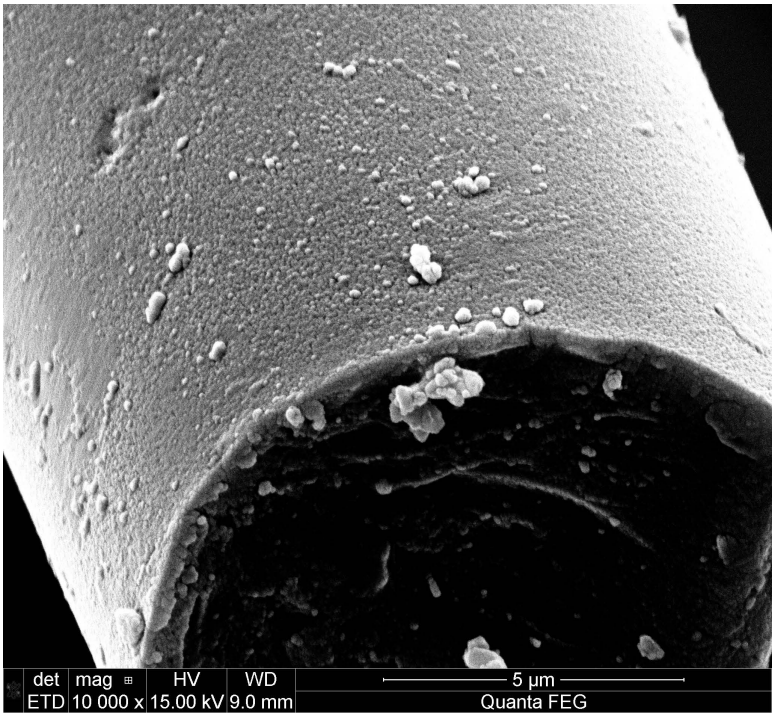

Figure 7.173: Hi-Nicalon S fiber specimen S40, tested in steam at 900°C at 353MPa

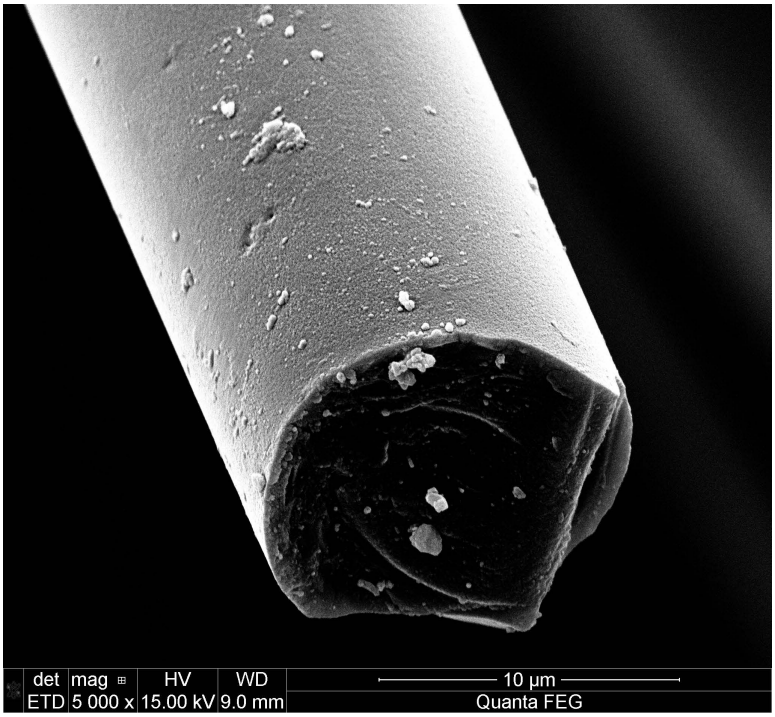

Figure 7.174: Hi-Nicalon S fiber specimen S40, tested in steam at 900°C at 353MPa

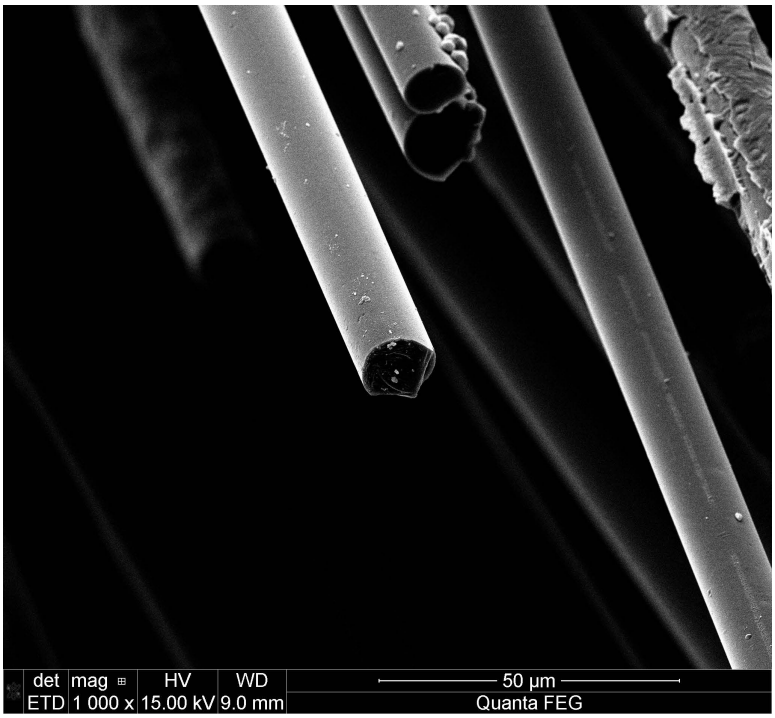

Figure 7.175: Hi-Nicalon S fiber specimen S40, tested in steam at 900°C at 353MPa

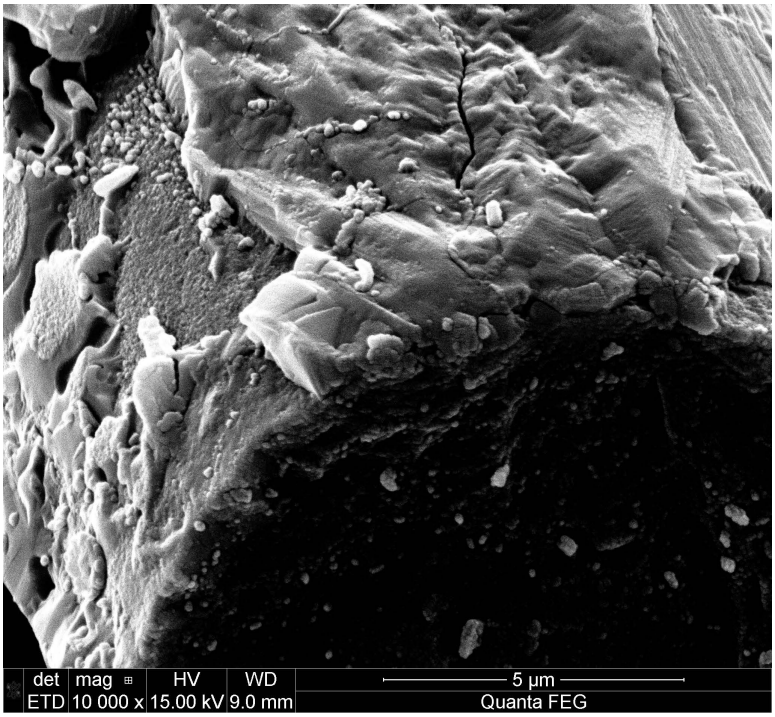

Figure 7.176: Hi-Nicalon S fiber specimen S40, tested in steam at 900°C at 353MPa

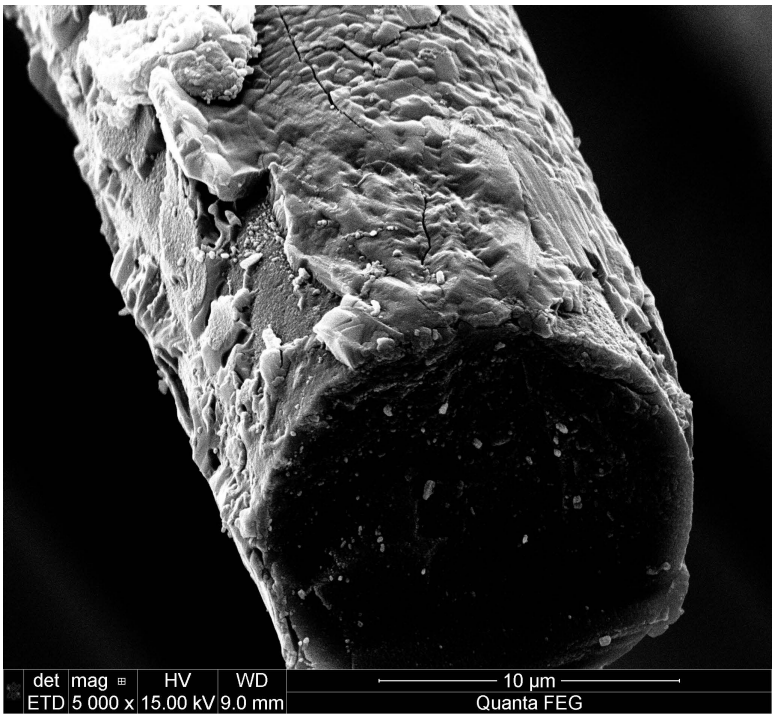

Figure 7.177: Hi-Nicalon S fiber specimen S40, tested in steam at 900°C at 353MPa

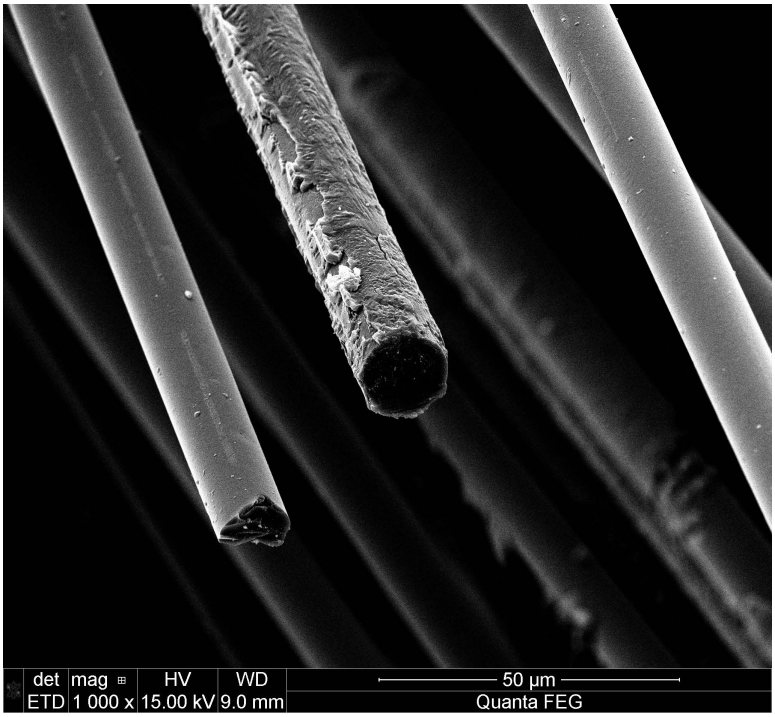

Figure 7.178: Hi-Nicalon S fiber specimen S40, tested in steam at 900°C at 353MPa

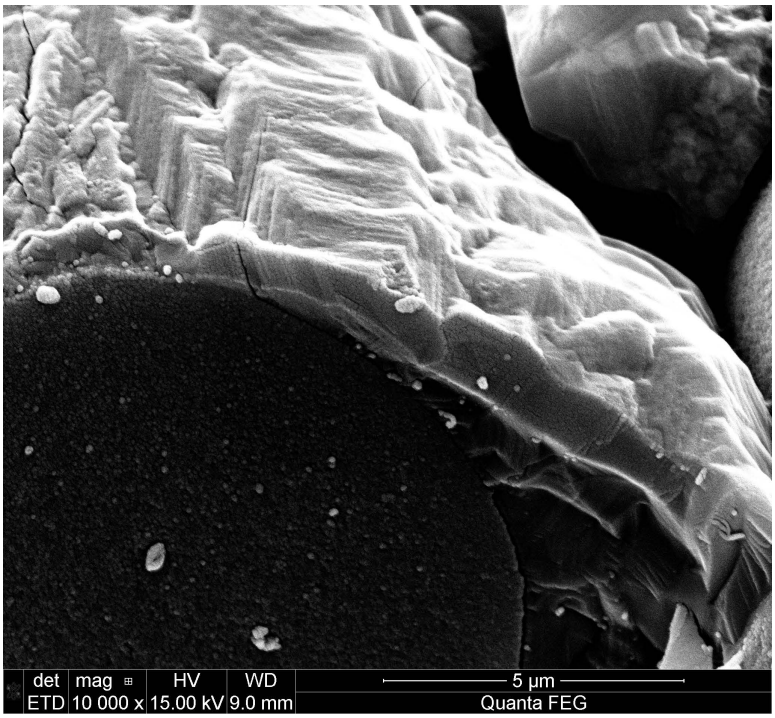

Figure 7.179: Hi-Nicalon S fiber specimen S40, tested in steam at 900°C at 353MPa

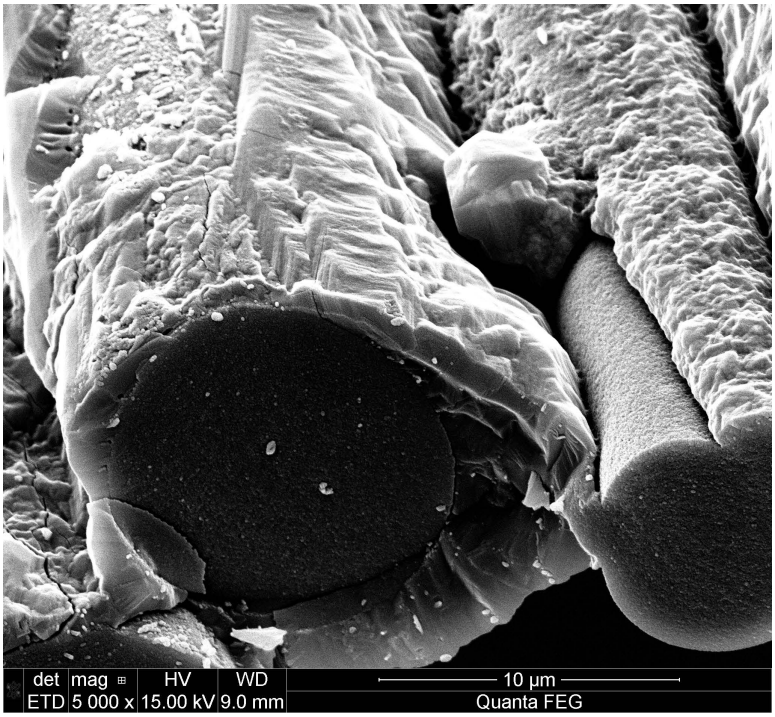

Figure 7.180: Hi-Nicalon S fiber specimen S40, tested in steam at 900°C at 353MPa

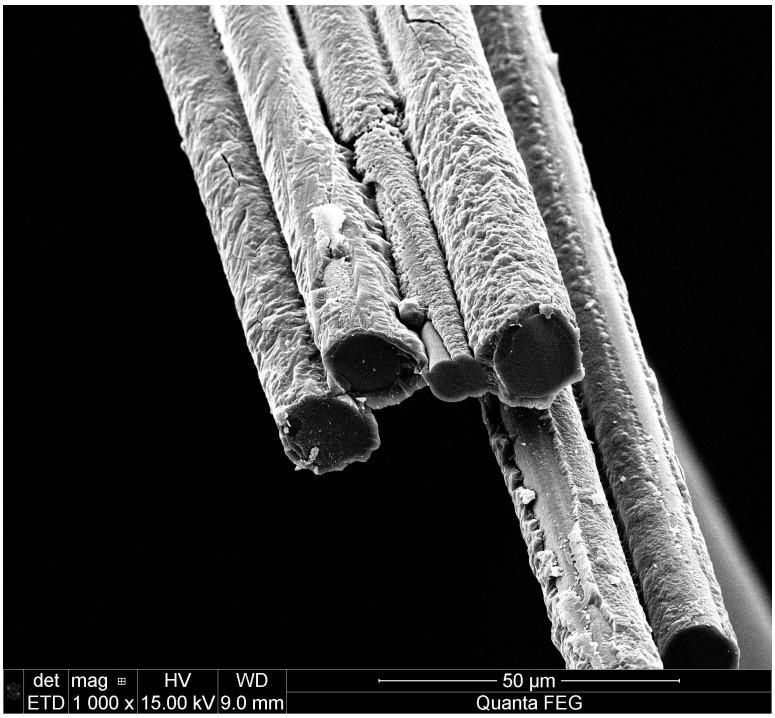

Figure 7.181: Hi-Nicalon S fiber specimen S40, tested in steam at 900°C at 353MPa

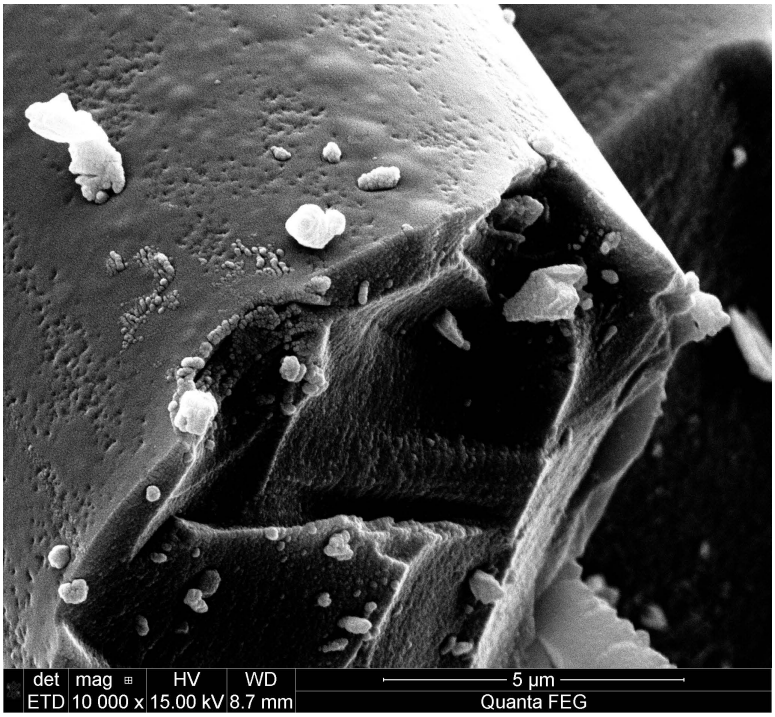

Figure 7.182: Hi-Nicalon S fiber specimen S38, tested in steam at 900°C at 353MPa

7.4.3 Fibers tested at 1000°C.

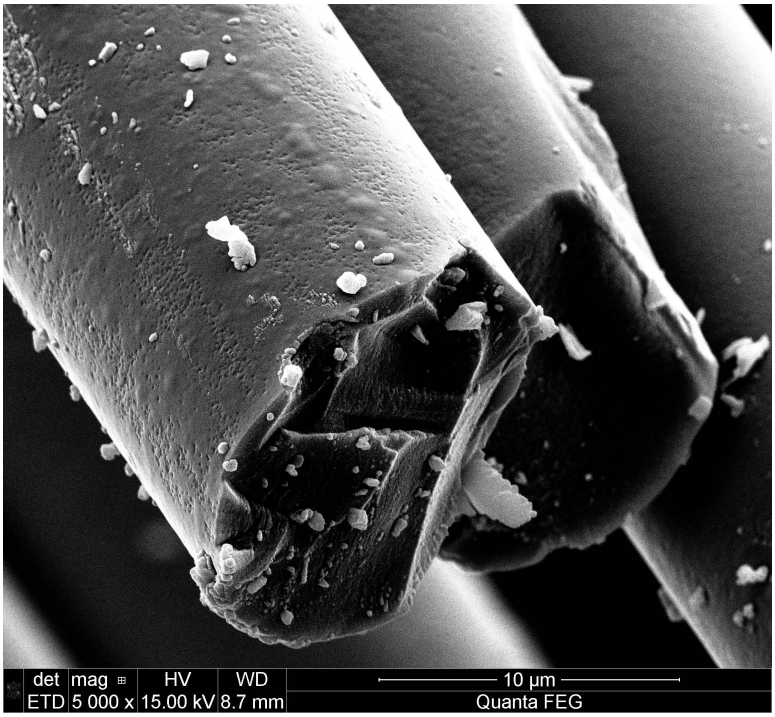

Figure 7.183: Hi-Nicalon S fiber specimen S38, tested in steam at 900°C at 353MPa

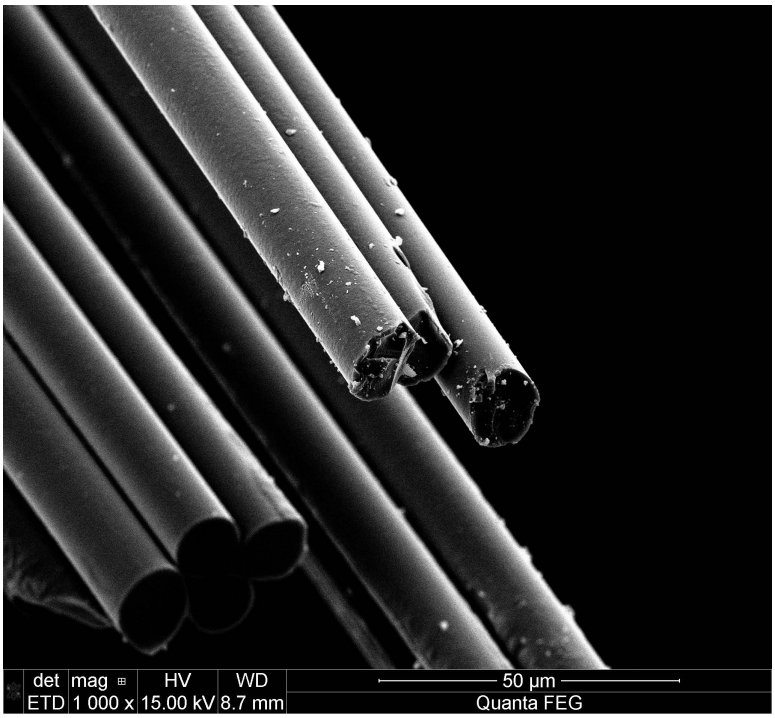

Figure 7.184: Hi-Nicalon S fiber specimen S38, tested in steam at 900°C at 353MPa

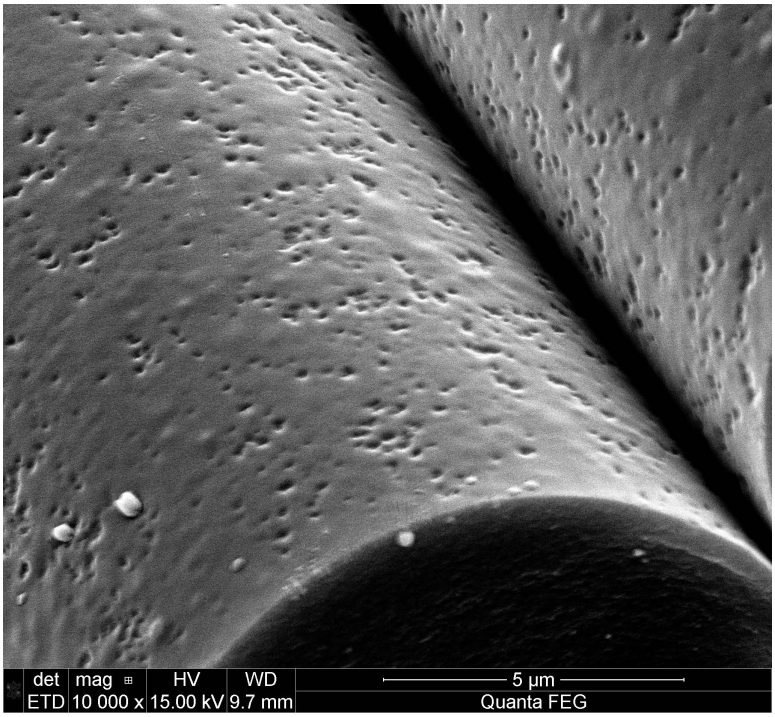

Figure 7.185: Hi-Nicalon S fiber specimen S38, tested in steam at 900°C at 353MPa

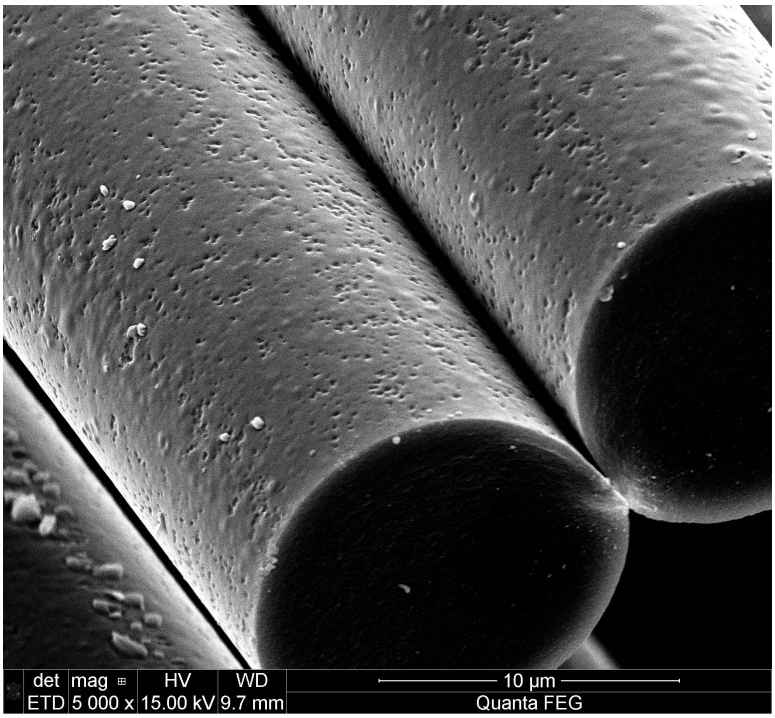

Figure 7.186: Hi-Nicalon S fiber specimen S38, tested in steam at 900°C at 353MPa

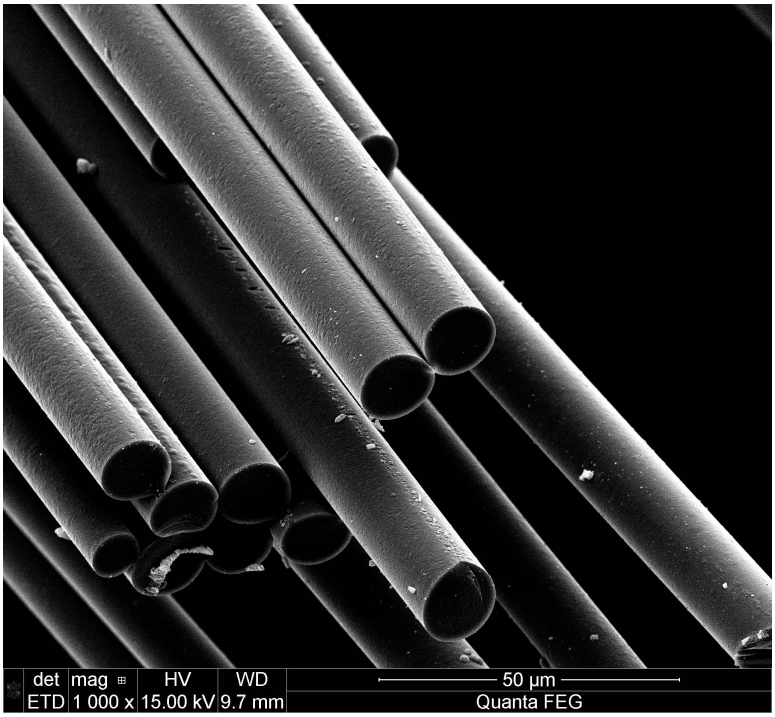

Figure 7.187: Hi-Nicalon S fiber specimen S38, tested in steam at 900°C at 353MPa

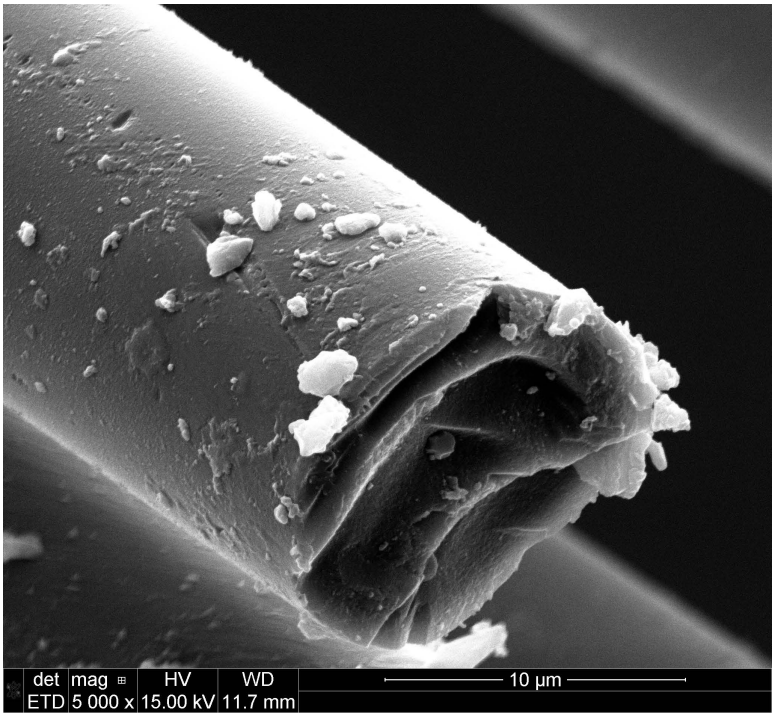

Figure 7.188: Hi-Nicalon S fiber specimen A42, tested in air at 1000°C at 700MPa

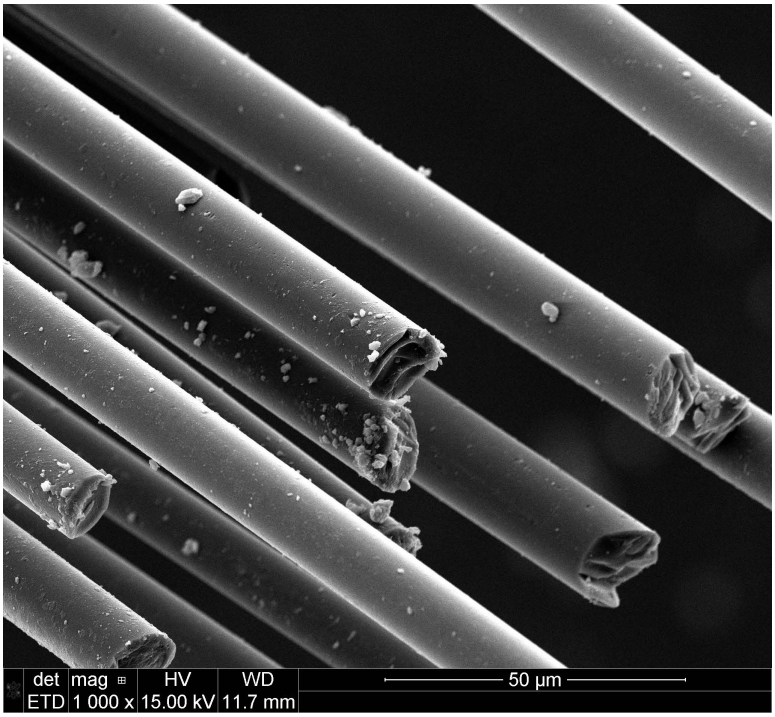

Figure 7.189: Hi-Nicalon S fiber specimen A42, tested in air at 1000°C at 700MPa

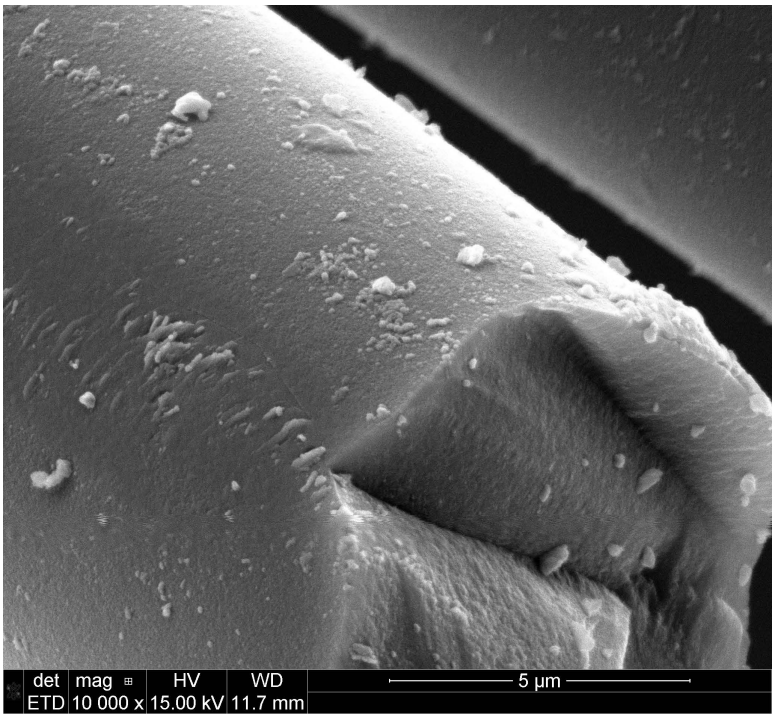

Figure 7.190: Hi-Nicalon S fiber specimen A42, tested in air at 1000°C at 700MPa

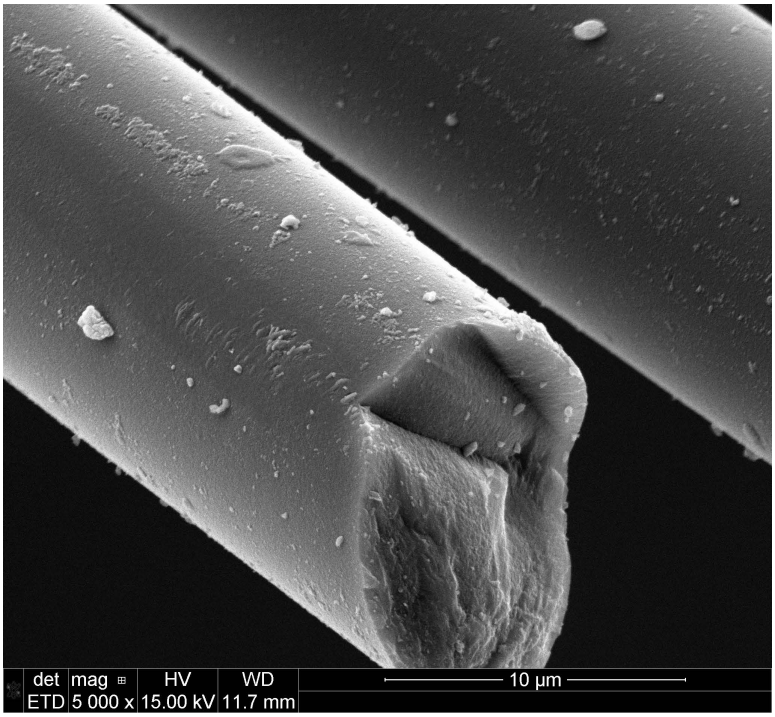

Figure 7.191: Hi-Nicalon S fiber specimen A42, tested in air at 1000°C at 700MPa

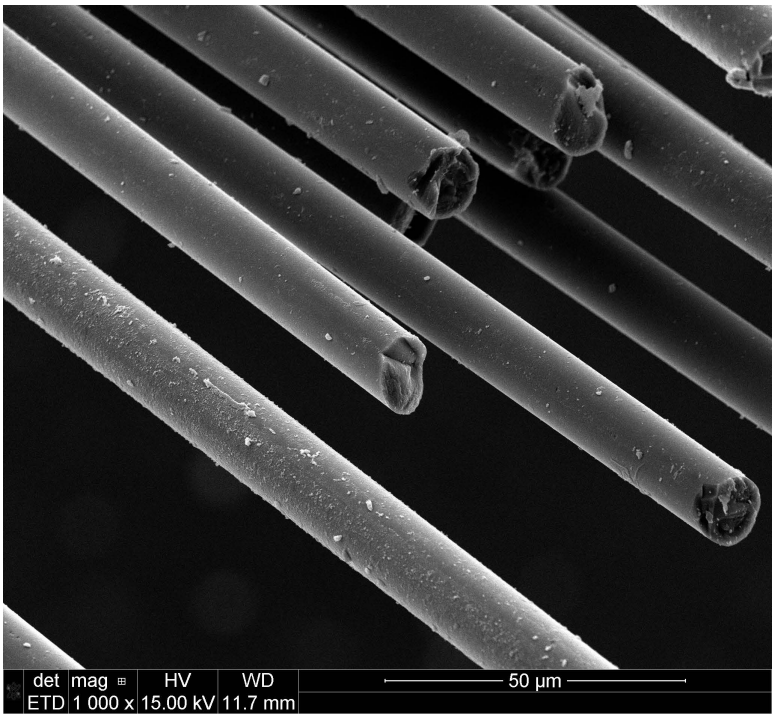

Figure 7.192: Hi-Nicalon S fiber specimen A42, tested in air at 1000°C at 700MPa

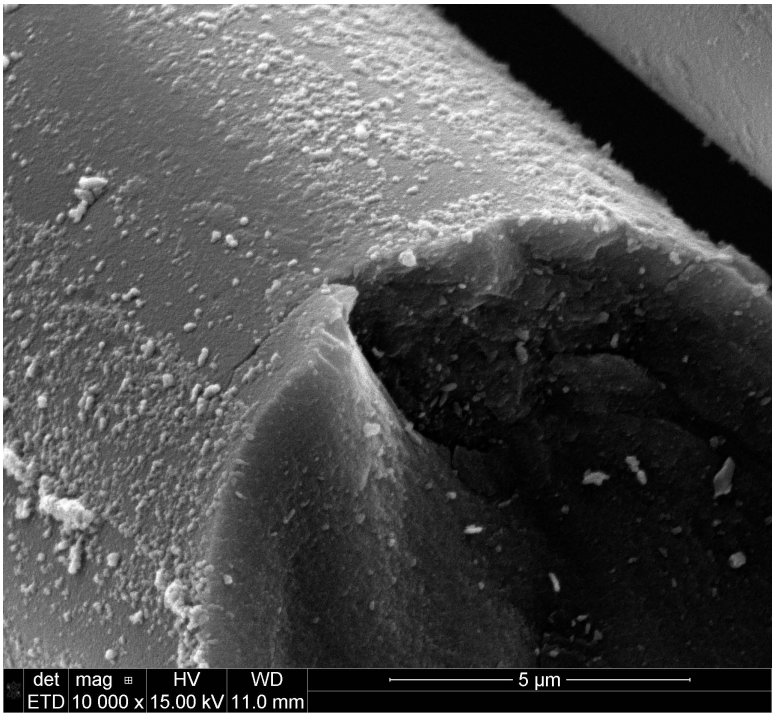

Figure 7.193: Hi-Nicalon S fiber specimen A43, tested in air at 1000°C at 700MPa

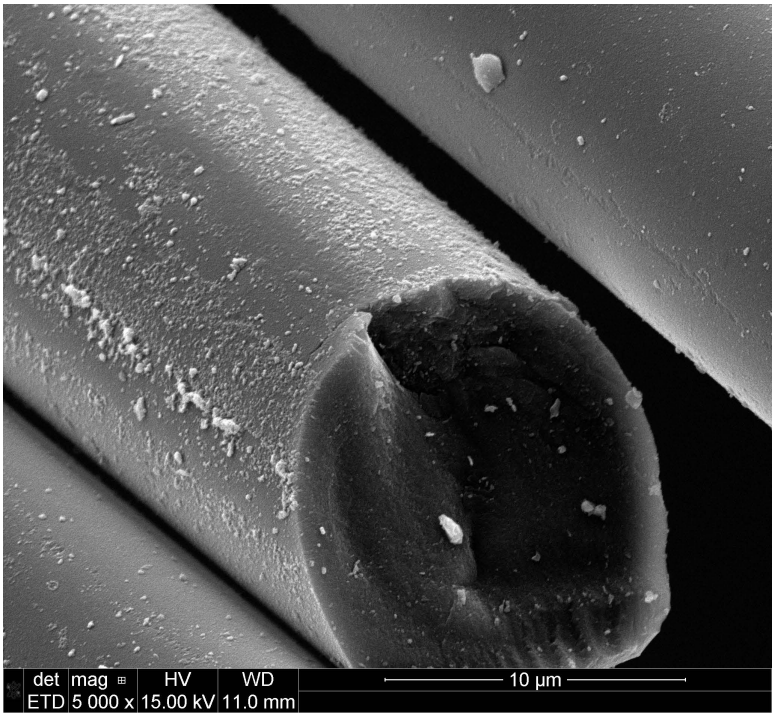

Figure 7.194: Hi-Nicalon S fiber specimen A43, tested in air at 1000°C at 700MPa

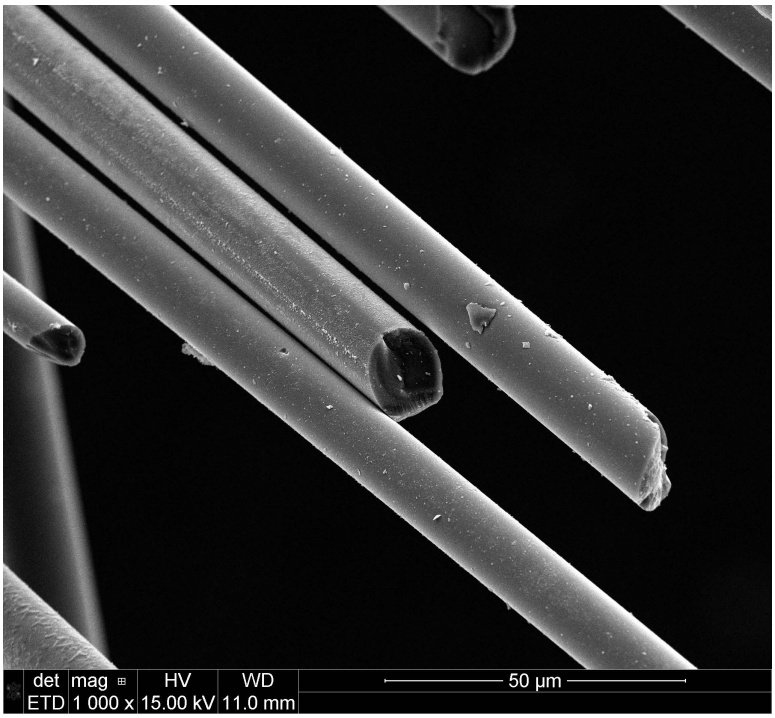

Figure 7.195: Hi-Nicalon S fiber specimen A43, tested in air at 1000°C at 700MPa

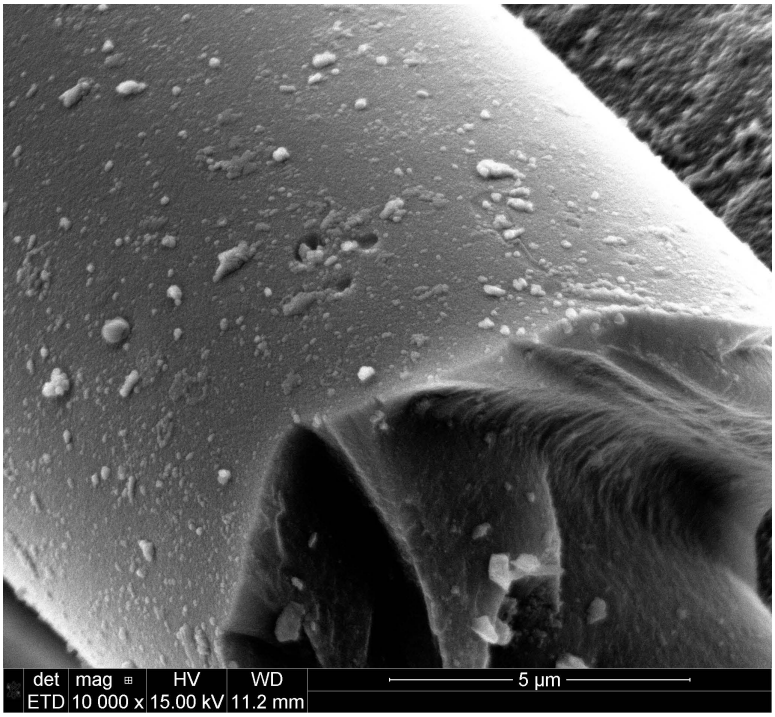

Figure 7.196: Hi-Nicalon S fiber specimen A43, tested in air at 1000°C at 700MPa

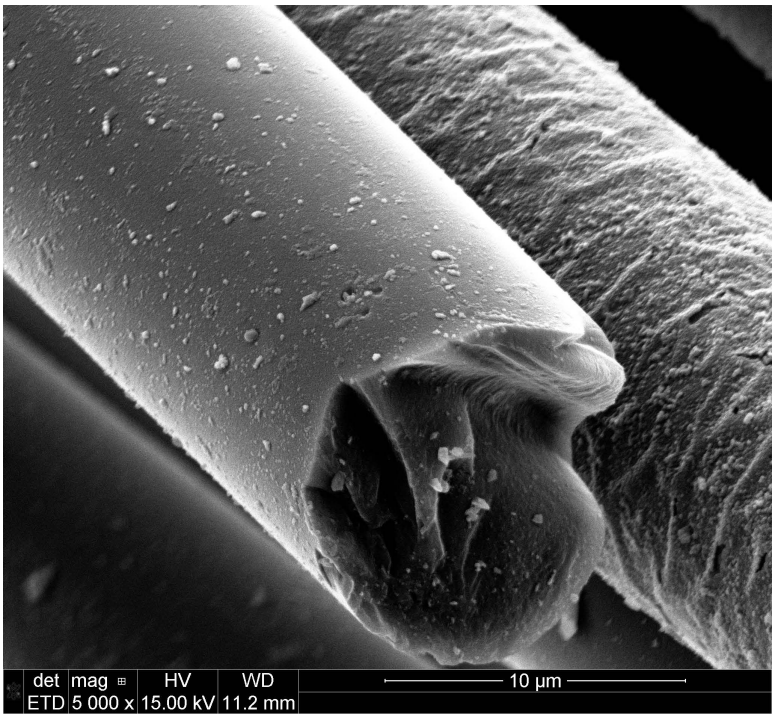

Figure 7.197: Hi-Nicalon S fiber specimen A43, tested in air at 1000°C at 700MPa

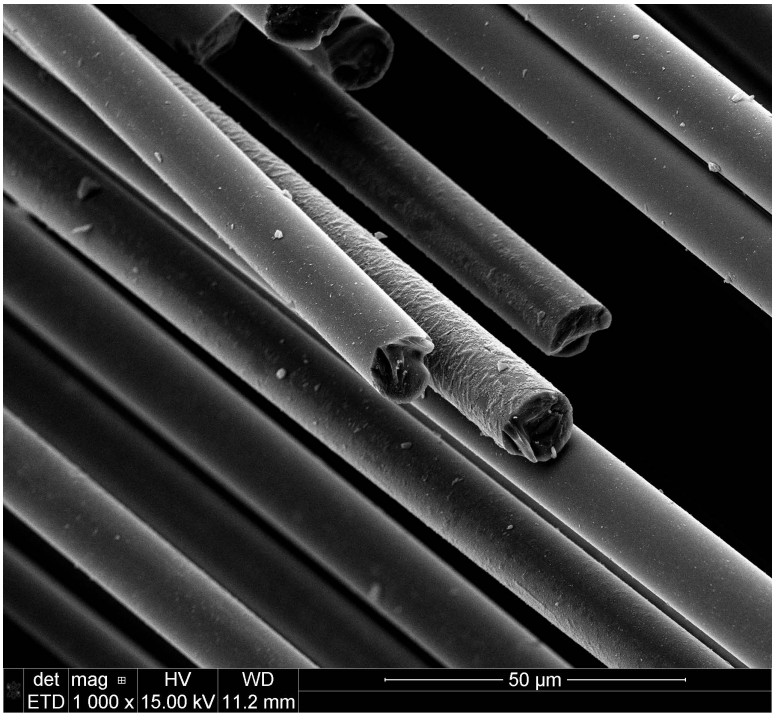

Figure 7.198: Hi-Nicalon S fiber specimen A43, tested in air at 1000°C at 700MPa

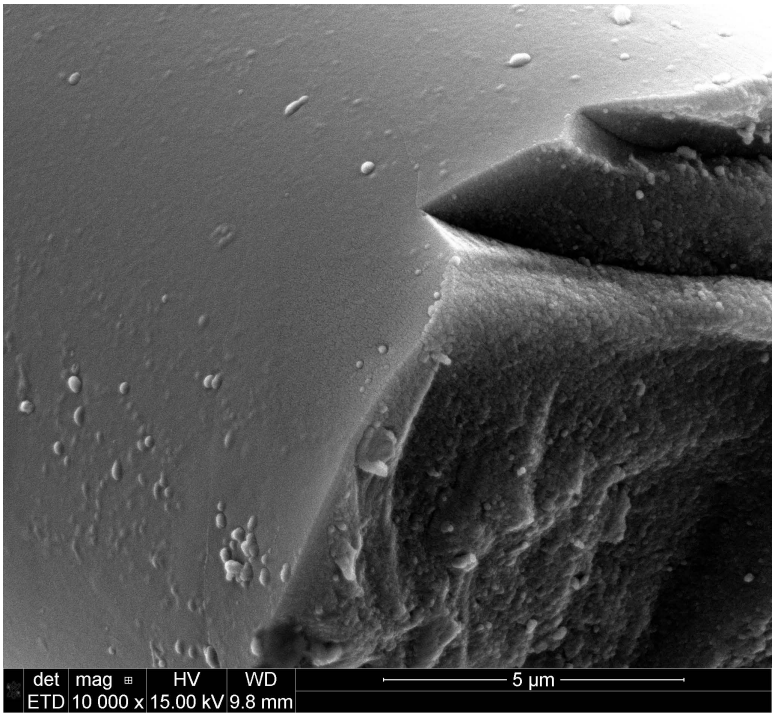

Figure 7.199: Hi-Nicalon S fiber specimen S47, tested in steam at 1000°C at 255MPa

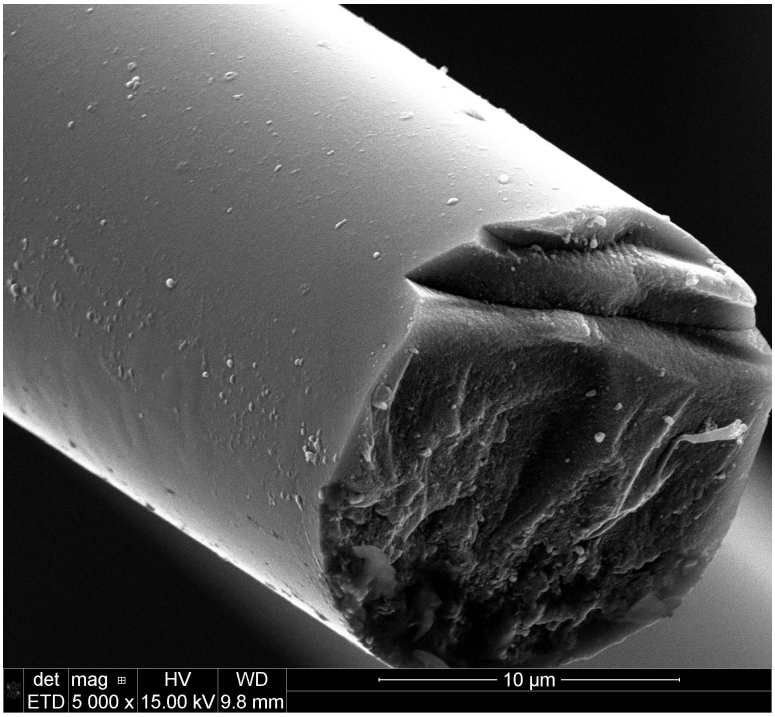

Figure 7.200: Hi-Nicalon S fiber specimen S47, tested in steam at 1000°C at 255MPa

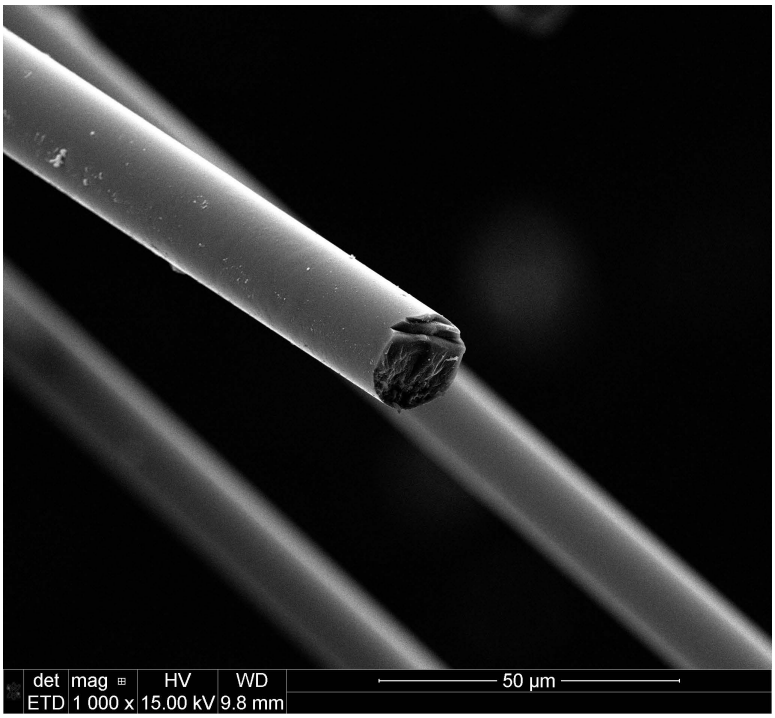

Figure 7.201: Hi-Nicalon S fiber specimen S47, tested in steam at 1000°C at 255MPa

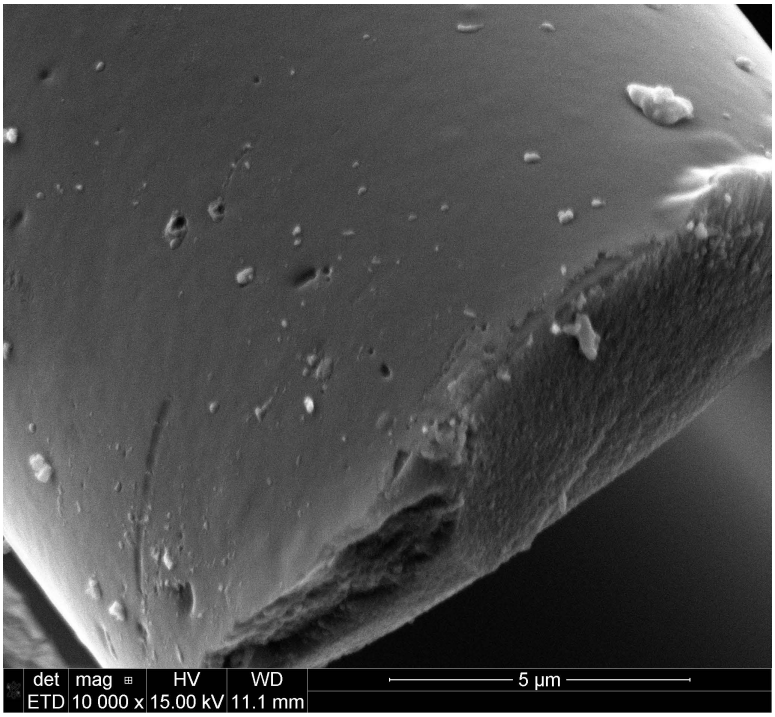

Figure 7.202: Hi-Nicalon S fiber specimen S47, tested in steam at 1000°C at 255MPa

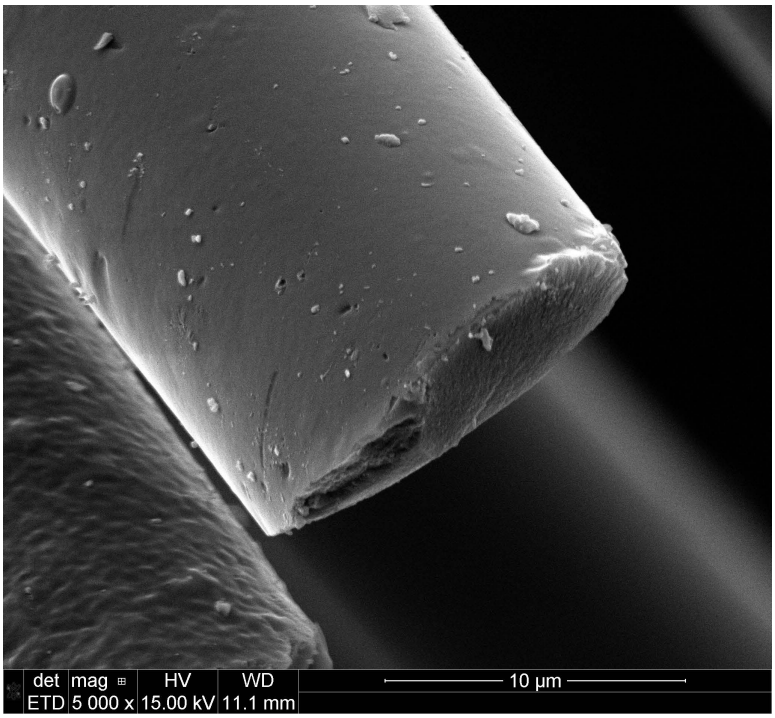

Figure 7.203: Hi-Nicalon S fiber specimen S47, tested in steam at 1000°C at 255MPa

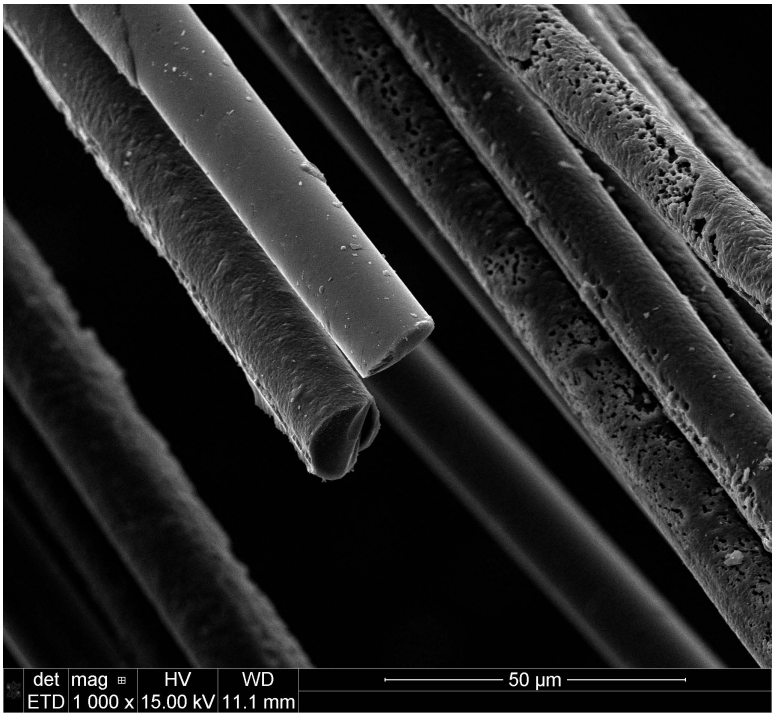

Figure 7.204: Hi-Nicalon S fiber specimen S47, tested in steam at 1000°C at 255MPa

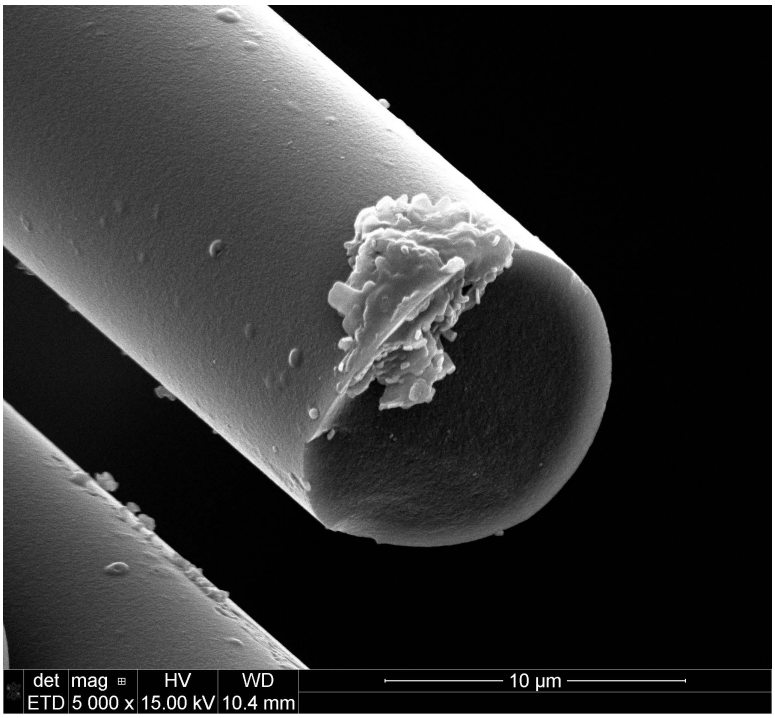

Figure 7.205: Hi-Nicalon S fiber specimen S47, tested in steam at 1000°C at 255MPa

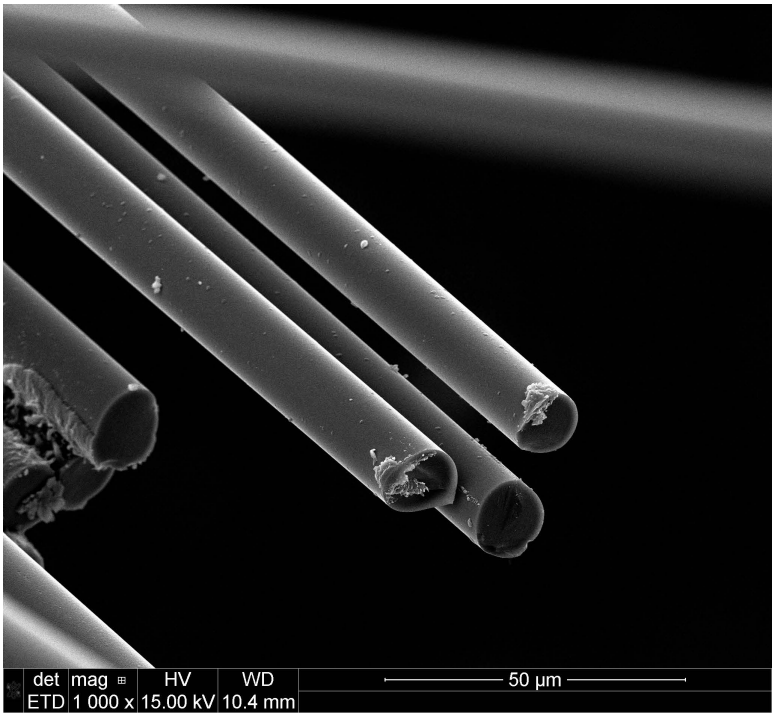

Figure 7.206: Hi-Nicalon S fiber specimen S47, tested in steam at 1000°C at 255MPa

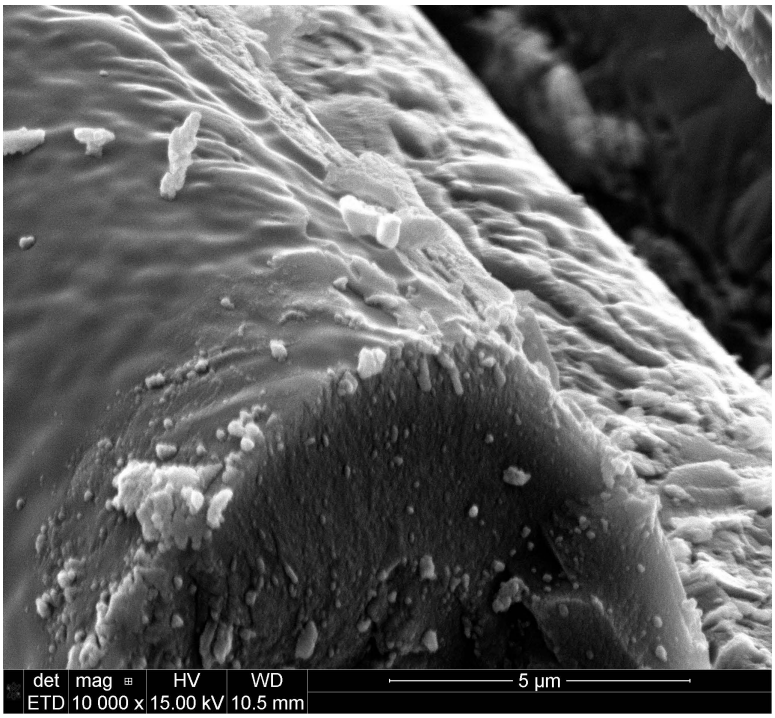

Figure 7.207: Hi-Nicalon S fiber specimen S47, tested in steam at 1000°C at 255MPa

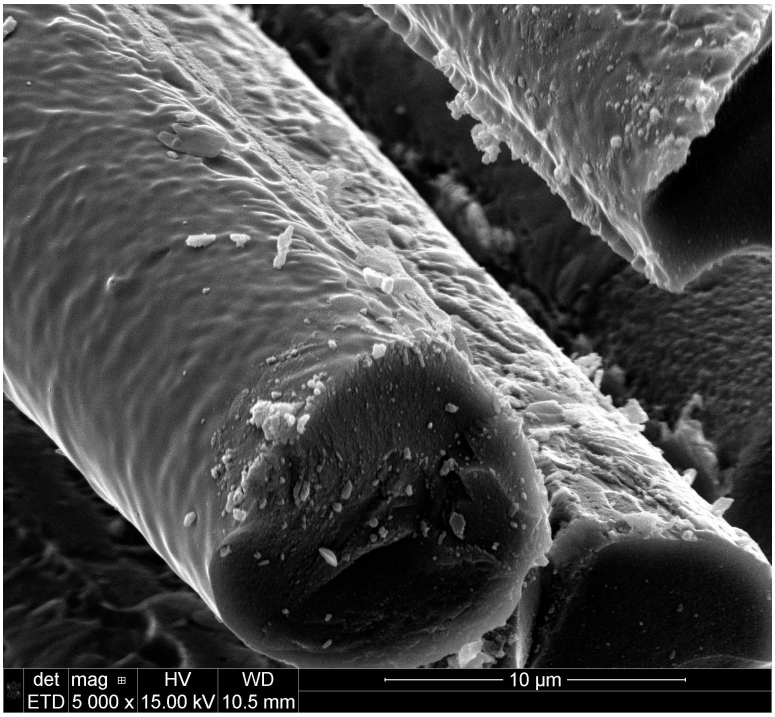

Figure 7.208: Hi-Nicalon S fiber specimen S47, tested in steam at 1000°C at 255MPa

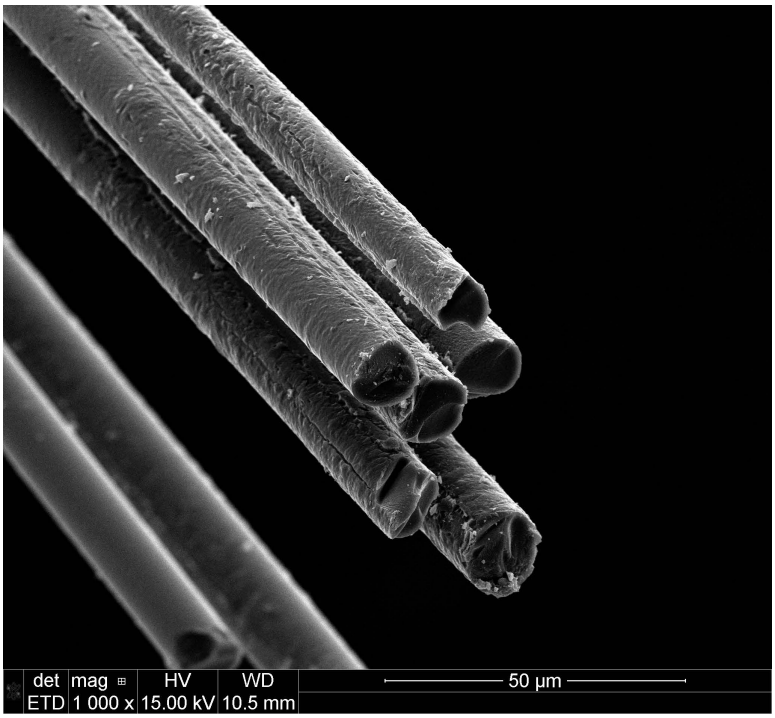

Figure 7.209: Hi-Nicalon S fiber specimen S47, tested in steam at 1000°C at 255MPa

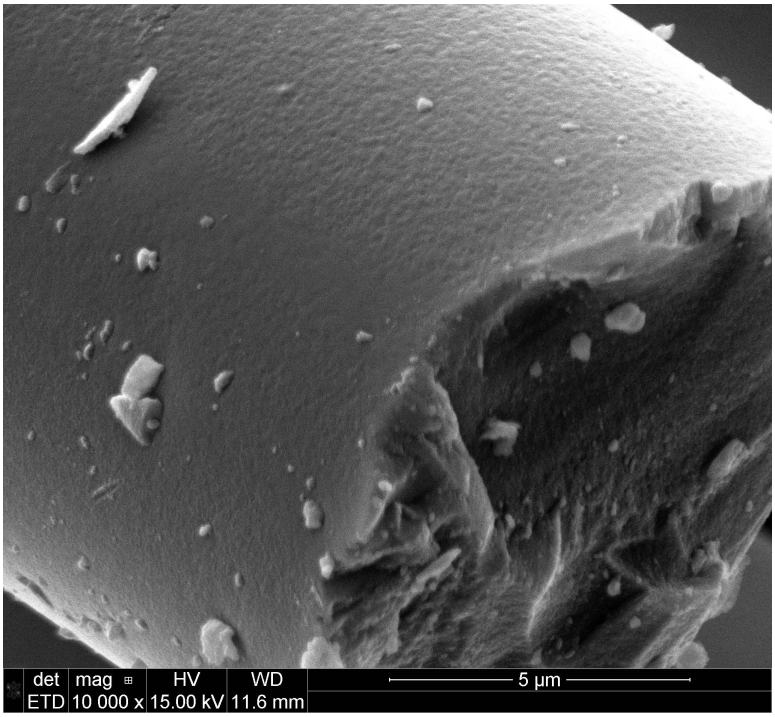

Figure 7.210: Hi-Nicalon S fiber specimen S44, tested in steam at 1000°C at 353MPa

7.4.4 Fibers tested at 1100°C.

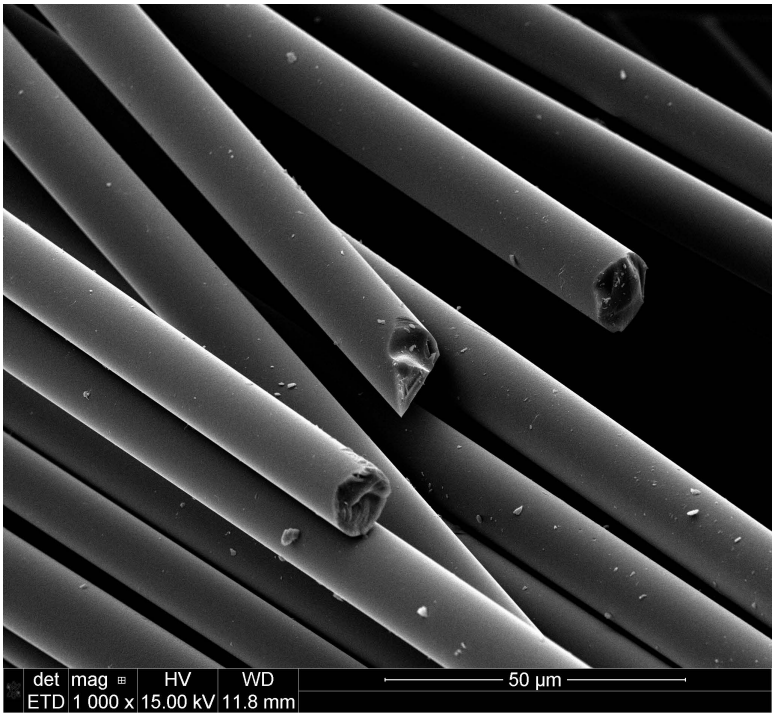

Figure 7.211: Hi-Nicalon S fiber specimen S44, tested in steam at 1000°C at 353MPa

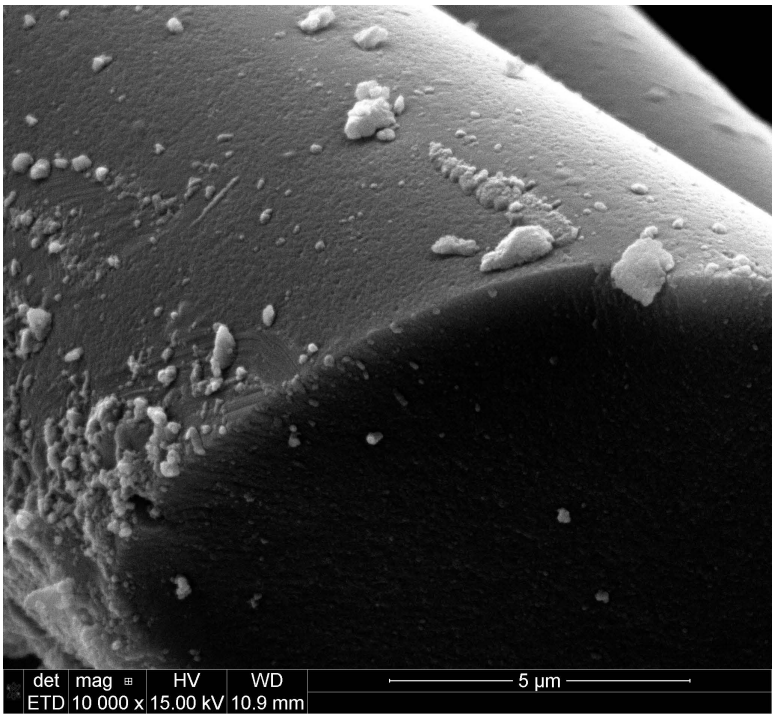

Figure 7.212: Hi-Nicalon S fiber specimen S45, tested in steam at 1000°C at 400MPa

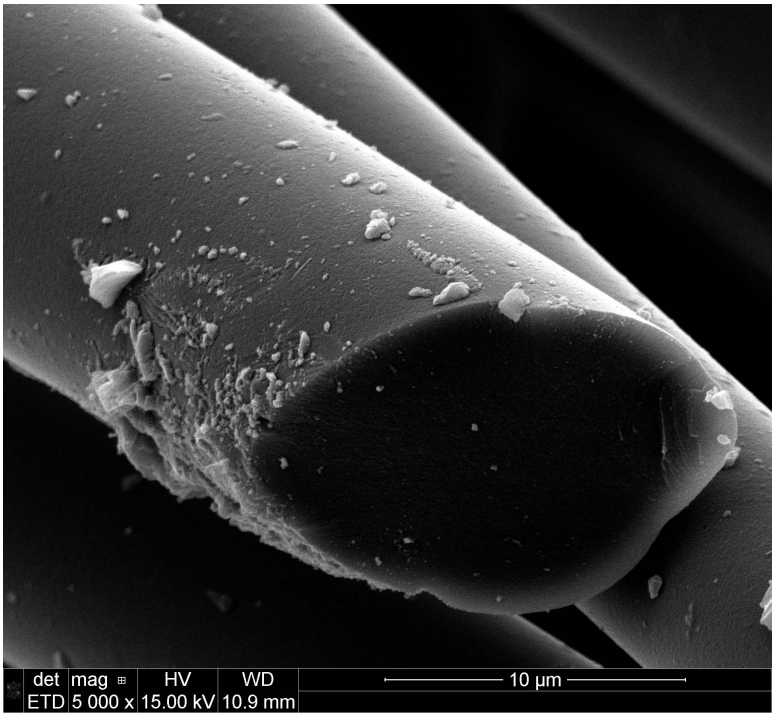

Figure 7.213: Hi-Nicalon S fiber specimen S45, tested in steam at 1000°C at 400MPa

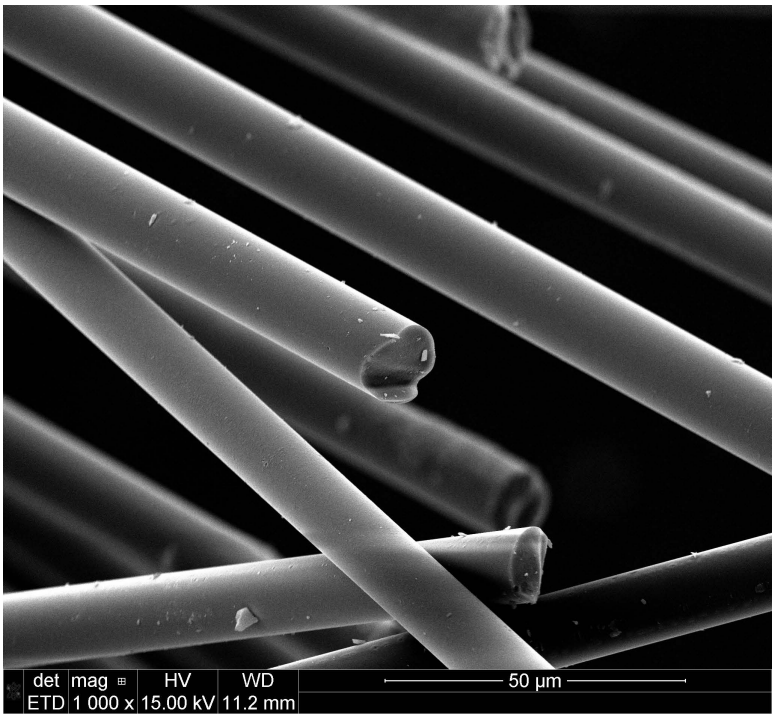

Figure 7.214: Hi-Nicalon S fiber specimen S45, tested in steam at 1000°C at 400MPa

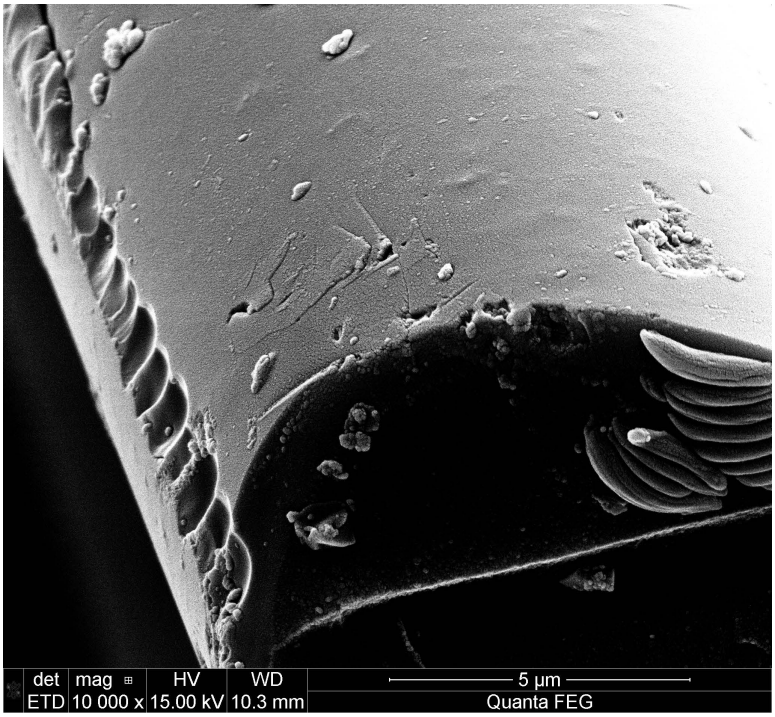

Figure 7.215: Hi-Nicalon S fiber specimen A27, tested in air at 1100°C at 154MPa

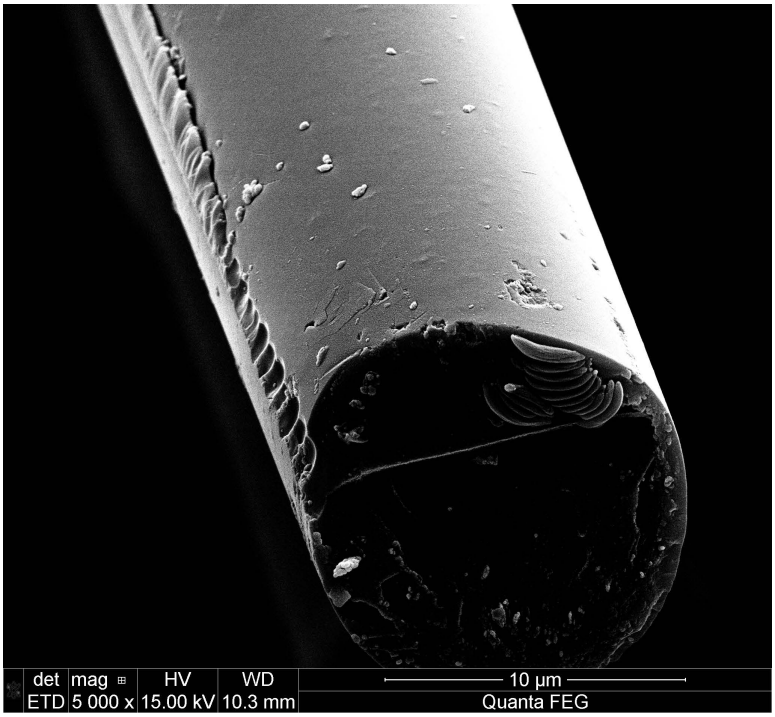

Figure 7.216: Hi-Nicalon S fiber specimen A27, tested in air at 1100°C at 154MPa

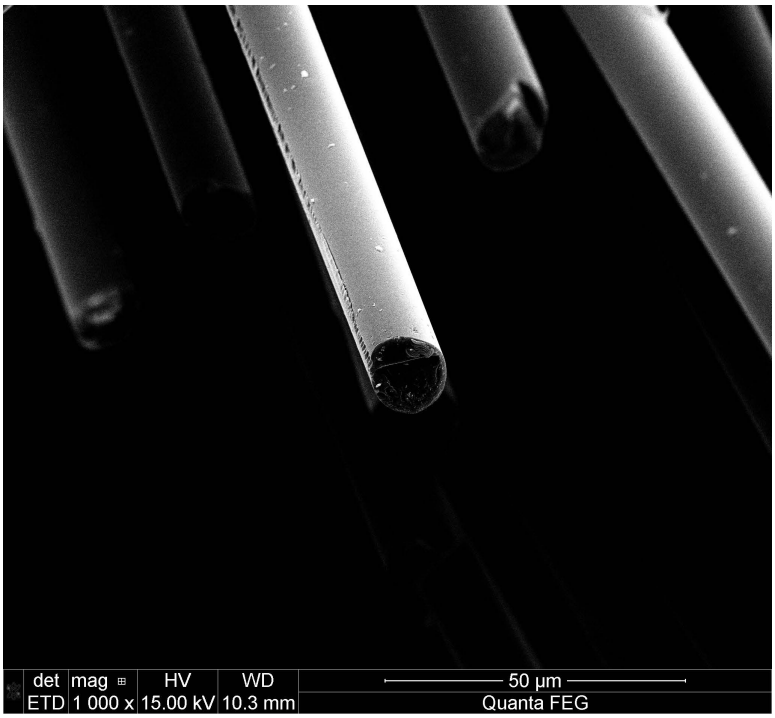

Figure 7.217: Hi-Nicalon S fiber specimen A27, tested in air at 1100°C at 154MPa

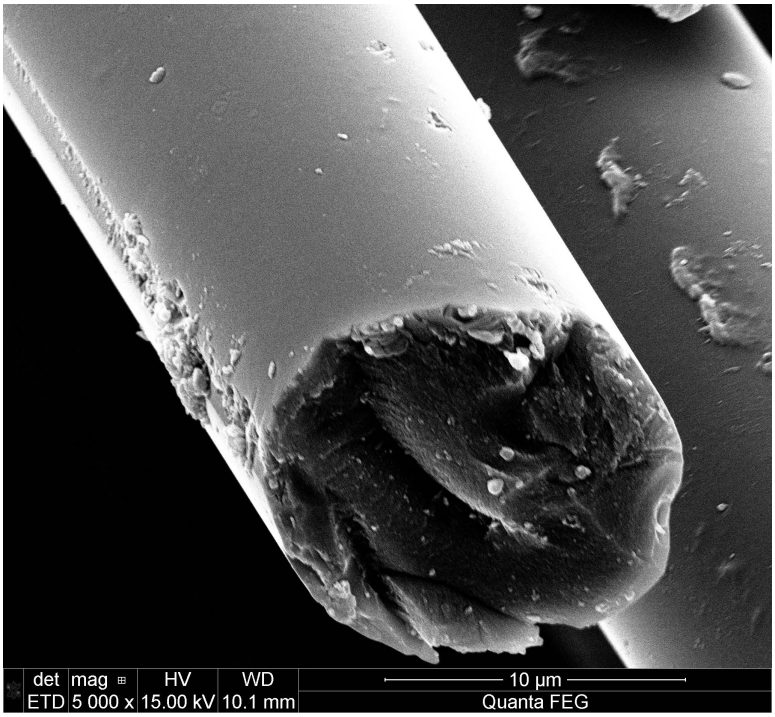

Figure 7.218: Hi-Nicalon S fiber specimen A27, tested in air at 1100°C at 154MPa

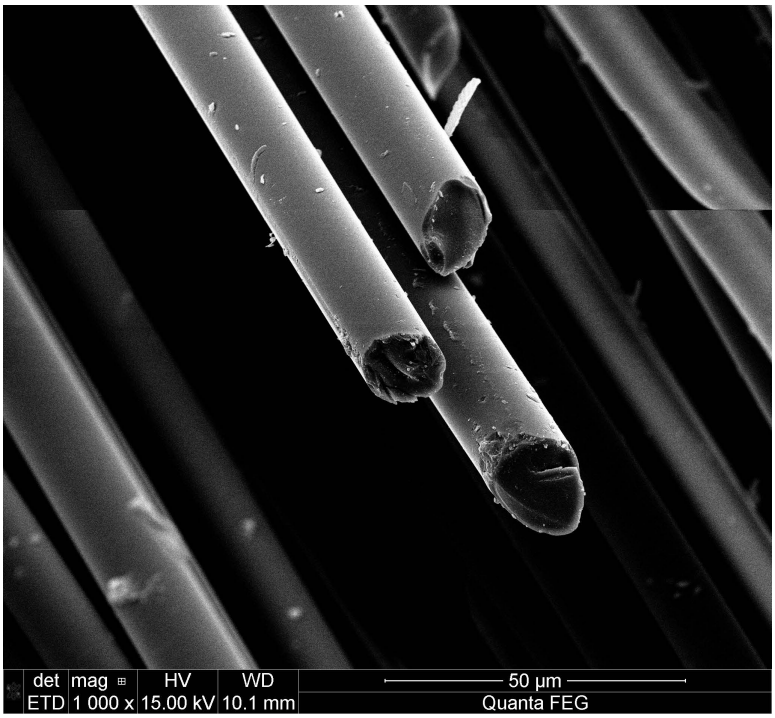

Figure 7.219: Hi-Nicalon S fiber specimen A27, tested in air at 1100°C at 154MPa

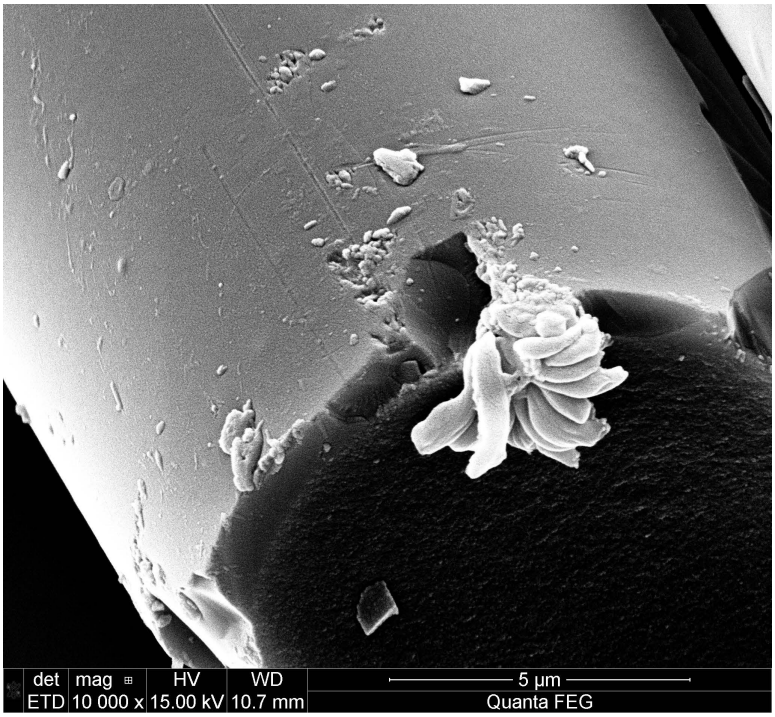

Figure 7.220: Hi-Nicalon S fiber specimen A30, tested in air at 1100°C at 255MPa

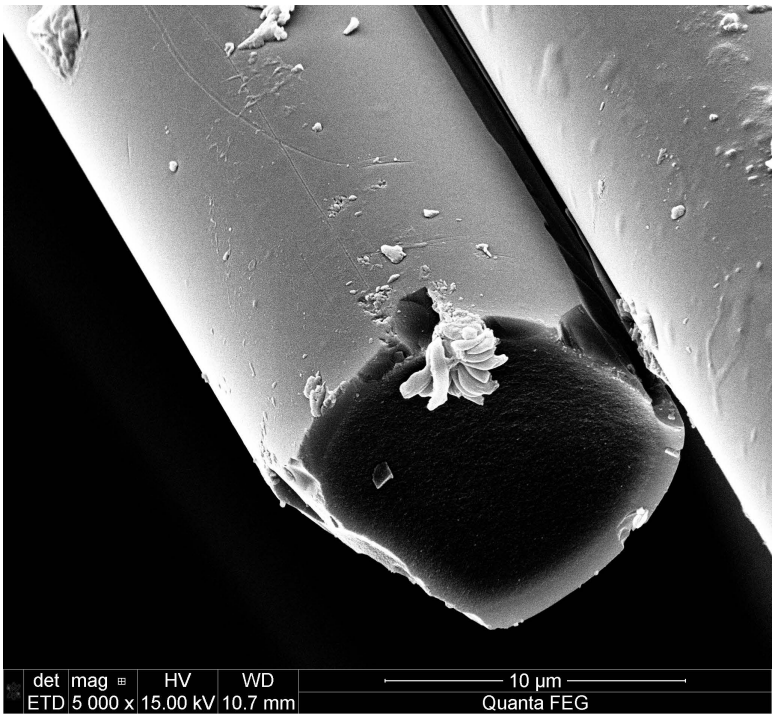

Figure 7.221: Hi-Nicalon S fiber specimen A30, tested in air at 1100°C at 255MPa

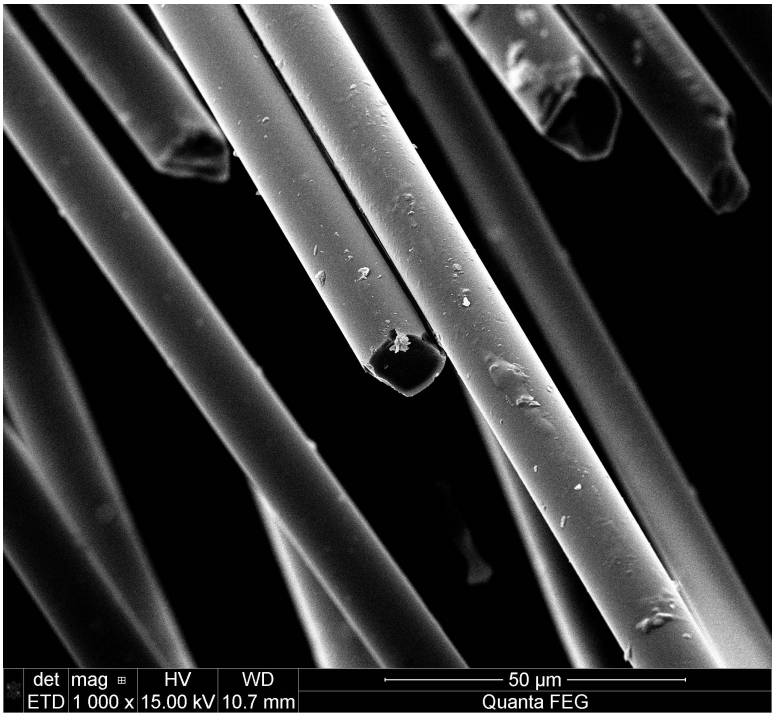

Figure 7.222: Hi-Nicalon S fiber specimen A30, tested in air at 1100°C at 255MPa

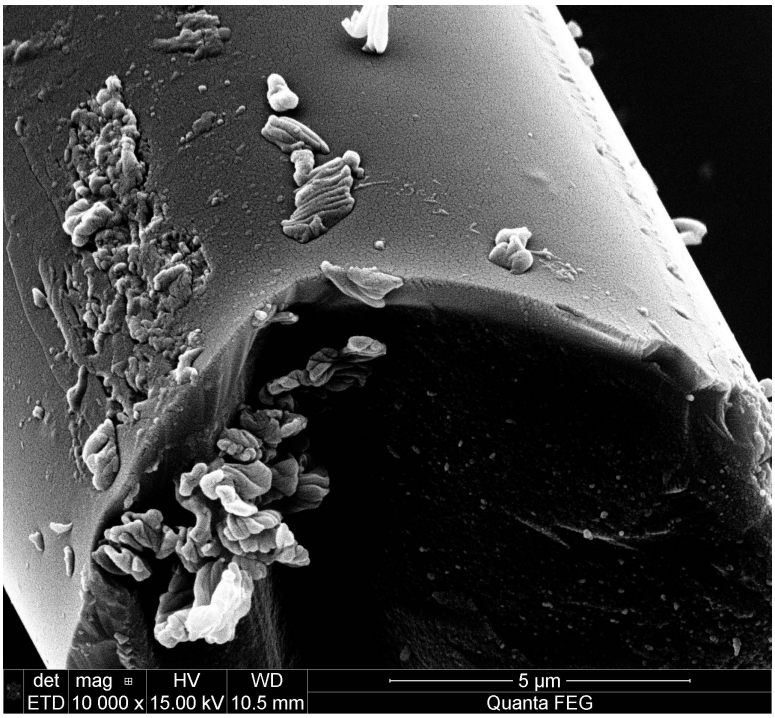

Figure 7.223: Hi-Nicalon S fiber specimen A30, tested in air at 1100°C at 255MPa

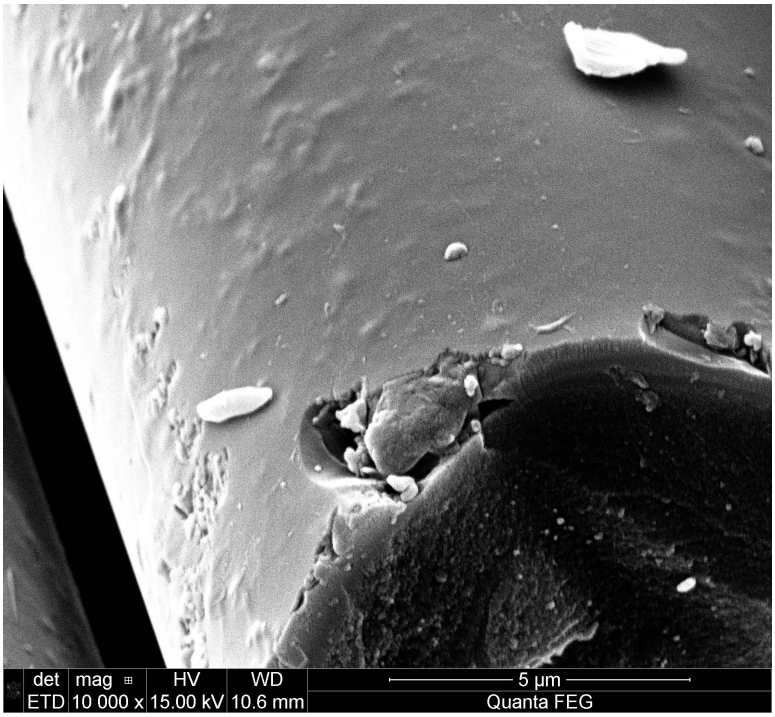

Figure 7.224: Hi-Nicalon S fiber specimen A30, tested in air at 1100°C at 255MPa

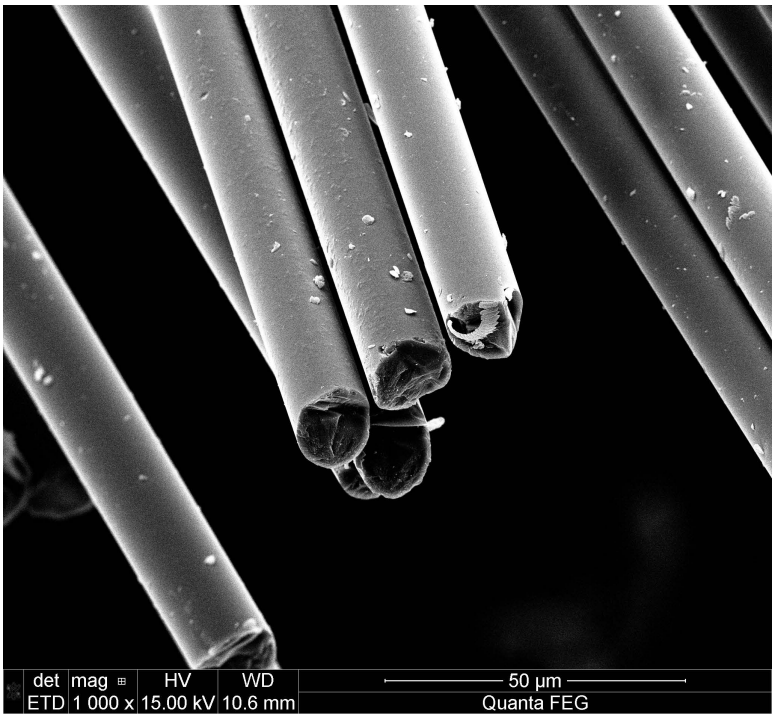

Figure 7.225: Hi-Nicalon S fiber specimen A30, tested in air at 1100°C at 255MPa

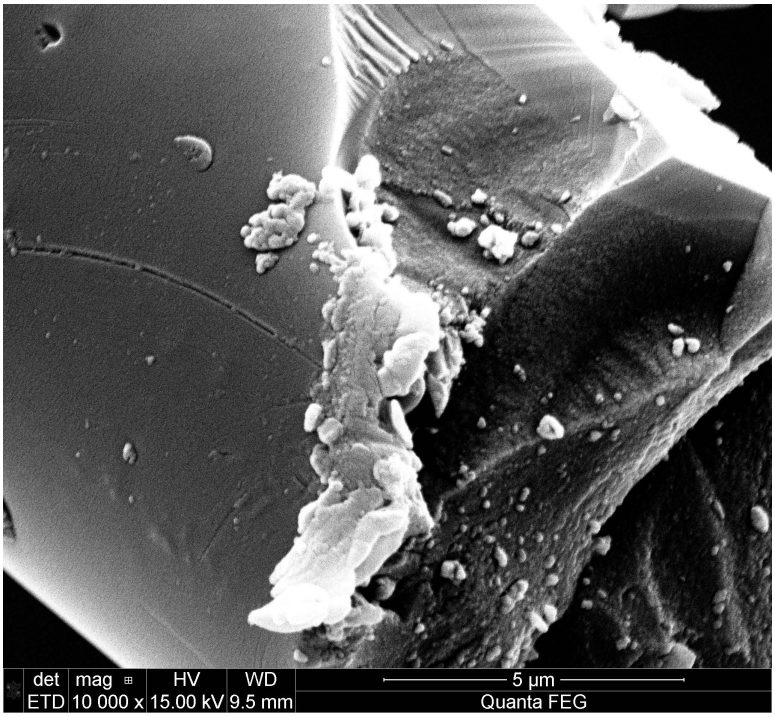

Figure 7.226: Hi-Nicalon S fiber specimen A35, tested in air at 1100°C at 353MPa

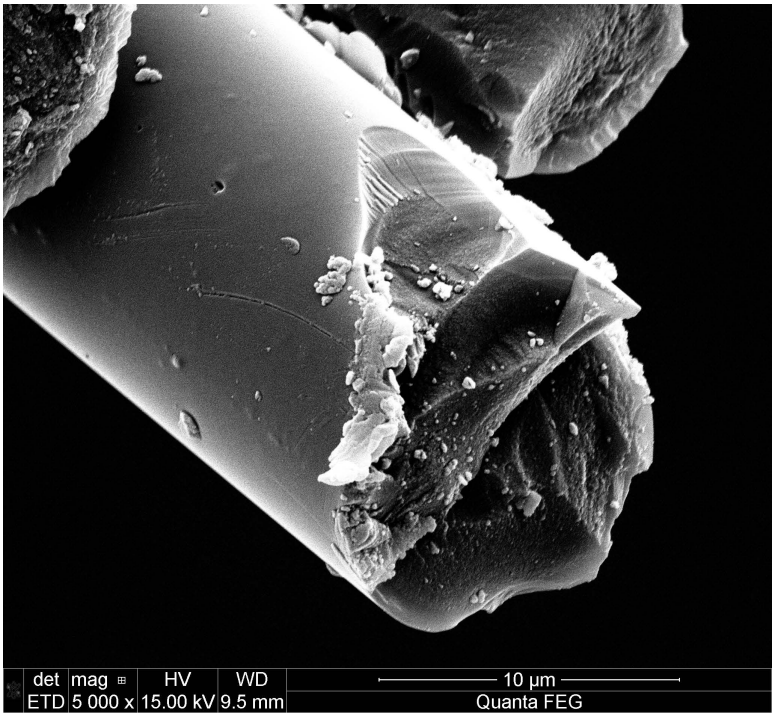

Figure 7.227: Hi-Nicalon S fiber specimen A35, tested in air at 1100°C at 353MPa

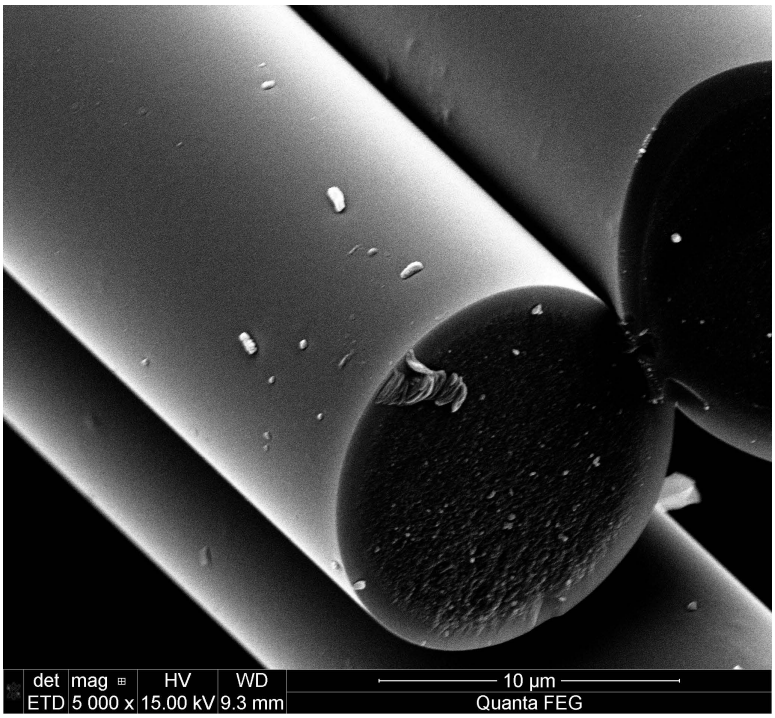

Figure 7.228: Hi-Nicalon S fiber specimen A35, tested in air at 1100°C at 353MPa

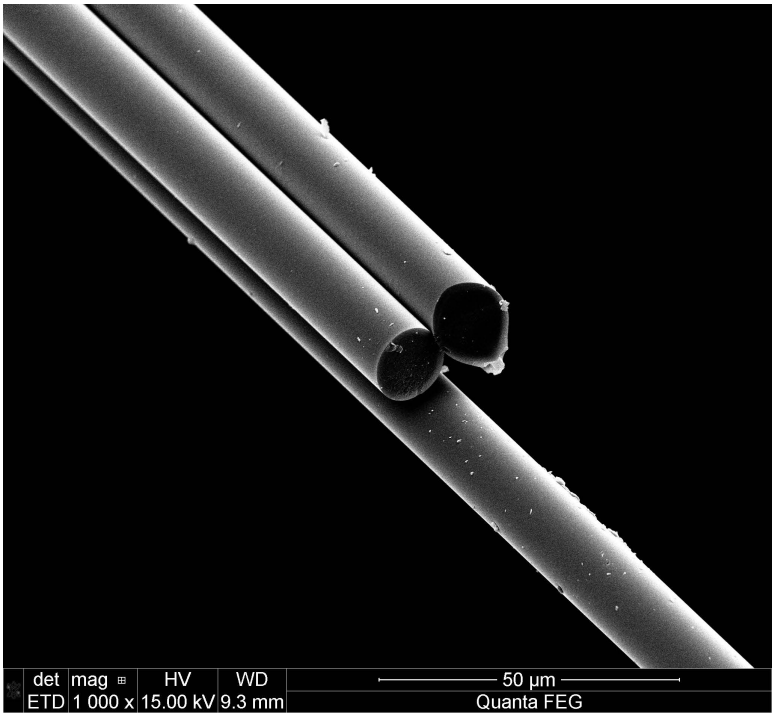

Figure 7.229: Hi-Nicalon S fiber specimen A35, tested in air at 1100°C at 353MPa

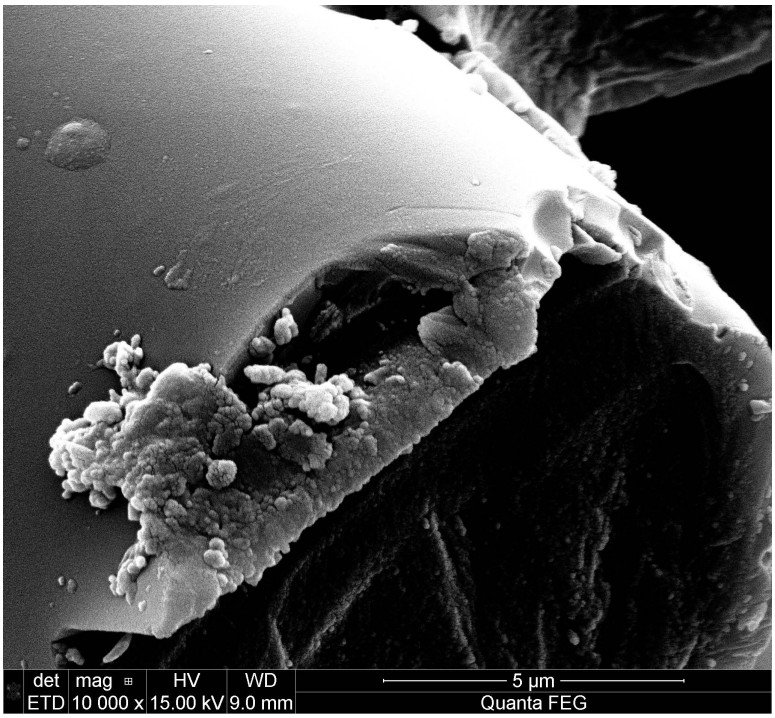

Figure 7.230: Hi-Nicalon S fiber specimen A35, tested in air at 1100°C at 353MPa

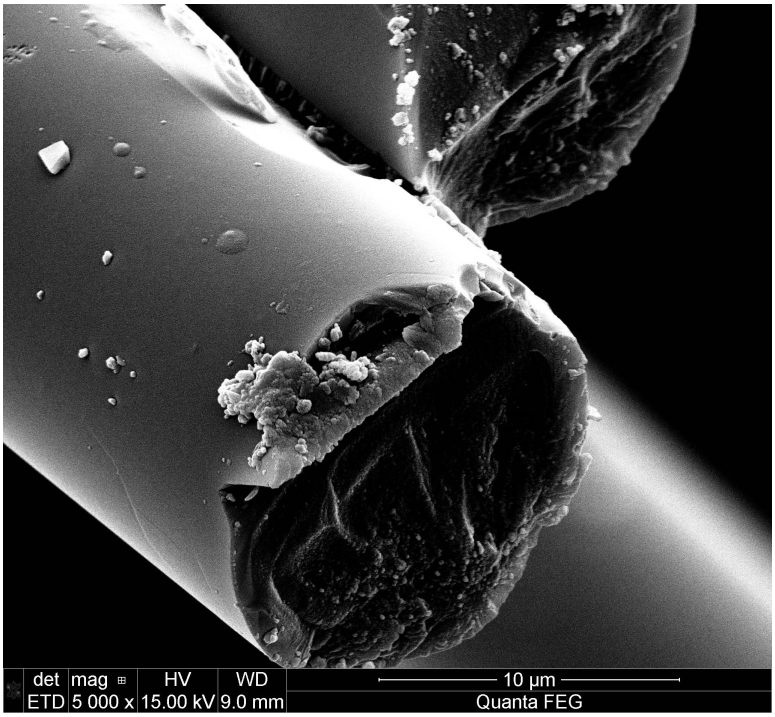

Figure 7.231: Hi-Nicalon S fiber specimen A35, tested in air at 1100°C at 353MPa

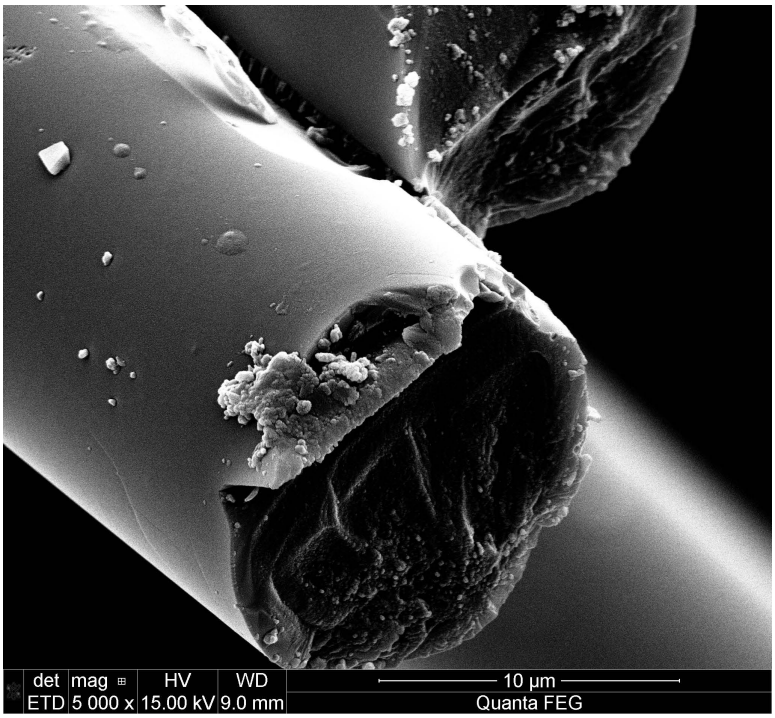

Figure 7.232: Hi-Nicalon S fiber specimen A35, tested in air at 1100°C at 353MPa

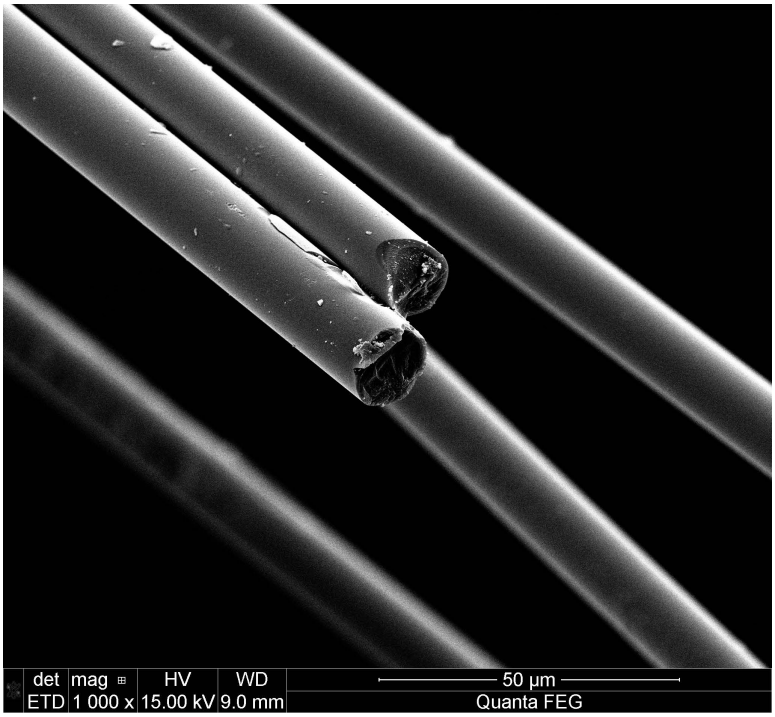

Figure 7.233: Hi-Nicalon S fiber specimen A35, tested in air at 1100°C at 353MPa

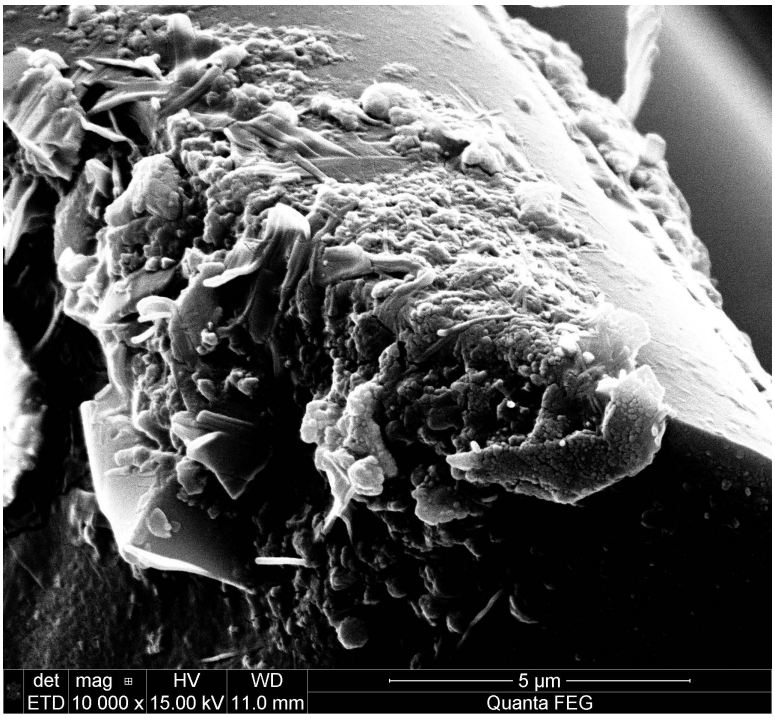

Figure 7.234: Hi-Nicalon S fiber specimen A28, tested in air at 1100°C at 450MPa

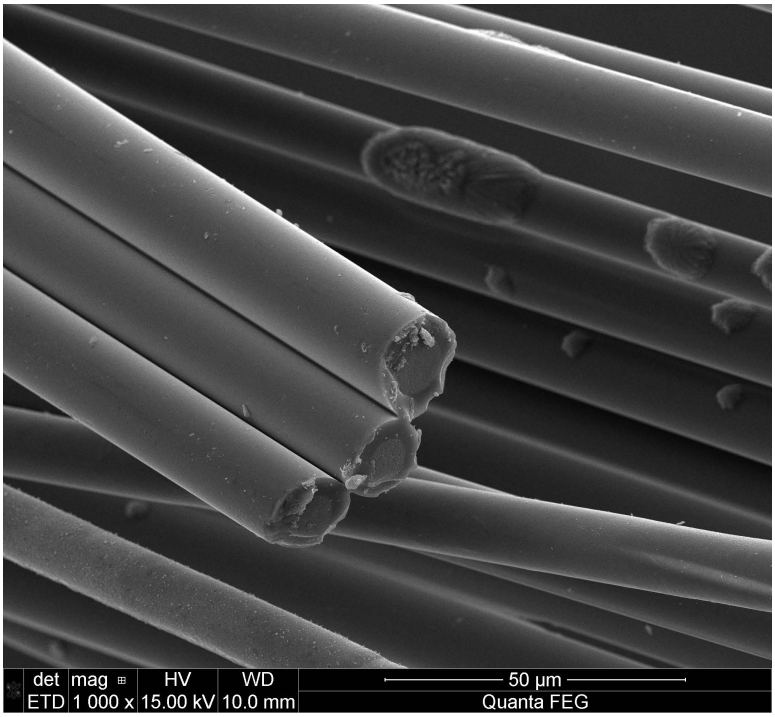

Figure 7.235: Hi-Nicalon S fiber specimen S25, tested in steam at 1100°C at 154MPa

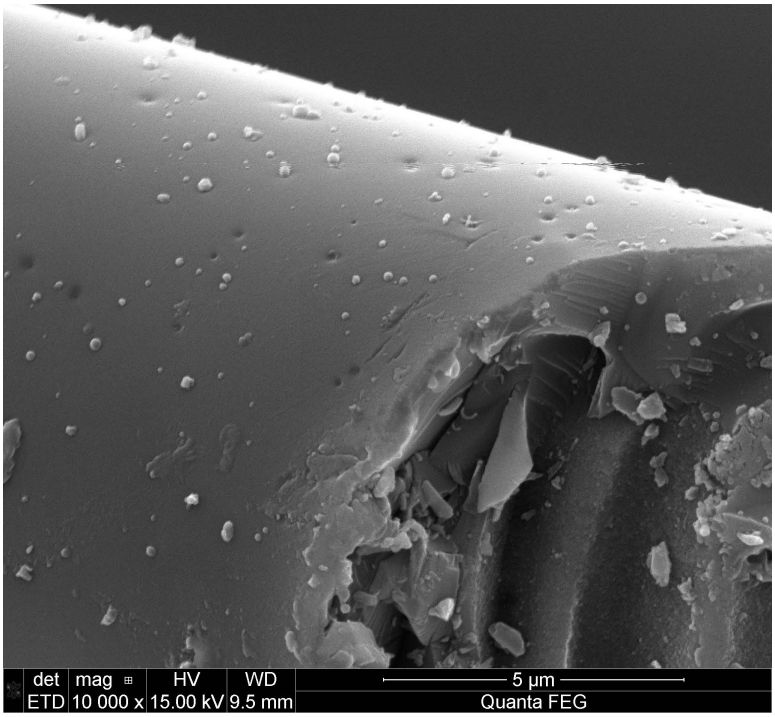

Figure 7.236: Hi-Nicalon S fiber specimen S25, tested in steam at 1100°C at 154MPa

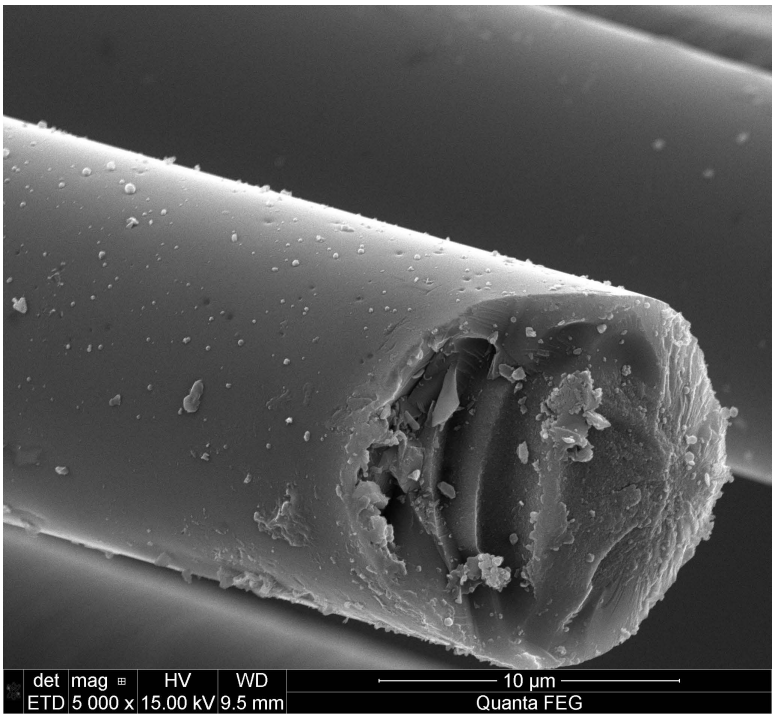

Figure 7.237: Hi-Nicalon S fiber specimen S25, tested in steam at 1100°C at 154MPa

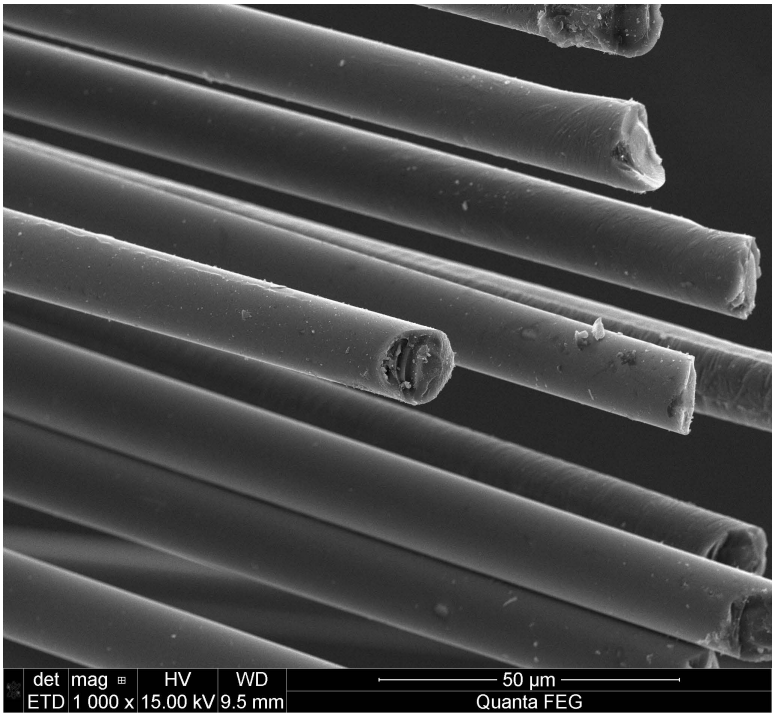

Figure 7.238: Hi-Nicalon S fiber specimen S25, tested in steam at 1100°C at 154MPa

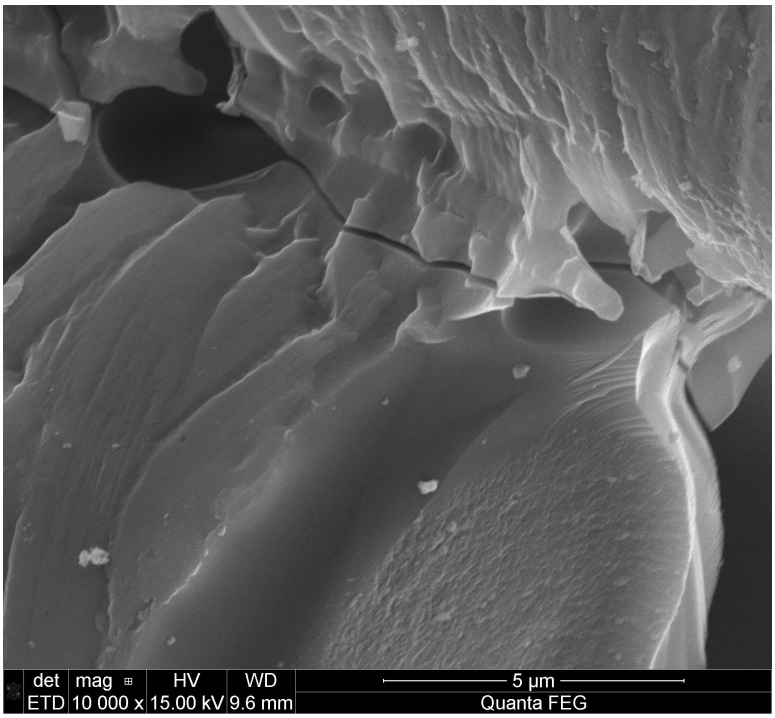

Figure 7.239: Hi-Nicalon S fiber specimen S25, tested in steam at 1100°C at 154MPa

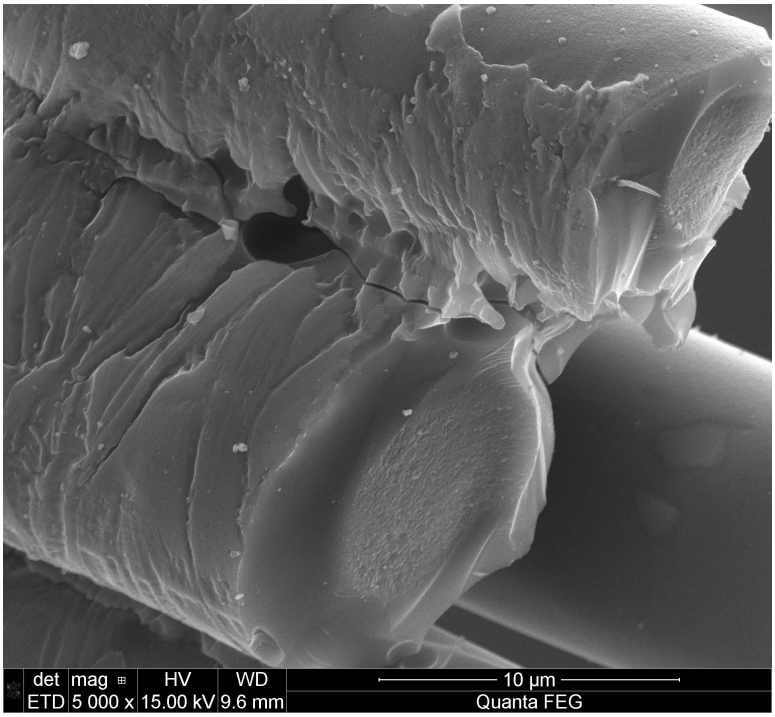

Figure 7.240: Hi-Nicalon S fiber specimen S25, tested in steam at 1100°C at 154MPa

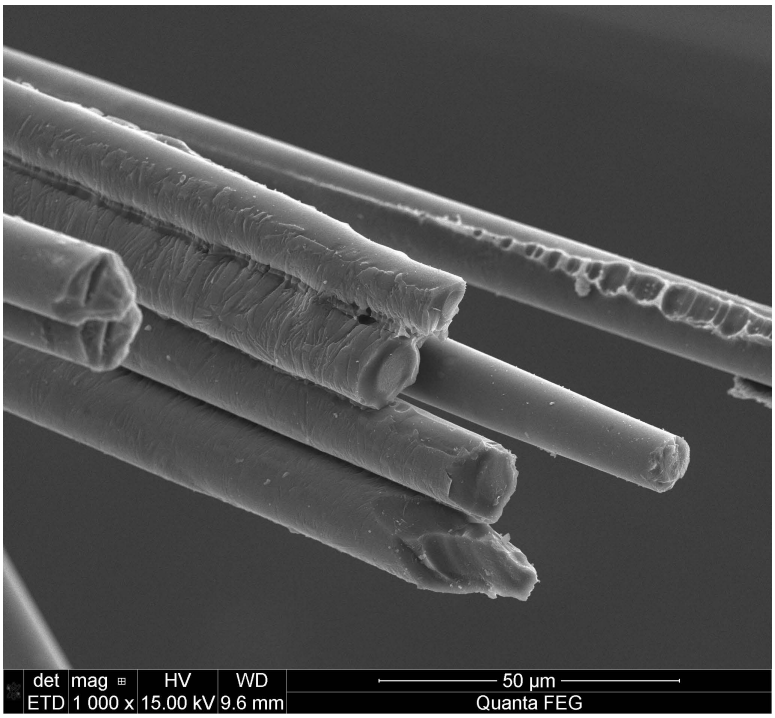

Figure 7.241: Hi-Nicalon S fiber specimen S25, tested in steam at 1100°C at 154MPa

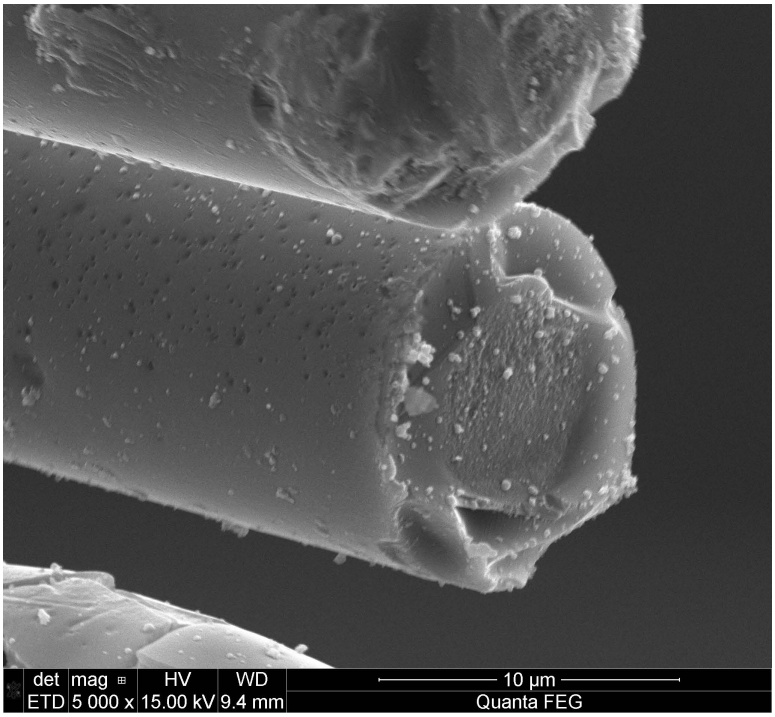

Figure 7.242: Hi-Nicalon S fiber specimen S25, tested in steam at 1100°C at 154MPa

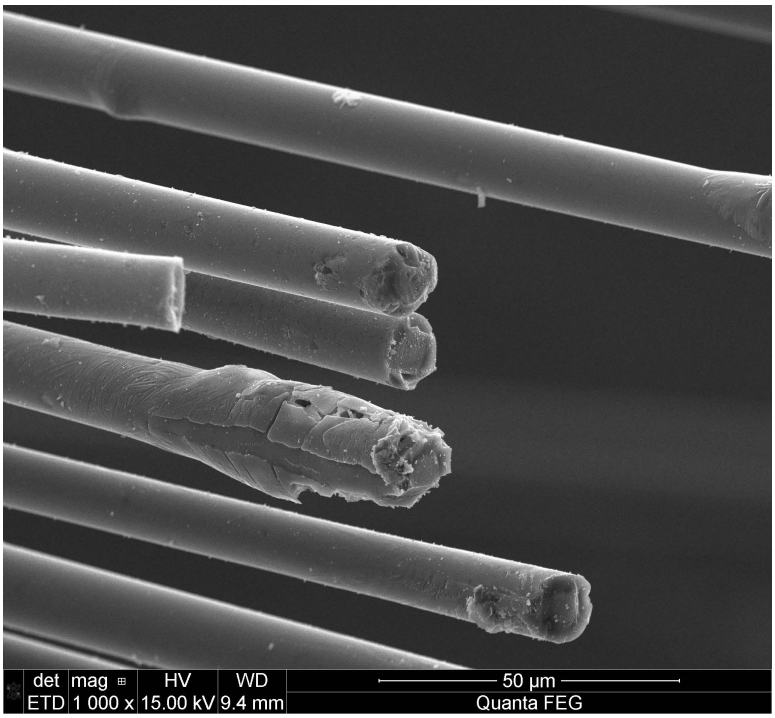

Figure 7.243: Hi-Nicalon S fiber specimen S25, tested in steam at 1100°C at 154MPa

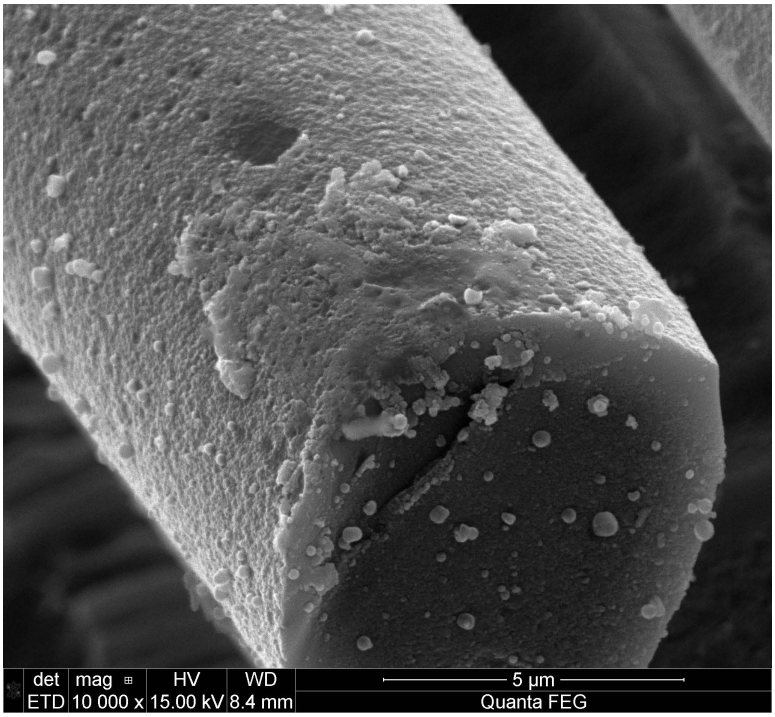

Figure 7.244: Hi-Nicalon S fiber specimen S26, tested in steam at 1100°C at 255MPa

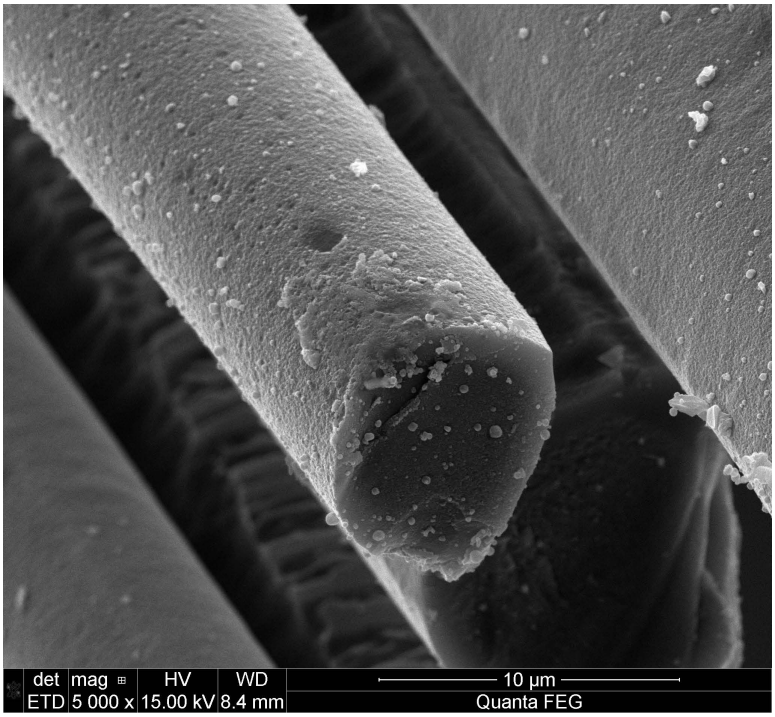

Figure 7.245: Hi-Nicalon S fiber specimen S26, tested in steam at 1100°C at 255MPa

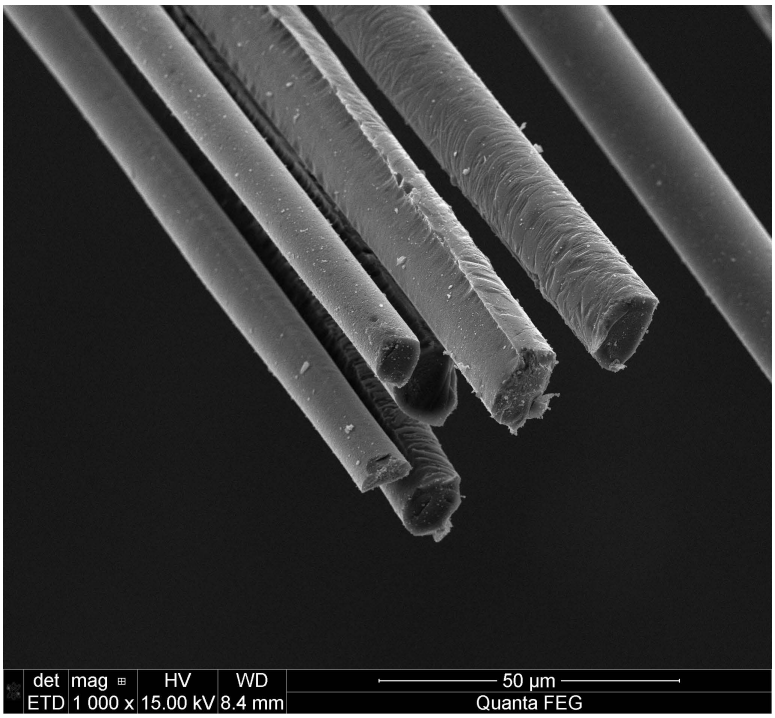

Figure 7.246: Hi-Nicalon S fiber specimen S26, tested in steam at 1100°C at 255MPa

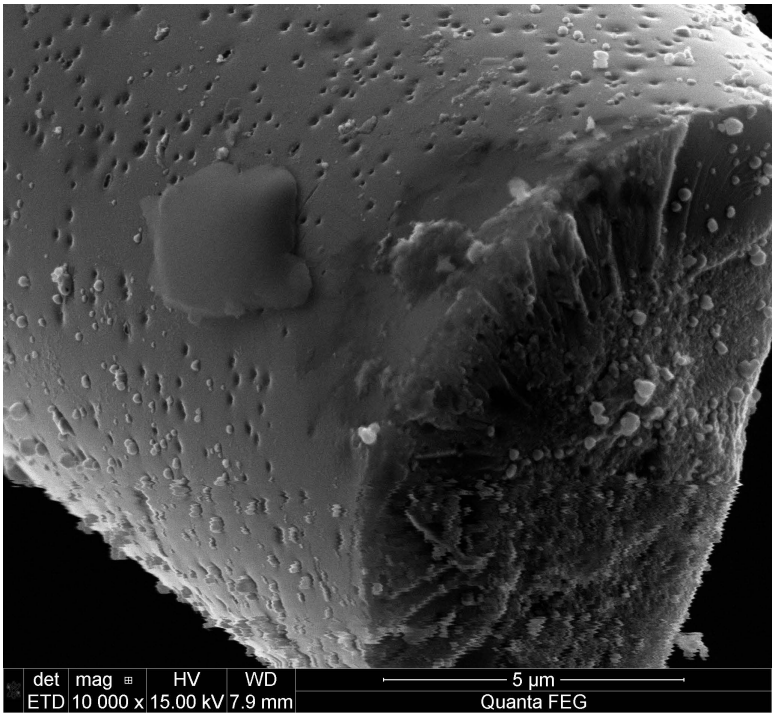

Figure 7.247: Hi-Nicalon S fiber specimen S26, tested in steam at 1100°C at 255MPa

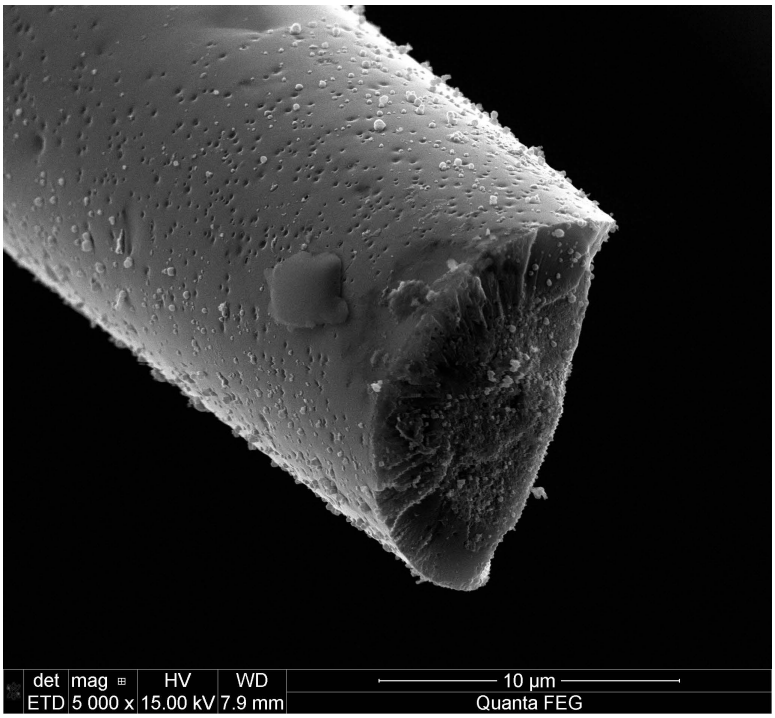

Figure 7.248: Hi-Nicalon S fiber specimen S26, tested in steam at 1100°C at 255MPa

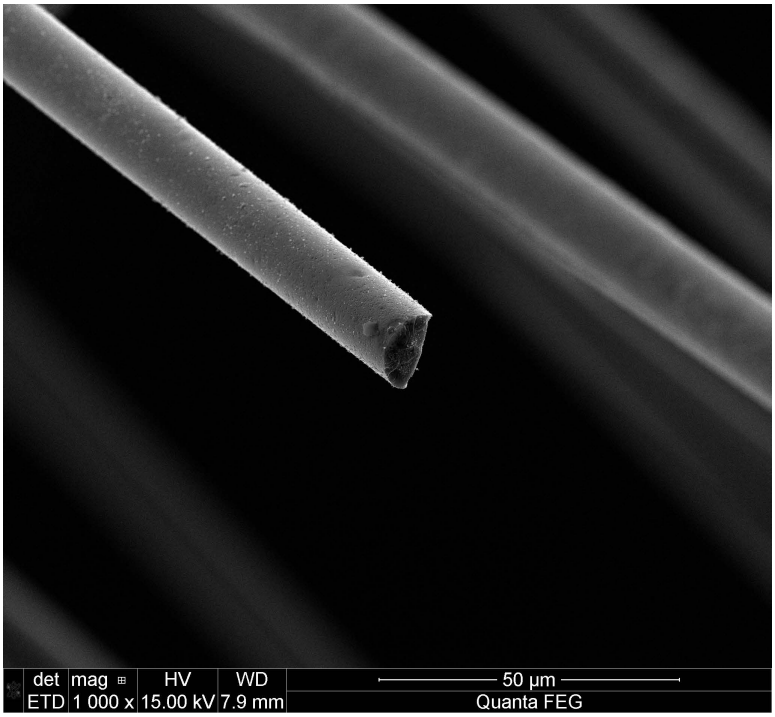

Figure 7.249: Hi-Nicalon S fiber specimen S26, tested in steam at 1100°C at 255MPa

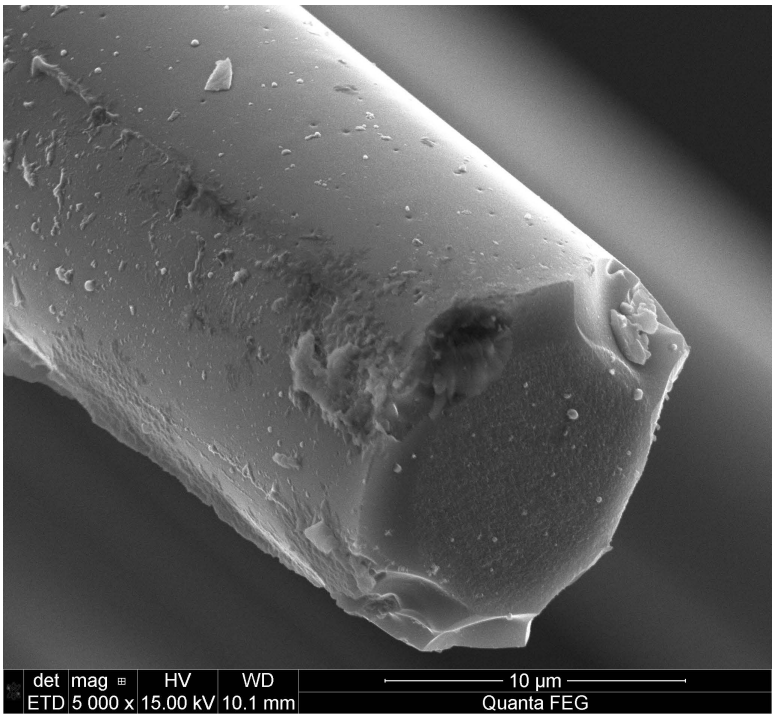

Figure 7.250: Hi-Nicalon S fiber specimen S26, tested in steam at 1100°C at 255MPa

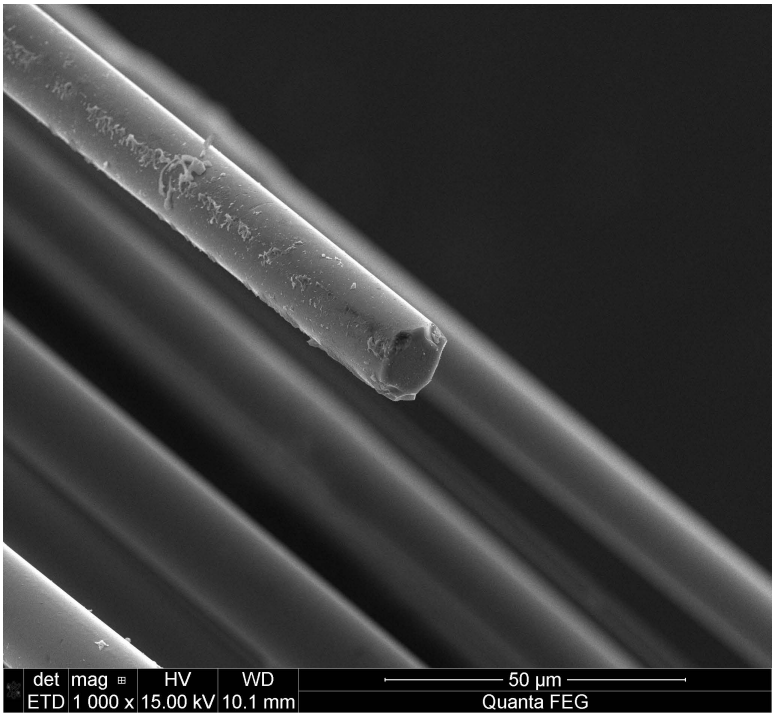

Figure 7.251: Hi-Nicalon S fiber specimen S26, tested in steam at 1100°C at 255MPa

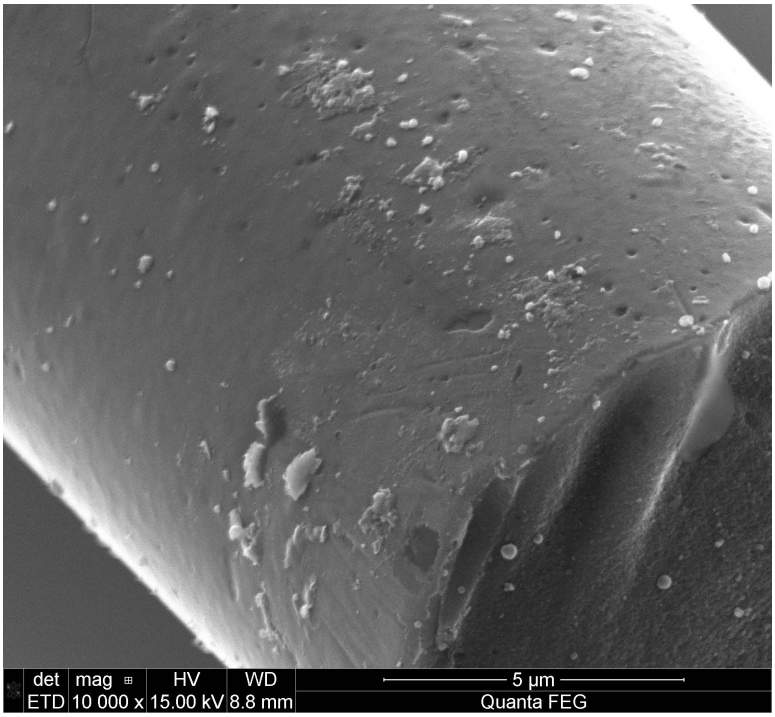

Figure 7.252: Hi-Nicalon S fiber specimen S33, tested in steam at 1100°C at 353MPa

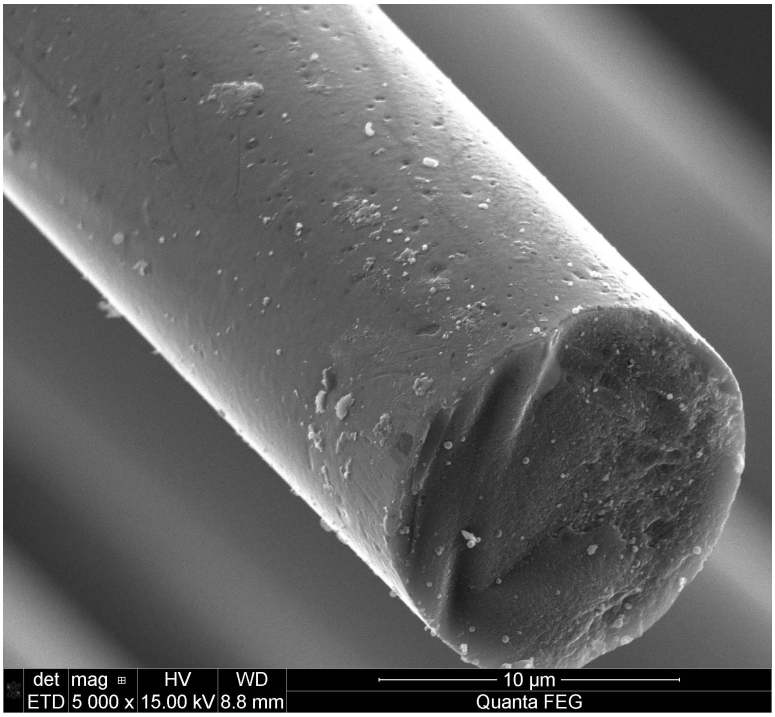

Figure 7.253: Hi-Nicalon S fiber specimen S33, tested in steam at 1100°C at 353MPa

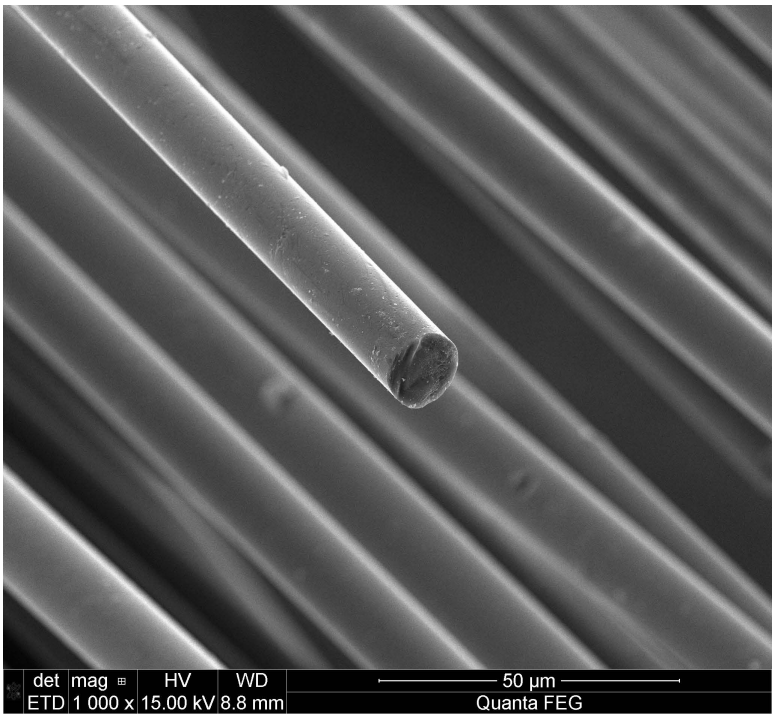

Figure 7.254: Hi-Nicalon S fiber specimen S33, tested in steam at 1100°C at 353MPa

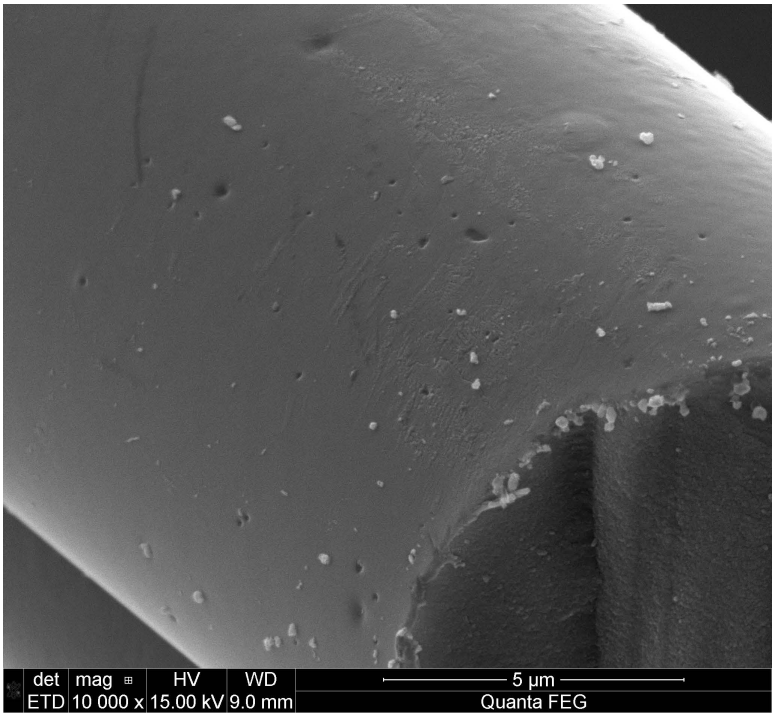

Figure 7.255: Hi-Nicalon S fiber specimen S33, tested in steam at 1100°C at 353MPa

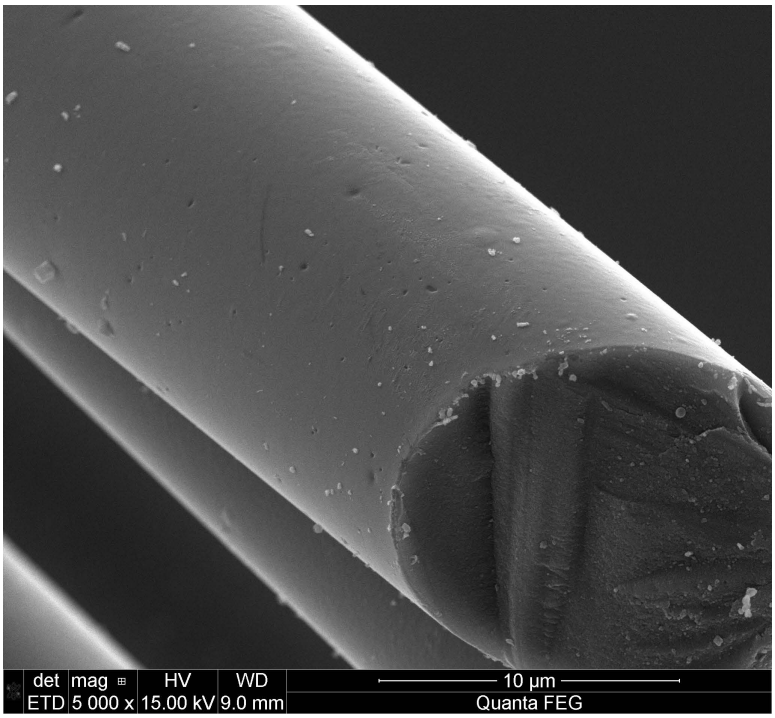

Figure 7.256: Hi-Nicalon S fiber specimen S33, tested in steam at 1100°C at 353MPa

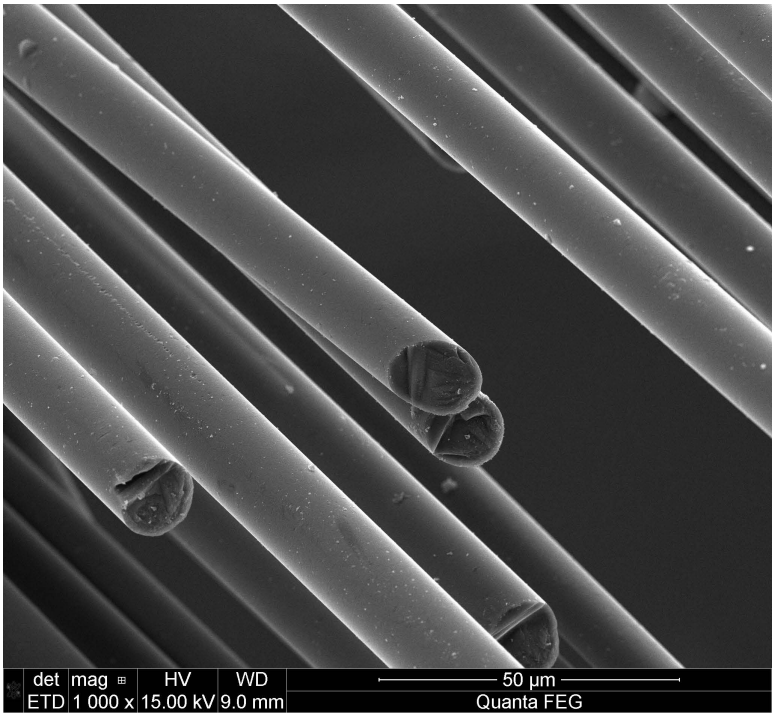

Figure 7.257: Hi-Nicalon S fiber specimen S33, tested in steam at 1100°C at 353MPa

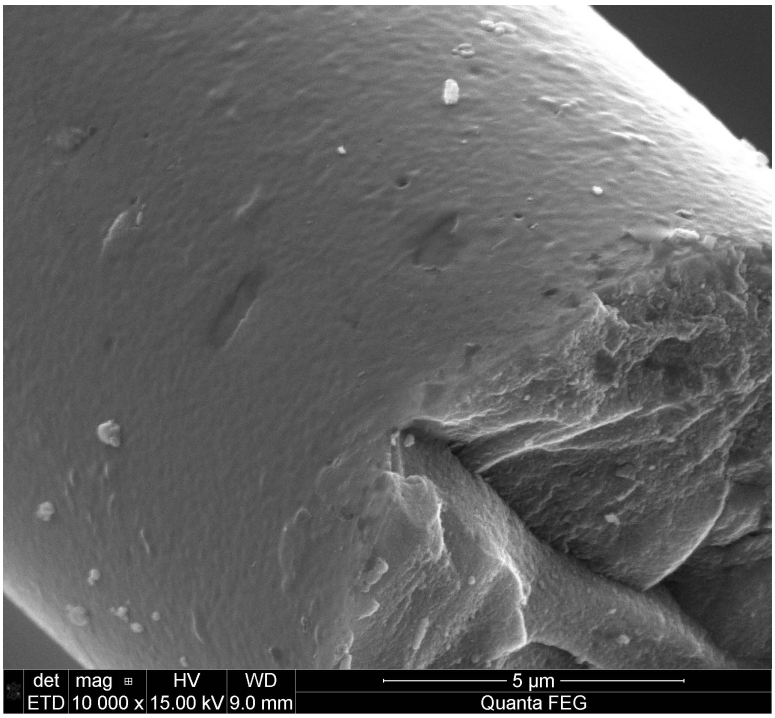

Figure 7.258: Hi-Nicalon S fiber specimen S33, tested in steam at 1100°C at 353MPa

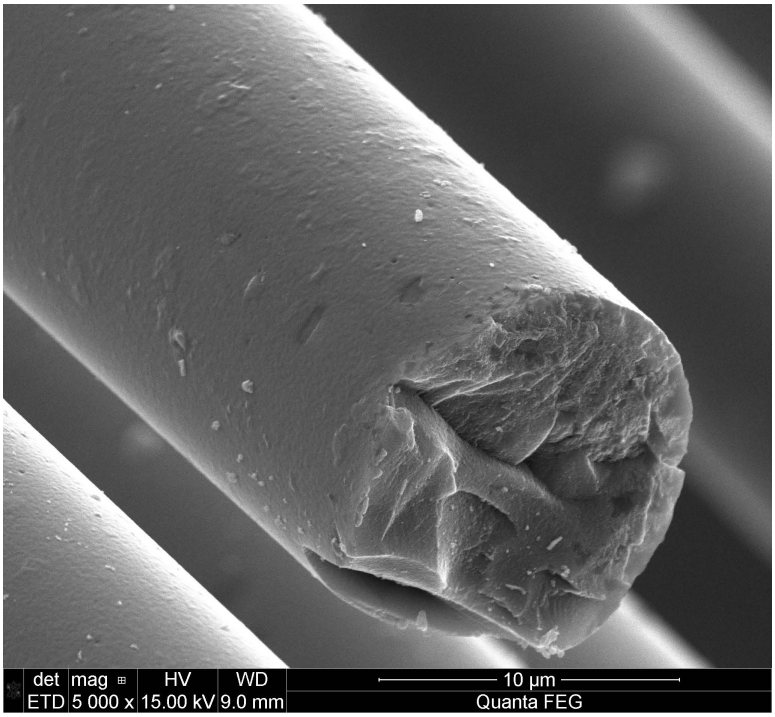

Figure 7.259: Hi-Nicalon S fiber specimen S33, tested in steam at 1100°C at 353MPa

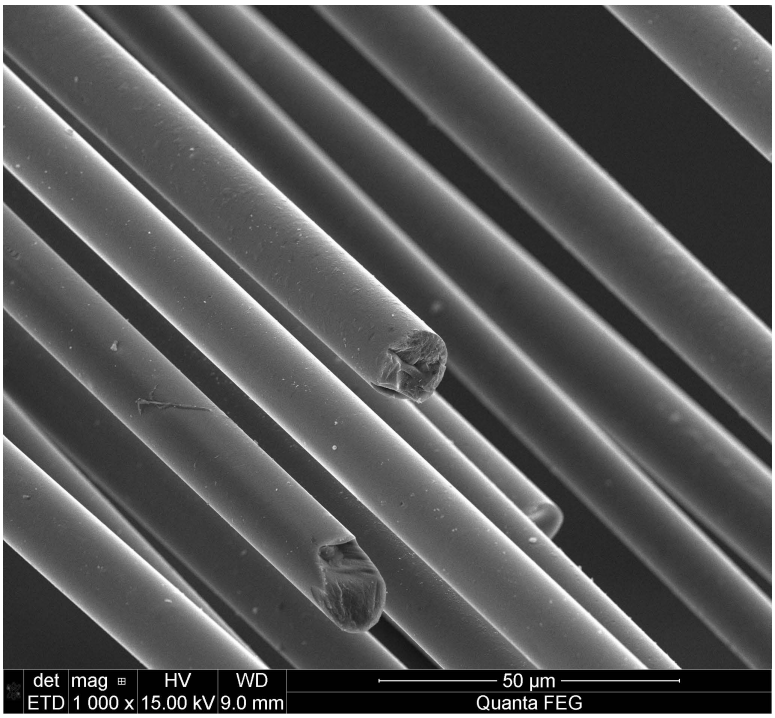

Figure 7.260: Hi-Nicalon S fiber specimen S33, tested in steam at 1100°C at 353MPa

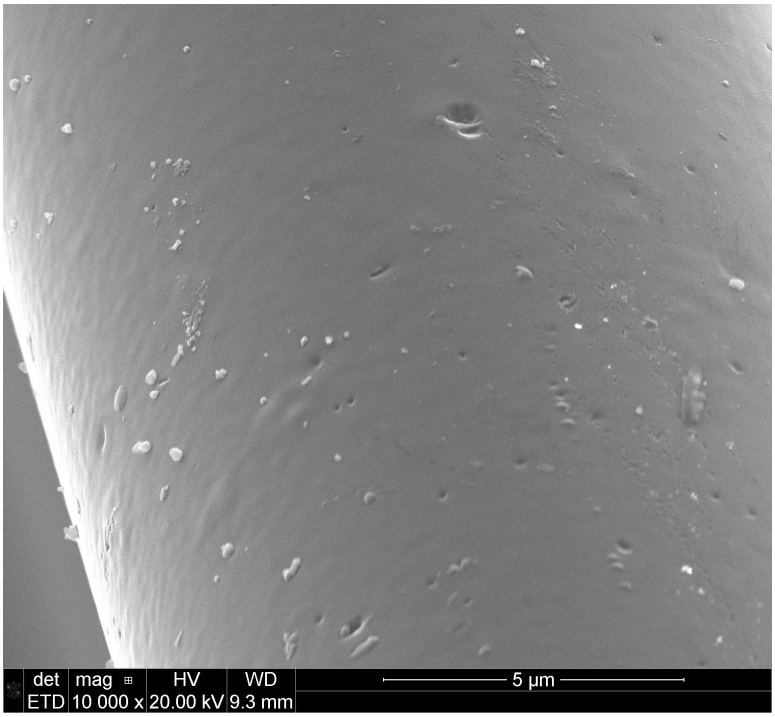

Figure 7.261: Hi-Nicalon S fiber specimen S33, tested in steam at 1100°C at 353MPa

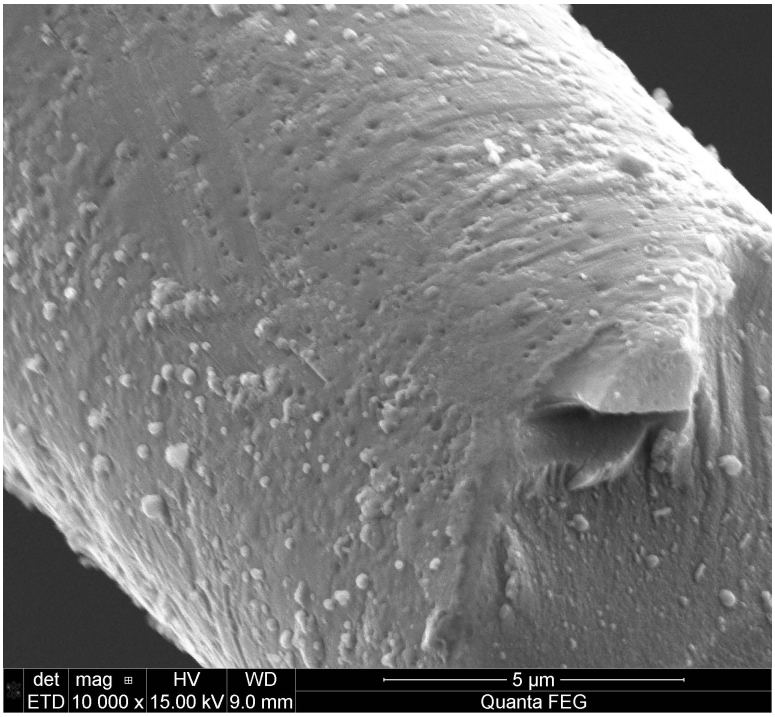

Figure 7.262: Hi-Nicalon S fiber specimen S32, tested in steam at 1100°C at 400MPa

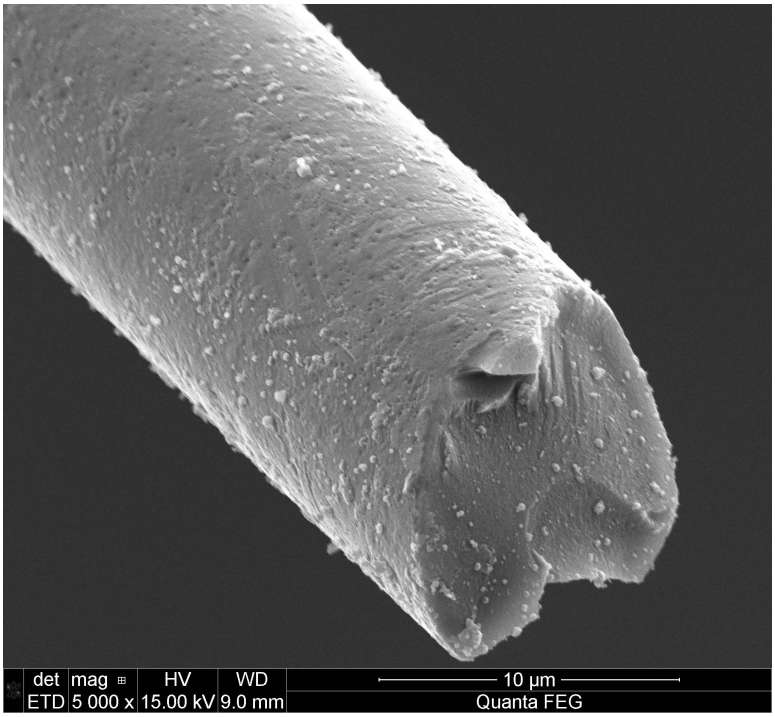

Figure 7.263: Hi-Nicalon S fiber specimen S32, tested in steam at 1100°C at 400MPa

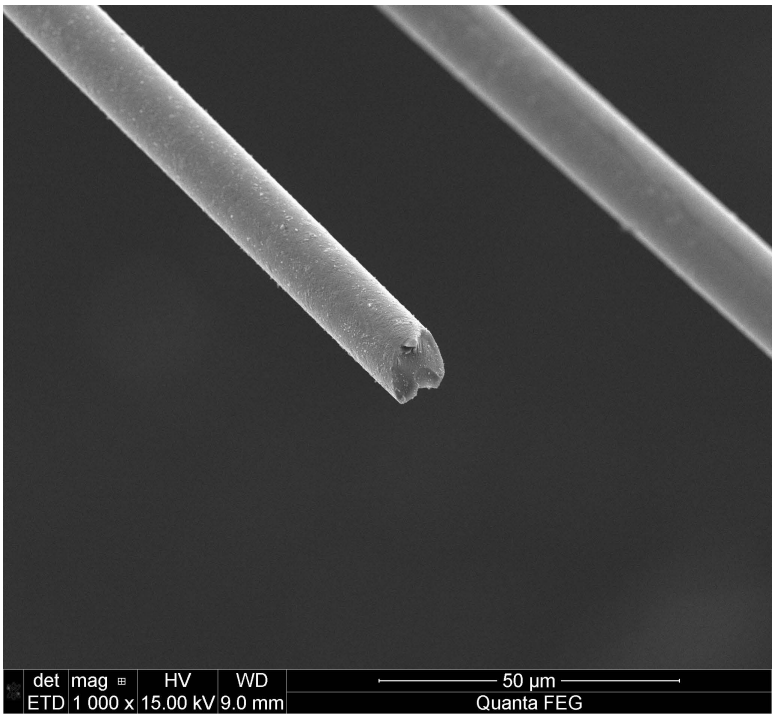

Figure 7.264: Hi-Nicalon S fiber specimen S32, tested in steam at 1100°C at 400MPa

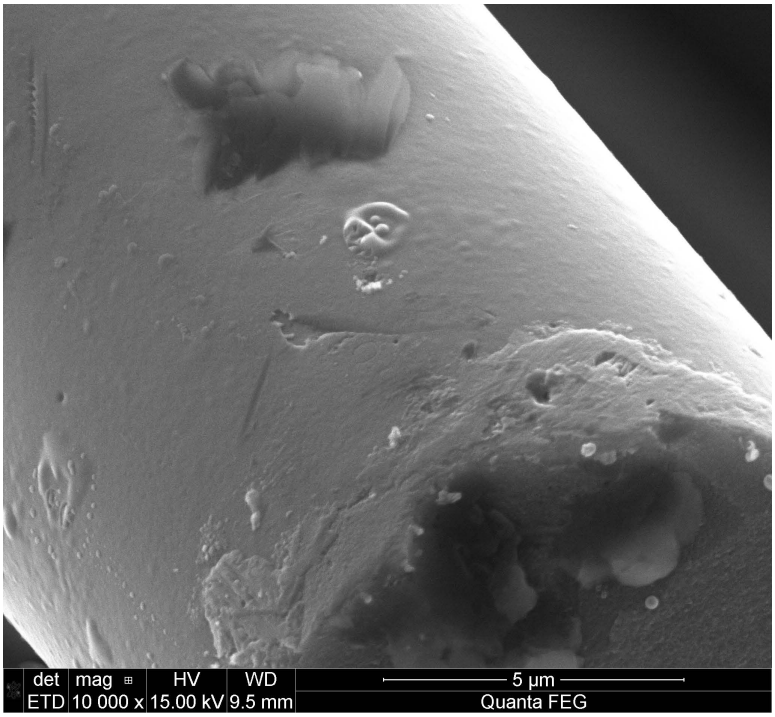

Figure 7.265: Hi-Nicalon S fiber specimen S32, tested in steam at 1100°C at 400MPa

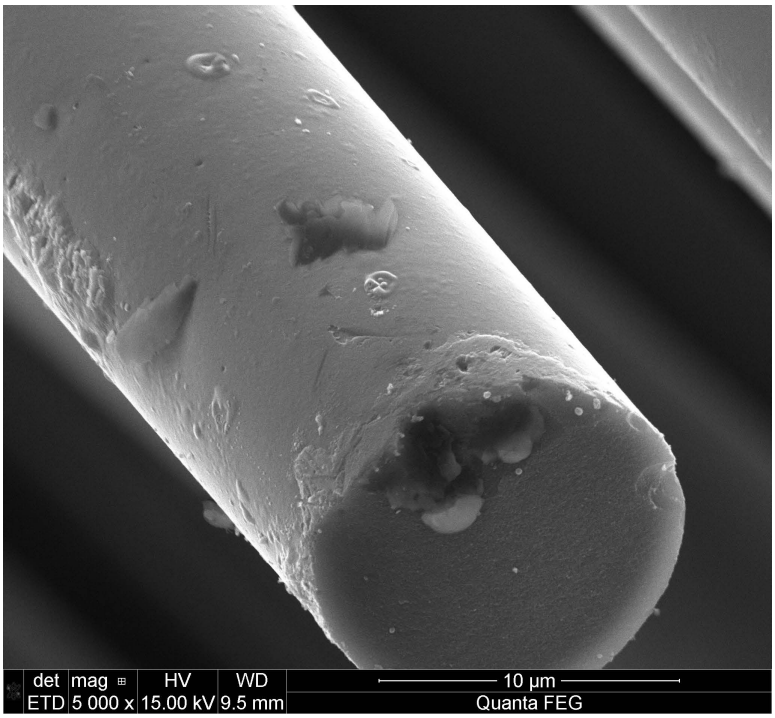

Figure 7.266: Hi-Nicalon S fiber specimen S32, tested in steam at 1100°C at 400MPa

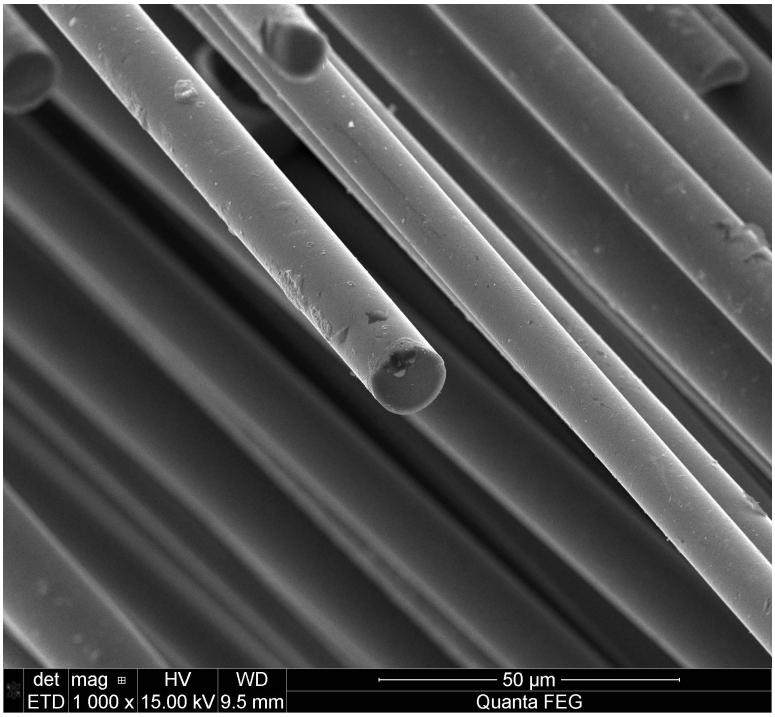

Figure 7.267: Hi-Nicalon S fiber specimen S32, tested in steam at 1100°C at 400MPa

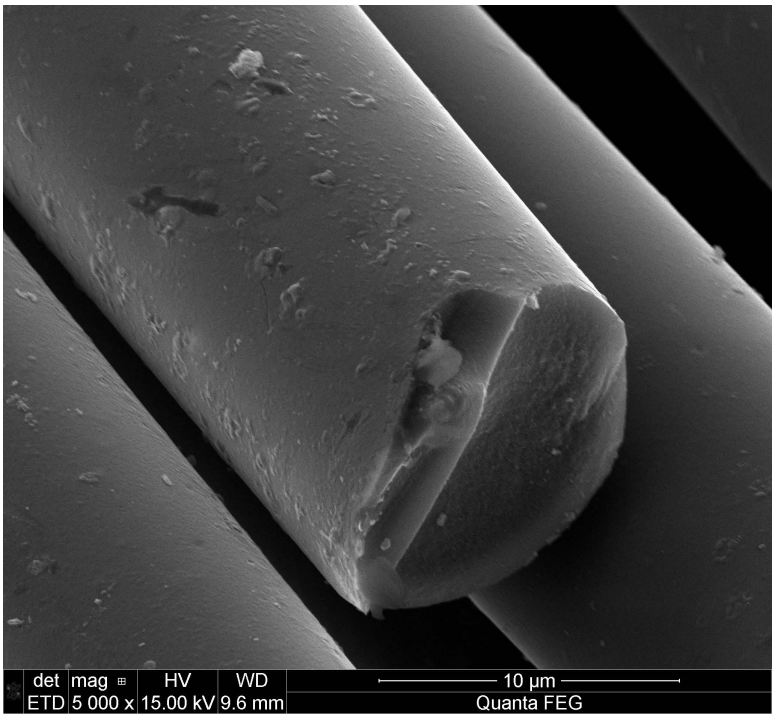

Figure 7.268: Hi-Nicalon S fiber specimen S32, tested in steam at 1100°C at 400MPa

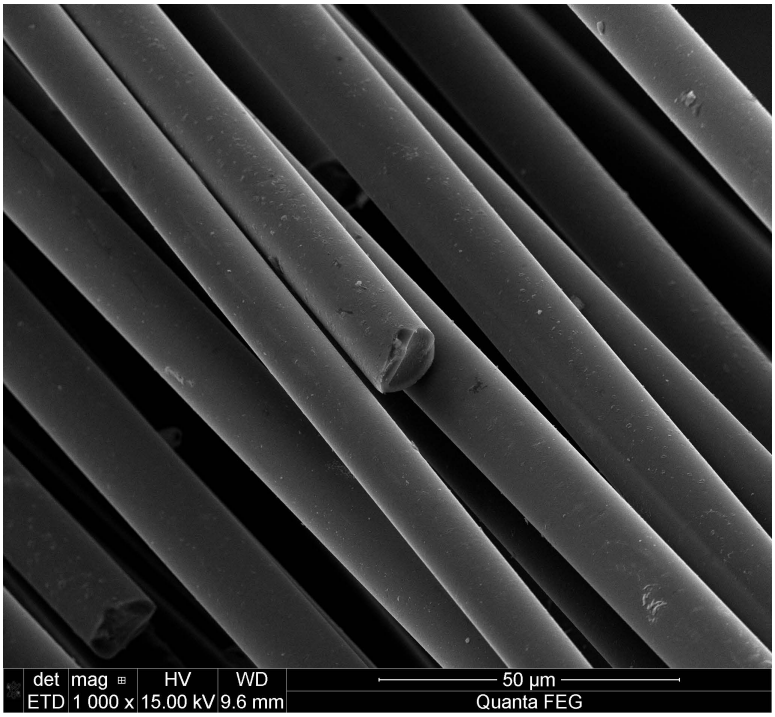

Figure 7.269: Hi-Nicalon S fiber specimen S32, tested in steam at 1100°C at 400MPa

VIII. Bibliography

[1] "Ceramic Matrix Composites". *Composite Materials Handbook, vol. 5*. Department of Defense, 2002.

[2] Armani, C. *Creep performance of oxide ceramic fiber materials at elevated temperature in air and in steam.* Phd dissertation, Air Force Institute of Technology (AU), March 2011.

[3] Bae, S. I. and S. Baik. "Sintering and grain growth of ultrapure alumina". *Journal of Materials Science*, 28(15):4197–4204, 1993.

[4] Bertrand, S., R. Pailler, and J. Lamon. "Influence of Strong Fiber/Coatings Interfaces on the Mechanical Behavior and Lifetime of Hi-Nicalon/Pyc/SiC)n/SiC Minicomposites". *J. Am. Ceram. Soc.*, 84(4):787–794, 2001.

[5] Bewlay, B., M. Jackson, and H. Lipsitt. "The balance of mechanical and environmental properties of a multi element niobium-niobium silicide-based composite". *Metallurgical and Materials Transactions*, 27(12):3801–3808, 1996.

[6] Brewer, D. "HSR/EPM combustor materials development program". *Mater. Sci. Eng. A*, A261:284–291, 1999.

[7] Brewer, D., F. Ojard, and Gibler M. "Ceramic matrix composite combustor liner rig test". *ASME Turbo Expo 2000*, ASME Paper 2000–GT–0670, 2000.

[8] Bunsell, A. and A. Piant. "A review of the development of three generations of small diameter silicon carbide fibres". *J. Mater. Sci*, 41:823–839, 2006.

[9] Calard, V. and J. Lamon. "Failure of fiber bundles". *Composites Science and Technology*, 64(5):701–710, 2004.

[10] Chawla, Krishan K. *Ceramic Matrix Composites*. Kluwer Academic Publishers, 2003.

[11] Christensen, D.T. *Fatigue behavior of an advanced SiC/SiC composite at elevated temperature in air and in steam.* Master's thesis, Air Force Institute of Technology, December 2009.

[12] Clauser, H. R. "Advanced composite materials". *Scientific American*, 229(1):36–44, 1973.

[13] Coleman, B. D. "On the strength of classical fibres and fibre bundles". *Journal of the Mechanics and Physics of Solids*, 7:60, 1958.

[14] Corman, G. S. and K. Luthra. "Silicon melt infiltrated ceramic composites (HiPerComp)". N. Bansal (editor), *Handbook of ceramic composites*, 99–115. Kluwer Academic, NY, 2005.

[15] Dassios, K. G., M. Steen, and C. Filiou. "Mechanical properties of alumina Nextel 720 fibres at room and elevated temperatures: tensile bundle testing". *Materials Science and Engineering A*, 349(1-2):63–72, 2003.

[16] DiCarlo, J. A. "Property goals and test methods for high temperature ceramic fibre reinforcement". *Ceram. Int.*, 23(4):283–289, 1997.

[17] DiCarlo, J. A. and H. M. Yun. "Fiber Test Development for Ceramic Composite Thermomechanical Properties". M. G. Jenkins, E. Lara-Curzio, and S. T. Gonczy (editors), *Mechanical, Thermal, and Environmental Testing and Performance of Cermaic Composties and Components, ASTM STP 1392*. West Conshohocken, PA, 2000.

[18] DiCarlo, J. A., H. M. Yun, G. N. Morscher, and R. T. Bhatt. "SiC/SiC Composites for 1200°C and Above". *Handbook for Ceramic Composites*. 2005.

[19] Dowling, Norman E. *Mechanical Behavior of Materials: Engineering Methods of Deformation, Fracture, and Fatigue 3rd ed.* Pearson Prentice Hall, 2007.

[20] Evans, A.G. and F. W. Zok. "Review: the Physics and Mechanics of Fiber Reinforced Brittle Matrix Composites". *J. Mater. Science*, 30:3857–3896, 1994.

[21] Ferber, M. K., H. T. Lin, and J. R. Keiser. "Oxidation behavior of non-oxide ceramics in a high-pressure, high-temperature steam environment, editor = Jenkins, M. G. and Lara-Curzio, E. and Gonczy, S. T., booktitle= Mechanical, Thermal, and Environmental Testing and Performance of Ceramic Composites and Components, publisher= ASTM STP 1392, address= American Society for Testing and Materials, pages= 210-215". 2000.

[22] Forio, P., F. Lavaire, and J. Lamon. "Delayed Failure at Intermediate Temperatures (600°C-700°C) in Air in Silicon Carbide Multifilament Tows". *J. Am. Ceram. Soc.*, 87(5):888–893, 2004.

[23] Gauthier, W. and J. Lamon. "Delayed Failure of Hi-Nicalon and Hi-Nicalon S Multifilament Tows and Single Filaments at Intermediate Temperatures (500-800°C)". *J. Am. Ceram. Soc.*, 92(3):702–709, 2009.

[24] Gauthier, W., F. Pailler, J. Lamon, and R. Pailler. "Oxidation of Silicon Carbide Fibers During Static Fatigue in Air at Intermediate Temperatures". *J. Am. Ceram. Soc.*, 92(9):2067–2073, 2009.

[25] Hammond, V. H. *Creep Rupture of an Oxide/Oxide Composite Fiber*. Phd dissertation, University of Virginia, 2001.

[26] Herakovich, C. T. *Mechanics of Fibrous Composites*. John Wiley & Sons, 1998.

[27] Heredia, F. E., J. C. McNulty, F. W. Zok, and A. G. Evans. "An oxidation embrittlement probe for ceramic matrix composites". *J. Am. Ceram. Soc.*, 78:2097–2100, 1995.

[28] Hillig, W. B. *Tailoring Multiphase Composite Ceramics*. Plenum Press, 1985.

[29] Ichikawa, H., K. Okamura, and T. Seguchi. "High temperature ceramic matrix composites II". A. G. Evans and R. Naslain (editors), *Ceramic Transactions*, 65. American Ceramic Soc., West Conshohocken, PA, 1995.

[30] Ishikawa, T. "Advances in Inorganic Fibers". *Polymeric and Inorganic Fibers*, 178, 2005.

[31] Kandil, F.A. and B.F. Dyson. "Tensile Creep of Ceramics: the Development of a Testing Facility". *Int. J. High Technol. Ceram.*, 4(2-4):243, 1988.

[32] Kerans, R., R. Hay, T. Parthasarathy, and M. Cinibulk. "Interface Design for Oxidation-Resistant Ceramic Composites". *J. Am. Ceram. Soc.*, 85(11):2599–2632, 2002.

[33] Kerans, R. J., R. S. Hay, N. J. Pagano, and T. A. Parthasarathy. "The Role of the fiber Matrix Interface in Ceramic Composites". *Am. Ceram. Soc. Bull*, 68(2):429–442, 1989.

[34] Kerans, R. J. and T. A. Parthasarathy. "Crack Deflection in Ceramic Composites and Fiber coating Design Criteria". *Composites: Part A*, 30:521–524, 1999.

[35] Kiser, J.D. et al. "SiC/SiC Ceramic Matrix Composites Developed for High-Temperature Space Transportation Applications". *NASA Glenn Research Center*, 2005.

[36] Ladeveze, P. and M. Genet. "A new approach to the subcritical cracking of ceramic fibers". *Composites Science and Technology*, 70:1575–1583, 2010.

[37] Mah, T., N. L. Hecht, D. E. McCullum, J. R. Hoenigman, H. M. Kim, A. P. Katz, and H. A. Libsitt. "Thermal Stability of SiC Fibres (Nicalon)". *J. Mater. Sci.*, 19:1191–1201, 1984.

[38] Manson, S.S. and G.R. Halford. "Fatigue and Durability of Structural Materials". *ASM International*, 316–317, 2006.

[39] McNulty, J. C., M. Y. He, and F. W. Zok. "Notch sensitivity of fatigue life in a Sylramic^T *M*/SiC composite at elevated temperature". *Comp. Sci. Tech*, 61:1331–1338, 2001.

[40] Moeller, H. H. "Tensile testing of ceramic fiber tows". *Ceram. Eng. Sci. Proc.*, 6:558, 1985.

[41] More, K. L., P. F. Tortorelli, M. K. Ferber, and J. R. Keiser. "Observations of accelerated silicon carbide recession by oxidation at high water-vapor pressure". *J. Am. Cer. Soc.*, 83(1):211–213, 2000.

[42] More, K. L., P. F. Tortorelli, M. K. Ferber, L. R. Walker, J. R. Keiser, W. D. Brentnall, N. Miralya, and J. B. Price. "Exposure of ceramic and ceramic-matrix composites in simulated and actual combustor environments". *Proceedings of international gas turbine and aerospace congress*. Paper No. 99-GT-292, 1999.

[43] Morrell, R.M. "A tensile creep-testing apparatus for ceramic materials using simple knife-edge universal joints." *Journal of Physics E (Scientific Instruments*, 5(5):465–467, 1972.

[44] Morscher, G. N., G. Ojard, R. Miller, Y. Gowayed, U. Santhosh, J. Ahmad, and R. John. "Tensile creep and fatigue of Sylramic-iBN melt-infiltrated SiC matrix

composites: retained properties, damage development, and failure mechanisms". *Comp. Sci. Tech*, 68:3305–3313, 2008.

[45] Naslain, R. "Ceramic Matrix Composites". *European White Book on fundamental Research in Materials Science*. Max-Planck-Institut fur Metallforschung, Stuttgart, Germany, 2001.

[46] Naslain, R. "Design, preparation and properties of non-oxide CMCs for applicaiton in engines and nuclear reactors: an overview". *Composites Science and Technology*, 64(1):155–170, 2004.

[47] Opila, E.J. "Variation of the Oxidation Rate of Silicon Carbide with Water-Vapor Pressure". *J. Am. Ceram. Soc.*, 82(3):625–636, 1999.

[48] Opila, E.J. "Oxidation and Volatilization of Silica Formers in Water Vapor". *J. Am. Ceram. Soc.*, 86(8):1238–1248, 2003.

[49] Prewo, K. M. and J. A. Batt. "The oxidative stability of carbon fibre reinforced glass-matrix composites". *J. Mater. Sci.*, 23:523–527, 1988.

[50] Sauder, C. and J. Lamon. "Tensile Creep Behavior of SiC-Based Fibers With a Low Oxygen Content". *J. Am. Ceram. Soc.*, 94(4):1146–1156, 2007.

[51] Schmidt, S., H. Knabe, H. Immich, R. Mestring, and A. Gessler. "Advanced Ceramic Matrix Composite Material for Current and Future Propulsion Technology Applications". *Acta Astronautica*, 55:409–420, 2004.

[52] Steffens, B. *Creep of Hi-Nicalon S ceramic fiber tows at elevated temperature in air and in steam.* Master's thesis, Air Force Institute of Technology, March 2012.

[53] Vaughan, D. J. "Fiberglass Reinforcement". G. Lubin and S.T. Peters (editors), *Handbook of Composites, 2nd ed.* Chapman & Hall, New York, 1998.

[54] Yun, H. M., J. C. Goldsby, and J. A. DiCarlo. "Tensile creep and stress-rupture behavior of polymer derived SiC fibers". NASA TM–106692, 1994.

[55] Zawada, L. P., J. Staehler, and S. Steel. "consequence of INtermittent Exposure to Moisture and Salt Fog on the High-Temperature Fatigue Durability of Several Ceramic-Matrix Composites". *J. Am. Ceram. Soc.*, 86(8):1282–1291, 2003.

[56] Zok, F. W. and C. G. Levi. "Mechanical properties of porous-matrix ceramic composites". *Advanced Engineering Materials*, 3(1):15–23, 2001.

REPORT DOCUMENTATION PAGE

Form Approved
OMB No. 0704–0188

1. REPORT DATE (DD–MM–YYYY)	2. REPORT TYPE	3. DATES COVERED *(From — To)*
21-03-2013	Master's Thesis	Oct 2011-Mar 2013

4. TITLE AND SUBTITLE
Creep of Hi-Nicalon S Fiber Tows at Elevated Temperature in Air and in Steam

5a. CONTRACT NUMBER
5b. GRANT NUMBER
5c. PROGRAM ELEMENT NUMBER

6. AUTHOR(S)
Shillig, Theodore R., Captain, USAF

5d. PROJECT NUMBER
5e. TASK NUMBER
5f. WORK UNIT NUMBER

7. PERFORMING ORGANIZATION NAME(S) AND ADDRESS(ES)
Air Force Institute of Technology
Graduate School of Engineering and Management (AFIT/ENY)
2950 Hobson Way
WPAFB OH 45433-7765

8. PERFORMING ORGANIZATION REPORT NUMBER
AFIT-ENY-13-M-31

9. SPONSORING / MONITORING AGENCY NAME(S) AND ADDRESS(ES)
Dr. Geoff Fair, Dr. Randy Hay
AFRL-RXCC
2977 Hobson Way Wright-Patterson AFB, OH 45433-7734
(937) 255-9791

10. SPONSOR/MONITOR'S ACRONYM(S)
AFRL/RXCC

11. SPONSOR/MONITOR'S REPORT NUMBER(S)

12. DISTRIBUTION / AVAILABILITY STATEMENT
APPROVED FOR PUBLIC RELEASE; DISTRIBUTION UNLIMITED

13. SUPPLEMENTARY NOTES This material is declared a work of the U.S. Government and is not subject to copyright protection in the United States.

14. ABSTRACT

Structural aerospace components require materials that have superior long-term mechanical properties and can withstand severe environmental conditions, such as high temperatures, high pressures and moisture. Ceramic-matrix composites (CMCs) are capable of maintaining excellent strength and creep resistance at high temperatures, which makes them attractive candidate materials for aerospace applications, particularly in propulsion components. Silicon Carbide (SiC) ceramic fibers have been used as constituent materials in CMCs, although oxidation of the SiC to SiO_2 has been a known fiber degradation mechanism. Recently developed near stoichiometric Hi-Nicalon-S fibers have shown significant improvements in thermo-chemical stability. Creep of the Hi-Nicalon-S fibers at elevated temperature in air and in inert gas environments has been examined. However performance of these new fibers at elevated temperatures in steam environments has not been studied thoroughly. The objective of this thesis is to investigate creep of near stoichiometric Hi-Nicalon-S SiC fiber tows at elevated temperatures in air and in steam.

The creep response of Hi-Nicalon-S SiC fiber tows was investigated at 800°C, 900°C, 1000°C and 1100°C in laboratory air and in steam. The creep stresses ranged from 154 MPa to 1250 MPa. Creep run-out was defined as 100 h at creep stress. The presence of steam degraded the creep performance of the fiber tows at all temperatures. However, the negative effects of steam became less pronounced as the temperature increased. Less degradation due to steam at higher temperature is attributed to the transition from passive oxidation at 800°C-1000°C to active oxidation at 1100°C of the Hi-Nicalon-S SiC fibers.

15. SUBJECT TERMS
Material, Mechanical, Ceramic, Creep, Environmental,

16. SECURITY CLASSIFICATION OF:			17. LIMITATION OF ABSTRACT	18. NUMBER OF PAGES	19a. NAME OF RESPONSIBLE PERSON
a. REPORT	b. ABSTRACT	c. THIS PAGE	UU	235	Dr. Marina B. Ruggles-Wrenn (ENY)
U	U	U			19b. TELEPHONE NUMBER (Include Area Code) (937)255-3636, ext 4641 Marina.Ruggles-Wrenn@afit.edu